17.0

ANSYS reaction DESIGN

Chemkin Theory Manual

Chemkin® Software

CK-THE-15151-1601-UG-1
January 2016

Licensing:

For licensing information, please contact Reaction Design at (858) 550-1920 (USA) or licensing@ansys.com.

Technical Support:

Reaction Design provides an allotment of technical support to its Licensees free of charge. To request technical support, please include your license number along with input or output files, and any error messages pertaining to your question or problem. Requests may be directed in the following manner: E-mail: reactiondesign-support@ansys.com, Fax: (858) 550-1925, Phone: (858) 550-1920.
Additional technical support hours may also be purchased. Please contact Reaction Design for the hourly rates.

Copyright:

Trademark:

Limitation of Warranty:

The software is provided “as is” by Reaction Design, without warranty of any kind including, without limitation, any warranty against infringement of third party property rights, fitness or merchantability, or fitness for a particular purpose, even if Reaction Design has been informed of such purpose. Furthermore, Reaction Design does not warrant, guarantee, or make any representations regarding the use or the results of the use, of the software or documentation in terms of correctness, accuracy, reliability or otherwise. No agent of Reaction Design is authorized to alter or exceed the warranty obligations of Reaction Design as set forth herein. Any liability of Reaction Design, its officers, agents or employees with respect to the software or the performance thereof under any warranty, contract, negligence, strict liability, vicarious liability or other theory will be limited exclusively to product replacement or, if replacement is inadequate as a remedy or in Reaction Design’s opinion impractical, to a credit of amounts paid to Reaction Design for the license of the software.

Literature Citation for CHEMKIN:

ANSYS Chemkin Theory Manual 17.0 (15151) should be cited as:
ANSYS Chemkin Theory Manual 17.0 (15151), Reaction Design: San Diego, 2015.

Contents

Table of Contents

Contents

List of Tables

Contents

List of Figures

Acknowledgments

ANSYS acknowledges the following contributions.

ANSYS acknowledges researchers from Nissan Motor Co., Ltd., Dr. Noda and Mr. Kassai, for their helpful advice and technical review of the CHEMKIN Zonal SI Engine Model.

The content of this document is based, in part, on the following publications:

M. E. Coltrin, R. J. Kee, G. H. Evans, E. Meeks, F. M. Rupley, and J. F. Grcar, *SPIN (Version 3.83): A Fortran Program for Modeling One-Dimensional Rotating-Disk/Stagnation-Flow Chemical Vapor Deposition Reactors*, Sandia National Laboratories Report SAND91-8003, 1991.

M. E. Coltrin, R. J. Kee, F. M. Rupley, and E. Meeks, *SURFACE CHEMKIN III: A Fortran Package for Analyzing Heterogeneous Chemical Kinetics at a Solid-Surface - Gas-Phase Interface*, Sandia National Laboratories Report SAND96-8217, 1996.

M. E. Coltrin and H. K. Moffat, *SURFTHERM: A Program to Analyze Thermochemical and Kinetic Data in Gas-phase and Surface Chemical Reaction Mechanisms*, Sandia National Laboratories Report SAND94-0219, 1994.

M. E. Coltrin, H. K. Moffat, R. J. Kee, and F. M. Rupley, *CRESLAF (Version 4.0): A Fortran Program for Modeling Laminar, Chemically Reacting, Boundary-Layer Flow in Cylindrical or Planar Channels*, Sandia National Laboratories Report SAND93-0478, 1993.

R. J. Kee, G. Dixon-Lewis, J. Warnatz, M. E. Coltrin, and J. A. Miller, *A Fortran Computer Code Package for the Evaluation of Gas-Phase Multicomponent Transport Properties*, Sandia National Laboratories Report SAND86-8246, (1986).

R. J. Kee, J. F. Grcar, M. D. Smooke, and J. A. Miller, *A Fortran Program for Modeling Steady Laminar One-Dimensional Premixed Flames*, Sandia National Laboratories Report SAND85-8240 (1985).

R. J. Kee, J. A. Miller, and T. H. Jefferson, *Chemkin: A General-Purpose, Problem-Independent, Transportable, Fortran Chemical Kinetics Code Package*, Sandia National Laboratories Report SAND80-8003, 1980.

R. J. Kee, F. M. Rupley, E. Meeks, and J. A. Miller, *Chemkin-III: A Fortran Chemical Kinetics Package for the Analysis of Gas-Phase Chemical and Plasma Kinetics*, Sandia National Laboratories Report SAND96-8216, 1996.

R. J. Kee, F. M. Rupley, and J. A. Miller, *Chemkin-II: A Fortran Chemical Kinetics Package for the Analysis of Gas-Phase Chemical Kinetics*, Sandia National Laboratories Report SAND89-8009, 1990.

R. J. Kee, F. M. Rupley, and J. A. Miller, *The Chemkin Thermodynamic Data Base*, Sandia National Laboratories Report SAND87-8215B, 1990.

R. S. Larson, *A Fortran Program for the Analysis of Plug Flow Reactors with Gas-Phase and Surface Chemistry*, Sandia National Laboratories Report SAND96-8211, 1996.

A. E. Lutz, R. J. Kee, J. F. Grcar, and F. M. Rupley, *OPPDIF: A Fortran Program for Computing Opposed-flow Diffusion Flames*, Sandia National Laboratories Report 96-8243, 1996.

A. E. Lutz, R. J. Kee, and J. A. Miller, *SENKIN: A Fortran Program for Predicting Homogeneous Gas Phase Chemical Kinetics with Sensitivity Analysis*, Sandia National Laboratories Report 87-8248, 1988.

E. Meeks, H. K. Moffat, J. F. Grcar, and R. J. Kee, *AURORA: A Fortran Program for Modeling Well Stirred Plasma and Thermal Reactors with Gas and Surface Reactions*, Sandia National Laboratories Report SAND96-8218, 1996.

R. E. Mitchell and R. J. Kee, *SHOCK: A General Purpose Computer Code for Predicting Chemical Kinetic Behavior Behind Incident and Reflected Shocks*, Sandia National Laboratories Report 82-8205, 1982.

W. C. Reynolds, *The Element Potential Method for Chemical Equilibrium Analysis: Implementation in the Interactive Program STANJAN*, Department of Mechanical Engineering, Stanford University (1986).

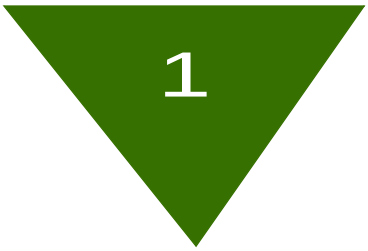

1 Introduction

Successful application of Chemkin to engineering and chemistry problems requires some basic understanding of the theory and formulations behind chemically reacting flow simulations. The *ANSYS Chemkin Theory Manual* provides a broad overview of the relationships and formulations used in calculations of chemical property and source terms. It also provides brief derivations and explanations of the governing equations solved by Chemkin Reactor Models, as well as a discussion of numerical solution techniques and sensitivity analysis employed in the models. In most cases these descriptions contain references to more rigorous treatments of the theoretical background that are available in the open literature. For further background information, we recommend a textbook written by several of ANSYS Chemkin's original authors: *Chemically Reacting Flow: Theory and Practice*.[1]

1.1 Chemistry—Species and Phases

Before discussion of the theoretical background for reacting-flow simulations, it is important to introduce the concepts of phases, and the species that reside in those phases and take part in the chemical reactions of the system. The Chemkin phase nomenclature builds from that of Eriksson,[2] but has been extended to account for surface sites. Currently, Chemkin defines three types of species: gas-phase, surface, and bulk. In the gas phase, a species is part of an ideal-gas mixture that may be flowing or stagnant. When reactive surfaces are present, the gas phase is considered to be "above" the surface. A bulk species is one that resides in a solid or condensed material, or "below" the surface. A surface species resides at the bulk-gas interface or is defined to be a chemical species on the top-most layer of a solid or condensed material. Each surface species occupies one or more "sites," where the total number

1. Robert J. Kee, Michael E. Coltrin, and Peter Glarborg, *Chemically Reacting Flow: Theory and Practice*, John Wiley and Sons, Hoboken, New Jersey (2003).
2. G. Eriksson, *Acta Chem. Scand.* **25**:2651 (1971).

of sites is usually conserved in the system. Only gas-phase species participate in gas-phase reactions, but all types of species may participate in heterogeneous gas-surface reactions. In writing elementary reactions for a surface mechanism in a kinetic model, mass, elemental composition, and charge must all be conserved.

In actuality there is no constraint that the surface must be only one atom thick. However, defining a “surface” that is several monolayers thick may be conceptually much more difficult to deal with.

Beyond the basic gas, surface, and bulk species, we also use the notion of different physical “phases” to group the chemical species in a problem. For example, there can be more than one type of site on the surface. This may be used to specify that a surface consists of “ledge” sites and “plane” sites, where the number of sites of each type might be a characteristic of the solid crystal face. Alternatively, a particular site type may consist of “active” sites vs. “non-active” sites, where different reaction rates are defined on each type. There can be any number of site types. The user may define a species that only resides on a certain type of site. For example, the thermodynamic properties of a hydrogen atom on a ledge site might be different from a hydrogen on a plane site, and they could be specified as different species (even though their elemental composition is the same). The population of different species occupying a given type of site is specified by site fractions. The sum of the site fractions of the species on a given site is 1. (Thus an “open site'' is considered as a distinct species.) This general formalism provides the user extensive flexibility in defining surface chemistry problems, whether they involve material deposition, surface catalysis, or simple radical recombination.

In the bulk there can also be different types of bulk species. The simplest bulk phase consists of a pure (single) species. There can be any number of pure bulk phases. It is also possible to specify a bulk mixture with components A and B, for example. The composition of the bulk phase may then be specified using the “activities” of each of the bulk-phase components.

For gas-phase and surface site species, the mole fractions of the species correspond directly to the species activities. In general this is not true for condensed-phase mixtures unless the bulk phase is either an ideal mixture or a pure bulk species.

When defining problems in Chemkin, a user may define a chemistry set that is gas-phase only. In all cases one or more gas-phase species must be defined, but problems may be defined that include no gas-phase reactions. When surface chemistry is included, it may include only surface species, only bulk species, or both surface site and bulk species. Reactions may involve any combination of species from different phases, as long as conservation rules are obeyed.

1.2 Species Indexing Conventions

Within Chemkin programs, information about a species (e.g., a thermodynamic property) is presumed to be available in ordered arrays beginning with the first gas-phase species. When surface chemistry is included, the species array continues from the last gas-phase species, through the surface species, and ending with the last bulk species. In the expressions and equations in this manual, we presume that there are a total of K species in the system. We use the index or subscript k to refer to a specific species in the array. There are K_g gas-phase species, which, by convention, are always the first entries in the species arrays. The index of the first gas-phase species is K_g^f ($K_g^f = 1$ by our convention) and the last gas-phase species index is K_g^l ($K_g^l = K_g$). Thus, the gas-phase species indices are $K_g^f \le k \le K_g^l$. In a similar way surface species indices are in the range $K_s^f \le k \le K_s^l$ and bulk species are in the range $K_b^f \le k \le K_b^l$. The surface species may be arranged on any number of sites, and the bulk species may exist in any number of bulk mixtures. Furthermore, many situations occur where there are no surface species and/or no bulk species.

As discussed in *Section 1.1*, the species are grouped in “phases.” The first (and often only) phase is the gas phase, whose index $n = 1$. When surface and/or bulk phases are considered, it is possible to have multiple surface site phases as well as multiple bulk (condensed) phases. In terms of indexing and nomenclature, the next N_s phases after the gas phase will be the surface sites, whose phase indices are bounded by $N_s^f \le n \le N_s^l$. The final N_b phases are the bulk mixtures, whose indices are bounded by $N_b^f \le n \le N_b^l$. In each phase n there are $K_{\text{phase}}(n)$ species, and those species have indices in the range $K_{\text{phase}}^f(n) \le k \le K_{\text{phase}}^l(n)$.

In most cases, users do not need to be concerned with the internal indexing of species within Chemkin. However, users who wish to create their own Chemkin-based programs will need to be aware of the use of species and phase arrays in passing information back and forth through the Chemkin/API. Also, these conventions are used extensively in the mathematical descriptions of our governing equations and rate formulations, so some familiarity is helpful in following the discussions here.

1.3 Footnote Notation

In this manual, footnotes can refer to a reference citation that originally occurred some distance previously in the chapter. In this case, you see a footnote that gives the footnote number and the page on which that footnote occurs:

Stewart, Larson, and Golden.[9, p. 48]

Means citation #9, occurring on page 48 in this manual.

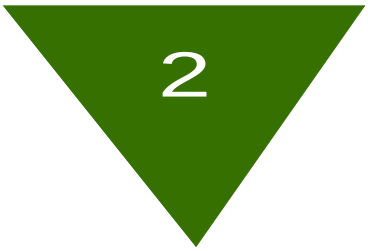

2 Thermodynamic Expressions

In defining the chemistry used in a Chemkin reactor simulation, users must first supply the thermodynamic data for each species in the chemical system. These data are in the form of polynomial fits to temperature, for species enthalpy, entropy, and specific heat capacity. Sources of this data, as well as the utility that generates the needed polynomial-fit parameters, are described in detail in the *Geting Started with ANSYS Chemkin*. Once these data are defined, they are used during a Chemkin simulation to determine species thermodynamic properties, thermal transport properties, and reaction equilibrium constants. This chapter describes the mathematical relationships, formulations, and conversions used in such calculations.

These formulas are used internally within Chemkin program executables. In addition, the CHEMKIN/API, allows users to call Chemkin subroutines to perform many of the calculations described within their own programs. Such calls can be made from a user's C, C++, or FORTRAN program or to create interfaces to 3rd-party programs. Details on the API for such calls are provided in the *ANSYS Chemkin Application Programming Interface Manual*. However, to aid in programming and formulation of a problem, the descriptions of formulas and conversions in the following section contain references to the CHEMKIN/API, giving the name of the subroutine that performs the particular calculation.

Species can exist in the gas phase, on surface sites, or in bulk mixtures. In some cases it is desirable to refer to information about species without regard to the phases, and in other cases it is desirable to determine information about species in one particular phase or group of phases. Therefore, before discussing surface state variables, it is helpful to first introduce a nomenclature that facilitates the mathematical expression of species information.

2.1 State Variables

The formulation of any chemically reacting-flow problem requires selection of a set of state variables. State variables define the thermodynamic and chemical state of the fluid mixture. When surface chemistry is considered, the state variables may also include the chemical state of a solid material and/or of the surface or interface between the fluid and the solid.

2.1.1 Gas-phase State Variables

In Chemkin, we allow the user to select either pressure or density, temperature(s), and either mass fraction, mole fraction, or molar concentration, to describe the state of a gas mixture. In other words, to define the state of a gas, one variable must be selected from each column of the array below.

$$\begin{bmatrix} P & T_k & Y_k \\ \rho & & X_k \\ & & [X_k] \end{bmatrix}$$

In making these options available from among the many possible, we provide combinations of variables that are natural ones for a wide class of chemically reacting-flow problems. For example, pressure is a natural choice in situations where pressure is fixed, and density is a natural variable where volume is fixed. Moreover, density is a natural variable in many problems involving fluid mechanics because it is determined directly from the mass continuity equation. Temperature is always taken as a natural variable because the thermodynamic properties and the chemical rate constants both depend directly on temperature. Mass fraction and mole fraction are convenient variables for describing the composition of a gas. Molar concentration ($[X_k]$, in moles/cm^3) is sometimes a convenient variable because the rate of progress of chemical reactions depends directly on the molar concentration of the reactants and products. In general, most Chemkin Reactor Models use species mass fractions to track variations in chemical composition, because of the direct relation to mass conservation principles. The formulas (and their related subroutines) in the following sections show the calculations necessary to convert between state variables, which are used in assembling reaction rates-of-production, thermodynamic properties, and other terms in the reactor governing equations.

2.1.2 Surface State Variables

On the surface sites or phases, we can describe the chemical state in terms of an array of surface species site fractions, Z_k. Surface site fractions are also often referred to as “site coverages.” Like gas-species fractions, surface site fractions become dependent variables in the chemically reacting-flow problem when multiple surface site species are included in the chemistry set.

The array of surface site fractions is of length K_s. It is composed of N_s sections containing the site fractions of each of the species on a given site (phase) n. The site fractions on each site are normalized, such that

Equation 2-1

$$\sum_{k=K_s^f(n)}^{K_s^l(n)} Z_k(n) = 1 \qquad (n = N_s^f, \ldots, N_s^l)$$

The sum in *Equation 2-1* runs from the first species in phase n to the last species in phase n. The surface molar concentration of a species is then

Equation 2-2

$$[X_k] = Z_k(n)\Gamma_n / \sigma_k(n)$$

where Γ_n is the density of sites of phase n (in moles/cm^2) and $\sigma_k(n)$ is the number of sites that each species k occupies. Note that *Equation 2-2* assumes that the surface site density is constant as a function of time. It is possible to override this requirement in the surface chemistry reaction set, in which case use of this equation should ensure that the correct value of $\Gamma_n(t)$ is used. Non-conservation of sites is discussed further in *Section 4.11*.

For the sake of parallelism, we adopt the nomenclature for bulk species:

Equation 2-3

$$[X_k] = a_k \qquad (k = K_b^f, \ldots, K_b^l)$$

SURFACE KINETICS takes the approach that the activity, a_k, of bulk species k is used in all chemical rate expressions. In the limiting case of an ideal solution, the activity of a species is equal to its mole fraction. However, SURFACE KINETICS does not explicitly evaluate the relationship between bulk mole fraction and the bulk activities. In most

existing Chemkin executables, ideal solutions are assumed when bulk mixtures are present, although it is recognized that this approximation is often not a good one. Typically bulk activities become dependent variables in the reacting-flow problem only if there are more than one bulk species in any one bulk phase.

2.2 Gas Equation of State and Conversion Formulas

The equation of state used throughout Chemkin is that of an ideal, multi-fluid gas. The multi-fluid gas formulation allows for a temperature to be specified for each species, T_k. This formulation collapses to the more usual thermal-equilibrium relation in the case where all species temperatures, T_k, are equal to the gas temperature. The general equation of state is given by:

Equation 2-4 CKPY, CKPX, CKPC

$$P = \sum_{k=1}^{K} [X_k] R T_k$$

while the mean mass density is defined by:

Equation 2-5 CKRHOY, CKRHOX, CKRHOC

$$\rho = \sum_{k=1}^{K} [X_k] W_k$$

The mean molecular weight may be defined variously as

Equation 2-6 CKMMWY

$$\overline{W} = \frac{1}{\sum_{k=1}^{K} Y_k / W_k}$$

or

Equation 2-7 CKMMWX

$$\overline{W} = \sum_{k=1}^{K} X_k W_k$$

or

Equation 2-8 CKMMWC

$$\overline{W} = \frac{\sum_{k=1}^{K} [X_k] W_k}{\sum_{k=1}^{K} [X_k]}$$

As stated above, It is often convenient to represent a gas-mixture species composition as either mass fraction, mole fraction, or molar concentration. The following sections contain the formulas used to convert between these different ways of describing the mixture composition.

2.2.1 Mass Fraction to Mole Fraction

Equation 2-9 CKYTX

$$X_k = \frac{Y_k}{W_k \sum_{j=1}^{K} Y_j / W_j} = \frac{Y_k \overline{W}}{W_k}$$

2.2.2 Mass Fraction to Molar Concentration

Equation 2-10 CKYTCP

$$[X_k] = \frac{P(Y_k / W_k)}{R \sum_{j=1}^{K} Y_j T_j / W_j}$$

Equation 2-11 CKYTCR

$$[X_k] = \rho \frac{Y_k}{W_k}$$

2.2.3 Mole Fraction to Mass Fraction

Equation 2-12 CKXTY

$$Y_k = \frac{X_k W_k}{\sum_{j=1}^{K} X_j W_j} = \frac{X_k W_k}{\overline{W}}$$

2.2.4 Mole Fraction to Molar Concentration

Equation 2-13 CKXTCP

$$[X_k] = X_k \frac{P}{R \sum X_k T_k}$$

Equation 2-14 CKXTCR

$$[X_k] = X_k \frac{\rho}{\overline{W}}$$

2.2.5 Molar Concentration to Mass Fraction

Equation 2-15 CKCTY

$$Y_k = \frac{[X_k]W_k}{\sum_{j=1}^{K}[X_j]W_j}$$

2.2.6 Molar Concentration to Mole Fraction

Equation 2-16 CKCTX

$$X_k = \frac{[X_k]}{\sum_{j=1}^{K}[X_j]}$$

2.3 Standard-state Thermodynamic Properties

Chemkin's GAS-PHASE and SURFACE KINETICS utilities presume that the standard-state thermodynamic properties of all species (regardless of phase) are functions of temperature only. For gas-phase species, this assumption corresponds to the gas being thermally "perfect". The temperature-dependent properties are input in the form of polynomial fits.

2.3.1 Specific Heat Capacity at Constant Pressure

Using arbitrary-order polynomial fits, the molar heat capacities at constant pressure are defined as:

Equation 2-17

$$\frac{C_{pk}^{o}}{R} = \sum_{m=1}^{M} a_{mk}T_k^{(m-1)}$$

The superscript ^{o} refers to the standard-state. For gas-phase species, the standard state is an ideal gas at 1 atmosphere. For perfect gases, however, the heat capacities are independent of pressure, and the standard-state values become the actual values.

For surface species the standard state of species k refers to the case of a chemical potential for a surface of pure species k (i.e., $Z_k \rightarrow 1$) with a fixed standard-state site density, Γ_n^o. Moreover, a perfect solution (i.e., non-interacting) is assumed for the surface phase, which is independent of the system pressure. Under these assumptions the chemical potential for surface species k on surface site n may be written as

Equation 2-18

$$\mu_k(T, P, Z) = \mu_k^o(T) + RT\ln(\Gamma_n Z_k / \Gamma_n^o)$$

The activity of a bulk species is defined in terms of the following equation for the chemical potential:

Equation 2-19

$$\mu_k(T, P, X) = \mu_k^o(T) + RT\ln(a_k(T, P, X))$$

where μ_k^o is the standard state chemical potential of species k at temperature T and at the standard pressure P, 1 atm, and a_k is the species activity. The vector X represents an array of the mole fractions of the species. Two conventions are normally used to complete the specification of the activity coefficient:

1. If the standard state is defined as a pure bulk phase of k at temperature T and 1 atm, then a_k is further defined to approach X_k as X_k approaches 1 at 1 atm (Raoult's Law).
2. If the standard state is defined as the hypothetical state of species k in infinite dilution in bulk-phase species j at temperature T and 1 atm, then is further defined to approach X_k as X_k approaches 0 at 1 atm (Henry's Law).

Both conventions for the standard state work with SURFACE KINETICS, as do any other definitions that conform to the formalism expressed by *Equation 2-19* for μ. $\mu_k^o(T)$ is specified through the entry for species k in the thermodynamics data file. The value of $a_k(T, P, X)$ is required as input to all SURFACE KINETICS subroutines that calculate bulk phase thermodynamic quantities and reaction rates. Therefore, if desired, advanced users can construct their own subroutines to calculate $a_k(T, P, X)$, possibly incorporating models for non-ideality of the bulk phase, and can have the consequences properly incorporated into the surface kinetics mechanism. Although the activities of all components of an ideal solution must sum to 1, this condition is not enforced in SURFACE KINETICS. (It is, however, enforced in many of the Chemkin program executables that employ SURFACE KINETICS.)

Other thermodynamic properties are given in terms of integrals of the molar heat capacities.

2.3.2 Species Molar Enthalpy

First, the standard-state molar enthalpy is given by

Equation 2-20

$$H_k^o = \int_0^{T_k} C_{pk}^o dT + H_k^o(0)$$

so that

Equation 2-21

$$\frac{H_k^o}{RT_k} = \sum_{m=1}^{M} \frac{a_{mk} T_k^{(m-1)}}{m} + \frac{a_{M+1,k}}{T_k}$$

where a_{mk} is the coefficients of the polynomial that fits the thermodynamic property (in this case, the enthalpy h) with units [1/K^{M-1}] and M is the total number of coefficients of the polynomial (7). The constant of integration, $a_{M+1,k}R$, is the standard heat of formation at 0 K. Normally, however, this constant is evaluated from knowledge of the standard heat of formation at 298 K, since the polynomial representations are usually not valid down to 0 K.

2.3.2.1 Surface-coverage Dependent Enthalpy for Surface Species

Within the thermodynamic data, it is possible to specify the enthalpy of surface species to be dependent on surface coverage of other species. This is an added functionality for addressing surface coverage dependencies, which allows for modification of heat of reaction and therefore reaction rate, based on local surface coverage calculated during a simulation. The theory is explained in *Section 4.5*. The implementation in Chemkin of the coverage-dependent enthalpy formulation was based on collaborative discussions with researchers at MIT,[3] where the need for this capability was defined for use in estimating thermodynamically consistent and reversible reaction rates for reactions of gas-phase species on metal catalysts.

3. Anantharaman, B., Green, W. H., and McRae, G. J., Chemical Engineering Department, Massachusetts Institute of Technology, personal communication, March 2005.

Coverage dependency is specified in the thermodynamic data using the HFCOV keyword. This option affects the chemisorption enthalpies. *Equation 2-22* relates the heat of formation of surface species at any coverage to the heat of formation at zero coverage. The coverage-dependent coefficient that is input to the model is c. The $H_j(\theta = 0)$ is calculated using *Equation 2-3* in the *ANSYS Chemkin Input Manual*.

Equation 2-22

$$H_j = H_j(\underline{\theta} = 0) + \sum_m c_{j,m}\,\theta_m$$

The coverage parameters also affect the activation energy of the reverse reaction. Chemkin calculates the reverse reaction rate constant using the equilibrium constant, and the enthalpy impacts the temperature-dependent equilibrium constant through the Gibbs free energy, as shown below.

Equation 2-23

$$k_{reverse} = \frac{k_{forward}}{K_{equilibrium}} = \frac{A_{forward}\,\exp\left(-E_{forward}/RT\right)}{\exp\left(-\left[\Delta H - T\Delta S\right]/RT\right)}$$

The reverse reaction activation energy thus has the following dependence on the coverage-dependent enthalpy.

$$E_r = E_f - \Delta H$$

HFCOV thus allows for a more complex impact of coverage dependence on the activation energies of surface reactions, especially since coverages will change during the course of the simulation. This option is particularly useful when using approaches such as Bond Order Conservation (BOC) (also known as Unity Bond Index-Quadratic Exponential Potential approach)[4].

For *j*th surface species, the coverage dependence on *m*th species is specified by $c_{j,m}$. Thermodynamic consistency is enforced in the coverage dependent coefficients for heats of formation in that the partial derivative of heat of formation of *j*th species with respect to the coverage of *m*th species is same as the partial derivative of heat of formation of the *m*th species with respect to the coverage of *j*th species:

4. Shustorovich, E., "The Bond-Order Conservation Approach to Chemisorption and Heterogeneous Catalysis: Applications and Implications", *Advances in Catalysis*, **37**, 101-163 (1990).

Equation 2-24

$$\frac{\partial H_j}{\partial \theta_m} = \frac{\partial H_m}{\partial \theta_j}$$

or

$$c_{j,m} = c_{m,j}$$

The coverage-dependent coefficients are typically estimated from experimental data on the heat of formation of surface species under various coverages of the same or other species, often measured by Temperature Programmed Desorption (TPD).

2.3.3 Species Molar Entropy

The standard-state molar entropy is written as

Equation 2-25

$$S_k^o = \int_{298}^{T_k} \frac{C_p^o k}{T} dT + S_k^o(0)$$

so that

Equation 2-26

$$\frac{S_k^o}{R} = a_{1k} \ln T_k + \sum_{m=2}^{M} \frac{a_{mk} T_k^{(m-1)}}{(m-1)} + a_{M+2,k}$$

where the constant of integration $a_{M+2,k}R$ is evaluated from knowledge of the standard-state entropy at 298 K.

2.3.4 Standard Form of Polynomial Fits

The above equations are stated for an arbitrary-order polynomial, but the GAS-PHASE KINETICS package is designed by default to work with thermodynamic data in the form used in the NASA chemical equilibrium code.[5] In this case, seven coefficients are needed for each of two temperature ranges. These fits take the following form, where the temperatures are in Kelvin:

5. S. Gordon and B. J. McBride, *Computer Program for Calculation of Complex Chemical Equilibrium Compositions, Rocket Performance, Incident and Reflected Shocks and Chapman-Jouguet Detonations*, NASA Report SP-273, 1971.

Equation 2-27 CKCPOR, SKCPOR

$$\frac{C_{pk}^o}{R} = a_{1k} + a_{2k}T_k + a_{3k}T_k^{\,2} + a_{4k}T_k^{\,3} + a_{5k}T_k^{\,4}$$

Equation 2-28 CKHORT, SKHORT

$$\frac{H_k^o}{RT_k} = a_{1k} + \frac{a_{2k}}{2}T_k + \frac{a_{3k}}{3}T_k^{\,2} + \frac{a_{4k}}{4}T_k^{\,3} + \frac{a_{5k}}{5}T_k^{\,4} + \frac{a_{6k}}{T_k}$$

Equation 2-29 CKSOR, SKSOR

$$\frac{S_k^o}{R} = a_{1k}\ln T_k + a_{2k}T_k + \frac{a_{3k}}{2}T_k^{\,2} + \frac{a_{4k}}{3}T_k^{\,3} + \frac{a_{5k}}{4}T_k^{\,4} + a_{7k}$$

The GAS-PHASE and SURFACE KINETICS Pre-processors allow for additional temperature ranges. Details of the thermodynamic data format options are included in *Chapter 2* of the *ANSYS Chemkin Input Manual*.

2.3.5 Other Species Molar Properties

Other thermodynamic properties are easily given in terms of C_p^o, H^o, and S^o.

For gas-phase only, the specific heat capacity at constant volume C_{vk}^o is:

Equation 2-30 CKCVML

$$C_{vk}^o = C_{pk}^o - R$$

For all phases, the internal energy U_k^o is

Equation 2-31 CKUML, SKHML

$$U_k^o = H_k^o - RT_k$$

The standard-state Gibb's free energy G_k^o is

Equation 2-32 CKGML, SKGML

$$G_k^o = H_k^o - T_k S_k^o$$

and the standard-state Helmholtz free energy A_k^o is

Equation 2-33 CKAML, SKAML

$$A_k^o = U_k^o - T_k S_k^o$$

2.3.6 Specific (Mass-based) Species Properties

Often, specific thermodynamic properties are needed in mass units (per gram) rather than in molar units (per mole). The conversion is made by dividing the property in molar units by the molecular weight. The specific properties are thus

Equation 2-34 CKCPMS, SKCPMS

$$c_{pk}^o = \frac{C_{pk}^o}{W_k}$$

Equation 2-35 CKHMS, SKHMS

$$h_k^o = \frac{H_k^o}{W_k}$$

Equation 2-36 CKSMS, SKSMS

$$s_k^o = \frac{S_k^o}{W_k}$$

Equation 2-37 CKCVMS

$$c_{vk}^o = \frac{C_{vk}^o}{W_k}$$

Equation 2-38 CKUMS, SKUMS

$$u_k^o = \frac{U_k^o}{W_k}$$

Equation 2-39 CKGMS, SKGMS

$$g_k^o = \frac{G_k^o}{W_k}$$

and

Equation 2-40 CKCAMS, SKAMS

$$a_k^o = \frac{A_k^o}{W_k}$$

2.3.7 Molar and Specific Properties of Gas Mixtures

One also often needs mixture-averaged thermodynamic properties. As with the pure-species properties, the GAS-PHASE KINETICS thermodynamics subroutines return properties in either mass or molar units. Since, for a perfect gas mixture, the standard-state specific heats, enthalpies, and internal energies are also the actual values, we drop the superscript ^{o} for these quantities.

The mixture-averaged specific heats are

Equation 2-41 CKCPBL

$$\overline{C}_p = \sum_{k=1}^{K} C_{pk} X_k$$

Equation 2-42 CKCPBS

$$\bar{c}_p = \sum_{k=1}^{K} c_{pk} Y_k = \overline{C}_p / \overline{W}$$

Equation 2-43 CKCVBL

$$\overline{C}_v = \sum_{k=1}^{K} C_{vk} X_k$$

and

Equation 2-44 CKCVBS

$$\bar{c}_v = \sum_{k=1}^{K} c_{vk} Y_k = \overline{C}_v / \overline{W}$$

the enthalpies are

Equation 2-45 CKHBML

$$\overline{H} = \sum_{k=1}^{K} H_k X_k$$

and

Equation 2-46 CKHBMS

$$\bar{h} = \sum_{k=1}^{K} h_k Y_k = \overline{H}/\overline{W}$$

and the internal energies are

Equation 2-47 CKUBML

$$\overline{U} = \sum_{k=1}^{K} U_k X_k$$

and

Equation 2-48 CKUBMS

$$\bar{u} = \sum_{k=1}^{K} u_k Y_k = \overline{U}/\overline{W}$$

The mixture properties are more complex for the entropies and the Gibb's and Helmholtz free energies. Here the actual values are not the same as the standard-state values and we must account for the appropriate pressure and entropy-of-mixing terms. The entropy is then

Equation 2-49

$$S_k = S_k^o - R\ln X_k - R\ln(P/P_{\text{atm}})$$

Thus the mixture-averaged entropies are

Equation 2-50 CKSBML

$$\bar{S} = \sum_{k=1}^{K} (S_k^o - R\ln X_k - R\ln(P/P_{\text{atm}}))X_k$$

and

Equation 2-51 CKSBMS

$$\bar{s} = \bar{S}/\overline{W}$$

Similarly, the mixture-averaged Gibb's and Helmholtz free energies are

Equation 2-52 CKGBML

$$\overline{G} = \sum_{k=1}^{K} [H_k - T_k(S_k^o - R\ln X_k - R\ln(P/P_{\text{atm}}))]X_k$$

Equation 2-53 CKGBMS

$$\bar{g} = \overline{G}/\overline{W}$$

Equation 2-54 CKABML

$$\overline{A} = \sum_{k=1}^{K} [U_k - T_k(S_k^o - R\ln X_k - R\ln(P/P_{\text{atm}}))]X_k$$

and

Equation 2-55 CKABMS

$$\bar{a} = \overline{A}/\overline{W}$$

2.3.8 Properties of Surface or Bulk Mixtures

At present, CHEMKIN/API does not provide routines to return mixture-averaged properties for surface- or bulk-phase species. In cases where such mixture properties are required within a Chemkin reactor model, the reactor model will compute them directly, in a manner appropriate to the application.

3

3 Gas-phase Chemical Rate Expressions

Gas-phase reactions describe interactions of gas-phase species. Each species in a reaction must be associated with thermodynamic data. The thermodynamic data are used to calculate equilibrium constants and reverse-rate coefficients for a reaction. In this way the chemical rate expressions build on the thermodynamic expressions discussed in the previous chapter. Chemkin provides the user with a wide array of options for expressing gas-phase chemical reactions, where reaction rates can depend on species composition, temperature, and pressure. While elementary reactions that obey the law of mass action are the default formulation, the user has available a variety of optional formulations for specifying global or lumped rate expressions. In this chapter, we begin here by describing the more common elementary-reaction relations and then discuss the exceptions and user options in subsequent sections.

3.1 Basic Rate Expressions

Consider elementary reversible (or irreversible) reactions involving K chemical species that can be represented in the general form

Equation 3-1

$$\sum_{k=1}^{K} \upsilon'_{ki} \chi_k \Leftrightarrow \sum_{k=1}^{K} \upsilon''_{ki} \chi_k \qquad (i = 1,\ldots, I)$$

The stoichiometric coefficients υ_{ki} are integer numbers and χ_k is the chemical symbol for the *k*th species. The superscript $'$ indicates forward stoichiometric coefficients, while $''$ indicates reverse stoichiometric coefficients. Normally, an elementary reaction involves only three or four species; hence the υ_{ki} matrix is quite sparse for a large set of reactions. For non-elementary reactions, *Equation 3-1* also represents the reaction expression, but the stoichiometric coefficients may be non-integers.

Global reactions are sometimes stated with non-integer stoichiometric coefficients. Chemkin can accommodate non-integer stoichiometric coefficients.

The production rate $\dot{\omega}_k$ of the *k*th species can be written as a summation of the rate-of-progress variables for all reactions involving the *k*th species

Equation 3-2 CKWYP, CKWYR, CKWXP, CKWXR, CKWC, CKCONT

$$\dot{\omega}_k = \sum_{i=1}^{I} \upsilon_{ki} q_i \qquad (k = 1,\ldots, K)$$

where

Equation 3-3 CKNU

$$\upsilon_{ki} = \upsilon''_{ki} - \upsilon'_{ki}$$

The rate of progress variable q_i for the *i*th reaction is given by the difference of the forward and reverse rates as

Equation 3-4 CKQYP, CKQYR, CKQXP, CKQXR, CKQC, CKCONT, SKROP

$$q_i = k_{fi} \prod_{k=1}^{K} [X_k]^{\upsilon'_{ki}} - k_{ri} \prod_{k=1}^{K} [X_k]^{\upsilon''_{ki}}$$

where X_k is the molar concentration of the *k*th species and k_{fi} and k_{ri} are the forward and reverse rate constants of the *i*th reaction. As indicated in *Equation 3-4*, the rate-of-progress of a reaction is evaluated, by default, using the concentration of each reactant or product species raised to the power of its stoichiometric coefficient. Thus, the rate-of-progress of a reaction that includes species A with a coefficient of 2 will be second-order with respect to the concentration of A. *Equation 3-4* is always valid when mass-action kinetics are obeyed, and when the mechanism is written in

terms of elementary reactions. As it is often useful to work with reduced chemistry, GAS-PHASE KINETICS includes an option allowing the user to define an arbitrary reaction order for a species in place of the coefficients used in *Equation 3-4*. This option is described further below.

The forward rate constants for the I reactions are generally assumed to have the following Arrhenius temperature dependence:

Equation 3-5 CKABE, SKABE, SKRAEX

$$k_{fi} = A_i T^{\beta_i} \exp\left(\frac{-E_i}{R_c T}\right)$$

where the pre-exponential factor A_i, the temperature exponent β_i, and the activation energy E_i are specified. These three parameters are required input to the GAS-PHASE KINETICS package for each reaction.

Two gas constants, R and R_c are used throughout this chapter and within Chemkin programs. R_c is used only in conjunction with the activation energy E_i and has compatible units. The reason for the duality is that many users would rather use units of cal/mole for the activation energies even though other energy units are used elsewhere.

In *Equation 3-5* through *Equation 3-10*, T refers to the gas temperature, unless auxiliary reaction information is provided to indicate that the reaction depends on a temperature associated with a particular species. Such information would be specified using the auxiliary keyword, `TDEP`, which is described further in *Table 3-6* of the *ANSYS Chemkin Input Manual*. In the case where the `TDEP` keyword is included for reaction i, T represents the temperature of the species whose name follows the `TDEP` keyword.

In thermal systems, the reverse rate constants k_{ri} are related to the forward rate constants through the equilibrium constants by

Equation 3-6

$$k_{ri} = \frac{k_{fi}}{K_{ci}}$$

Although K_{ci} is given in concentration units, the equilibrium constants are more easily determined from the thermodynamic properties in pressure units; they are related by

Equation 3-7 CKEQYP, CKEQYR, CKEQXP, CKEQXR, CKEQC

$$K_{ci} = K_{pi}\left(\frac{P_{\text{atm}}}{RT}\right)^{\sum_{k=1}^{K}\upsilon_{ki}}$$

The equilibrium constants K_{pi} are obtained with the relationship

Equation 3-8

$$K_{pi} = \exp\left(\frac{\Delta S_i^o}{R} - \frac{\Delta H_i^o}{RT}\right)$$

The Δ refers to the change that occurs in passing completely from reactants to products in the *i* th reaction; specifically,

Equation 3-9

$$\frac{\Delta S_i^o}{R} = \sum_{k=1}^{K}\upsilon_{ki}\frac{S_k^o}{R}$$

Equation 3-10

$$\frac{\Delta H_i^o}{RT} = \sum_{k=1}^{K}\upsilon_{ki}\frac{H_k^0}{RT}$$

For reactions involving electrons, the use of equilibrium constants to determine reverse rates is usually not appropriate. In some cases, detailed balancing on electron-driven reactions can be applied using the Saha equation (see, for example, Mitchner and Kruger[6]) that relates the ionization and electron-third-body recombination reactions to the species partition functions. While such relations can be used to calculate explicitly reverse rates from forward rates, they are not part of the built-in features of GAS-PHASE KINETICS. To avoid erroneous results, it is therefore required that all reactions involving electron species must either be specified as forward reactions only, or must include the reverse rate parameters explicitly stated using auxiliary keywords. The specification of reverse-rate parameters is described in more detail in the REV entry in *Table 3-6* of the *ANSYS Chemkin Input Manual*).

6. M. Mitchner and J. Charles H. Kruger, *Partially Ionized Gases*, John Wiley & Sons, New York, 1973.

3.2 Non-integer Stoichiometric Coefficients

Early versions of Chemkin allowed only integer stoichiometric coefficients. This was based upon the assumption that kinetic mechanisms would deal with elementary chemical reactions, for which it makes little sense to talk about a fraction of a molecule participating as a product or reactant. However, in many real-world applications the elementary reactions are not known. Instead, the kinetics may only be summarized in terms of global expressions. GAS-PHASE KINETICS and SURFACE KINETICS therefore allow use of non-integer stoichiometric coefficients. Examples of reactions with such non-integer coefficients are

Equation 3-11

$$\mathrm{H(s)} \leftrightarrow 0.5\mathrm{H_2(g)}$$

and

Equation 3-12

$$\mathrm{C_2H_6} \leftrightarrow 0.72\mathrm{C_2H_4} + 0.56\mathrm{H} + 0.28\mathrm{CH_4} + 0.28\mathrm{CH_2}$$

The rate-of-progress of a reaction is, by default, still evaluated via *Equation 3-4*, with the coefficients υ'_{ki} and υ''_{ki} defined as real numbers instead of integers. The GAS-PHASE KINETICS and SURFACE KINETICS Pre-processors automatically allow real coefficients for reactions without requiring any special flags or keywords. An executable can call subroutine SKIRNU to find out which reactions were declared to the Pre-processor with real coefficients, and get arrays of the coefficients.

3.3 Reactions with Arbitrary Reaction Order

By default, the rate-of-progress of a reaction is evaluated by *Equation 3-4*, which uses the concentration of each reactant or product species raised to the power of its stoichiometric coefficient. Thus, the rate-of-progress of a reaction that includes species A with a coefficient of 2 will be second-order with respect to the concentration of A. *Equation 3-4* would always be valid when mass-action kinetics are obeyed, and the mechanism is written in terms of elementary reactions.

Often, these elementary assumptions do not apply to the global reactions of interest. For example, an experimental measurement may show that the rate of reaction is proportional to the concentration of a species raised to an arbitrary power (different from its stoichiometric coefficient). In such cases, Chemkin allows the user to declare that the rate-of-progress of a reaction is proportional to the concentration of any species (regardless of whether that species even appears as a reactant or a product

in the reaction) raised to any specified power. To modify the reaction order for the reaction in the forward or reverse direction, the user must declare the FORD or RORD auxiliary keywords, respectively, in the Pre-processor input file. These keywords are discussed in *Table 3-6* of the *ANSYS Chemkin Input Manual*. These options are available both for gas-phase and surface reactions.

When the order-dependence of reaction i is changed via the FORD or RORD keywords, the rate-of-progress variable q_i for the reaction is evaluated by

Equation 3-13

$$q_i = k_{fi} \prod_{k=1}^{K} [X_k]^{F_{ki}} - k_{ri} \prod_{k=1}^{K} [X_k]^{R_{ki}}$$

where F_{ki} is the reaction order specified through the FORD keyword and R_{ki} is the reaction order specified through the RORD keyword for species k. The default for species participating in reaction i is the normal mass-action kinetics values

Equation 3-14

$$F_{ki} = \upsilon'_{ki}$$

and

Equation 3-15

$$R_{ki} = \upsilon''_{ki}$$

if an order-change parameter is not given for species k.

The user should exercise caution when specifying a change of reaction order, as such a change may produce unexpected and unphysical results in a kinetic simulation. For example, the user should consider the kinetics of the reverse reaction when changing reaction-orders for the forward reaction. Such a reaction may no longer satisfy microscopic reversibility. At equilibrium, elementary kinetics ensure that

Equation 3-16

$$k_{ri}/k_{fi} = \prod_{k=1}^{K} [X_k]^{\upsilon'_{ki}} / \prod_{k=1}^{K} [X_k]^{\upsilon''_{ki}} = \prod_{k=1}^{K} [X_k]^{\upsilon'_{ki} - \upsilon''_{ki}}$$

A reaction for which one has specified a change in reaction order will not have the proper equilibrium behavior unless

Equation 3-17

$$F_{ki} - R_{ki} = \upsilon'_{ki} - \upsilon''_{ki} \qquad (k = 1,\ldots, K)$$

The user specifying F_{ki} may also wish to adjust R_{ki} such that *Equation 3-17* is satisfied; GAS-PHASE KINETICS does not do this automatically. Another alternative would be to simply specify that the reaction is irreversible. A user program can call subroutine `CKIORD` for gas-phase reactions and `SKIORD` for surface reactions, to determine if a reaction has user-specified orders and the values of those parameters.

3.4 Three-body Reactions

In some reactions a “third body” is required for the reaction to proceed; this is often the case in dissociation or recombination reactions, such as

$H + O_2 + M \Leftrightarrow HO_2 + M$

When a third body is needed, the concentration of the effective third body must appear in the expression for the rate-of-progress variable. Accordingly, the rate-of-progress variable is different from *Equation 3-4* by the first factor in the equation

Equation 3-18 CKQYP, CKQYR, CKQXP, CKQXR, CKQC, CKTHB

$$q_i = \left(\sum_{k=1}^{K} (a_{ki})[X_k] \right) \left(k_{fi} \prod_{k=1}^{K} [X_k]^{\upsilon'_{ki}} - k_{ri} \prod_{k=1}^{K} [X_k]^{\upsilon''_{ki}} \right)$$

If all species in the mixture contribute equally as third bodies, then $a_{ki} = 1$ for all k, and the first factor is the total concentration of the mixture,

Equation 3-19

$$[M] = \sum_{k=1}^{K} [X_k]$$

However, it is often the case that some species act more efficiently as third bodies than do others. The a_{ki} that differ from 1 must be specified by auxiliary input to the GAS-PHASE KINETICS Pre-processor, as described in *Section 3.5.3.1* of the *ANSYS Chemkin Input Manual*.

3.5 Collision Frequency Efficiency Expression

Making some simple assumptions about spherical collisions leads to the bi-molecular collision rate:

Equation 3-20

$$Z_{AB} = c_A c_B N_{Av} d^2 \sqrt{\frac{8\pi RT}{W_{AB}}}$$

Where N_{Av} is Avogadro's constant, d is the average diameter of the two spherical particles, R is the universal gas constant, T is temperature, W_{AB} is the reduced molar mass of the two species, and c_X is the concentration of the species X.

This expression is the theoretical limit that two spherical entities A and B collide. Using this as a basis for chemical kinetic rates, a formulation for a reaction rate constant is derived.

Equation 3-21

$$k_{fi} = \gamma_i N_{Av} d^2 \sqrt{\frac{8\pi RT}{W_{AB}}}$$

The new term γ_i is a correction factor, sometimes called the probability factor or the steric factor. This factor encompasses the probability of a bimolecular collision leading to reaction, and for Chemkin the factor is expressed in Arrhenius form.

Equation 3-22

$$\gamma_i = \min\left[1, a_i T^{b_i} \exp\left(\frac{-c_i}{R_c T}\right)\right]$$

This expression limits the probability factor to be less than or equal to one. A probability factor of unity means that every collision leads to reaction, which is valid for many radical-radical recombination reactions, but represents an upper limit for other bimolecular reactions.

3.6 Pressure-dependent Reactions

Under certain conditions, some reaction rate expressions depend on pressure as well as temperature. GAS-PHASE KINETICS provides for two kinds of such reactions: unimolecular/recombination fall-off reactions and chemically activated bimolecular reactions. Generally speaking, the rate for unimolecular/recombination fall-off

reactions increases with increasing pressure, while the rate for chemically activated bimolecular reactions decreases with increasing pressure. In both cases, GAS-PHASE KINETICS makes available various expressions that blend smoothly between high- and low-pressure limiting rate expressions.

ANSYS Chemkin makes the selection of pressure-dependent rate formulation equation based only on whether the LOW or HIGH keyword is specified in the auxiliary input for the rate coefficients. When LOW is specified, the coefficients given on the reaction line are assumed to represent the high-pressure limit and the pressure-falloff formulation is used. When HIGH is specified, the coefficients given on the reaction line are assumed to represent the low-pressure limit and the chemically activated reaction formulation is used.

3.6.1 Unimolecular/Recombination Fall-off Reactions

As an example of a unimolecular/recombination fall-off reaction, consider methyl recombination. In the high-pressure limit, the appropriate description of the reaction is $CH_3 + CH_3 \Leftrightarrow C_2H_6$. In the low-pressure limit, a third-body collision is required to provide the energy necessary for the reaction to proceed, i.e., the appropriate description is $CH_3 + CH_3 + M \Leftrightarrow C_2H_6 + M$. When such a reaction is at either limit, the (solely temperature-dependent) rate expressions discussed in the preceding paragraphs are applicable. However, when the pressure and temperature are such that the reaction is between the limits, the rate expressions are more complicated. To denote a reaction that is in this “fall-off” region, we write the reaction with the positive + M enclosed in parentheses,

$$\mathbf{CH_3 + CH_3(+ M) \Leftrightarrow C_2H_6(+ M)}$$

There are several methods of representing the rate expressions in this fall-off region. The simplest one is due to Lindemann.[7] There are also now two other (and related) methods that provide a more accurate description of the fall-off region than does the simple Lindemann form. The GAS-PHASE KINETICS package handles all three of these forms as options.

We begin with the Lindemann approach. Arrhenius rate parameters are required for both the high- and low-pressure limiting cases, and the Lindemann form for the rate coefficient relates them in a pressure-dependent rate expression. In Arrhenius form, the parameters are given for the high-pressure limit k_∞ and the low-pressure limit k_0 as follows:

7. F. Lindemann, *Trans. Faraday Soc.***17**:598 (1922).

Equation 3-23

$$k_0 = A_0 T^{\beta_0} \exp(-E_0 / R_c T)$$

Equation 3-24

$$k_\infty = A_\infty T^{\beta_\infty} \exp(-E_\infty / R_c T)$$

The rate constant at any pressure is then taken to be

Equation 3-25

$$k = k_\infty \left(\frac{P_r}{1 + P_r} \right) F$$

where the reduced pressure P_r is given by

Equation 3-26

$$P_r = \frac{k_0 [M]}{k_\infty}$$

and $[M]$ is the concentration of the mixture, possibly including enhanced third-body efficiencies.

It is also possible that the third body in the fall-off region could be a specific species rather than the mixture as a whole. In such a case, the reaction could be written, for example, as $CH_3 + CH_3 (+N_2) \Leftrightarrow C_2H_6 (+N_2)$. In this case, the concentration of Nitrogen $[N_2]$ would replace the total concentration in the mixture $[M]$ in these equations.

For this example, note that the units for k are 1/sec, k_0 are cm^6/(mole^2 • sec^2), and k_∞ are cm^3/(mole • sec). If the F in *Equation 3-10* is unity, then this is the Lindemann form. The other descriptions involve more complex expressions for the function F.

In the Troe form,[8] F is given by

Equation 3-27

$$\log F = \left[1 + \left[\frac{\log P_r + c}{n - d(\log P_r + c)} \right]^2 \right]^{-1} \log F_{\text{cent}}$$

The constants in *Equation 3-27* are

8. R. G. Gilbert, K. Luther, and J. Troe, *Ber. Bunsenges. Phys. Chem.* **87**:169 (1983).

Equation 3-28

$$c = -0.4 - 0.67 \log F_{\text{cent}}$$

Equation 3-29

$$n = 0.75 - 1.27 \log F_{\text{cent}}$$

Equation 3-30

$$d = 0.14$$

and

Equation 3-31

$$F_{\text{cent}} = (1 - \alpha)\exp(-T/T^{***}) + \alpha\exp(-T/T^{*}) + \exp(-T^{**}/T)$$

The four parameters α, T^{***}, T^{*}, and T^{**} must be specified as auxiliary input to the GAS-PHASE KINETICS Pre-processor, as described in Neutral Third Body and Pressure Dependent Parameters (*Section 3.5.3.1* of the *ANSYS Chemkin Input Manual*). It is often the case that the parameter T^{**} is not used. Thus GAS-PHASE KINETICS provides for the use of either three or four parameters.

The approach taken at SRI International by Stewart, et al.[9] is in many ways similar to that taken by Troe, but the blending function F is approximated differently. Here, F is given by

Equation 3-32

$$F = d\left[a\exp\left(\frac{-b}{T}\right) + \exp\left(\frac{-T}{c}\right)\right]^X T^e$$

where

Equation 3-33

$$X = \frac{1}{1 + (\log P_r)^2}$$

In addition to the six Arrhenius parameters—three each for the low-pressure limit k_0 and high-pressure limit k_∞ expressions—the user must supply the parameters a, b, and c in the F expression. The parameters d and e were not discussed by Stewart, et al., but we have included them as additional optional parameters to increase flexibility. If one wishes, d and e can be considered parameters that define a weak-collision efficiency factor, in the event that one wants to compute strong-collision rate parameters and correct them with such a factor.

Figure 3-1 Rate constant as a function of pressure at fixed temperature for a unimolecular fall-off reaction

The Troe and Lindemann forms are illustrated as are the low- and high-pressure limiting forms.

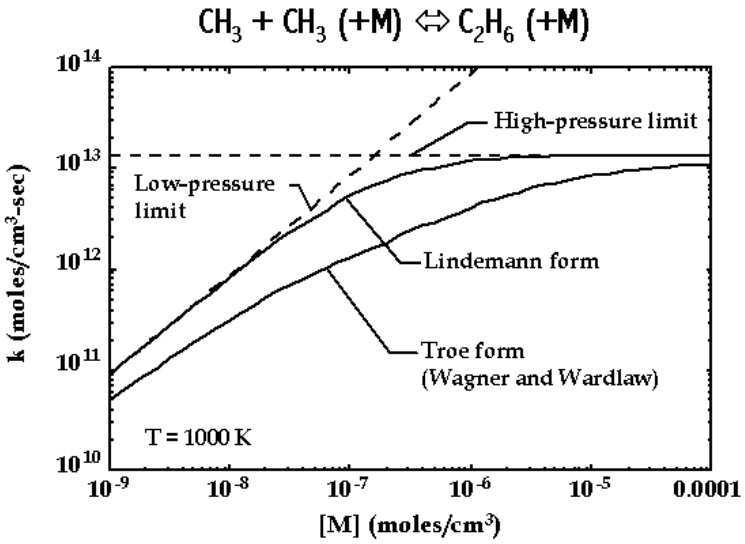

9. P. H. Stewart, C. W. Larson, and D. M. Golden, *Combustion and Flame* **75**:25 (1989).

Figure 3-1 illustrates the pressure dependence of rate expressions for the example reaction, $CH_3 + CH_3(+ M) \Leftrightarrow C_2H_6(+ M)$, evaluated at a fixed temperature of 1000 K. Both the Lindemann and the Troe forms are shown, as well as the low- and high-pressure limits. The specific constants in fits to the Troe form ($A_0 = 1.135\text{E}36$, $\beta_0 = -5.246$, $E_0 = 1704.8\text{cal/mole}$, $A_\infty = 6.22\text{E}16$, $\beta_\infty - 1.174$, $E_\infty = 653.8\text{cal/mole}$, $\alpha = 0.405$, $T^{***} = 1120\text{K}$, $T^{*} = 69.6\text{K}$) are taken from Wagner and Wardlaw.[10] For the relatively simple Lindemann case ($F = 1$), the limiting behavior is apparent. In the low-pressure limit, $[\text{M}] \to 0$, the denominator in *Equation 3-25* approaches unity and the rate expression becomes $k \to k_0[\text{M}]$. In the high-pressure limit, $[\text{M}] \to \infty$, the pressure-ratio factor approaches one, and the rate expression becomes $k \to k_\infty$, i.e., a constant. For both the Troe and SRI forms, F approaches unity for both high and low pressures. Thus, all expressions recover the correct limiting behavior.

3.6.2 Chemically Activated Bimolecular Reactions

As an example of a chemically activated bimolecular reaction, consider the reaction $CH_3 + CH_3(+ M) \Leftrightarrow C_2H_5 + H(+ M)$. This reaction, which is endothermic, occurs through the same chemically activated C_2H_6* adduct as does the recombination reaction $CH_3 + CH_3(+ M) \Leftrightarrow C_2H_6(+ M)$. *Figure 3-2* helps to illustrate the competition between these alternative channels using a reaction-energy diagram. As the pressure increases, deactivating collisions of C_2H_6* with other molecules cause the rate coefficient for C_2H_6 formation to increase. At the same time, these deactivating collisions preclude the dissociation of C_2H_6* into $C_2H_5 + H$, thus causing this rate coefficient to decrease with increasing pressure.

We assume the rate coefficient for a chemically activated bimolecular reaction to be described by the following function:

Equation 3-34

$$k = k_0\left(\frac{1}{1+P_r}\right)F$$

where $1/(1+P_r)$ is analogous to the Lindemann form of *Equation 3-25*. Note that in *Equation 3-34*, k_0 is the pressure-independent factor, whereas in *Equation 3-25* it is k_∞. The three choices for the F function are exactly the same as for the unimolecular fall-off reactions, i.e., the Lindemann ($F = 1$), Troe, or SRI forms.

10. A. F. Wagner and D. M. Wardlaw, *Journal of Physical Chemistry* **92**:2462 (1988).

Figure 3-2 Energy versus reaction coordinate diagram

Energy versus reaction coordinate diagram that illustrates the competition between a three-body recombination reaction,

$CH_3 + CH_3(+ M) \Leftrightarrow C_2H_6(+ M)$

and a chemically activated bimolecular reaction

$CH_3 + CH_3(+ M) \Leftrightarrow C_2H_5 + H(+ M)$

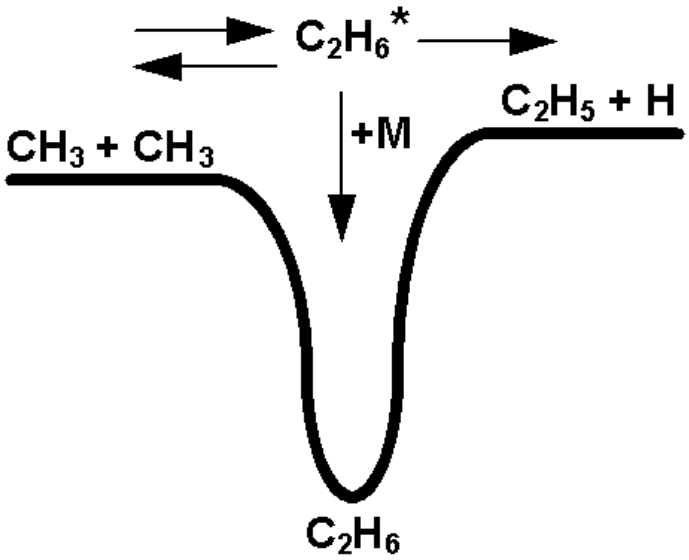

Figure 3-3 illustrates the rate-expression behavior for the example chemically activated reaction, $CH_3 + CH_3(+ M) \Leftrightarrow C_2H_5 + H(+ M)$. Both the Lindemann and the SRI formulations are shown, as well as the high- and low-pressure limiting cases. The specific constants for the SRI form ($A_0 = 10^{12.698}$, $\beta_0 = 0.0099$, $E_0 = 10600\,\mathrm{cal/mole}$, $A_\infty = 10^{-6.42}$, $\beta_\infty = 4.838$, $E_\infty = 7710\,\mathrm{cal/mole}$, $a = 1641$, $b = 4334$, $c = 2725$) are taken from Stewart, Larson, and Golden.[9, p. 48] For this example, note that the units for k are cm^3/(mole • sec), k_0 are cm^3/(mole • sec), and k_∞ are 1/sec. The limiting cases are recognized easily from the behavior of *Equation 3-34*. In the low-pressure limit, $[\mathrm{M}] \to 0$, $P_r \ll 1$, causing the pressure-ratio factor in *Equation 3-34* to approach unity. Hence, $k \to k_0$, i.e., a pressure-independent function. In the high-pressure limit, $[\mathrm{M}] \to \infty$, $P_r \gg 1$ and $k \to k_0/P_r \gg k_\infty/[\mathrm{M}]$.

Figure 3-3 Rate constant as a function of pressure at fixed temperature for a chemically activated reaction

The SRI and Lindemann forms are illustrated as are the low- and high-pressure limiting forms

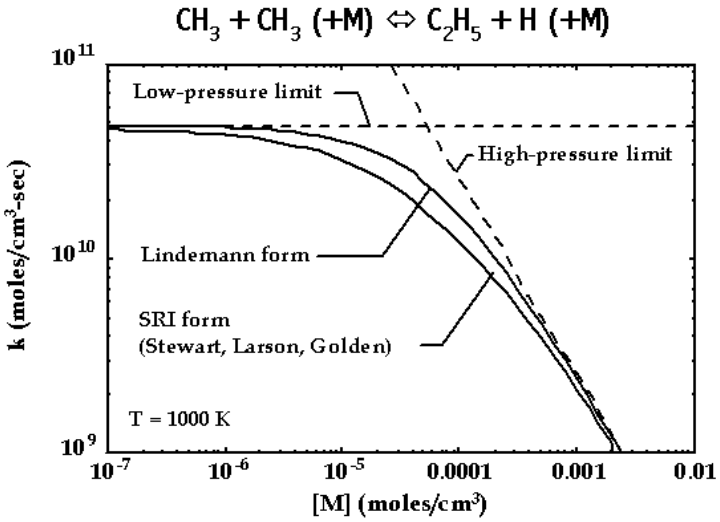

3.6.3 General Pressure Dependence Using Logarithmic Interpolation

"In the discussions and equations in this manual, "log" means $\log_{10}$, and "ln" means "natural logarithm".

Miller and Lutz[11] developed a generalized method for describing the pressure dependence of a reaction rate based on direct interpolation of reaction rates specified at individual pressures. In this formulation, the reaction rate is described in terms of the standard modified Arrhenius rate parameters. Different rate parameters are given for discrete pressures within the pressure range of interest. When the actual reaction rate is computed, the rate parameters will be determined through logarithmic interpolation of the specified rate constants, at the current pressure from the simulation. This approach provides a very straight-forward way for users to include rate data from more than one pressure regime.

For a given reaction, then, the user would supply rate parameters $k(T, P_j) = A_j T^{\beta_j} \exp(E_j / R_c T)$ for a set of P_j pressures. The set of pressure points for which rate parameters are specified must include at least two different pressures. If the rate at a given pressure cannot be described by a single set of Arrhenius parameters, more than one set may be provided. In such cases, the reaction rates will be treated in a similar manner as for `DUPLICATE` reactions, meaning that Chemkin will use the sum of the sets of rates provided for the given pressure.

11. J. A. Miller and A. E. Lutz, personal communication, August 2003.

During a simulation, if the current pressure is within 1% of one of the pressures for which rate constants were provided, then that set of rate parameters will be used directly. However, If the current pressure is in between the pressure points provided, then the rate will be obtained by a linear interpolation of $\ln k$ as a function of $\ln P$ (natural logarithms). For P between P_i and P_{i+1}, k is obtained using *Equation 3-35*.

Equation 3-35

$$\ln k = \ln k_i + (\ln k_{i+l} - \ln k_i)\frac{\ln P - \ln P_i}{\ln P_{i+l} - \ln P_i}$$

If the rate of the reaction is desired for a pressure lower than any of those provided, the rate parameters provided for the lowest pressure are used. Likewise, if rate of the reaction is desired for a pressure higher than any of those provided, the rate parameters provided for the highest pressure are used.

This logarithmic interpolation method can be used as an alternative approach to describing any type of pressure dependence, including the multiple-well, multiple-channel reactions discussed in *Section 3.6.4*. It has the advantage of being conceptually straightforward to implement. However, the resolution or accuracy of the pressure dependence will depend on the number of pressure points included for each reaction.

3.6.4 Multiple-well Multiple-channel Reactions Using Chebyshev Polynomials

An example of the multiple-well, multiple-channel chemically activated reaction is the reaction of the ethyl radical with oxygen, $C_2H_5 + O_2$. This chemically activated reaction occurs through three wells. The initial well corresponds to the chemically activated molecule CH_3CH_2OO formed by the radical addition process via a loose transition state. This activated molecule can further isomerize to the hydroperoxy radicals CH_2CH_2OOH and CH_2CHOOH leading to different products.[12] The Lindemann based methods described in the previous sections, i.e., the Lindemann, Troe, and SRI forms, although accurate for representing the falloff behavior of single-well reactions, do not apply well to multiple-well reactions.[13] A method based on the Chebyshev expansions are proposed by Venkatesh, et al.[13, p. 52] for approximating the pressure and temperature-dependent behavior of multiple-well reactions. The Chebyshev expansions provide accurate approximations over any given temperature and pressure domain for single- and multiple-well reactions. However, these approximates should not be used for extrapolative studies outside their defined domain.

12. P. K. Venkatesh, *J Phys. Chem. A* **104(2)**:280-287 (2000).
13. P. K. Venkatesh, A.Y. Chang, A.M. Dean, M. H. Cohen and R.W. Carr, J. *AIChE* **43**:1331-1340 (1997).

The implementation of pressure-dependent reaction rates through the use of Chebyshev polynomials is based on the work of Jeff Ing, Chad Sheng, and Joseph W. Bozzelli at the New Jersey Institute of Technology.[14]

Instead of using the modified Arrhenius form for the rate coefficient, the Chebyshev expansions approximate the logarithm of the rate coefficient directly as a truncated bivariate Chebyshev series in the reverse temperature and logarithm of the pressure. Since the Chebyshev polynomials are only defined in the interval of [-1, +1], the temperature and pressure boundaries for the approximation must be established first, i.e.,

$$T_{\min} \le T \le T_{\max}$$

and

$$P_{\min} \le P \le P_{\max}$$

The $T - P$ domain is then mapped onto a square bounded by ±1 using the transformations[15]

Equation 3-36

$$\tilde{T} = \frac{2T^{-1} - T_{\min}^{-1} - T_{\max}^{-1}}{T_{\max}^{-1} - T_{\min}^{-1}}$$

and

Equation 3-37

$$\tilde{P} = \frac{2\log P - \log P_{\min} - \log P_{\max}}{\log P_{\max} - \log P_{\min}}$$

The logarithm of the rate coefficient is approximated by the Chebyshev expansions as

14. Jeff Ing, Chad Sheng, and Joseph W. Bozzelli, personal communication, 2002.
15. *Equation 3-36* is the form implemented in Chemkin, which is based on the original work at the New Jersey Institute of Technology, and does not reproduce an error from the journal articles cited earlier (**12**, **13**).

Equation 3-38

$$\log k(\tilde{T},\tilde{P}) \approx \sum_{n=1}^{N} \sum_{m=1}^{M} a_{nm} \varphi_n(\tilde{T}) \varphi_m(\tilde{P})$$

where the Chebyshev polynomials of the first kind of degree $n-1$ are given by

Equation 3-39

$$\varphi(x) = \cos((n-1)\cos^{-1}(x)) \qquad n = 1, 2, \ldots$$

with $-1 \le x \le +1$. The integers N and M denote the number of basis functions along the temperature and the pressure axis, respectively. The accuracy of the approximates will increase monotonically with N and M. The $\mathrm{N} \times \mathrm{M}$ coefficients, a_{nm}, of the Chebyshev expansions are determined from a least-squares fit to a set of rate coefficient data points, $k(\tilde{T},\tilde{P})$, computed from a detailed theory such as the Rice-Ramsperger-Kassel-Marcus (RRKM) theory. To ensure the approximation is uniform over the desired domain, the computed rate coefficient data must be on the Gauss-Chebyshev grid. For example, if the computed rate coefficient data is on a Gauss-Chebyshev grid, its coordinates, $\tilde{T}_i$ and $\tilde{P}_j$, must be the roots of a high-order Chebyshev polynomial of the first kind given by

Equation 3-40

$$\tilde{T}_i = \cos\left(\frac{2i-1}{2d_T}\pi\right)$$

Equation 3-41

$$\tilde{P}_j = \cos\left(\frac{2j-1}{2d_P}\pi\right)$$

where $1 \le i \le d_T$ and $1 \le j \le d_P$. The integers d_T and d_P are the resolutions of the computed rate coefficient data in the temperature and the pressure direction, respectively. As a necessary condition, the number of basis functions in each direction of the Chebyshev expansions should be no greater than the data resolution of that direction, i.e., $\mathrm{N} \le d_T$ and $\mathrm{M} \le d_P$.

To use the Chebyshev expansions to represent the rate coefficient of a reaction, the user should provide the temperature and pressure limits of the expansion, $T_{\max}$, $T_{\min}$, (auxiliary keyword TCHEB) and $P_{\max}$, $P_{\min}$ (auxiliary keyword PCHEB) the number of basis functions used in each direction, N and M, and the $\mathrm{N} \times \mathrm{M}$ coefficients, a_{nm}, (auxiliary keyword CHEB). See *Table 3-6* and *Figure 3-4* of the *ANSYS Chemkin Input Manual* for more information about the use of these keywords.

3.7 Landau-Teller Formulation of the Rate Expressions

For reactions such as vibrational energy transfer processes, the Arrhenius form of the rate expression *Equation 3-5* is often not used. Instead, it is common to use the Landau-Teller expression,

Equation 3-42

$$k_{fi} = A_i \exp\left(\frac{B_i}{T^{1/3}} + \frac{C_i}{T^{2/3}}\right)$$

In GAS-PHASE KINETICS, we have provided the possibility to blend the Arrhenius expression with the Landau-Teller expression in the general expression, as follows:

Equation 3-43

$$k_{fi} = A_i T^{\beta_i} \exp\left(\frac{-E_i}{R_c T} + \frac{B_i}{T^{1/3}} + \frac{C_i}{T^{2/3}}\right)$$

Clearly, by setting B_i and C_i to zero, the Arrhenius expression is recovered, and by setting β_i and E_i to zero, the standard Landau-Teller expression is recovered. If appropriate, however, all the parameters can be used together to provide more flexibility in the reaction-rate expression than could be afforded by one of the forms alone.

3.8 Other Allowable Rate Constant Fitting Options

In the accommodation of plasma reactions, we have included two new rate-expression forms in GAS-PHASE KINETICS. These fits require auxiliary keywords to specify additional parameters and to distinguish the rate expression from the default of a modified Arrhenius form.

One form includes a polynomial fit to the logarithm of the temperature on which the reaction depends, as follows:

Equation 3-44

$$k_{fi} = A_i T^{\beta_i} \exp\left(\frac{E_i}{T} + \sum_{n=1}^{9} b_{ni} (\ln T)^{n-1}\right)$$

This form is consistent with the rate-constant fits for electron-hydrogen and electron-helium processes in a publication by Janev, Langer, Evans, and Post,[16] when the Arrhenius parameters β_i and E_i are zero. The user can specify this rate-constant fit option using the auxiliary keyword `JAN`, followed by the nine b_{ni} parameters.

A second form introduces a power series within the exponential of a modified Arrhenius expression, as follows:

Equation 3-45

$$k_{fi} = A_i T^{\beta_i} \exp \sum_{n=1}^{4} \frac{b_{ni}}{T^n}$$

The user may specify this rate-constant expression using the auxiliary keyword `FIT1`, followed by the four b_{ni} parameters. The use of auxiliary keywords are described in more detail in the *Section 3.5.3* of the *ANSYS Chemkin Input Manual*.

3.9 Rates of Creation and Destruction of Species

It is often convenient to separate the species chemical production rates into creation and destruction rates. Furthermore, some numerical approaches take advantage of this separation. Therefore, we provide subroutines that return the chemical rates in the following form:

Equation 3-46 CKCDYP, CKCDYR, CKCDXP, CKCDXR, CKCDC

$$\dot{\omega}_k = \dot{C}_k - \dot{D}_k$$

where, for non-three-body reactions, the creation rate is

16. R. K. Janev, W. D. Langer, J. K. Evans, and J. D. E. Post, *Elementary Processes in Hydrogen-Helium Plasmas*, Springer-Verlag, New York, 1987.

Equation 3-47

$$\dot{C}_k = \sum_{i=1}^{I} \upsilon'_{ki} k_{ri} \prod_{j=1}^{K} [X_j]^{\upsilon''_{ji}} + \sum_{i=1}^{I} \upsilon''_{ki} k_{fi} \prod_{j=1}^{K} [X_j]^{\upsilon'_{ji}}$$

and the destruction rate is

Equation 3-48

$$\dot{D}_k = \sum_{i=1}^{I} \upsilon'_{ki} k_{fi} \prod_{j=1}^{K} [X_j]^{\upsilon'_{ji}} + \sum_{i=1}^{I} \upsilon''_{ki} k_{ri} \prod_{j=1}^{K} [X_j]^{\upsilon''_{ji}}$$

When third body reactions are involved, each sum in the above equations is multiplied by the third-body concentration

$$[M] = \sum_{k=1}^{K} \alpha_{ki} [X_k]$$

Another useful form for the chemical production rates is found by defining a creation rate and characteristic time for the destruction rate, i.e.,

Equation 3-49 CKCTYP, CKCTYR, CKCTXP, CKCTXR, CKCTC

$$\dot{\omega}_k = \dot{C}_k - \frac{[X_k]}{\tau_k}$$

Here the characteristic time for destruction is given in terms of $\dot{D}_k$ as

Equation 3-50

$$\tau_k = \frac{[X_k]}{\dot{D}_k}$$

As a precaution against $[X_k]$ and $\dot{D}_k$ simultaneously approaching zero, the GAS-PHASE KINETICS implementation of the destruction time is written as

Equation 3-51 CKCTYP, CKCTYR, CKCTXP, CKCTXR, CKCTC

$$\tau_k = \frac{[X_k]}{\dot{D}_k + \varepsilon}$$

where ε is an arbitrary small number, say 10^{-30}.

The computer-dependent “small” number used in *Equation 3-51* is set in the GAS-PHASE KINETICS Subroutine Library at the time that the library is created.

3.10 Separating Temperature from Composition Dependence

In some numerical solution algorithms for chemically reacting flow, it is a significant computational savings to separate the temperature-dependent part of the rate expressions (i.e., the rate constants in most cases) from the concentration-dependent contribution. In particular, evaluation of Jacobian matrix elements through perturbation of solution variables often relies on numerous function evaluations and hence numerous calls to GAS-PHASE KINETICS to evaluate rate expressions. The temperature-dependent portion of the rate expression contains an exponential, which is computationally expensive to evaluate. When the temperature variable is not being perturbed, it is unnecessary to repeat this evaluation.

To facilitate a more computationally efficient solution algorithm, Chemkin provides additional subroutines that either provide the temperature-dependent rate coefficients or, given these rate coefficients, return the species’ net rates of production. The subroutine for evaluating the temperature-dependent rate constant for each reaction is called `CKKFRT`, while the subroutine that takes the rate constant as input and returns the species net rates of production is called `CKWYPK`. The use of these subroutines is described in more detail in the *ANSYS Chemkin Application Programming Interface Manual*, specifically in *Section 4.13* and *Chapter 7*.

4 Surface Chemical Rate Expressions

Heterogeneous reactions may occur at the interface between a solid surface and an adjacent gas. Such reactions are central to many important chemical processes including thin-film deposition, chemical or plasma etching, catalytic oxidation, and catalytic conversion processes. Chemkin SURFACE KINETICS utilities are based on general and systematic conventions that allow users to describe any level of complexity for such gas-surface interactions.

Surface reactions can involve gas-phase species, surface-site species, and bulk-phase or condensed species. There can be multiple surface (site) phases and multiple bulk phases. Surface reactions may involve conversion between any phases or may involve only one phase. The definitions of these phases and the species that reside in them are provided in more detail in *Chapter 2* of this manual. As with gas-phase reactions, surface reactions must conserve mass, elements, electronic charge, and (usually) surface sites.

This chapter describes basic rate expressions and default assumptions, as well as the wide array of options available to users for describing different types of reactions. While the default formulation assumes elementary reactions, where law of mass action is assumed, users may also easily specify global reaction rates. Global rate expressions can use arbitrary reaction orders and non-integer stoichiometric coefficients. In addition, users can directly input parameters to express Langmuir-Hinshelwood and Eley-Rideal rate expressions.

4.1 Atomic vs. Open Site Reaction Formalism

In this section, we consider in more detail how to write chemical reactions involving surface and bulk species. For clarity, we will write our rate expressions using a suffix (g) on our gas-phase species symbolic names, (s) for surface site species, and (b) for bulk-phase species.

A chemical species on the top layer of the solid, i.e., a surface species, occupies a site. For example, an arsine molecule adsorbed on a surface could occupy a site, and might be denoted $AsH_3(s)$. Another example might be a bare gallium atom, Ga(s), on top of a gallium arsenide (bulk) crystal. If another species, say a gas-phase $AsH_3(g)$, lands on top of the Ga(s), it might "stick" or adsorb on that site, as shown in *Figure 4-4*. In this case the gallium atom that was at the surface is now covered up, such that it is no longer accessible to react with the gas and therefore no longer a surface species. In our nomenclature it has become a bulk species. The adsorbed AsH_3 molecule now occupies the top-most layer at this site, so it has become the surface species $AsH_3(s)$. In our formalism, we might write the adsorption reaction in *Figure 4-4* as

Figure 4-1 Absorption Reaction of $AsH_3(s)$

$$\mathbf{AsH_3(g) + Ga(s) \rightarrow AsH_3(s) + Ga(b)}$$

In this reaction, the number of sites included on the left-hand side of the reaction equals the number on the right-hand side; the reaction conserves sites.

Suppose that we had wanted to describe the reverse reaction, i.e., desorption of AsH_3 from the surface. We would then write the reaction as

Figure 4-2 Desorption Reaction of $AsH_3(s)$

$$\mathbf{AsH_3(s) + Ga(b) \rightarrow AsH_3(g) + Ga(s)}$$

Here, Ga(b) is included as a reactant in order to achieve site and elemental balance. We refer to the formalism described in *Figure 4-1* and *Figure 4-2* as the **Atomic Site Formalism**.

An alternate way of posing the example reaction above is to consider the situation on the left side of *Figure 4-4* not as having a surface gallium atom on a site, but to say that this is really an "open" site at which some event may take place (see *Figure 4-5*). From this viewpoint, we could write the reaction of *Figure 4-5* as

Figure 4-3 Open Site Formalism

$$\mathbf{O(s) + AsH_3(g) \rightarrow AsH_3(s)}$$

where the symbol O(s) is used to denote an open site. In specifying thermodynamic data for O(s), we would include no elements in the composition. Since O(s) contains no elements, this reaction conserves both sites and elements. We refer to this alternative formalism described in *Figure 4-3* as the **Open Site Formalism**.

The Atomic Site and Open Site Formalisms are equally valid ways of stating these surface reactions. Either is allowed by the SURFACE KINETICS Pre-processor. Personal preference or, perhaps, the nature of a particular problem might dictate one over the other. Note that an “open” site must be considered as a species and therefore must have thermodynamic data specified (even if all the data for the “species” are zeroes).

Figure 4-4 Illustration of an Adsorption Reaction using the Atomic Site Formalism

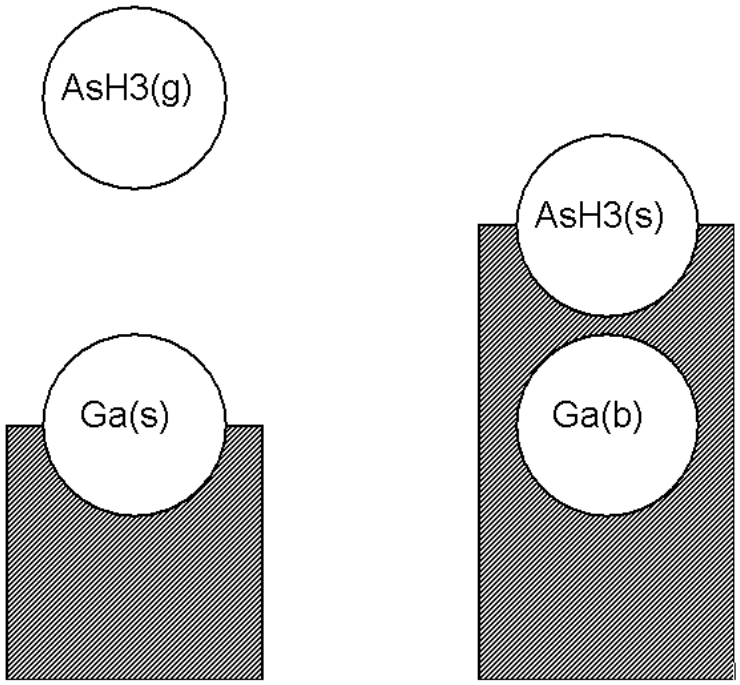

Figure 4-5 Illustration of an Adsorption Reaction using the Open Site Formalism

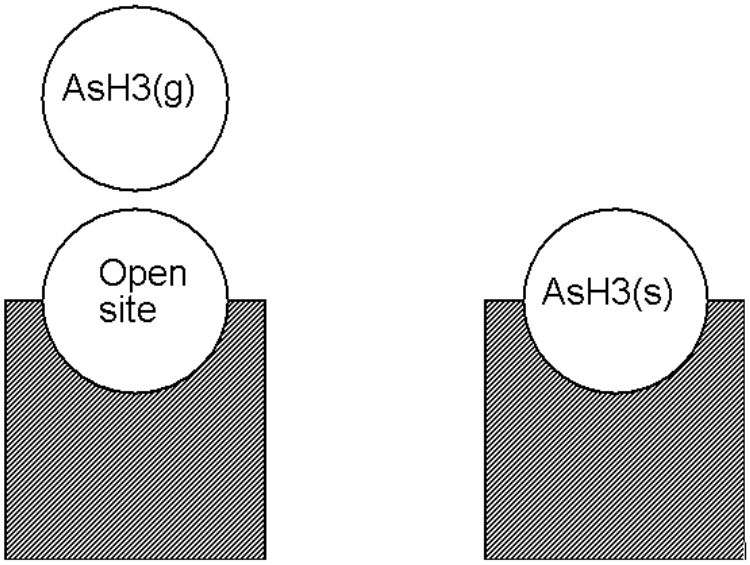

Next we consider the thermodynamical implications of stating reactions such as *Figure 4-1* and *Figure 4-3*. In the Atomic Site Formalism, the interpretation is straightforward. In *Figure 4-1* we have converted AsH_3(g) and Ga(s) into AsH_3(s) and Ga(b). Thus, the change in a thermochemical property, e.g., ΔH_{rxn}, is the difference in the heats of formation of the products and the reactants.

For the Open Site Formalism, we need to consider the properties of the open-site species, which may be less easy to define. Since the open-site formalism describes an identical physical event to the atomic-site formalism, the properties of the open site must be related to those of Ga(b) and Ga(s). For example, the heat of formation of this open site is

Equation 4-1

$$\Delta H_f(\mathrm{O(s)}) = \Delta H_f(\mathrm{Ga(s)}) - \Delta H_f(\mathrm{Ga(b)})$$

Thus, if the thermodynamic properties of Ga(s) were taken to be equivalent to those of Ga(b), then the heat of formation of the open site would be zero. In most cases the thermodynamic behavior of the surface is considered only in relative, not absolute, terms. For this reason, it is important to specify thermodynamic property values of surface sites relative to one species (such as a solid bulk species) in the system and to use this convention, as well as the choice of atomic vs. open-site formalism, throughout the surface reaction mechanism.

4.2 Basic Surface Reaction Rate Expressions

A SURFACE KINETICS mechanism may include I surface reactions that involve up to K chemical species, where K is the total number of species (gas, surface, bulk) in the system. The reactions can be represented in a general form that is equivalent to that stated in *Equation 3-1* for gas-phase reactions in *Section 3.1*. As with gas-phase reactions, reactions may be reversible, where both forward and reverse rates are included, or irreversible where only forward rates are considered.

For surface reactions, the net production rate $\dot{s}_k$ is in units of (**mole/cm^2/sec**) for each of the K species, regardless of phase. The net production rate for each species is the sum of the rates-of-production for all reactions involving the *k*th species, as shown in *Equation 4-2*.

Equation 4-2 SKRAT

$$\dot{s}_k = \sum_{i=1}^{I} \upsilon_{ki} q_i \qquad (k = 1, \ldots, K)$$

As with gas-phase reactions, the stoichiometric coefficients may be non-integers for global rate expressions, and the net stoichiometric coefficient is given by *Equation 3-3*. Net stoichiometric coefficients for surface reactions are determined by SURFACE KINETICS library routine SKNU. Again, the rate-of-progress variable q_i for the ith reaction is given by the difference of the forward rates and the reverse rates. By default, the law of mass action, as stated in *Equation 3-4* is used to determine the forward and reverse rates based on the stoichiometric coefficients and the species concentrations. This assumption can be over-ridden as described in later sections of this chapter. For surface reactions, the SURFACE KINETICS library routine SKROP is used to determine net rates of progress.

As discussed in *Section 2.1.2*, the form of the concentrations $[X_k]$ depends upon whether species k is in the gas-phase, on the surface, or in the bulk. Furthermore, the units of the rate constants will depend on the identity of the reactants and products in a particular reaction.

The forward rate constants k_{fi} for the I reactions are (by default) assumed to have the Arrhenius temperature dependence, as given in *Equation 3-5*. The three Arrhenius parameters (returned by SURFACE KINETICS library routines SKABE and SKRAEX) are required input to the SURFACE KINETICS Pre-processor for each reaction. However, there are a number of ways in which the rate expression for a reaction can be altered from this basic expression. These alternative formulations are described in the remaining sections of this chapter.

For reversible reactions, the reverse rate constants k_{ri} are related to the forward rate constants through the equilibrium constants, as stated in *Equation 3-6*. The user can over-ride this use of the equilibrium constant by explicitly declaring Arrhenius coefficients for the reverse reaction in the Pre-processor input via the auxiliary keyword REV. This option is explained in the *Table 4-6* of the *ANSYS Chemkin Input Manual*. An executable can call the SURFACE KINETICS library routine SKIREV to find out if reverse coefficients were explicitly input for a given reaction and the coefficient values.

4.3 Equilibrium Constants for Reactions Involving Surface Species

In pressure units, the equilibrium constant K_{pi} has the same form as for gas-phase reactions, as stated in *Equation 3-8*. The pressure equilibrium constant is directly related to the net Gibb's free energy of the reaction, as determined by the thermodynamic properties of the species involved in the reaction. In deriving the equilibrium constant in concentration units, however, the surface state as well as the gas state must be taken into account. For surface reactions, then, K_{ci} takes the form:

Equation 4-3 SKEQ

$$K_{ci} = \left(\frac{P_{\text{atm}}}{RT}\right)^{\sum_{k=1}^{K_g} \upsilon_{ki}} \prod_{n=N_s^f} \left(\Gamma_n^o\right)^{\sum_{k=K_s^f(n)}^{K_s^l(n)} \upsilon_{ki}} \prod_{k=K_s^f(n)} \sigma_k^{-\upsilon_{ki}} K_{pi}$$

where P_{atm} denotes a pressure of 1 atm, and Γ_n^o is the standard-state surface site density of site type n. The sum in the first exponent runs only over the gas-phase species, and the sum in the second exponent runs only over surface species in surface phase n.

4.4 Non-integer Stoichiometric Coefficients and Arbitrary Reaction Orders

As described in *Section 3.2* and *Section 3.3*, respectively, SURFACE KINETICS reaction expressions can included non-integer stoichiometric coefficients for participating species and arbitrary, user-specified reaction orders for any species in the system.

The user is advised to exercise caution when specifying a change of reaction order. Such a change may produce unexpected and unphysical results in a kinetic simulation. The user should also consider the kinetics of the reverse reaction when changing reaction orders for the forward reaction.

4.5 Surface-coverage Modification of Rate Expression

In some cases there are experimental data that indicate that the Arrhenius expression for the rate constant, *Equation 3-5*, is modified by the coverage (concentration) of some surface or bulk species. Chemkin SURFACE KINETICS allows optional coverage parameters to be specified for species k and reaction i, through use of the auxiliary keyword COV, described in *Table 4-6* of the *ANSYS Chemkin Input Manual*. In this case, the rate constant for the forward reaction is modified as

Equation 4-4

$$k_{fi} = A_i T^{\beta_i} \exp\left(\frac{-E_i}{RT}\right) \prod_{k=K_s^f(N_s^f)}^{K_s^l(N_s^l)} 10^{\eta_{ki}[Z_k(n)]} [Z_k(n)]^{\mu_{ki}} \exp\left(\frac{-\varepsilon_{ki}[Z_k(n)]}{RT}\right) \prod_{k=K_b^f(N_b^f)}^{K_b^l(N_b^l)} 10^{\eta_{ki}[a_k(n)]} [a_k(n)]^{\mu_{ki}} \exp\left(\frac{-\varepsilon_{ki}[a_k(n)]}{RT}\right)$$

where the three coverage parameters are η_{ki}, μ_{ki}, and ε_{ki} for species k and reaction i. The product in *Equation 4-4* runs over only those surface species that are specified as contributing to the coverage modification. Note that the surface site fractions appear in *Equation 4-4* rather than molar concentrations $[X_k]$ (mole/cm^2) for surface species, while bulk activities appear for bulk species. The term associated with μ_{ki} now makes it possible for the rate-of-progress of a reaction to be proportional to any arbitrary power of a surface species concentration. Also, using this modified expression for k_{fi}, the net pre-exponential factor may be a function of coverage

Equation 4-5

$$\log A = \log A_i + \sum_{k=K_s^f(N_s^f)}^{K_s^l(N_s^l)} \eta_{ki}[Z_k(n)] + \sum_{k=K_b^f(N_b^f)}^{K_b^l(N_b^l)} \eta_{ki}[a_k(n)]$$

and the activation energy is a function of the coverage

Equation 4-6

$$E = E_i + \sum_{k=K_s^f(N_s^f)}^{K_s^l(N_s^l)} \varepsilon_{ki}[Z_k(n)] + \sum_{k=K_b^f(N_b^f)}^{K_b^l(N_b^l)} \varepsilon_{ki}[a_k(n)]$$

For reactions with optional coverage dependence, the rate of progress is calculated employing *Equation 3-4*, with the forward rate coefficient from *Equation 4-4*. The reverse rate constant is calculated via *Equation 3-6*.

If the form of *Equation 4-4* is not flexible enough to describe a certain coverage behavior, one can repeat the same reaction several times with different values for the coverage parameters such that the sum of the rate constants approximates the desired form.

4.6 Sticking Coefficients

For some simple surface reaction mechanisms we have found it convenient to specify the surface reaction rate constant in terms of a “sticking coefficient” (probability), rather than an actual reaction rate. This approach is only allowed when there is exactly one gas-phase species reacting with a surface. Sticking-coefficient reactions may include any number of surface site or bulk-phase species as reactants, and any number of species of any phase as products

In such cases, one might have a measurement or intuition about the probability that a certain process takes place when a collision between a given gas-species occurs with the surface. For consistency in expressing each surface reaction in terms of a rate constant, we provide a conversion between this sticking coefficient form and the usual rate expression. The actual reaction rate (in moles/cm^2/sec) is derived from this probability together with the physical gas-surface collision frequencies, as discussed further below.

The unitless sticking coefficients’ functional form has an “Arrhenius-like” form as follows:

Equation 4-7

$$\gamma_i = \min\left[1, a_i T^{b_i} \exp\left(\frac{-c_i}{R_c T}\right)\right]$$

In this case, γ_i, a_i and b_i are unitless and c_i has units compatible with $R_c T$, the real-gas constant used for reaction activation energies multiplied by temperature. SURFACE KINETICS also allows for surface-coverage modification of a sticking coefficient, analogous to *Equation 4-4*.

Because γ_i is defined as a probability, it must lie between 0 and 1 to make physical sense. Therefore, SURFACE KINETICS checks the value of γ_i, and an unphysical sticking coefficient greater than 1 is changed to the value 1. Some earlier versions of SURFACE KINETICS did not truncate the values at 1.

To illustrate the use of sticking coefficients, we give three successively complex examples of using sticking coefficients. First, to specify that $SiH_2(g)$ reacts with probability γ_i upon each collision with the surface, one could write the reaction

Figure 4-6 Sticking Coefficient for $SiH_2(g)$—Collision Probability

$SiH_2(g) \rightarrow Si(b) + H_2$

In this example, we have not explicitly included the surface in writing *Figure 4-6*.

A somewhat more detailed way of using the sticking-coefficient specification would be to say that $SiH_2(g)$ reacts with probability γ_i upon each collision with a bare surface silicon atom, Si(s):

Figure 4-7 Sticking Coefficient for $SiH_2(g)$—Collision Probability with Si(s)

$SiH_2(g) + Si(s) \rightarrow Si(s) + Si(b) + H_2$

If the surface site fraction of Si(s) were unity, then a fraction γ_i of the collisions of SiH_2 with the surface would result in a reaction. However, for Si(s) coverages less than 1, the reaction rate decreases in proportion with the coverage of Si(s).

In a third (contrived) example, suppose there is a probability γ_i for a reaction to occur when SiH_2 collides with both a Si(s) and a C(s) reaction such as

Figure 4-8 Sticking Coefficient for $SiH_2(g)$—Collision Probability with Si(s) and C(s)

$SiH_2(g) + Si(s) + C(s) \rightarrow Si(b) + SiH(s) + CH(s)$

The rate of this reaction would be proportional to both the coverage of Si(s) and C(s).

Conversion of a sticking coefficients γ_i to the usual mass-action kinetic rate constants uses the collision frequency of the gas species with the solid surface, as shown in *Equation 4-8*.

Equation 4-8

$$k_{fi} = \gamma_i \frac{\prod_{j=1} \sigma_j^{v'_{ji}}}{(\Gamma_{\text{tot}})^m} \sqrt{\frac{RT}{2\pi W_k}}$$

Here, R is the universal gas constant, W_k is the molecular weight of the gas-phase species, Γ_{tot} is the total surface site concentration summed over all surface phases (number of moles of surface sites per unit area), and m is the sum of all the stoichiometric coefficients of reactants that are surface species. The term involving Γ_{tot} raised to the m power is needed to convert from the unitless sticking coefficient form to units appropriate for a rate constant, and the term in the square root accounts for the gas/surface collision frequency. In the third example given above, *Figure 4-8*, the value of m is 2, because there are two surface sites appearing as reactants, i.e., Si(s) and C(s). The product term in *Equation 4-8* is the product of the site-species occupancies, raised to a power equal to the reaction order for that species, for all site species that are reactants. Here, σ_j is the number of sites that the surface species occupies, and v_j is the reaction order for that species. The product term will be equal to one when there are unity site occupancies for all of the surface species in the reaction.

Implicit in the sticking coefficient description just presented is an assumption that the sticking coefficient is relatively small, i.e., much less than one. In this case the molecular motion in the vicinity of the solid surface is random and the collision frequency of gas-phase species with the surface is not affected by the surface itself. However, when the sticking coefficient is large, i.e., close to one, then the velocity distribution becomes skewed. Species whose random motion carries them close to the surface have a high probability of staying there, which causes a non-Maxwellian velocity distribution that, in turn, alters the net species flux near the surface. Motz and Wise[17] analyzed this situation and suggested a correction factor that modified *Equation 4-8* to become:

17. H. Motz and H. Wise, *Journal of Chemical Physics* **32**:1893 (1960)

Equation 4-9

$$k_{fi} = \left(\frac{\gamma_i}{1-\gamma_i/2}\right)\frac{\prod_{j=1}\sigma_j^{\upsilon'_{ji}}}{(\Gamma_{\text{tot}})^m}\sqrt{\frac{RT}{2\pi W_k}}$$

Goodwin and Gavillet[18] have incorporated this effect in their analysis of chemical vapor deposition of diamond films. However, in most cases sticking coefficients are derived from empirical data rather than theory, in which case it is usually inappropriate to apply the Motz-Wise correction. Users may turn this option on by including `MWON` in the `REACTIONS` line of their SURFACE KINETICS input file.

Early versions of SURFACE KINETICS always applied *Equation 4-9*. Later versions allow optional use of *Equation 4-8* to relate the sticking coefficient to rate constants through use of the keyword `MWOFF` on the `REACTIONS` line. *Currently, the default usage is Equation 4-8, or* `MWOFF`. Users can invoke *Equation 4-9* using `MWON` in the `REACTIONS` line. (*Section 4.5.1* of the *ANSYS Chemkin Input Manual*)

Using the kinetic rate constant derived from the sticking probability, the rate-of-progress is calculated using *Equation 3-4*, as usual. The sticking coefficient specification is only allowed for the forward reaction. If the reaction is written as reversible, the reverse reaction rate constant would be calculated from *Equation 3-6* to assure microscopic reversibility.

4.7 Langmuir-Hinshelwood and Eley-Rideal Reactions

Surface reactions are often described using global reactions rather than as a series of elementary reactions. Some of the most common global rate expressions used for surface reactions are the Langmuir-Hinshelwood (LH) and Eley-Rideal (ER) rate expressions. The former applies to the case where adsorption and desorption are assumed to be in equilibrium, and a reaction on the surface between adsorbed species is rate determining. The latter applies to the case of a reaction between a gas-phase species and an adsorbed species being rate-limiting. Although originally developed for specific cases, these names are now used to refer to a variety of rate expressions with similar forms. If a LH reaction is used, a single global reaction might constitute the entire surface chemistry mechanism. The “Langmuir” part of the name for the LH rate expression originates from the inclusion of the Langmuir adsorption

18. D. G. Goodwin and G. G. Gavillet, *Journal of Applied Physics*, **68**:6393 (1990)

isotherm, which assumes that the adsorption sites on the surface are independent from each other (single site adsorption), the sites are equivalent, and the surface coverage decreases the number of sites available for adsorption only, but does not alter the energetics of adsorption/desorption.

The following example of a LH reaction illustrates its features. Species A and B coadsorb onto the surface, react to products C and D, which can then desorb. The reaction between adsorbed A and adsorbed B is assumed to be rate-limiting and irreversible, while the adsorption/desorption processes are assumed to be in equilibrium. In the LH formulation, the elementary chemical reactions shown in *Figure 4-9* would be replaced by the single overall reaction shown in *Figure 4-10*, which does not explicitly include any surface species.

Figure 4-9 Langmuir-Hinshelwood Elementary Chemical Reactions

A + O(s) $\leftrightarrow$ A(s)
B + O(s) $\leftrightarrow$ B(s)
A(s) + B(s) $\rightarrow$ C(s) + D(s)
C(s) $\leftrightarrow$ C + O(s)
D(s) $\leftrightarrow$ D + O(s)

Figure 4-10 Langmuir-Hinshelwood Single Overall Reaction

A + B $\rightarrow$ C + D

The effects of surface-sites being blocked by various species are included via the adsorption/desorption equilibria. This “lumping” of a number of elementary steps together results in a rate expression that differs substantially from a simple mass-action rate expression. The rate of progress variable is given by:

Equation 4-10

$$q = \frac{kK_A[X_A]K_B[X_B]}{(1 + K_A[X_A] + K_B[X_B] + K_C[X_C] + K_D[X_D])^2}$$

where the Ks are the equilibrium constants for the adsorption/desorption steps and $[X_i]$ s are the concentrations of the species. As product species, C and D do not appear in the numerator, but as adsorbed species they can block surface sites, so they do appear in the denominator. The k is expressed in terms of Arrhenius parameters, as are the Ks. The equilibrium constant is defined as $K = AT^{\beta}\exp(-H/RT)$, in parallel with the standard expression for rate constants. Often, the equilibrium constants in the numerator are lumped into a representative rate constant, giving:

Equation 4-11

$$q = \frac{k'[X_A][X_B]}{(1 + K_A[X_A] + K_B[X_B] + K_C[X_C] + K_D[X_D])^2}$$

The generalized form of the above expression is:

Equation 4-12

$$q = k' \frac{\prod_i [X_i]^{\nu_i}}{\left(1 + \sum_i K_i [X]_i\right)^2}$$

where i represents gas-phase species in the reaction, and the exponent of 2 in the denominator comes from the fact that the reaction rate is determined by the reaction between two adsorbed species. In practice, this rate form is often used for empirical parameter fitting, so we further generalize it to:

Equation 4-13

$$q = k' \frac{\prod_i [X_i]^{l_i}}{\left(1 + \sum_i K_i [X_i]^{n_i}\right)^m}$$

where:

1. the chemical species in the rate law are not limited to the reactants and products in the reaction description,
2. the exponents (l_i) for the chemical species concentrations in the numerator of *Equation 4-13* may differ from the stoichiometric coefficients (ν_i) and may be fractional,
3. the overall exponent in the denominator (m) of *Equation 4-13* may differ from 2, and may be fractional,
4. the exponents (n_i) for the concentrations of species in the denominator may differ from 1 or the stoichiometric coefficients, and may be fractional.

For example, hydrogen (H2) and toluene (T) can react over a catalyst to produce methane (M) and benzene (B):

$C_6H_5CH_3 + H_2 \rightarrow C_6H_6 + CH_4$

The rate law for hydrodemethylation of toluene at 600 C is given by the Langmuir-Hinshelwood form as[19]:

Equation 4-14

$$q' = \frac{1.4 \times 10^{-8} P_{H2} P_T}{1 + 1.26 P_B + 1.01 P_T} \qquad \text{mol/g cat-sec}$$

where P_i is partial pressure in atm.

Because reaction rates in SURFACE KINETICS are area-based, the catalyst-mass-based rate given in *Equation 4-14* has to be converted accordingly. By assuming each gram of catalyst provides 0.5 cm^2 of active surface area, the area-based rate law is found to be:

Equation 4-15

$$q = \frac{2.8 \times 10^{-8} P_{H2} P_T}{1 + 1.26 P_B + 1.01 P_T} \qquad \text{mol/cm}^2\text{-sec}$$

By comparing Equation (2) to the generalized LH rate expression given by *Equation 4-13*, the reaction for hydrodemethylation of toluene can be presented in SURFACE KINETICS format as:

```
C6H5CH3  +  H2 => C6H6 + CH4          2.8E-8   0.0      0.0
    LANG /C6H6     1.26  0.0  0.0  1.0/
    LANG /C6H5CH3  1.01  0.0  0.0  1.0/
    LHDE /1/
    LHPR /atm/
```

Auxiliary keywords for the Langmuir-Hinshelwood reaction are described in *Table 4-6* of the *ANSYS Chemkin Input Manual*.

Eley-Rideal (also called Rideal-Eley) reactions are less common than LH reactions. The following example illustrates its features. Species A adsorbs onto the surface, then reacts with gas-phase species B to produce C, which can then desorb. The reaction between adsorbed A and gas-phase B is assumed to be rate-limiting and irreversible, while the adsorption/desorption processes are assumed to be in equilibrium. In the ER formulation, the elementary chemical reactions shown in *Figure 4-11* would be replaced by the single overall reaction shown in *Figure 4-12*, which does not explicitly include any surface species.

19. Fogler, H.S., *Elements of Chemical Reaction Engineering*, 2nd ed., Prentice Hall, 281.

Figure 4-11 Eley-Rideal Elementary Chemical Reaction

A + O(s) ↔ A(s)
A(s) + B → C(s)
C(s) ↔ C + O(s)

Figure 4-12 Eley-Rideal Single Overall Reaction

A + B → C

In this case, the rate of progress variable is given by:

Equation 4-16

$$q = \frac{kK_A[X_A][X_B]}{(1 + K_A[X_A] + K_C[X_C])}$$

or

Equation 4-17

$$q = \frac{k'[X_A][X_B]}{(1 + K_A[X_A] + K_C[X_C])}$$

The generalized form of this is:

Equation 4-18

$$q = k' \frac{\prod_i [X_i]^{\nu_i}}{\left(1 + \sum_i K_i [X]_i\right)}$$

which is the same as the *Equation 4-12* above for LH kinetics, except that the denominator has an overall exponent (m) of one rather than two. ER reactions are thus treated as a special case of the LH rate law.

Using the LH option requires paying careful attention to the units of the reaction rates. The discussion above assumes that the rate expressions are given in terms of gas concentrations, which is the standard for GAS-PHASE KINETICS. However, literature values for LH rate parameters, especially equilibrium constants, are often provided in pressure units. To reduce the number of units conversions required of the user, equilibrium constants may be input in either pressure units or concentration units. This option is currently limited to the LH rate expression and **only** for the equilibrium constants. Rate parameters still must be input in concentration units. In SURFACE

KINETICS, the default units, unless altered on the REACTIONS line, for the rate of a reaction are moles $cm^{-2}sec^{-1}$. Rate parameters given in pressure units, for example in atm sec^{-1}, do not have the same dimensions as moles $cm^{-2}sec^{-1}$. Such a rate would need to be divided both by RT and the surface-area to volume ratio (AV), before use. Rates given in terms of weight of catalyst need to be converted to a rate expressed in terms of the effective surface area of the catalyst via the surface area per unit weight of catalyst and the dispersion. Rates given on a per site basis should also be converted to a per area basis.

4.8 Plasma-surface Interactions

For chemistry sets that involve electrons and ions, some special formulations of surface reactions are available. These formulations allow modification of the ion flux as well as the ion impact energy for ion-surface collisions.

Ion fluxes are often not determined by a “thermal” collision frequency (as used in our sticking-coefficient formulations). Instead, ion fluxes are often limited by transport from the plasma to the edge of the plasma sheath, which an electric field that exists near surfaces adjacent to a plasma gas. For non-thermal plasmas, the limiting flux is then defined by the Bohm criterion,[20] which depends on the ion mass and the electron temperature. Chemkin SURFACE KINETICS allows a user to indicate that certain reactions are governed by the Bohm flux.

In addition, there are many examples in materials processing, where ions interact with surfaces to alter the morphology, sputter material, or enhance heterogeneous chemical reactions. Ions are often accelerated through a plasma sheath to grounded or electrically biased materials. In this way, the directed energy of ions encountering a surface may be significantly greater than that represented by the ion temperature in the plasma gas. SURFACE KINETICS therefore makes the provision for a reaction-rate constant to depend upon the energy of a positive ionic reactant species, E_{ion}.

Details of the ion flux and ion-energy options are described in this section.

4.8.1 Bohm Rate Expression for Ionic Reactions

The rate constant for a reaction involving a positive ion can be modified by applying a Bohm velocity correction, as follows

20. M. A. Lieberman and A. J. Lichtenberg, *Principles of Plasma Discharges and Materials Processing*, John Wiley and Sons, New York (1994).

Equation 4-19

$$k_{fi,\,\mathrm{Bohm}} = a_i T^{b_i} e^{-c_i/R_c T} \frac{\prod_{j=1} \sigma_j^{v'_{ji}}}{(\Gamma_{\mathrm{tot}})^m} \sqrt{\frac{RT_e}{W_{\mathrm{ion}}}}$$

In *Equation 4-19*, the reaction-rate expression is similar to that of *Equation 4-8*, used to describe sticking coefficients. As with a sticking coefficient, Bohm reactions allow the user to specify a probability for the reaction to occur, rather than a reaction rate. Also, the Bohm reaction formulation is only valid for reactions where there is exactly one gas-phase ion that is a reactant. The units of the pre-exponential, temperature exponent term, and activation energy correspond to the parameters in a sticking coefficient. The main difference, however, is that the resulting probability is multiplied by the Bohm velocity expression (the term in the square root in *Equation 4-19*), rather than the thermal velocity of the ion species. The Bohm velocity is based on the electron temperature, rather than the thermodynamic temperature of the gas.

For use of the Bohm reaction option, the electron must be declared as a gas-phase species in the list of species names in the GAS-PHASE KINETICS Pre-processor input.

The molecular weight in the last term is that of the positive ion. Bohm reactions can be declared through the Pre-processor input via the auxiliary keyword `BOHM`. An executable can find out which reactions were declared as Bohm reactions by a call to `SKIBHM`. Use of the `BOHM` keyword is only allowed for irreversible reactions.

4.8.2 General Ion-energy-dependent Rate Expression

To account for ion-impact energy on a reaction-rate, the following general form is available, as well as the more specific ion-yield form described in *Section 4.8.3*. For the general functional form, the reaction-rate constant can be modified as follows:

Equation 4-20

$$k_i(E_{\mathrm{ion}}) = k_i(\mathrm{thermal}) \cdot \max\left[0, (E_{\mathrm{ion}}^{f_i} - E_{\mathrm{ion},\,0}^{f_i})^{g_i}\right]$$

In this case, the reaction rate depends upon a threshold energy, $E_{\mathrm{ion},\,0}$, and the energy expressions can be raised to a specified power in two different ways through the use of the parameters f_i and g_i. Ion-energy dependent reactions are declared in the Pre-processor input via the auxiliary keyword `ENRGDEP`. An executable can find out which reactions were declared as ion-energy-dependent reactions and get an array of the parameters by a call to `SKIENR`. Because the subroutines that evaluate

rate constants in SURFACE KINETICS take temperature as an argument, and not species energy, subroutine SKRPAR must be called to input an array of ion energies, ENRGI before the rate constant routine is called. Use of the ENRGDEP keyword is only allowed for irreversible reactions.

4.8.3 Ion-enhanced Reaction Yield Expression

In modeling plasma systems, it is sometimes necessary to include reactions where the energy of the incident ion determines not only the reaction rate, but also the number of product species formed. For example, in physical etching the incident ion energy determines the number of species etched from the surface. Such surface reactions can be modeled in SURFACE KINETICS using a “yield enhancement” factor to account for the variable stoichiometry.

Consider the case in which a positive ion, I(g) hits a surface and knocks off a variable number ψ of surface species, S(s). For each surface species S(s) destroyed, the example reaction produces two gas-phase products, P(g) and leaves behind some other surface species, O(s); another gas species Q(g) is produced by the reaction, but its stoichiometric coefficient is not dependent upon the number of surface species etched.

Figure 4-13 Stoichiometric Coefficient with a Positive Ion

$$\mathbf{I(g) + \psi S(s) \rightarrow \psi 2P(g) + \psi O(s) + Q(g)}$$

The coefficient ψ is essentially a variable stoichiometric coefficient, which depends upon the energy of the positive ionic reactant I(g).

A reaction written like *Figure 4-13* is required to satisfy mass, charge, and elemental balance (as is every reaction in a SURFACE KINETICS mechanism). For this always to be the case, the “sub-reaction”

Figure 4-14 Stoichiometric Coefficient Sub-reaction

$$\mathbf{S(s) \rightarrow 2P(g) + O(s)}$$

consisting of all of the species in the original reaction that are multiplied by the coefficient ψ, must also satisfy mass, charge, and elemental balance. In addition, unless the NONCON auxiliary keyword was declared on the REACTIONS line (described later), the sub-reaction must also conserve the number of surface sites.

An example of a reaction using the ion-enhanced yield option in the form accepted by the SURFACE KINETICS Pre-processor is

```
E + CL+ + #SICL3(S) + #SI(B) + SICL(S) => SICL2(S) + #SICL2 +
#SICL(S)
```

The special character # identifies the energy-dependent multiplicative factor for the stoichiometric coefficient. Notice that the sub-reaction consisting of every species preceded by the # sign balances mass, elements, charge, and number of surface sites. The "yield" of this reaction (per incident CL+ ion) depends upon the energy of the ion.

We allow the following functional form for the yield enhancement:

Equation 4-21

$$\psi(E_{\text{ion}}) = h_{\text{yield}} \max\left[0, (E_{\text{ion}}^{t_i} - E_{\text{yield, 0}}^{t_i})^{u_i}\right]$$

The ion-enhanced yield can depend upon a threshold energy, $E_{\text{yield, 0}}$, and the energy expressions can be raised to a specified power in two different ways through the use of the parameters t_i and u_i. Ion-enhanced-yield reactions can be declared through the Pre-processor input via the auxiliary keyword YIELD. An executable can find out which reactions were declared as ion-enhanced yield reactions and get an array of the parameters via a call to SKIYLD. Because the subroutines that evaluate rate constants in SURFACE KINETICS take temperature as an argument, and not species energy, subroutine SKRPAR must be called to input an array of ion energies, ENRGI, before the rate constant routine is called. Use of the YIELD keyword is only allowed for irreversible reactions.

4.9 Manipulation of Chemical Rate Sensitivity Coefficients

Sensitivity analysis is a powerful tool in interpreting the results of computational simulations. Sensitivity analysis is used to determine quantitatively the dependence of a solution on certain parameters that appear in a model's definition. The "raw" first-order sensitivity coefficient matrices $S_{li} = \partial\Phi_l / \partial\alpha_i$ report the partial derivatives of the dependent variable vector Φ (e.g., temperature, mass fractions, surface composition) with respect to a parameter vector α_i (e.g., reaction rate constants). Since there is much mathematical literature on sensitivity analysis and various methods to compute the sensitivity coefficients from the solution, we do not discuss the computation of S_{li} here.

However, given the sensitivity matrix it is possible to manipulate it further to obtain the sensitivities of species production rates with respect to the dependent variables:

Equation 4-22

$$\frac{d\dot{s}_k}{d\alpha_i} = \frac{\partial \dot{s}_k}{\partial \alpha_i} + \sum_l \frac{\partial \dot{s}_k}{\partial [X_l]} \frac{\partial [X_l]}{\partial \Phi_l} \frac{\partial \Phi_l}{\partial \alpha_i}$$

where the components of Φ are the mass fractions, site fractions, and activities for gas-phase, surface, and bulk species, respectively. The term $\partial [X_l] / \partial \Phi_l$ converts from concentration units to the units of Φ:

Equation 4-23

$$\frac{\partial [X_l]}{\partial \Phi_l} = \begin{cases} \left(\frac{P}{RT}\right)\left\{\frac{\overline{W}}{W_l} - \frac{Y_l \overline{W}^2}{W_l^2}\right\} & K_g^f \le l \le K_g^l \\ \Gamma_n / \sigma_k(n) & K_s^f(N_s^f) \le l \le K_s^l(N_s^l) \\ 1 & K_b^f(N_b^f) \le l \le K_b^l(N_b^l) \end{cases}$$

We have included two subroutines in the SURFACE KINETICS Subroutine Library to facilitate calculation of these terms. The first gives the partial derivative of the production rate of species k with respect to the pre-exponential constant of the Arrhenius expression for surface reaction i:

Equation 4-24 SKDRDA

$$\frac{\partial \dot{s}_k}{\partial \alpha_i} = \upsilon_{ki} q_i / \alpha_i$$

Note that subroutine SKDRDA calculates the derivative with respect to the Arrhenius pre-exponential if the reaction was originally stated in standard Arrhenius form, or with respect to the sticking coefficient pre-exponential if a sticking coefficient was used.

The production rate of species k due to reaction i is

Equation 4-25

$$\dot{s}_k = \upsilon_{ki} q_i$$

Therefore, the dependence of $\dot{s}_k$ upon the concentration of some species l is

Equation 4-26

$$\frac{\partial \dot{s}_k}{\partial [X_l]} = \upsilon_{ki} q_i^f \left[\frac{\upsilon'_{li}}{[X_l]} + \left(\frac{\sigma_k(n)}{\Gamma_n} \right) \left\{ \eta_{li} \ln(10) + \frac{\mu_{li}}{[X_l]} - \frac{\dot{\varepsilon}_{li}}{R_c T} \right\} \right] - \upsilon_{ki} q_i^r \left[\frac{\upsilon''_{li}}{[X_l]} + \left(\frac{\sigma_k(n)}{\Gamma_n} \right) \left\{ \eta_{li} \ln(10) + \frac{\mu_{li}}{[X_l]} - \frac{\varepsilon_{li}}{R_c T} \right\} \right]$$

The terms inside the curled braces will only be present if species l modifies the rate of reaction i through coverage parameters, as in *Equation 4-4*. The partial of the production rate of species k due to all reactions with respect to the concentration of species l is then

Equation 4-27 SKDRDC

$$\frac{\partial \dot{s}_k}{\partial [X_l]} = \sum_{i=1}^{I} \frac{\partial \dot{s}_{ki}}{\partial [X_l]}$$

These terms can all be combined to calculate the desired $\partial \dot{s}_k / \partial \alpha_i$ in the executable.

4.10 Flux-matching Conditions at a Gas-surface Interface

Heterogeneous reactions at a gas-surface interface affect the mass and energy balance at the interface, and thus have an important influence on the boundary conditions in a chemically reacting flow simulation. The convective and diffusive mass fluxes of gas-phase species at the surface are balanced by the production (or depletion) rates of gas-phase species by surface reactions. This relationship is

Equation 4-28

$$\bar{n} \cdot [\rho Y_k (\bar{V}_k + \bar{u})] = -\dot{s}_k W_k \qquad (k = 1, \ldots, K_g)$$

where $\bar{n}$ is the unit inward-pointing normal vector to the surface, and the gas-phase diffusion velocities are related to the species and temperature gradients by

Equation 4-29

$$\bar{V}_k = \frac{1}{X_k \bar{W}} \sum_{j \neq k}^{K_g} W_j D_{k,j} \nabla X_j - \frac{D_k^T}{\rho Y_k} \frac{\nabla T}{T} \qquad (k = 1, \ldots, K_g)$$

Here the X_k are the gas-phase mole fractions, the Y_k are the gas-phase mass fractions, $\bar{W}$ is the mean molecular weight, $D_{k,j}$ is the ordinary multicomponent diffusion coefficient matrix, and the D_k^T are the thermal diffusion coefficients. (Both types of diffusion coefficients can be evaluated by calls to the TRANSPORT Package) In nonreacting fluid mechanics the fluid velocity normal to a solid wall is zero. However, if there are chemical reactions at the wall, then the velocity can be nonzero. This so-called Stefan flow velocity occurs when there is a net mass flux between the surface and the gas. The induced Stefan velocity is given by

Equation 4-30

$$\bar{n} \cdot \bar{u} = -\frac{1}{\rho} \sum_{k=1}^{K_g} \dot{s}_k W_k$$

The expression for the Stefan velocity is easily obtained from the interfacial mass balance (*Equation 4-28*) by summing over all K species and noting that the mass fractions must sum to one, i.e.,

Equation 4-31

$$\sum_{k=1}^{K_g} Y_k = 1$$

and that the sum of the diffusion fluxes must be zero, i.e.,

Equation 4-32

$$\sum_{k=1}^{K_g} Y_k V_k = 0$$

Exothermicity (or endothermicity) of surface reactions contributes to the energy balance at an interface. Diffusive and convective fluxes in the gas phase are balanced by thermal radiative and chemical heat release at the surface. This balance is stated as

Equation 4-33

$$\bar{n}\cdot\left[-\lambda\nabla T|_{gas}+\sum_{k=1}^{K_g}\rho Y_k(\bar{V}_k+\bar{u})h_k\right]=\sigma\varepsilon(T^4-T_o^4)+\sum_{k=K_s^f(N_s^f)}^{K_b^l(N_b^l)}\dot{s}_k W_k h_k-\bar{n}\cdot\lambda_{bulk}\nabla T|_{bulk}$$

The summation on the right-hand side runs over all surface and bulk species. It is interesting to note that by substituting *Equation 4-28* into the flux term on the left-hand side, the energy balance can be written in a more compact form as

Equation 4-34

$$-\bar{n}\cdot\lambda\nabla T|_{gas}=\sigma\varepsilon(T^4-T_o^4)+\sum_{k=1}^{K}\dot{s}_k W_k h_k-\bar{n}\cdot\lambda_{bulk}\nabla T|_{bulk}$$

Now the reaction-rate summation on the left-hand side runs over all species, including the gas-phase species.

The SURFACE KINETICS package allows the user to specify mass densities ρ_k for the bulk species. A possible use for the densities would be to convert surface reaction rate-of-production of a bulk species (in mole/cm^2/sec) into a growth rate G (in cm/sec). The needed relationship is

Equation 4-35

$$G=\sum_{k=K_b^f(N_b^f)}^{K_b^l(N_b^l)}\frac{\dot{s}_k W_k}{\rho_k}$$

4.11 Surface Site Non-conservation

Most current Chemkin Reactor Models do not accommodate situations where the surface site density is not constant for a specific surface-site phase. However, It is possible for a user to write their own programs that include equations for performing site-density balances where a non-zero net rate of production of surface sites is allowed. In such cases, it is possible that a given surface reaction (or reactions) will not conserve the number of surface sites. When sites are not conserved, the density of sites Γ_n is not necessarily a constant. One must then be sure to use the correct value of $\Gamma_n(t)$ in relationships such as *Equation 2-2*, which relating a site fraction and a surface molar concentration. It may be necessary to add equations to calculate the

current value of the total site concentration of each surface phase. Because surface site non-conservation is an issue that can alter the basic governing equations of the system, we require that one acknowledge its use by adding a keyword on the REACTIONS line (*Section 4.5.1* of the *ANSYS Chemkin Input Manual*). It is up to the user's program to ensure that the current site concentrations are correct. Subroutines SKRAT, SKRATI, which return an array of species production rates, also return an array of surface *phase* production rates, which would all be zero if sites are conserved in every reaction.

In the case where the user overrides the default of site conservation, the production rate $\dot{\Gamma}_n$ (in moles/cm^2/sec) for each surface phase is given by:

Equation 4-36

$$\dot{\Gamma}_n = \sum_{i=1}^{I} \Delta\sigma(n,i) q_i \qquad (n = N_s^f, \ldots, N_s^l)$$

where

Equation 4-37 SKRAT, SKRATI

$$\Delta\sigma(n,i) = \sum_{k=K_s^f(n)}^{K_s^l(n)} \upsilon_{ki}\sigma_k(n)$$

Here, the term $\Delta\sigma(n,i)$ is the net change in the number of surface sites of type n for surface reaction i.

5

5 Gas-phase Species Transport Properties

In solving chemically reacting-flow problems, chemical production and destruction is often balanced by transport due to convection, diffusion, or conduction. In some cases, such as perfectly stirred reactors or plug-flow reactors, the determination of composition and temperature fields are assumed to be kinetically limited. In such cases, transport is assumed to be infinitely fast within the section of gas considered and the effects of transport properties can be neglected. In many other important cases, however, transport of species and energy can become rate limiting. Examples where transport properties play a key role in determining the gas state are laminar premixed and diffusion flames, as well as many chemical vapor deposition systems.

Characterizing the molecular transport of species, momentum, and energy in a multicomponent gaseous mixture requires the evaluation of diffusion coefficients, viscosities, thermal conductivities, and thermal diffusion coefficients. Although evaluation of pure species properties follows standard kinetic theory expressions, one can choose from a range of possibilities for evaluating mixture properties. Moreover, computing the mixture properties can be expensive, and depending on the use of the results, it is often advantageous to make simplifying assumptions to reduce the computational cost.

For most applications, gas mixture properties can be determined from pure species properties via certain approximate mixture averaging rules. However, there are some applications in which the approximate averaging rules are not adequate. Chemkin therefore addresses both the mixture-averaged approach and the full multicomponent approach to transport properties. The TRANSPORT package is designed for use with the Chemkin Thermodynamic Database and the GAS-PHASE KINETICS utilities. The multicomponent methods are based on the work of Dixon-Lewis[21] and the methods for mixture-averaged approach are reported in Warnatz[22] and Kee, *et al*.[23]

21. G. Dixon-Lewis, *Proceedings of the Royal Society A.* **304**:111 (1968)
22. J. Warnatz, in *Numerical Methods in Flame Propagation*, edited by N. Peters and J. Warnatz Friedr. Vieweg and Sohn, Wiesbaden, 1982.

The multicomponent formulation has several important advantages over the relatively simpler mixture formulas. The first advantage is accuracy. The mixture formulas are only correct asymptotically in some special cases, such as in a binary mixture, or in diffusion of trace amounts of species into a nearly pure species, or systems in which all species except one move with nearly the same diffusion velocity.[24] A second deficiency of the mixture formulas is that overall mass conservation is not necessarily preserved when solving the species continuity equations. To compensate for this shortcoming one has to apply some *ad hoc* correction procedure.[23, p. 84, 25] The multicomponent formulation guarantees mass conservation without any correction factors, which is a clear advantage. The only real deficiency of the multicomponent formulation is its computational expense. Evaluating the ordinary multicomponent diffusion coefficients involves inverting a $K \times K$ matrix, and evaluating the thermal conductivity and thermal diffusion coefficients requires solving a $3K \times 3K$ system of algebraic equations, where K is the number of species.

To maximize computational efficiency, TRANSPORT is structured to do a large portion of the calculations in a Pre-processor that provides information to Chemkin through a Linking File. Polynomial fits are thus computed *a priori* for the temperature-dependent parts of the kinetic theory expressions for pure species viscosities and binary coefficients. (The pure species thermal conductivities are also fit, but are only used in the mixture-averaged formulation.) The coefficients from the fit are passed to subroutines in the TRANSPORT Subroutine Library, which can be used to return either mixture-averaged properties or multicomponent properties. With this fitting procedure, expensive operations, such as evaluation of collision integrals, are only done once and not every time a property value is needed.

5.1 Pure Species Viscosity and Binary Diffusion Coefficients

The single component viscosities are given by the standard kinetic theory expression,[26]

23. R. J. Kee, J. Warnatz, and J. A. Miller, *A Fortran Computer Code Package for the Evaluation of Gas-Phase Viscosities, Conductivities, and Diffusion Coefficients*, Sandia National Laboratories Report SAND83-8209, 1983.
24. R. B. Bird, W. E. Stewart, and E. N. Lightfoot, *Transport Phenomena*, John Wiley and Sons, New York, 1960.
25. T. P. Coffee and J. M. Heimerl, *Combustion and Flame* **43**:273 (1981)
26. J. O. Hirschfelder, C. F. Curtiss, and R. B. Bird, *Molecular Theory of Gases and Liquids*, John Wiley and Sons, New York, 1954.

Equation 5-1

$$\eta_k = \frac{5}{16}\frac{\sqrt{\pi m_k k_B T}}{\pi\sigma_k^2\Omega^{(2,2)*}}$$

where σ_k is the Lennard-Jones collision diameter, m_k is the molecular mass, k_B is the Boltzmann constant, and T is the temperature. The collision integral $\Omega^{(2,2)*}$ depends on the reduced temperature, given by

Equation 5-2

$$T_k^* = \frac{k_B T}{\varepsilon_k}$$

and the reduced dipole moment, given by

Equation 5-3

$$\delta_k^* = \frac{1}{2}\frac{\mu_k^2}{\varepsilon_k\sigma_k^3}$$

In the above expression ε_k is the Lennard-Jones potential well depth and μ_k is the dipole moment. The collision integral value is determined by a quadratic interpolation of the tables based on Stockmayer potentials given by Monchick and Mason.[27]

The binary diffusion coefficients[26, p. 84] are given in terms of pressure and temperature as

Equation 5-4

$$D_{kj} = \frac{3}{16}\frac{\sqrt{2\pi k_B^3 T^3/m_{jk}}}{P\pi\sigma_{jk}^2\Omega^{(1,1)*}}$$

where m_{jk} is the reduced molecular mass for the (j, k) species pair

27. L. Monchick and E. A. Mason, *Journal of Chemical Physics* **35:**1676 (1961).

Equation 5-5

$$m_{jk} = \frac{m_j m_k}{m_j + m_k}$$

and σ_{jk} is the reduced collision diameter. The collision integral $\Omega^{(1,1)*}$ (based on Stockmayer potentials) depends on the reduced temperature, T_{jk}^{*} which in turn may depend on the species dipole moments μ_k, and polarizabilities α_k. In computing the reduced quantities, we consider two cases, depending on whether the collision partners are polar or nonpolar. For the case that the partners are either both polar or both nonpolar the following expressions apply:

Equation 5-6

$$\frac{\varepsilon_{jk}}{k_B} = \sqrt{\left(\frac{\varepsilon_j}{k_B}\right)\left(\frac{\varepsilon_k}{k_B}\right)}$$

Equation 5-7

$$\sigma_{jk} = \frac{1}{2}(\sigma_j + \sigma_k)$$

Equation 5-8

$$\mu_{jk}^2 = \mu_j \mu_k$$

For the case of a polar molecule interacting with a nonpolar molecule:

Equation 5-9

$$\frac{\varepsilon_{np}}{k_B} = \xi^2 \sqrt{\left(\frac{\varepsilon_n}{k_B}\right)\left(\frac{\varepsilon_p}{k_B}\right)}$$

Equation 5-10

$$\sigma_{np} = \frac{1}{2}(\sigma_n + \sigma_p)\xi^{-\frac{1}{6}}$$

Equation 5-11

$$\mu_{np}^2 = 0$$

where,

Equation 5-12

$$\xi = 1 + \frac{1}{4}\alpha_n^* \mu_p^* \sqrt{\frac{\varepsilon_p}{\varepsilon_n}}$$

In the above equations α_n^* is the reduced polarizability for the nonpolar molecule and μ_p^* is the reduced dipole moment for the polar molecule. The reduced values are given by

Equation 5-13

$$\alpha_n^* = \frac{\alpha_n}{\sigma_n^3}$$

Equation 5-14

$$\mu_p^* = \frac{\mu_p}{\sqrt{\varepsilon_p \sigma_p^3}}$$

The table look-up evaluation of the collision integral $\Omega^{(1,1)*}$ depends on the reduced temperature

Equation 5-15

$$T_{jk}^* = \frac{k_B T}{\varepsilon_{jk}}$$

and the reduced dipole moment,

Equation 5-16

$$\delta_{jk}^* = \frac{1}{2}\mu_{jk}^{*2}$$

Although one could add a second-order correction factor to the binary diffusion coefficients[28] we have chosen to neglect this since, in the multicomponent case, we specifically need only the first approximation to the diffusion coefficients. When higher accuracy is required for the diffusion coefficients, we therefore recommend using the full multicomponent option.

28. T. R. Marrero and E. A. Mason, *J. of Phys. and Chem. Ref. Data* **1**:3 (1972).

5.2 Pure Species Thermal Conductivities

The pure species thermal conductivities are computed only for the purpose of later evaluating mixture-averaged thermal conductivities; the mixture conductivity in the multicomponent case does not depend on the pure species formula stated in this section. Here we assume the individual species conductivities to be composed of translational, rotational, and vibrational contributions as given by Warnatz.[29]

Equation 5-17

$$\lambda_k = \frac{\eta_k}{W_k}(f_{\text{trans.}}C_{\upsilon,\text{ trans.}} + f_{\text{rot.}}C_{\upsilon,\text{ rot.}} + f_{\text{vib.}}C_{\upsilon,\text{ vib.}})$$

where

Equation 5-18

$$f_{\text{trans.}} = \frac{5}{2}\left(1 - \frac{2}{\pi}\frac{C_{\upsilon,\text{ rot.}}}{C_{\upsilon,\text{ trans.}}}\frac{A}{B}\right)$$

Equation 5-19

$$f_{\text{rot.}} = \frac{\rho D_{kk}}{\eta_k}\left(1 + \frac{2}{\pi}\frac{A}{B}\right)$$

Equation 5-20

$$f_{\text{vib.}} = \frac{\rho D_{kk}}{\eta_k}$$

Equation 5-21 and,

Equation 5-22

$$A = \frac{5}{2} - \frac{\rho D_{kk}}{\eta_k}$$

29. J. Warnatz, in *Numerical Methods in Flame Propagation*, edited by N. Peters and J. Warnatz Friedr. Vieweg and Sohn, Wiesbaden, 1982.

Equation 5-23

$$B = Z_{\text{rot.}} + \frac{2}{\pi}\left(\frac{5}{3}\frac{C_{\upsilon,\text{ rot.}}}{R} + \frac{\rho D_{kk}}{\eta_k}\right)$$

The molar heat capacity C_υ relationships are different depending on whether (or not) the molecule is linear (or not). In the case of a linear molecule,

Equation 5-24

$$\frac{C_{\upsilon,\text{ trans.}}}{R} = \frac{3}{2}$$

Equation 5-25

$$\frac{C_{\upsilon,\text{ rot.}}}{R} = 1$$

Equation 5-26

$$C_{\upsilon,\text{ vib.}} = C_\upsilon - \frac{5}{2}R$$

In the above, C_υ is the specific heat at constant volume of the molecule and R is the universal gas constant. For the case of a nonlinear molecule,

Equation 5-27

$$\frac{C_{\upsilon,\text{ trans.}}}{R} = \frac{3}{2}$$

Equation 5-28

$$\frac{C_{\upsilon,\text{ rot.}}}{R} = \frac{3}{2}$$

Equation 5-29

$$C_{\upsilon,\text{ vib.}} = C_\upsilon - 3R$$

The translational part of C_υ is always the same,

Equation 5-30

$$C_{\upsilon,\text{ trans.}} = \frac{3}{2}R$$

In the case of single atoms (H atoms, for example) there are no internal contributions to C_υ, and hence,

Equation 5-31

$$\lambda_k = \frac{\eta_k}{W_k}\left(f_{\text{trans.}}\frac{3}{2}R\right)$$

where $f_{\text{trans.}} = 5/2$. The “self-diffusion” coefficient comes from the following expression,

Equation 5-32

$$D_{kk} = \frac{3}{8}\frac{\sqrt{\pi k_B^3 T^3/m_k}}{P\pi\sigma_k^2\Omega^{(1,1)*}}$$

The density comes from the equation of state for an ideal gas,

Equation 5-33

$$\rho = \frac{PW_k}{RT}$$

with P being the pressure and W_k the species molecular weight.

The rotational relaxation collision number is a parameter that we assume is available at 298 K (included in the database). It has a temperature dependence given in an expression by Parker[30] and Brau and Jonkman,[31]

Equation 5-34

$$Z_{\text{rot.}}(T) = Z_{\text{rot.}}(298)\frac{F(298)}{F(T)}$$

where,

Equation 5-35

$$F(T) = 1 + \frac{\pi^{\frac{3}{2}}}{2}\left(\frac{\varepsilon/k_B}{T}\right)^{\frac{1}{2}} + \left(\frac{\pi^2}{4}+2\right)\left(\frac{\varepsilon/k_B}{T}\right) + \pi^{\frac{3}{2}}\left(\frac{\varepsilon/k_B}{T}\right)^{\frac{3}{2}}$$

30. J. G. Parker, *Physics of Fluids* **2**:449 (1959).
31. C. C. Brau and R. M. Jonkman, *Journal of Chemical Physics* **52**:447 (1970).

5.3 The Pure Species Fitting Procedure

To expedite the evaluation of transport properties in Chemkin, we fit the temperature dependent parts of the pure species property expressions. Then, rather than evaluating the complex expressions for the properties, only comparatively simple fits need to be evaluated.

We use a polynomial fit of the logarithm of the property versus the logarithm of the temperature. For the viscosity

Equation 5-36

$$\ln \eta_k = \sum_{n=1}^{N} a_{n,k} (\ln T)^{n-1}$$

and the thermal conductivity,

Equation 5-37

$$\ln \lambda_k = \sum_{n=1}^{N} b_{n,k} (\ln T)^{n-1}$$

The fits are done for each pair of binary diffusion coefficients in the system.

Equation 5-38

$$\ln D_{kj} = \sum_{n=1}^{N} d_{n,jk} (\ln T)^{n-1}$$

By default TRANSPORT uses third-order polynomial fits (i.e., $N = 4$) and we find that the fitting errors are well within one percent. The fitting procedure must be carried out for the particular system of gases that is present in a given problem. Therefore, the fitting cannot be done “once and for all,” but must be done once at the beginning of each new problem.

The viscosity and conductivity are independent of pressure, but the diffusion coefficients depend inversely on pressure. The diffusion coefficient fits are computed at unit pressure; the later evaluation of a diffusion coefficient is obtained by simply dividing the diffusion coefficient as evaluated from the fit by the actual pressure.

Even though the single component conductivities are fit and passed to the TRANSPORT Subroutine Library, they are not used in the computation of multicomponent thermal conductivities; they are used only for the evaluation of the mixture-averaged conductivities.

5.4 The Mass, Momentum, and Energy Fluxes

The momentum flux is related to the gas mixture viscosity and the velocities by

Equation 5-39

$$\tau = -\eta(\nabla v + (\nabla v)^{\mathrm{T}}) + \left(\frac{2}{3}\eta - \kappa\right)(\nabla \cdot v)\hat{\delta}$$

where v is the velocity vector, ∇v is the dyadic product, $(\nabla v)^{\mathrm{T}}$ is the transpose of the dyadic product, and $\hat{\delta}$ is the unit tensor.[24, p. 84] The Chemkin TRANSPORT package provides average values for the mixture viscosity, η, but no information on the bulk viscosity, κ.

The energy flux is given in terms of the thermal conductivity λ_0 by

Equation 5-40

$$\mathbf{q} = \sum_{k=1}^{K} \mathbf{j}_k h_k - \lambda_0 \nabla T - \sum_{k=1}^{K} \frac{RT}{W_k X_k} D_k{}^T \mathbf{d}_k$$

where,

Equation 5-41

$$\mathbf{d}_k = \nabla X_k + (X_k - Y_k)\frac{1}{P}\nabla P$$

The multicomponent species flux is given by

Equation 5-42

$$\mathbf{j}_k = \rho Y_k V_k$$

where Y_k are the mass fractions and the diffusion velocities are given by

Equation 5-43

$$\mathbf{V}_k = \frac{1}{X_k \overline{W}} \sum_{j \neq k}^{K} W_j D_{k,j} \mathbf{d}_j - \frac{D_k^T}{\rho Y_k} \frac{1}{T} \nabla T$$

The species molar masses are denoted by W_k and the mean molar mass by $\overline{W}$. $D_{k,j}$ are the ordinary multicomponent diffusion coefficients, and D_k^T are the thermal diffusion coefficients.

By definition in the mixture-average formulations, the diffusion velocity is related to the species gradients by a Fickian formula as,

Equation 5-44

$$\mathbf{V}_k = -\frac{1}{X_k} D_{km} \mathbf{d}_k - \frac{D_k^T}{\rho Y_k} \frac{1}{T} \nabla T$$

The mixture diffusion coefficient for species k is computed as[32]

Equation 5-45

$$D_{km} = \frac{1 - Y_k}{\sum_{j \neq k}^{K} X_j / D_{jk}}$$

A potential problem with this expression is that it is not mathematically well defined in the limit of the mixture becoming a pure species. Even though diffusion itself has no real meaning in the case of a pure species, the numerical implementation must ensure that the diffusion coefficients behave reasonably and that the program does not “blow up” when the pure species condition is reached. We circumvent these problems by evaluating the diffusion coefficients in the following equivalent way.

Equation 5-46

$$D_{km} = \frac{\sum_{j \neq k}^{K} X_j W_j}{\overline{W} \sum_{j \neq k}^{K} X_j / D_{jk}}$$

In this form the roundoff is accumulated in roughly the same way in both the numerator and denominator, and thus the quotient is well behaved as the pure species limit is approached. However, if the mixture is exactly a pure species, the formula is still undefined.

32. R. B. Bird, W. E. Stewart, and E. N. Lightfoot, *Transport Phenomena*, John Wiley and Sons, New York, 1960.

To overcome this difficulty we always retain a small quantity of each species. In other words, for the purposes of computing mixture diffusion coefficients, we simply do not allow a pure species situation to occur; we always maintain a residual amount of each species. Specifically, we assume in the above formulas that

Equation 5-47

$$X_k = \hat{X}_k + \varepsilon$$

where $\hat{X}_k$ is the actual mole fraction and ε is a small number that is numerically insignificant compared to any mole fraction of interest, yet which is large enough that there is no trouble representing it on any computer. A value of 10^{-12} for ε works well.

In some cases (for example, Warnatz[33] and Coltrin, *et al*.[34]) it can be useful to treat multicomponent diffusion in terms of an equivalent Fickian diffusion process. This is sometimes a programming convenience in that the computer data structure for the multicomponent process can be made to look like a Fickian process. To do so supposes that a mixture diffusion coefficient can be defined in such a way that the diffusion velocity is written as *Equation 5-44* rather than *Equation 5-43*. This equivalent Fickian diffusion coefficient is then derived by equating *Equation 5-43* and *Equation 5-44* and solving for D_{km} as

Equation 5-48

$$D_{km} = -\frac{\sum_{j \neq k}^{K} W_j D_{k,j} \mathbf{d}_j}{\overline{W} \mathbf{d}_k}$$

Unfortunately, this equation is undefined as the mixture approaches a pure species condition. To help deal with this difficulty a small number ($\varepsilon = 10^{-12}$) may be added to both the numerator and denominator to obtain

Equation 5-49

$$D_{km} = -\frac{\sum_{j \neq k}^{K} W_j D_{kj} \mathbf{d}_j + \varepsilon}{\overline{W}(\mathbf{d}_k + \varepsilon)}$$

Furthermore, for the purposes of evaluating the "multicomponent" D_{km}, it may be advantageous to compute the $\mathbf{d}_k$ in the denominator using the fact that $\nabla X_k = -\sum_{j \neq k}^{K} \nabla X_j$. In this way the summations in the numerator and the denominator accumulate any rounding errors in roughly the same way, and thus the

33. J. Warnatz, *Ber. Bunsenges. Phys. Chem.* **82**:193 (1978).
34. M. E. Coltrin, R. J. Kee, and J. A. Miller, *Journal of the Electrochemical Society* **133**:1206 (1986).

quotient is more likely to be well behaved as the pure species limit is approached. Since there is no diffusion due to species gradients in a pure species situation, the exact value of the diffusion coefficient is not as important as the need for it to be well defined, and thus not cause computational difficulties.

In practice we have found mixed results using the equivalent Fickian diffusion to represent multicomponent processes. In some marching or parabolic problems, such as boundary-layer flow in channels,[34, p. 94] we find that the equivalent Fickian formulation is preferable. However, in some steady state boundary value problems, we have found that the equivalent Fickian formulation fails to converge, whereas the regular multicomponent formulation works quite well. Thus, we cannot confidently recommend which formulation should be preferred for any given application.

5.5 The Mixture-averaged Properties

Our objective in this section is to determine mixture properties from the pure species properties. In the case of viscosity, we use the semi-empirical formula due to Wilke[35] and modified by Bird, et al.[24, p. 84] The Wilke formula for mixture viscosity is given by

Equation 5-50

$$\eta = \sum_{k=1}^{K} \frac{X_k \eta_k}{\sum_{j=1}^{K} X_j \Phi_{kj}}$$

where

Equation 5-51

$$\Phi_{Kj} = \frac{1}{\sqrt{8}}\left(1 + \frac{W_k}{W_j}\right)^{-\frac{1}{2}}\left(1 + \left(\frac{\eta_k}{\eta_j}\right)^{\frac{1}{2}}\left(\frac{W_j}{W_k}\right)^{\frac{1}{4}}\right)^2$$

for the mixture-averaged thermal conductivity we use a combination averaging formula[36]

35. C. R. Wilke, *Journal of Chemical Physics* **18**:517 (1950).
36. S. Mathur, P. K. Tondon, and S. C. Saxena, *Molecular Physics* **12**:569 (1967).

Equation 5-52

$$\lambda = \frac{1}{2}\left(\sum_{k=1}^{K} X_k \lambda_k + \frac{1}{\sum_{k=1}^{K} X_k / \lambda_k}\right)$$

5.6 Thermal Diffusion Ratios

The thermal diffusion coefficients are evaluated in the following section on multicomponent properties. This section describes a relatively inexpensive way to estimate the thermal diffusion of light species into a mixture. This method is included here for the sake of backward compatibility. However, this approximate method is considerably less accurate than the thermal diffusion coefficients that are computed from the multicomponent formulation. It is therefore recommended that users employ the multicomponent formulation when thermal diffusion is likely to be important.

A thermal diffusion ratio Θ_k can be defined such that the thermal diffusion velocity W_k is given by

Equation 5-53

$$W_{ki} = -\frac{D_{km}\Theta_k}{X_k}\frac{1}{T}\frac{\partial T}{\partial x_i}$$

where x_i is a spatial coordinate. The mole fractions are given by X_k, and the D_{km} are mixture diffusion coefficients *Equation 5-44*. In this form we only consider thermal diffusion in the trace, light component limit (specifically, species k having molecular mass less than 5). The thermal diffusion ratio[37] is given by

Equation 5-54

$$\Theta_k = \sum_{j \neq k}^{K} \theta_{kj}$$

where

37. S. Chapman and T. G. Cowling, *The Mathematical Theory of Non-Uniform Gases* Cambridge University Press, Cambridge, 1970.

Equation 5-55

$$\theta_{kj} = \frac{15}{2}\frac{(2A^*_{kj}+5)(6C^*_{kj}-5)}{A^*_{kj}(16A^*_{kj}-12B^*_{kj}+55)}\frac{W_k - W_j}{W_k + W_j}X_k X_j$$

Three ratios of collision integrals are defined by

Equation 5-56

$$A^*_{ij} = \frac{1}{2}\frac{\Omega^{(2,2)}_{ij}}{\Omega^{(1,1)}_{ij}}$$

Equation 5-57

$$B^*_{ij} = \frac{1}{3}\frac{5\Omega^{(1,2)}_{ij} - \Omega^{(1,3)}_{ij}}{\Omega^{(1,1)}_{ij}}$$

Equation 5-58

$$C^*_{ij} = \frac{1}{3}\frac{\Omega^{(1,2)}_{ij}}{\Omega^{(1,1)}_{ij}}$$

We have fit polynomials to tables of A^*_{ij}, B^*_{ij}, and C^*_{ij}.[27, p. 85]

In the TRANSPORT Pre-processor (where the pure species properties are fit) we also fit the temperature dependent parts of the pairs of the thermal diffusion ratios for each light species diffusing into all the other species. That is, we fit $\theta_{kj}/(X_j X_k)$ for all species pairs in which $W_k < 5$. Since the θ_{kj} depend weakly on temperature, we fit to polynomials in temperature, rather than the logarithm of temperature. The coefficients of these fits are written onto the TRANSPORT Linking File.

5.7 The Multicomponent Properties

The multicomponent diffusion coefficients, thermal conductivities, and thermal diffusion coefficients are computed from the solution of a system of equations defined by what we call the L matrix[38]. It is convenient to refer to the L matrix in terms of its nine block sub-matrices, and in this form the system is given by

38. Dixon-Lewis, Proceedings of the Royal Society A. 304:111 (1968).

Equation 5-59

$$\begin{pmatrix} L^{00,00} & L^{00,10} & 0 \\ L^{10,00} & L^{10,10} & L^{10,01} \\ 0 & L^{01,10} & L^{01,01} \end{pmatrix} \begin{pmatrix} a^1_{00} \\ a^1_{10} \\ a^1_{01} \end{pmatrix} = \begin{pmatrix} 0 \\ X \\ X \end{pmatrix}$$

where the right-hand side vector is composed of the mole fraction vectors X_k. The multicomponent diffusion coefficients are given in terms of the inverse of the $L^{00,00}$ block as

Equation 5-60

$$D_{i,j} = X_i \frac{16}{25} \frac{T}{P} \frac{\overline{W}}{W_j} (p_{ij} - p_{ii})$$

where

Equation 5-61

$$(p) = (L^{00,00^{-1}})$$

The thermal conductivities are given in terms of the solution to the system of equations by

Equation 5-62

$$\lambda_{0,\text{tr.}} = -4 \sum_{k=1}^{K} X_k a^1_{k10}$$

Equation 5-63

$$\lambda_{0,\text{int.}} = -4 \sum_{k=1}^{K} X_k a^1_{k01}$$

Equation 5-64

$$\lambda_0 = \lambda_{0,\text{tr.}} + \lambda_{0,\text{int.}}$$

and the thermal diffusion coefficients are given by

Equation 5-65

$$D_k^T = \frac{8 m_k X_k}{5R} a_{k00}^1$$

The components of the L matrix are given by Dixon-Lewis,[21, p. 83]

Equation 5-66

$$L_{ij}^{00,00} = \frac{16T}{25P} \sum_{k=1}^{K} \frac{X_k}{m_i D_{ik}} \{ m_j X_j (1 - \delta_{ik}) - m_i X_j (\delta_{ij} - \delta_{jk}) \}$$

Equation 5-67

$$L_{ij}^{00,10} = \frac{8T}{5P} \sum_{k=1}^{K} X_j X_k (\delta_{ij} - \delta_{ik}) \frac{m_k (1.2 C_{jk}^* - 1)}{(m_j + m_k) D_{jk}}$$

Equation 5-68

$$L_{ij}^{10,00} = L_{ji}^{00,10}$$

Equation 5-69

$$L_{ij}^{01,00} = L_{ji}^{00,01} = 0$$

Equation 5-70

$$L_{ij}^{10,10} = \frac{16T}{25P} \sum_{k=1}^{K} \frac{m_i}{m_j} \frac{X_i X_k}{(m_i + m_k)^2 D_{jk}} \times \left\{ (\delta_{jk} - \delta_{ij}) \left[\frac{15}{2} m_j^2 + \frac{25}{4} m_k^2 - 3 m_k^2 B_{ik}^* \right] - 4 m_i m_k A_{ik}^* (\delta_{jk} + \delta_{ij}) \left[1 + \frac{5}{3\pi} \left(\frac{c_{i,\text{rot.}}}{k_B \xi_{ik}} + \frac{c_{k,\text{rot.}}}{k_B \xi_{ki}} \right) \right] \right\}$$

Equation 5-71

$$L_{ii}^{10,10} = -\frac{16 m_i X_i^2}{R \eta_i} \left(1 + \frac{10 c_{i,\text{rot.}}}{k_B \xi_{ii}} \right) - \frac{16T}{25P} \sum_{k \neq i}^{K} \frac{X_i X_k}{(m_i + m_k)^2 D_{ik}} \times \left\{ \frac{15}{2} m_i^2 + \frac{25}{4} m_k^2 - 3 m_k^2 B_{ik}^* + 4 m_i m_k A_{ik}^* \times \left[1 + \frac{5}{3\pi} \left(\frac{c_{i,\text{rot.}}}{k_B \xi_{ik}} + \frac{c_{k,\text{rot.}}}{k_B \xi_{ki}} \right) \right] \right\}$$

Equation 5-72

$$L_{ij}^{10,01} = \frac{32T}{5\pi P c_{j,\,\mathrm{int.}}} \sum_{k=1}^{K} \frac{m_j A_{jk}^*}{(m_j + m_k) D_{jk}} (\delta_{ik} + \delta_{ij}) X_j X_k \frac{c_{j,\,\mathrm{rot.}}}{k_B \xi_{jk}}$$

Equation 5-73

$$L_{ii}^{10,01} = \frac{16}{3\pi R} \frac{m_i X_i^2 k_B}{\eta_i c_{i,\,\mathrm{int.}}} \frac{c_{i,\,\mathrm{int.}}}{k_B \xi_{ii}} + \frac{32 T k_B}{5\pi P c_{i,\,\mathrm{int.}}} \sum_{k \neq i}^{K} \frac{m_i A_{ik}^*}{(m_i + m_k) D_{ik}} X_i X_k \frac{c_{i,\,\mathrm{rot.}}}{k_B \xi_{ik}}$$

Equation 5-74

$$L_{ij}^{01,10} = L_{ji}^{10,01}$$

Equation 5-75

$$L_{ii}^{01,10} = -\frac{8 k_B^k}{\pi c_{i,\,\mathrm{int.}}^2} \frac{m_i X_i^2}{R \eta_i} \frac{c_{i,\,\mathrm{rot.}}}{k_B \xi_{ii}} - \frac{4 k_B T}{c_{i,\,\mathrm{int.}} P} \left\{ \sum_{k=1}^{K} \frac{X_i X_k}{D_{i\mathrm{int.},\,k}} + \sum_{k \neq i}^{K} \frac{12 X_i X_k}{5\pi c_{i\mathrm{int.}}} \frac{m_i}{m_k} \frac{A_{ik}^*}{D_{ik}} \frac{c_{i\mathrm{rot.}}}{\xi_{ii}} \right\}$$

Equation 5-76

$$L_{ij}^{01,01} = 0 (i \neq j)$$

In these equations T is the temperature, P is the pressure, X_k is the mole fraction of species k, D_{ik} are the binary diffusion coefficients, and m_i is the molecular mass of species i. Three ratios of collision integrals A_{jk}^*, B_{jk}^*, and C_{jk}^* are defined by *Equation 5-56* through *Equation 5-58*. The universal gas constant is represented by R and the pure species viscosities are given as η_k. The rotational and internal parts of the species molecular heat capacities are represented by $c_{k,\,\mathrm{rot.}}$ and $c_{k,\,\mathrm{int.}}$. For a linear molecule

Equation 5-77

$$\frac{c_{k,\,\mathrm{rot.}}}{k_B} = 1$$

and for a nonlinear molecule

Equation 5-78

$$\frac{c_{k,\,\mathrm{rot.}}}{k_B} = \frac{3}{2}$$

The internal component of heat capacity is computed by subtracting the translational part from the full heat capacity as evaluated from the Chemkin Thermodynamic Database.

Equation 5-79

$$\frac{c_{k,\,\mathrm{int.}}}{k_B} = \frac{c_p}{k_B} - \frac{3}{2}$$

Following Dixon-Lewis,[21, p. 83] we assume that the relaxation collision numbers ξ_{ij} depend only on the species i, i.e., all $\xi_{ij} = \xi_{ii}$. The rotational relaxation collision number at 298 K is one of the parameters in the TRANSPORT database, and its temperature dependence was given in *Equation 5-34* and *Equation 5-35*.

For non-polar gases the binary diffusion coefficients for internal energy $D_{i\mathrm{int.},\,k}$ are approximated by the ordinary binary diffusion coefficients. However, in the case of collisions between polar molecules, where the exchange is energetically resonant, a large correction of the following form is necessary,

Equation 5-80

$$D_{p\mathrm{int.},\,p} = \frac{D_{pp}}{(1 + \delta'_{pp})}$$

Equation 5-81

$$\delta'_{pp} = \frac{2985}{\sqrt{T^3}}$$

when the temperature is in Kelvins.

There are some special cases that require modification of the L matrix. First, for mixtures containing monatomic gases, the rows that refer to the monatomic components in the lower block row and the corresponding columns in the last block column must be omitted. This is apparent by noting that the internal part of the heat capacity appears in the denominator of terms in these rows and columns (e.g., $L_{ij}^{10,\,01}$). An additional problem arises as a pure species situation is approached, because all X_k, except one, approach zero, and this causes the L matrix to become singular. Therefore, for the purposes of forming the L matrix, a pure species situation is not allowed to occur. We always retain a residual amount of each species by computing the mole fractions from

Equation 5-82

$$X_k = \frac{\overline{W} Y_k}{W_k} + \varepsilon$$

A value of $\varepsilon = 10^{-12}$ works well; it is small enough to be numerically insignificant compared to any mole fraction of interest, yet it is large enough to be represented on nearly any computer.

5.8 Species Conservation

Some care needs to be taken in using the mixture-averaged diffusion coefficients as described here. The mixture formulae are approximations, and they are not constrained to require that the net species diffusion flux is zero, i.e., the condition,

Equation 5-83

$$\sum_{k=1}^{K} \mathbf{V}_k Y_k = 0$$

is not automatically satisfied. Therefore, applying these mixture diffusion relationships in the solution of a system of species conservation equations may lead to some nonconservation, i.e., the resultant mass fractions will not sum to one. Therefore, one of a number of corrective actions must be invoked to ensure mass conservation. These corrections are implemented within Chemkin.

One attractive method is to define a “conservation diffusion velocity” as Coffee and Heimerl[39] recommend. In this approach we assume that the diffusion velocity vector is given as

39. T. P. Coffee and J. M. Heimerl, *Combustion and Flame* **43**:273 (1981).

Equation 5-84

$$\mathbf{V}_k = \hat{\mathbf{V}}_k + \mathbf{V}_c$$

where $\hat{\mathbf{V}}_k$ is the ordinary diffusion velocity *Equation 5-44* and $\mathbf{V}_c$ is a constant correction factor (independent of species, but spatially varying) introduced to satisfy *Equation 5-83*. The correction velocity is defined by

Equation 5-85

$$\mathbf{V}_c = -\sum_{k=1}^{K} Y_k \hat{\mathbf{V}}_k$$

This approach is the one used in OPPDIF, for example.

An alternative approach is attractive in problems having one species that is always present in excess. Here, rather than solving a conservation equation for the one excess species, its mass fraction is computed simply by subtracting the sum of the remaining mass fractions from unity. A similar approach involves determining locally at each computational cell which species is in excess. The diffusion velocity for that species is computed to require satisfaction of *Equation 5-83*. Chemkin includes both this trace-species approach and the correction-velocity approach as user options.

Even though the multicomponent formulation is theoretically forced to conserve mass, the numerical implementations can cause some slight nonconservation. Depending on the numerical method, even slight inconsistencies can lead to difficulties. Methods that do a good job of controlling numerical errors, such as the differential/algebraic equation solver DASSL,[40] for example, are especially sensitive to inconsistencies, and can suffer computational inefficiencies or convergence failures if mass is not strictly conserved. Therefore, even when the multicomponent formulation is used, it is often advisable to provide corrective measures such as those described above for the mixture-averaged approach. In the case of multicomponent formulations, however, the magnitude of any such corrections will be significantly smaller.

40. Petzold, L. R., “A description of DASSL: a differential/algebraic system solver,” Sandia National Laboratories Report SAND82-8637, (1982).

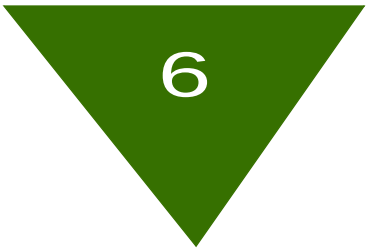

6 Determining Chemical Equilibria

In addition to chemically reacting flow applications, Chemkin includes an Equilibrium Reactor model. This model allows users to determine the chemical state of a mixture under equilibrium conditions. Any number of gas-phase or condensed (bulk) species can be included in an equilibrium calculation, while surface site species are ignored. In this way, the Equilibrium Reactor model can be used to determine phase equilibrium, between gas and condensed phases, as well as chemical equilibrium. All that is required is thermodynamic data for all species in each phase.

An established method for evaluating chemical equilibrium is the element-potential method embodied in the Stanford software STANJAN.[41] The Chemkin Equilibrium Reactor employs the STANJAN library of routines in it's solution method. The equilibrium determines composition equilibrium and/or phase equilibrium. The results depend only on the thermodynamic properties of the species in the user's chemistry set, as well as the starting composition and conditions specified. The starting composition determines the relative amount of chemical elements in the system. An initial estimate of the equilibrium temperature can sometimes be used to select a "burned" equilibrium state from an "unburned" equilibrium state in the case where two equilibrium states are possible.

Currently, the equilibrium program assumes that the gas-phase is a mixture of ideal gases and that condensed phases are ideal solutions. The user selects atomic populations through identity of initial species and their fraction in each phase, as well as the state parameters.

41. W. C. Reynolds, *The Element Potential Method for Chemical Equilibrium Analysis: Implementation in the Interactive Program STANJAN*, Department of Mechanical Engineering, Stanford University (1986).

The user may specify the state parameters in a number of different ways, including

a. temperature and pressure;
b. pressure and entropy;
c. enthalpy and pressure; and
d. volume and entropy.

Species composition can be “frozen” in a given calculation, or the equilibrium composition can be determined. Calculations may be linked through continuations, such that the conditions calculated from a previous equilibrium case can be used as the starting point for a subsequent case with different constraints. In this way, the user can employ the Equilibrium Reactor Model to analyze stages in a thermodynamic cycle.

The Equilibrium Reactor Model is also commonly used to determine adiabatic flame temperatures for combustible gas mixtures. Such a simulation is performed by specifying an initial (reagent) gas mixture and constraining equilibrium for constant enthalpy (adiabatic) and constant pressure. The calculation can also be performed using constant internal energy and constant volume. An initial guess for the equilibrium temperature of ~1000 K or above is usually needed to cause the equilibrium solver to find the burned-gas solution. For accurate adiabatic-flame temperature calculations, it is important to include all radical species that might occur in the flame, as well as stable reactants and products.

In the remainder of this chapter, we describe the equations solved and the methodology used for determining chemical and phase equilibria of arbitrary systems.

6.1 Minimization of Gibb’s Free Energy

The basic theory for the element-potential method of determining equilibrium is based on the minimization of Gibb’s free energy. The Gibb’s function of a system is:

Equation 6-1

$$G = \sum_{k=1}^{K} \bar{g}_k N_k$$

where $\bar{g}_k$ is the partial molal Gibb’s function and N_k is the number of moles of each species k in the system. K is the total number of species.

For ideal-gas mixtures or ideal solutions, the partial molal Gibb's functions are given by:

Equation 6-2

$$\bar{g}_k = g_k(T,P) + RT\ln X_k$$

where $g_k(T,P)$ is the Gibb's function for the pure species k, evaluated at the system temperature and pressure; R is the universal gas constant; and X_k is the mole fraction of the *k*th species.

The equilibrium solution at a given temperature and pressure is the distribution of N_k that minimizes the system Gibb's function, G, subject to atomic population constraints (and non-negative N_k). The atomic population constraints are:

Equation 6-3

$$\sum_{k=1}^{K} n_{jk}N_k = p_j \qquad j = 1, \ldots, M$$

where n_{jk} is the number of the *j*th atoms that appear in the *k*th molecule, is the total population in moles of the *j*th atom in the system, and M is the total number of different elements that are present in the system.

Details regarding the relationship between the partial molar Gibb's functions and the elemental potentials for the atoms, as well as the explicit form of the equations solved in the STANJAN library, are described in the STANJAN report.[41, p. 105]

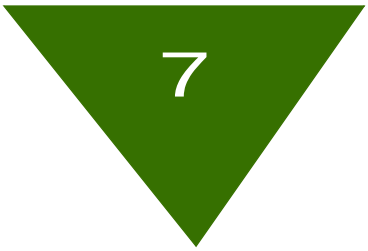

7 Normal Shock Equations

Although most Chemkin Reactor Models are concerned with sub-sonic flows, the Shock Reactor Model is used to simulate chemical kinetics behind a normal incident or reflected shock. A common use of the Shock Reactor Model is to simulate the behavior of a shock tube experiment for studying reaction kinetics. This model may also be used to look at reactions that occur behind a bow shock for a supersonic vehicle. In order to follow the evolution of chemical species after a shock has passed over, it is first important to determine the post-shock conditions. The initial conditions behind a shock wave are related to conditions in front of the shock by gas-dynamic relations that depend on the thermodynamic properties of the gas mixture.

In this chapter we introduce the gas-dynamic equations that are solved within the Shock Reactor Model. There are several options for specifying the shock conditions, which are described in *Section 7.1*. *Section 7.2* describes the gas-dynamic equations used to determine the conditions immediately behind a shock, while *Section 7.3* discusses the equations that are then solved to track the thermochemical state of the system as a function of time or distance after the shock has passed.

7.1 Shock Tube Experiments

The shock tube has found widespread use as an experimental device in which to investigate chemical kinetic behavior in reactive gas mixtures. Much can be learned by experiment alone, however such investigations are enhanced considerably when done in concert with computer simulations. To this end, the Shock Reactor Model simulates the chemical changes that occur after the shock heating of a reactive gas mixture. The Shock Reactor Model is designed to account for both incident and reflected normal shock waves. It makes allowances for the non-perfect gas behavior, boundary-layer effects and detailed finite-rate chemistry.

SHOCK provides flexibility in describing a wide variety of experimental conditions. Often people who perform shock tube experiments report their experimental conditions differently. The Shock Reactor Model allows input of these different conditions directly, without requiring hand calculations to prepare the input. The Shock Reactor Model works together with the GAS-PHASE KINETICS package.

The input options to the Shock Reactor Model coincide with the parameters most likely to be measured in shock tube experiments. For incident shock cases, the incident shock velocity and any two of the density, temperature and pressure, either before or behind the shock, can be specified. For reflected shocks, any two of the density, temperature and pressure behind the shock can be specified or conditions for the incident shock can be given. If the reflected shock velocity is specified, it is used in determining the temperature and pressure of the gas mixture behind the shock. Otherwise, the application determines that reflected shock velocity (and associated temperature and pressure), which renders the gas behind the shock at rest. Whenever gas conditions before the shock are given, the Shock Reactor Model calculates conditions behind the shock from the Rankine-Hugoniot equations using real gas thermodynamic properties for the test gas mixture.

A shock tube is a device in which a gas at high pressure (the driver gas) is initially separated from a gas at lower pressure (the test gas) by a diaphragm. When the diaphragm is suddenly burst, a plane shock wave propagates through the test gas raising it to new temperature and pressure levels. At the elevated temperature and pressure, chemical reaction commences. As the shock wave moves through the test gas, a rarefaction wave moves back into the high-pressure gas at the speed of sound. The test gas and the driver gas make contact at the “contact surface, which moves along the tube behind the shock front. Conventional notation represents the conditions in the unperturbed, low-pressure test gas by the subscript $_1$, so that the initial temperature and pressure in this region are denoted as p_1 and T_1, respectively. The region between the shock front and the contact surface is denoted by subscript $_2$; the region between the contact surface and the rarefaction wave by subscript $_3$. The initial conditions on the high-pressure side are given the subscript $_4$. If the shock wave is allowed to undergo reflection at the end of the tube, the pressure conditions in this region are given the subscript $_5$. *Figure 7-1* shows the ideal movement of the shock front, the contact surface, the rarefaction wave and the reflected shock wave in a distance-time diagram.

Figure 7-1 A distance-time diagram of a shock experiment

A distance-time diagram shows the movements of the shock front, contact surface, rarefaction wave, and reflected shock wave

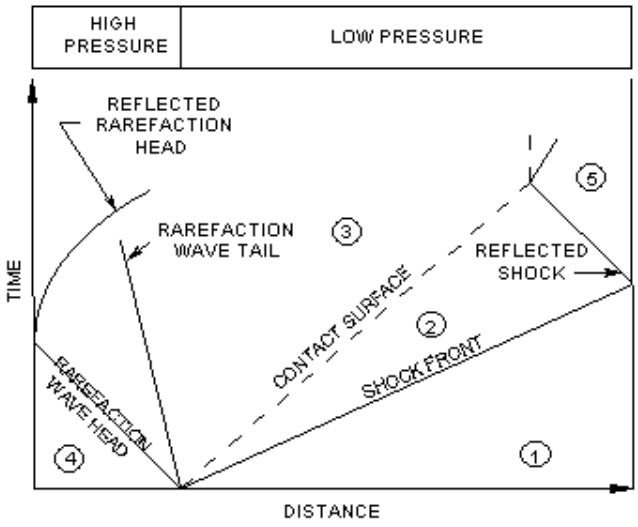

7.2 Rankine-Hugoniot Relations for Normal Shocks

Before tracking the species evolution behind the shock, the Shock Reactor Model first determines the initial conditions immediately behind the shock, using gas-dynamic relations. There are different relations employed for incident and for reflected shocks. To facilitate the discussion, we first familiarize the reader with the two time-frames that are relevant to this system: the shock tube “laboratory” time-frame and the gas “particle” time-frame. Understanding the relationships between these two time-frames is important to the interpretation of experimental data and application of the gas-dynamic equations.

7.2.1 Shock Tube Laboratory Time and Gas-particle Time

The experimentalist records changes in the test gas conditions (be it pressure, temperature, density or species concentration) after passage of the shock at some observation point. The time recorded on some external recording device is referred to as the laboratory time, t_l. Since the test gas is flowing however, it has been at the post-shock conditions for some time longer than the laboratory time. This longer time is referred to as the gas-particle time, t_p and is the time of interest with respect to rate processes in the test gas. A relationship between t_l and t_p can be derived. To do so, begin by considering the distance-time diagram in *Figure 7-2*. When the shock arrives at the observation point, measurements are made on the test gas for a period Δt_l. The test gas has been at the shock-heated conditions for a time Δt_p and has traveled a distance Δz since being shocked. The time that it took the shock wave to travel this same distance is $(\Delta t_p - \Delta t_l)$.

Hence, from the relationship between distance and time

Equation 7-1

$$\Delta z = U_s(\Delta t_p - \Delta t_l) = U\Delta t_p$$

Figure 7-2 Laboratory and gas-particle times

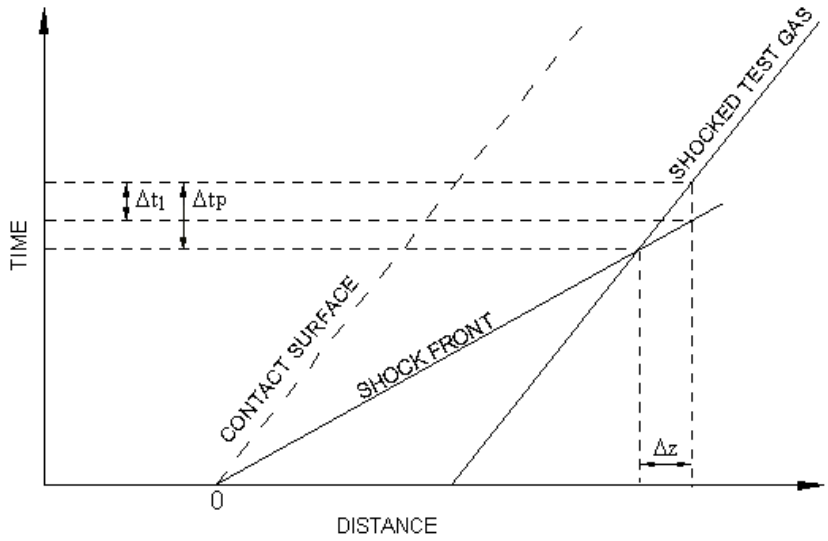

Taking the limit as Δz approaches zero results in the following ordinary differential equation relating gas particle and laboratory times:

Equation 7-2

$$\frac{dt_l}{dt_p} = 1 - \frac{U}{U_s}$$

For mass continuity across the shock wave, it can be shown that

Equation 7-3

$$\rho_1 A_1 / \rho A = 1 - U/U_s$$

and, therefore, *Equation 7-2* can be written as

Equation 7-4

$$\frac{dt_l}{dt_p} = \rho_1 A_1 / \rho A$$

Thus, when rate processes are measured, the time as measured must be multiplied by the density-area ratio across the shock to obtain the true rate referred to the test gas. In the Shock Reactor Model, *Equation 7-4* is integrated along with the other ordinary differential equations (ODEs) presented in *Section 7.3*, so that laboratory time as a function of gas-particle time is available. The Shock Reactor Model solves the coupled set of ODEs for either an incident or reflected shock problem.

The initial time for a problem, $t_p = 0$, is taken as the time immediately after the shock wave has elevated the test gas to new levels of temperature and pressure. The incident shock wave is assumed to instantaneously raise the test gas from initial conditions 1 to conditions 2; the reflected shock is assumed to instantaneously raise the test gas from conditions 2 to conditions 5. Gas composition immediately after passage of the shock is assumed to remain unchanged from the initial conditions. Vibrational and rotational energy relaxation processes are neglected.

7.2.2 Incident Shock Initial Conditions

In relating the pressures, temperatures and densities immediately across the shock, it is conventional to consider the gas motion in relation to the shock front. In such a frame of reference, the gas enters the shock at a relative velocity u_1, and leaves with a relative velocity u_2. In shock tube jargon, the shock is then considered to be at rest; u is the gas velocity measured in shock-fixed coordinates and U is that measured in laboratory-fixed coordinates. These two frames of reference are related by:

Equation 7-5

$$u_1 = U_s$$

Equation 7-6

$$u_2 = U_s - U_2$$

where U_s is the shock velocity. Gas conditions associated with the incident shock in the two coordinate systems are shown in *Figure 7-3*. The Rankine-Hugoniot relations for properties across the incident shock front are

Equation 7-7

$$\rho_1 u_1 = \rho_2 u_2$$

Equation 7-8

$$P_1 + \rho_1 u_1^2 = P_2 + \rho_2 u_2^2$$

Equation 7-9

$$h_1 + u_1^2/2 = h_2 + u_2^2/2$$

Utilizing the equation of state (Ideal Gas Law) and *Equation 7-7* to eliminate the velocity u_2 and ρ_2 from *Equation 7-8* and *Equation 7-9* results in the following expressions for the pressure and temperature ratios across the incident shock:

Equation 7-10

$$1 + \rho_1 u_1^2/P_1[1 - (T_2/T_1)(P_1/P_2)] - P_2/P_1 = 0$$

Equation 7-11

$$h_1 + u_1^2/2[1 - (P_1/P_2)^2(T_2/T_1)^2] - h_2 = 0$$

Figure 7-3 Laboratory-fixed and Incident-shock-fixed coordinate systems

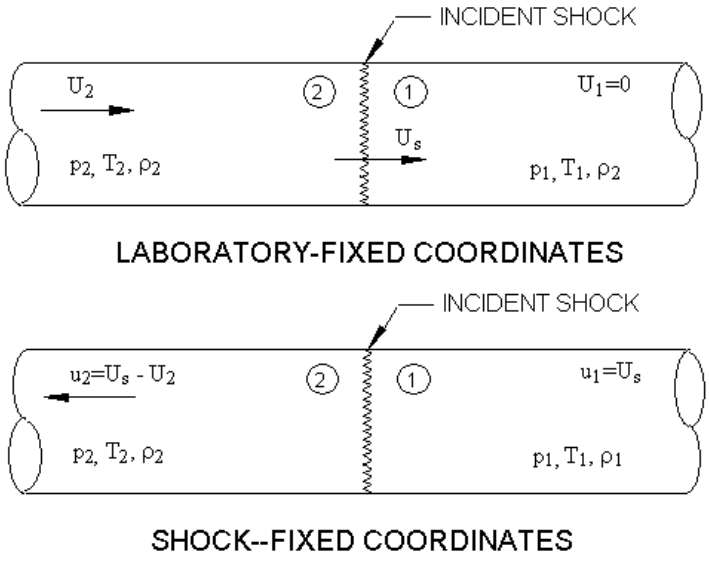

Since we assume no change in gas composition across the shock, h is a function of temperature alone and, hence, *Equation 7-10* and *Equation 7-11* represent a system of two equations in two unknowns. The solution gives P_2 and T_2 when conditions before the incident shock are specified. Knowing these, ρ_2 is determined from the equation of state and u_2 from *Equation 7-7*.

An iterative procedure is employed to solve *Equation 7-10* and *Equation 7-11* for P_2 and T_2. Letting α and β be the temperature and pressure ratios, respectively, across the shock, *Equation 7-10* can be solved for β in terms of α (see *Equation 7-13*) to yield

Equation 7-12

$$\beta = \frac{1}{2}\left[\left(1+\frac{\rho_1 u_1^2}{P_1}\right)+\sqrt{\left(1+\frac{\rho_1 u_1^2}{P_1}\right)^2-\frac{4\rho_1 u_1^2\alpha}{P_1}}\right]$$

This expression is then substituted into *Equation 7-11* to yield one equation with one unknown, α. Within Chemkin, a routine called ZEROIN[42], which finds the zeros of functions, is employed to determine the value of α that satisfies this equation. An initial guess for α is provided by assuming that the test gas is ideal (c_p and c_v are constant and independent of temperature). For ideal gases

Equation 7-13

$$\alpha = \frac{T_2}{T_1}\frac{\left(\gamma M_1^2-\frac{\gamma-1}{2}\right)\left(\frac{\gamma-1}{2}M_1^2+1\right)}{\left(\frac{\gamma+1}{2}\right)^2 M_1^2}$$

where γ is the specific heat ratio and M_1 is the Mach number of the incident shock.

Equation 7-14

$$M_1 = U_s\left(\frac{\rho_1}{\gamma P_1}\right)^{1/2}$$

Many times the experimentalist reports the incident shock speed, U_s, and temperature and pressure behind the shock, T_2 and P_2, respectively. Before the experiment can be modeled, however, the gas velocity behind the shock must be determined. Employing the equation of state in *Equation 7-10* to eliminate ρ_1/P_1 results in

42. L. F. Shampine and H. A. Watts, Zeroin, *A Root-Solving Code, Sandia National Laboratories Report* SC-TM-70-631, 1970.

Equation 7-15

$$1 + \frac{\rho_2 u_1^2}{P_2}(T_2/T_1)[1 - (T_2/T_1)(P_1/P_2)] - (P_2/P_1) = 0$$

This equation and *Equation 7-11* again represent two equations in two unknowns. The solution gives T_1 and P_1 and from these the density in region 1 is determined from the equation of state. The velocity behind the shock, u_2, is determined from *Equation 7-7*. The solution to *Equation 7-15* and *Equation 7-11* is analogous to that already described for *Equation 7-10* and *Equation 7-11*.

7.2.3 Reflected Shock Initial Conditions

For reflected shocks, shock-fixed and laboratory-fixed coordinates are again employed, but now shock-fixed coordinates refer to the reflected shock, which moves at velocity U_{rs}. Considering the reflected shock to be at rest, gas at condition 2 flows into the shock front and gas at condition 5 flows out. The velocities in the two coordinate systems are related by:

Equation 7-16

$$u'_2 = U_{rs} + U_2$$

and

Equation 7-17

$$u_5 = U_{rs} - U_5$$

The gas velocity measured in shock-fixed coordinates with respect to the reflected shock is u'. Gas conditions associated with the reflected shock in the two coordinate systems are shown in *Figure 7-4*.

Figure 7-4 Laboratory-fixed and reflected-shock-fixed coordinate systems

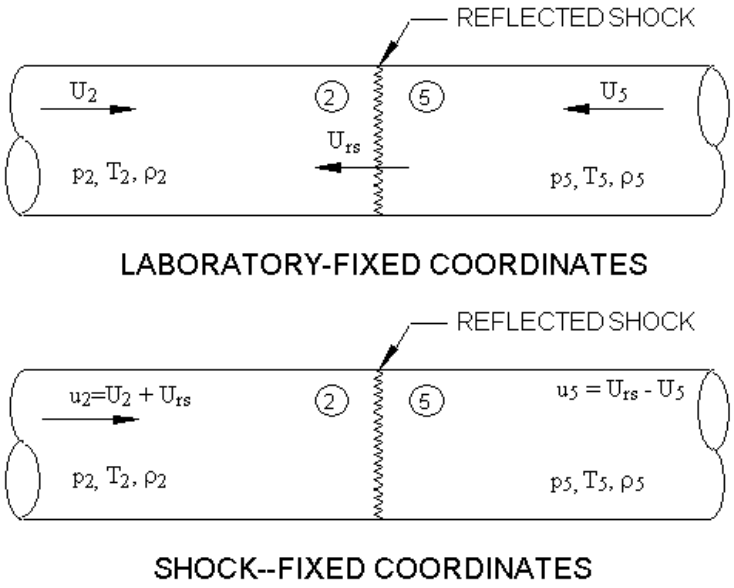

The Rankine-Hugoniot relations for properties across the reflected shock are

Equation 7-18

$$\rho_2 u'_2 = \rho_5 u_5$$

Equation 7-19

$$P_2 + \rho_2 (u'_2)^2 = P_5 + \rho_5 (u_5)^2$$

and

Equation 7-20

$$h_2 + (u'_2)^2/2 = h_5 + (u_5)^2/2$$

By analogy with *Equation 7-7*, *Equation 7-8* and *Equation 7-9*, the solution to the above set of coupled equations is found by finding the values of T_5 and P_5 which satisfy

Equation 7-21

$$1 + \frac{\rho_2 (u'_2)^2}{P_2}[1 - (T_5/T_2)(P_2/P_5)] - (P_5/P_2) = 0$$

and

Equation 7-22

$$h_2 + \frac{(u'_2)^2}{2}[1 - (P_2/P_5)^2 (T_5/T_2)^2] - h_5 = 0$$

where

Equation 7-23

$$u'_2 = U_{rs} + U_2 = U_{rs} + U_s - u_2$$

When the gas is assumed to be at rest behind the reflected shock (i.e., $U_5 = 0$), then the reflected shock velocity, U_{rs}, is given by

Equation 7-24

$$U_{rs} = \frac{(P_2/P_5)(T_5/T_2)(U_s - u_2)}{[1 - (P_2/P_5)(T_5/T_2)]}$$

Only in the ideal case is the gas behind the reflected shock at rest, however. Non-idealities cause the gas to move in the same direction as the incident shock and, hence, at conditions different from those calculated assuming $U_5 = 0$. Therefore, often the velocity of the reflected shock, as well as that of the incident shock, is measured. Then the values of T_5 and P_5 are computed so as to satisfy the Rankine-Hugoniot relationships using these measured velocities. Having determined T_5 and P_5, the density of the gas at condition 5 can be determined from the equation of state and u_5, from *Equation 7-18*.

Initial estimates for T_5 and P_5 can be obtained by again assuming ideal gas behavior. The temperature ratio across the incident shock when c_p and c_v are constant is given by *Equation 7-13* and the pressure ratio by

Equation 7-25

$$P_2/P_1 = \frac{2\gamma_1 M_1^2 - (\gamma_1 - 1)}{(\gamma_1 + 1)}$$

Letting η and ξ be defined as the following density ratios:

Equation 7-26

$$\eta = \rho_2/\rho_1$$

Equation 7-27

$$\xi = \rho_5/\rho_1$$

then the equation of state, *Equation 7-13* and *Equation 7-21* to *Equation 7-25* can be combined to show that for temperature-independent specific heats

Equation 7-28

$$\eta = \frac{M_1^2(\gamma_1 + 1)}{(\gamma_1 - 1)M_1^2 + 2}$$

Equation 7-29

$$\xi = \frac{\eta[M_1^2(\eta - 1)\gamma_1 + \eta]}{M_1^2(\eta - 1)(\gamma_1 - 1) + \eta}$$

Equation 7-30

$$P_5/P_1 = 1 + \frac{\gamma_1 M_1^2(\eta - 1)(\xi - 1)}{(\xi - \eta)}$$

Equation 7-31

$$T_5/P_1 = 1 + \frac{M_1^2(\gamma_1 - 1)(\eta - 1)(\xi - 1)}{\eta(\xi - \eta)}$$

and

Equation 7-32

$$U_{rs} = \frac{U_s(\eta - 1)}{(\xi - \eta)}$$

Even in the event that U_{rs} is specified, and hence U_5 is not necessarily zero, we still assume that the gas is at rest when solving the conservation equations. Only the initial state of the gas is modified by the non-ideal reflected shock velocity. Because of this, for reflected shock problems, we find it more convenient to use laboratory-time as the independent variable, since then the boundary-layer effects are of no consequence. For such cases, laboratory-time and gas-particle time are the same.

7.3 Downstream Model Equations

The set of equations, which describe the concentration, velocity and temperature distributions downstream of the shock, are derived from the well-established conservation laws of mass, momentum and energy transfer.

The flow is assumed to be adiabatic; transport phenomena associated with mass diffusion thermal conduction and viscous effects are assumed to be negligible. Test times behind shock waves are typically on the order of a few hundred microseconds; hence, neglect of these transport processes is of little consequence. Initial conditions for the governing equations are derived from the Rankine-Hugoniot relations for flow across a normal shock. The conservation equations for one-dimensional flow through an arbitrarily assigned area profile are stated below:

Equation 7-33 Continuity

$$\rho v A = \text{constant}$$

Equation 7-34 Momentum

$$\rho v \frac{dv}{dz} + \frac{dP}{dz} = 0$$

Equation 7-35 Energy

$$\frac{dh}{dz} + v\frac{dv}{dz} = 0$$

Equation 7-36 Species

$$\rho v \frac{dY_k}{dz} = \dot{\omega}_k W_k$$

Temperature is related to the specific enthalpy of the gas mixture through the relations:

Equation 7-37

$$h = \sum_{k=1}^{K} h_k Y_k$$

and

Equation 7-38

$$h_k = (h_k)_0 + \int_{T_0}^{T} c_{pk} dT$$

The net molar production rate of each species due to chemical reaction is denoted by $\dot{\omega}_k$. A detailed description of this term is given in the *Section 2.1* of the *ANSYS Chemkin Input Manual*. The equations of state relating the intensive thermodynamic properties is given by:

Equation 7-39

$$P\overline{W} = \rho RT$$

where the mixture molecular weight is determined from the local gas concentration via:

Equation 7-40

$$\overline{W} = \frac{1}{\sum_{k=1}^{K} Y_k / W_k}$$

In the shock tube experiments, the usual measurable quantities are density, species concentration, velocity and temperature as functions of time. It is therefore desirable to have time as the independent variable and not distance. Employing the relation

$$\frac{d}{dt} = v\frac{d}{dz}$$

differentiating *Equation 7-37*, *Equation 7-38*, *Equation 7-39*, and *Equation 7-40*, and combining the equations results in the following set of coupled, ordinary differential equations:

$$\frac{d\rho}{dt} = \left(\frac{1}{P + Pv^2/c_pT - Pv^2}\right)\left(\frac{R\rho}{\overline{W}c_p}\sum_{k=1}^{K}\dot{\omega}_k W_k\left(h_k - \frac{\overline{W}c_pT}{W_k}\right) + \frac{\rho^2 v^3}{A}\left(1 - \frac{R}{c_p\overline{W}}\right)\frac{dA}{dz}\right)$$

$$\frac{dY_k}{dt} = \frac{\dot{\omega}_k W_k}{\rho}$$

$$\frac{dv}{dt} = -\frac{v}{\rho}\frac{d\rho}{dt} - \frac{v^2}{A}\left(\frac{dA}{dz}\right)$$

$$\frac{dT}{dt} = -\frac{v^2}{\rho c_p}\frac{d\rho}{dt} - \frac{1}{\rho c_p}\sum_{k=1}^{K} h_k \dot{\omega}_k W_k + \frac{v^3}{A c_p}\left(\frac{dA}{dz}\right)$$

The time-histories of the measurable flow quantities should satisfy these relations. The distance of a fluid element from the shock, z, follows from *Equation* and is given by

Equation 7-41

$$\frac{dz}{dt} = v$$

These ODEs, *Equation* , *Equation* , *Equation* and *Equation* , are integrated along with *Equation 7-41*, for distance from the shock, and *Equation 7-4* for laboratory time, when gas-particle time is the independent variable. Values of the pressure, mean molecular weight and area as a function of gas-particle time are also determined.

7.3.1 Shock Tube Boundary-layer Effects

In a shock tube, the presence of the wall boundary-layer causes the shock to decelerate, the contact surface to accelerate and the flow behind the shock to be non-uniform. In this one-dimensional analysis, we must account empirically for effect that the flow of mass into the cold boundary-layer has on the free-stream variables. We take the approach developed by Mirels.[43] Assuming a laminar boundary-layer, Mirels proposed treating the flow as quasi-one-dimensional with the variation of the free-stream variables calculated from

43. H. Mirels, *Physics of Fluids* **6**:1201 (1963).

Equation 7-42

$$\frac{\rho v}{(\rho v)_2} = 1 - (z/l_m)^{1/2}$$

where l_m is the distance between the shock and contact surface at infinite distance from the diaphragm and the subscript 2 denotes conditions immediately behind the shock. He then obtained an expression for l_m by considering the simultaneous boundary-layer development and change in free-stream conditions external to the boundary-layer.

This expression is

Equation 7-43

$$l_m = \frac{d^2}{16\beta^2}\left(\frac{\rho_2}{\rho_w}\right)^2 \frac{1}{(w-1)}\left(\frac{u_2}{v_w}\right)$$

where

Equation 7-44

$$\beta = 1.59C\left(1 + \frac{1.796 + 0.802W}{(Zw-1)}\right)$$

with $Z = (\gamma+1)/(\gamma-1)$ and $w = u_w/u_2$. The effect of variable viscosity is accounted for by C, where

Equation 7-45

$$C = \left[\left(\frac{\rho_2}{\rho_w}\right)\left(\frac{\mu_2}{\mu_w}\right)\right]^{0.37}$$

The wall is assumed to remain at its initial temperature, while the pressure at the wall changes to P_2 after passage of the shock. The viscosity correction is based on numerical solutions for air. For the purposes of the boundary-layer corrections, we take the viscosity to be that of the diluent gas.

Hirschfelder, Curtiss and Bird[44] give the viscosity of a pure gas as

44. J. O. Hirschfelder, C. F. Curtiss, and R. B. Bird, *Molecular Theory of Gases and Liquids*, John Wiley and Sons, Inc., New York, 1967.

Equation 7-46

$$\mu = \frac{2.6693 \times 10^{-5} \sqrt{WT}}{\sigma^2 \Omega^{(2,2)^*} T^*}$$

where μ is the viscosity in gm/cm · sec; σ, the low-velocity collision cross-section for the species of interest in Angstroms; W, the molecular weight; T, the temperature in Kelvin; and $\Omega^{(2,2)^*}$, the reduced collision integral, a function of the reduced temperature T^* ($T^* = T/(\varepsilon/k)$) where (ε/k) is the potential parameter for the species of interest). The reduced collision integral represents an averaging of the collision cross-section over all orientations and relative kinetic energies of colliding molecules. Tabulated values of this integral at various reduced temperatures are given by Camac and Feinberg.[45]

The values can be fit to within 2% for $T^* > 2.7$ by the expression:

Equation 7-47

$$\Omega^{(2,2)^*} = 1.2516 (T^*)^{-0.1756}$$

Using this in the expression for the viscosity yields:

Equation 7-48

$$\mu = \left[\frac{2.1327 \times 10^{-5} \sqrt{W}}{\sigma^2 (\varepsilon/k)^{0.1756}} \right] T^{0.6756}$$

Evaluating the above equation at 300 K and using this as a reference point results in the following expression for the viscosity:

Equation 7-49

$$\mu = \mu_0 (T/300)^{0.6756}$$

A value for μ_0 for the diluent gas must be specified by the user when considering boundary-layer effects.

To derive an equation for the area variation, we first combine *Equation 7-33* and *Equation 7-42* to yield

45. M. Camac and R. M. Feinberg, in *Proceedings of the Eleventh Symposium (International) on Combustion*, The Combustion Institute, 1967, p. 137.

Equation 7-50

$$\frac{A_2}{A} = 1 - (z/l_m)^{1/2}$$

Then, the change in cross-sectional area with distance downstream of the shock is given by

Equation 7-51

$$\frac{1}{A}\frac{dA}{dz} = \frac{(z/l_m)^{-1/2}}{2l_m(1-(z/l_m)^{1/2})}$$

This expression is used in *Equation* , *Equation* and *Equation* . *Equation 7-51* allows us to account for the boundary-layer effects by computing the “effective” area through which the gas must flow.

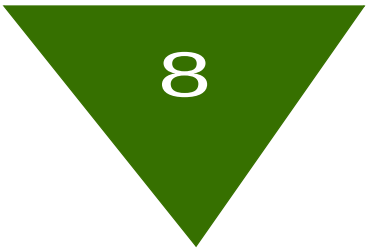

8 Homogeneous 0-D Reactor Models

In this chapter we derive the general equations for zero-dimensional homogenous systems, which include both open (with flow) and closed systems. The Chemkin reactor models that adhere to these general equations are:

1. Closed Homogeneous Reactor
2. IC HCCI Engine
3. Closed Plasma Reactor
4. Perfectly Stirred Reactor (PSR)
5. Plasma Reactor
6. Multi-Zone HCCI Engine Simulator
7. SI Engine Zonal Simulator

A PSR is also commonly referred to as a continuously stirred tank reactor (CSTR) in chemical engineering literature. All of the above reactor models may include both gas-phase and surface chemistry, and surface chemistry can be included for more than one material in the system. This allows investigation of systems with close coupling between gas-phase kinetics and surface kinetics, where kinetics dominate the system behavior.

All of the above reactor models allow simulation of dynamic reactor conditions. In addition, Reactors 4 and 5 allow efficient simulation of steady-state reactor systems through a modified Newton iteration solution algorithm. For dynamic systems, the user may specify controlling conditions that vary as a function of time. For steady-state systems, the models can compute a series of steady-state conditions varying one or more parameters, such as heat-loss or pressure, between simulations.

8.1 Reactor Clusters—Special Case of Reactor Networks

The open homogenous reactor models (Reactors 4 and 5) also includes an option to represent multiple PSRs that are connected in reactor network. In this case, a very special type of reactor network is formed, which we refer to as a reactor “cluster.” The difference is that the reactor “cluster” solution algorithm allows all reactor properties to be solved simultaneously. In this way recycling streams and heat flows between reactors can be included and resolved without external iteration in a computationally efficient manner. In contrast, other reactor networks (between different types of reactor models) involve series simulation of one reactor at time. For the reactor cluster, we assume that the effluent of the preceding reactor is the input to the next PSR by default. The user may add recycling streams and heat flow streams between any two reactors and additional inlets to each reactor. Each PSR in the cluster can have different temperatures, heating rates, volumes, and surface areas, for example. Clusters can be solved in both transient and dynamic modes.

8.2 Assumptions and Limitations

The contents of a well mixed or stirred reactor are assumed to be nearly spatially uniform due to high diffusion rates or forced turbulent mixing. In other words, the rate of conversion of reactants to products is controlled by chemical reaction rates and not by mixing processes. Thus we consider that the reactor is “limited” by reaction kinetics. An essential element of the stirred reactor model is the assumption that the reactor is sufficiently mixed to be described well by spatially averaged or bulk properties. For low-pressure processes (1 Torr and below), the dominance of species diffusion renders this assumption valid in many practical applications. For example, this is a very good assumption for the low-pressure, highly diffuse operating conditions of most plasma-etch reactors and some thermal CVD systems. The major advantage of the well stirred approximation lies in the relatively small computational demands of the mathematical model. Such a model allows investigators to easily consider and analyze large, detailed chemical reaction mechanisms or complex reactor networks.

In addition to fast mixing, the modeling of homogeneous reactors requires several assumptions. First, mass transport to the reactor walls is assumed to be infinitely fast. Therefore, the relative importance of surface reactions to gas-phase reactions is determined only by the surface-to-volume ratios of each material and the relative reaction rates (rather than by transport constraints). Second, the flow through the reactor must be characterized by a nominal residence time, which can be deduced from the flow rate and the reactor volume.

Further assumptions and limitations are described for specific model formulations in the following sections.

8.3 General Equations

Conservation of mass, energy, and species for a well mixed reactor or homogeneous system include net generation of chemical species within the reactor volume, and net loss of species and mass to surfaces in the reactor. Homogeneous systems include closed batch reactors, single-zone engine-cylinder models, perfectly stirred reactor approximations, well mixed (low-pressure) plasma processing reactors, for example. In closed batch reactors, there are no inlets or outlets flow during the period of interest, although there may or may not be heat flow to the external environment. Such batch systems are inherently transient, where the chemical state changes as production and destruction of species progress through chemical reaction. A perfectly stirred reactor (PSR) consists of a chamber, which may or may not allow heat loss, having inlet and outlet ducts. There may be more than one inlet defined for each reactor.

Figure 8-1 illustrates the conceptual representation of a generic reactor chamber. A steady flow of reactants is introduced through the inlet with a given species composition and temperature. For transient systems, there may be no flow, such that the system is closed with respect to mass transfer other than surface losses or gains. In some cases, the sum of the mass flow rates into the reactor, $\sum \dot{m}_i^*$, may not be equal to the mass flow rate out of the reactor, $\dot{m}$, due to deposition on or etching of surface materials. For open systems, the reactor pressure is specified, so that the conservation equations determine the volume outflow. Although *Figure 8-1* depicts a single surface in the reactor, an actual reactor may contain many different material surfaces, such as reactor walls, silicon wafer, substrate holder, etc. Each of these materials may have a different set of reaction kinetics associated with it. For this reason, we have included the capability of defining multiple surface materials that represent different fractions of the total surface area, with corresponding surface chemistry mechanisms.

Figure 8-1 Schematic Representation of a Well Mixed Reactor Module

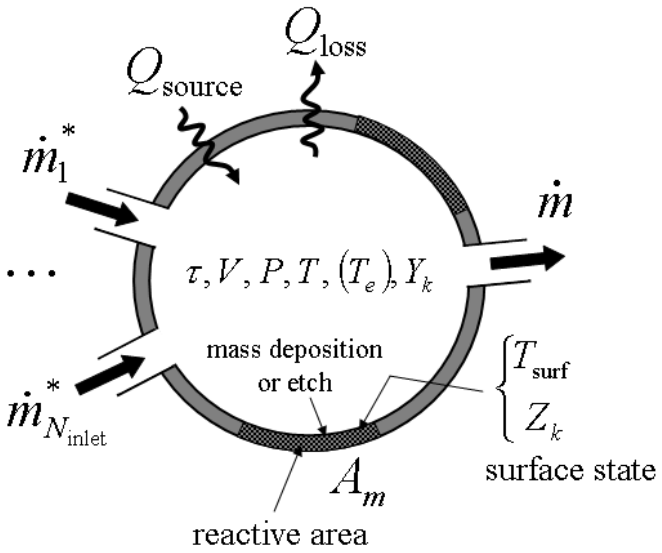

In addition to modeling a single well mixed reactor, Chemkin allows the user to build a reactor “cluster” composed of many reactor modules connected in series, with the possibility of “recycling” streams feeding back to upstream reactors or being directed forward to downstream reactors. A schematic of such a reactor cluster is given in *Figure 8-2*. This cluster is included for illustrative purposes only, to show the options for connecting reactors. The symbols **R11**, **R13,** and **R32** are examples of recycling streams, defined as fractions of total mass flow out of a reactor.

Reactor clusters are created using the Graphical User Interface Diagramming tool, as described in *Geting Started with ANSYS Chemkin*. This allows users to drag and drop reactors and connect them using mass-flow streams. Each inlet stream can be assigned it’s own attributes for flow rates, gas temperature, and composition. Recycling streams can be defined by specifying the fraction of the outflow from one reactor that will flow into another reactor. By default the outflow of a reactor will flow 100 percent into the next (downstream) reactor in series. When recycling streams are defined by the user, the mass flow from one PSR to the next in series will be one minus the sum of the recycle flows defined from that reactor to all other reactors (e.g., in *Figure 8-2*, `R12 = 1 - R11 - R13`).

As an example, the following set of keywords could be entered to define the reactor network shown in *Figure 8-2*:

```
INLET inletA 1  ! this indicates inletA is associated with reactor (PSR) 1
INLET inletB 1
INLET inletC 2
RECY  1  1  0.10  ! recycle 10% of PSR 1 outflow back into PSR 1
RECY  1  3  0.30  ! 30% of PSR 1 outflow into PSR 3
RECY  3  2  0.25  ! 25% of PSR 3 outflow recycled to PSR 2 ...
```

Figure 8-2 Schematic Representation of a Reactor Cluster

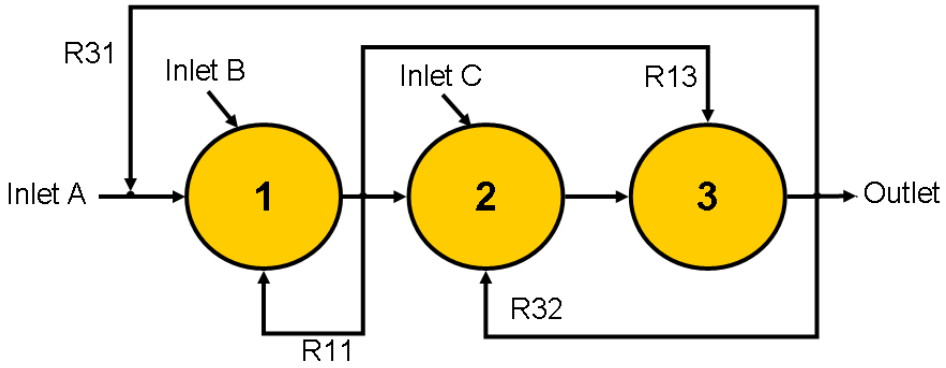

8.3.1 Mass Conservation and Gas-phase Species Equations

Chemkin includes several unique capabilities for well mixed reactor modeling. First, the model allows for the description of plasma kinetics, where a system is characterized by more than one temperature (e.g. the electron temperature, the ion temperature, or a neutral gas temperature). In these cases, some reaction rates may depend on one temperature, while other reaction rates may depend on another. This capability is incorporated through the use of the multi-fluid GAS-PHASE KINETICS package, and should not impact users who are only interested in systems that are in thermal equilibrium. Secondly, the model considers reaction kinetics on multiple surfaces within the reactor. Balances of surface species and bulk material species determine the surface state as well as net etch or deposition rates. This capability requires some hierarchy of information about gas-phase, surface-phase, and bulk-phase information. Only one gas phase is allowed, while more than one surface phase or bulk phase may be defined for each material. The details of this hierarchy are described in the *Section 2.1.2*.

Homogeneous 0-D reactor equations may address problems in both transient and steady-state environments. Even with steady-state equations, the computational algorithm often requires a partial solution of the related transient problem. Therefore, the transient conservation equations are presented here. We begin with global mass

conservation in the reactor volume, where the time-rate of change of the mass in the reactor is equal to the difference between the mass flow in and the mass flow out, plus any material that is added to or subtracted from the surfaces within the chamber. This equations is stated as:

Equation 8-1 Global Mass Balance Equation

$$\frac{d}{dt}(\rho V)^{(j)} = \sum_{i=1}^{N_{\text{inlet}^{(j)}}} \dot{m}_i^{*(j)} + \sum_{r=1}^{N_{\text{PSR}}} \dot{m}^{(r)} R_{rj} - \dot{m}^{(j)} + \sum_{m=1}^{M} A_m^{(j)} \sum_{k=1}^{K_g} \dot{s}_{k,m}^{(j)} W_k \qquad j = 1, N_{\text{PSR}}$$

Here j is the reactor number, ρ is the mass density, V is the reactor volume, $\dot{m}^*$ is the inlet mass flow rate, and $\dot{m}$ is the outlet mass flow rate. $N_{\text{inlet}^{(j)}}$ is the number of inlets for each reactor j, while N_{PSR} is the total number of reactor modules in the reactor network. R_{rj} is the fraction of the outflow of reactor r that is recycled into reactor j. The outlet mass flow differs from the sum of the inlet and recycled mass flow when deposition or etching of materials within the reactor occurs, as represented by the last term on the right-hand side. In this term, A_m is the surface area of the mth material defined within the reactor, and $\dot{s}_{k,m}$ is the molar surface production rate of the kth species on the mth material per unit surface area. There are K_g gas-phase species and M materials.

The time-dependent equation for mass conservation of each gas-phase species, including the implicit time dependence of ρ through its dependence on the temperature and molecular weight, is

Equation 8-2 Species Conservation Equation

$$(\rho V)^{(j)} \frac{dY_k^{(j)}}{dt} = \sum_{i=1}^{N_{\text{inlet}^{(j)}}} \dot{m}_i^{*(j)} (Y_{k,i}^* - Y_k) + \sum_{r=1}^{N_{\text{PSR}}} \dot{m}^{(r)} R_{rj} (Y_k^{(r)} - Y_k^{(j)})$$
$$- Y_k^{(j)} \sum_{m=1}^{M} A_m^{(j)} \sum_{k=1}^{K_g} \dot{s}_{k,m}^{(j)} W_k + (\dot{\omega}_k V)^{(j)} W_k + \sum_{m=1}^{M} A_m^{(j)} \dot{s}_{k,m}^{(j)} W_k$$

In *Equation 8-2*, Y_k is the mass fraction of the *k*th species, W_k is the molecular weight of the *k*th species, and $\dot{\omega}_k$ is the molar rate of production of the *k*th species by gas-phase chemical reaction per unit volume. The superscript * indicates inlet stream quantities.

For steady-state conditions, the nominal residence time τ in the reactor can be related to the reactor volume and the inlet mass flow rate as follows:

Equation 8-3 Definition of Residence Time

$$\tau = \frac{\rho V}{\left[\sum_{i=1}^{N_{\text{inlet}}^{(j)}} \dot{m}_i^{*(j)} + \sum_{r=1}^{N_{\text{PSR}}} \dot{m}^{(r)} R_{rj}\right]}$$

where the mass density ρ is related to the pressure, gas temperature and electron temperature through the multi-fluid ideal gas equation of state (see *Section 2.2*). The residence time is often used as a characteristic parameter of the reactor, rather than the mass flow rate for steady-state flow. In this case, $\dot{m}^*$ can be calculated from a specified residence time using *Equation 8-3*. Alternatively, the effective volume V can be calculated given specified values of both the residence time and the mass flow rates, also using *Equation 8-3*. If the mass flow rate is zero, then the reactor may not be characterized by residence time.

8.3.2 Surface Species Equations

To determine surface species site fractions, we begin with a conservation equation that balances the time rate of change of each surface species concentration with the net production rate of that surface species through chemical reactions at the surface. For each surface material there may be more than one surface phase; for example, sp^2 and sp^3 structures may be treated as two different phases in the surface mechanism. In addition, there may be several species defined for each phase representing, for example, open surface sites, physisorbed species, or chemisorbed

species. Each surface phase contains an independent set of surface species; in other words, a given surface species exists in only one phase on only one material. The surface species conservation equation is applied to every species in each surface phase n contained on each surface material m, as:

Equation 8-4

$$\frac{d}{dt}(A_m c_k W_k) = A_m W_k \dot{s}_k \qquad k = K_s^f(m), \ldots, K_s^f(m); m = 1, \ldots, M$$

Here A_m is the surface area of the *m*th material in the reactor and c_k is the molar concentration of the *k*th surface species (mole/cm^2).

Within the Chemkin reactor models, we use a strict ordering of species, species types, and surface materials that allows very general descriptions of the chemistry between species of all types in the reactor. The subscript k is then used for all species, whether gas-phase, surface-phase, or bulk-phase. For this reason, in *Equation 8-4* and subsequent equations, we introduce somewhat complicated indices for the range of surface species. Specifically, $K_s^f(N_s^f(m), m)$ refers to the first surface-phase species in the first surface phase of the material m, while $K_s^l(N_s^l(m), m)$ refers to the last surface-phase species of the last surface phase of the *m*th material. The total number of surface materials is M, with the total number of surface phases on each material given by $N_s(m)$ and the total number of bulk phases by $N_b(m)$. The surface phase index range for a material is given by $N_s^f(m) \le n \le N_s^l(m)$. The first phase defined in the system is always the gas-phase, with $n = 1$, such that $N_s^j(1) = 2$ and $K_s^f(2, 1) = K_g + 1$ in all cases where surface species are defined. In each phase, n, there are $K_{\text{phase}}(n, m)$ species, whose indices are in the range, $K_s^f(n, m) \le k \le K_s^l(n, m)$. When the species index range includes all surface species, as in *Equation 8-4*, we introduce a shorthand notation, where $K_s^f(m) = K_s^f(N_s^f(m), m)$ and $K_s^l(m) = K_s^l(N_s^l(m), m)$. Although this nomenclature is somewhat confusing on first glance, it need not unduly concern the user; all of this formalism is strictly maintained internally in the Chemkin software structure. For further insight into this nomenclature, see the *Chapter 1* explanation.

The molar concentration of a surface species is related to the total site density of a surface phase, $\rho_{n,m}$, to the site fraction of the *k*th surface species, and to the species coverage factor, σ_k, as follows:

Equation 8-5

$$c_k = \frac{\rho_{n,m} Z_k}{\sigma_k}$$

Assuming the surface areas of each material are constant, substituting *Equation 8-5* into *Equation 8-4*, and expanding the derivatives, we obtain:

Equation 8-6 Surface Site Conservation

$$\frac{dZ_k}{dt} = \sigma_k \frac{\dot{s}_{k,m}}{\rho_{n,m}} - \frac{Z_k}{\rho_{n,m}} \frac{d\rho_{n,m}}{dt} \qquad k = K_s^f(m), \ldots, K_s^l(m); m = 1, \ldots, M$$

The net change in surface-phase site densities is defined as:

Equation 8-7

$$\sum_{k = K_s^f(n,m)}^{K_s^l(n,m)} \sigma_k \dot{s}_{k,m} = \frac{d\rho_{n,m}}{dt} \qquad n = N_s^f(m), \ldots, N_s^l(m); m = 1, \ldots, M$$

Equation 8-7 is the surface site conservation equation that must hold true for each surface phase in each material. Here we note that, for the steady-state case, applying *Equation 8-6* to all surface species will lead to a singular Jacobian matrix. To obtain a well posed system of equations, one must introduce the additional requirement that all surface site fractions, Z_k, sum to one:

Equation 8-8

$$1 = \sum_{k = K_s^f(n,m)}^{K_s^l(n,m)} Z_k$$

Equation 8-8 may then be solved directly in place of one of the surface species balances in *Equation 8-6*. However, this approach results in the numerical round-off error in the calculation of the all of the $\dot{s}_k$'s to be assigned to one equation (*Equation 8-8*). This may cause problems in the case when that surface-site fraction is small. Instead, we chose to apportion the additional constraint represented by *Equation 8-8* over all of the equations represented by *Equation 8-6* for the surface phase n according to the size of the surface site fraction, as follows:

Equation 8-9

$$\frac{dZ_k}{dt} = \sigma_k \frac{\dot{s}_{k,m}}{\rho_{n,m}} - \frac{Z_k}{\rho_{n,m}} \frac{d\rho_{n,m}}{dt}$$

$$+ \frac{Z_k}{\tau}\left(1 - \sum_{l=K_s^f n,m}^{K_s^l n,m} Z_l\right) \qquad k = K_s^f(m), \ldots, K_s^l(m); m = 1, \ldots, M$$

Note that the time constant for the last term on the right-hand-side of *Equation 8-9* is arbitrary, and we have chosen τ because it is dimensionally correct and physically significant for the well mixed reactor model. For transient cases, the last term on the right-hand side is set to zero and a true transient for all species is solved. If *Equation 8-9* is summed over all surface species in phase n and combined with *Equation 8-7*, then the following relation results:

Equation 8-10

$$\frac{d\left(1 - \sum_{l=K_s^f(n,m)}^{l=K_s^l(n,m)} Z_l\right)}{dt} = -\frac{\left(1 - \sum_{l=K_s^f(n,m)}^{l=K_s^l(n,m)} Z_l\right)}{\rho_{n,m}} \frac{d\rho_{n,m}}{dt} - \frac{\left(1 - \sum_{l=K_s^f(n,m)}^{l=K_s^l(n,m)} Z_l\right)}{\tau}$$

which is equivalent to the sum of the Z_k's being equal to one, with a false transient.

8.3.3 Bulk Species Equations During Deposition

In the homogeneous, 0-D reactor models, Chemkin allows for the deposition and etching of bulk phase of materials in the reactor, although we do not account for changes in reactor volume or surface area with time due to etch or deposition processes. When there is only a single bulk species in a bulk phase, the bulk species mole fraction is trivially defined as one. When more than one bulk species exist in a bulk phase, the composition of the bulk phase may change with time, requiring

solution of the bulk-species mole fraction. For bulk phases that are being deposited, the mole fractions of the bulk-phase species are assumed to be initially unknown and are determined through time-dependent species balance equations for each bulk species:

Equation 8-11

$$\frac{d}{dt}(A_m L_{n,m} X_k^b C_{n,m}^b W_k) = A_m W_k \dot{s}_{k,m}$$

or

Equation 8-12

$$A_m L_{n,m} C_{n,m}^b W_k \frac{d}{dt}(X_k^b) + A_m W_k X_k^b \frac{d}{dt}(L_{n,m} C_{n,m}^b) = A_m W_k \dot{s}_{k,m}$$

Here X_k^b is the bulk species mole fraction of the *k*th species in phase n of the *m*th material. $L_{n,m}$ is the film thickness for the *n*th bulk phase of the *m*th material. $C_{n,m}^b$ is the average molar concentration of the species in the *n*th bulk phase of the *m*th material.

The molar growth rate of the bulk phase n, can be written as

Equation 8-13

$$\frac{d(A_m L_{n,m} C_{n,m}^b)}{dt} = \sum_{k = K_b^f(n,m)}^{K_b^l(n,m)} A_m \dot{s}_{k,m}$$

while the bulk mass density is defined as

Equation 8-14

$$\rho_{n,m}^b = C_{n,m}^b \overline{W}_{n,m}^b \qquad n = N_b^f(m), \ldots, N_b^l(m); m = 1, \ldots, M$$

where $\overline{W}_{n,m}^b$ is the mean molecular weight of the bulk phase. Combining *Equation 8-13* and *Equation 8-14* with *Equation 8-12* and rearranging gives the following relation:

Equation 8-15

$$A_m L_{n,m} \rho^b_{n,m} \frac{W_k}{\overline{W}^b_{n,m}} \frac{dX^b_k}{dt} = A_m W_k \dot{s}_{k,m} - A_m W_k X^b_k \sum_{l=K^f_b(n,m)}^{K^l_b(n,m)} \dot{s}_{l,m}$$

which simplifies to:

Equation 8-16

$$\frac{dX^b_k}{dt} = \frac{\overline{W}^b_{n,m}}{L_{n,m}\rho^b_{n,m}} \left[\dot{s}_{k,m} - X^b_k \sum_{l=K^f_b(n,m)}^{K^l_b(n,m)} \dot{s}_{l,m} \right]$$

We define the film-thickness length scale, $L_{n,m}$, somewhat arbitrarily. For steady-state, we define it as the linear growth rate of the bulk phase multiplied by the reactor residence time, as given in *Equation 8-17*. For transient cases, we use *Equation 8-17*, but replace the residence time with the time-step value.

Equation 8-17

$$L_{n,m} = \tau \frac{\overline{W}^b_{n,m}}{\rho^b_{n,m}} \sum_{k=K^f_b(n,m)}^{K^l_b(n,m)} \dot{s}_{k,m}$$

For deposition phases, then, *Equation 8-16* and *Equation 8-17* provide a false transient equation that is employed for the bulk species:

Equation 8-18

$$\frac{dX^b_k}{dt} = \frac{1}{\tau} \left[\frac{\dot{s}_{k,m}}{K^l_b n,m} - X^b_k \sum_{l=K^f_b n,m} \dot{s}_{l,m} \right]$$

Note that $L_{n,m}$ does not appear in *Equation 8-18*; Chemkin makes no assumption about the total amount of bulk-phase deposits, other than that their total amount is small compared to the total volume of the reactor. *Equation 8-18* is only used when the right-hand side is greater than zero; i.e., when there is net deposition of the bulk species. Under etching conditions, the bulk species equations must be treated differently.

8.3.4 Bulk Species Equations During Etch

When surface reactions that result in etching of a bulk phase are included in the surface reaction mechanism, the user must supply the initial composition of that phase (unless there is only one bulk species in the phase). The time-dependent equation for the bulk-phase species for phases that etch is then:

Equation 8-19

$$\frac{dX_k^b}{dt} = \frac{X_k^{b0} - X_k^b}{\tau} + \frac{X_k^b}{\tau}\left(1 - \sum_{l=K_b^f(n,m)}^{K_b^l(n,m)} X_l^b\right)$$

where X_k^{b0} is the user-supplied initial estimate for the mole fraction of species k in bulk phase n, normalized so that their sum over all bulk-phase species is equal to one. Here, the residence time in *Equation 8-19* is replaced with the time-step in transient simulations.

8.3.5 Non-constant Surface Phase Site Densities

Although surface site densities are very often considered physical constants associated with a particular surface structure, there are some cases when the surface site density may change with time. Chemkin allows the inclusion of reactions that do not conserve surface sites, if this is a desired feature of the problem. In such cases, the surface site density $\rho_{n,m}$, for every phase n whose total number of sites may not be conserved, becomes an additional solution unknown. The total number of surface phases on each material m, for which this condition may hold, is defined as equal to the variable $N_\rho(m)$. For each material m, there are $N_\rho(m)$ additional equations to be solved, corresponding to $N_\rho(m)$ additional unknowns. The equation for the time derivative of surface site densities is given by

Equation 8-20

$$\frac{d\rho_{n,m}}{dt} = \sum_{k=K_s^f(n,m)}^{K_s^l(n,m)} \sigma_k \dot{s}_{k,m} \qquad n = N_\rho^f(m), \ldots, N_\rho^l(m)$$

8.3.6 Gas Energy Equation

For the gas temperature, the user can specify either a fixed temperature value, or request solution of an energy balance in the reactor. The energy balance is determined by considering a control volume that includes the reactor, the reactor walls, and any deposited material therein. The following equation for the total internal energy of the reactor system is then

Equation 8-21 Gas Energy Equation

$$\frac{dU_{\text{sys}}^{(j)}}{dt} = \sum_{i=1}^{N_{\text{inlet}^{(j)}}} \dot{m}_i^{*(j)} \sum_{k=1}^{K_g} \left(Y_{k,i}^* h_{k,i}^*\right)^{(j)} + \sum_{r=1}^{N_{\text{PSR}}} \dot{m}^{(r)} R_{rj} \sum_{k=1}^{K_g} \left(Y_k h_k\right)^{(r)} - \left(\dot{m} \sum_{k=1}^{K_g} Y_k h_k\right)^{(j)}$$

$$- Q_{\text{loss}}^{(j)} + Q_{\text{source}}^{(j)} - P^{(j)} \frac{dV^{(j)}}{dt} \qquad j = 1, N_{\text{PSR}}$$

The total internal energy U_{sys} consists of the internal energy of the gas, surface phases, deposited or etched solid phases, and walls. Q_{loss} is the net heat flux directed out of the reactor. Q_{loss} can either be specified directly as a constant (`QLOS` keyword) or can be specified in terms of a constant heat transfer coefficient, h_t (`HTRN` keyword), and ambient temperature, T_o, as follows:

Equation 8-22

$$Q_{\text{loss}} = A h_t (T - T_o)$$

Q_{source} refers to energy deposited into the gas in the reactor. The term $P(dV/dt)$ represents the work done by the control volume on the external world. For plasma systems, this can represent the power deposited through Joule heating into the plasma by acceleration of charged species along electric fields. This term will be discussed in more detail in the description of the electron energy equation below.

The time derivative of the internal energy can be equated with the time derivative of the enthalpy, minus the time rate of change of the product of pressure and volume:

Equation 8-23

$$U_{\text{sys}} = H_{\text{sys}} - PV$$

Equation 8-24

$$U_{\text{sys}} = H_{\text{gas}} + \sum_{m=1}^{M} \sum_{n=N_s^f}^{N_b^l} (H_n(m) - PV_n) + H_{\text{walls}} - PV - PV_{\text{walls}^*}$$

The left-hand side of *Equation 8-21* then becomes:

Equation 8-25

$$\frac{dU_{\text{sys}}}{dt} = \frac{dH_{\text{gas}}}{dt} + \sum_{m=1}^{M} \sum_{n=N_s^f}^{N_b^l} \frac{dH_n(m)}{dt} + \frac{dH_{\text{walls}}}{dt} - P\frac{dV}{dt} - V\frac{dP}{dt}$$

We neglect the term on the right-hand-side that represents the heat capacity contribution from the walls. Expansion of the gas-phase contribution in *Equation 8-25* yields a heat balance for each reactor module:

Equation 8-26

$$\frac{dH_{\text{gas}}}{dt} = \frac{d(\rho V\bar{h})}{dt} = \rho V\left(\sum_{k=1}^{K_g} Y_k c_{pk}\frac{dT_k}{dt}\right) + \rho V\left(\sum_{k=1}^{K_g} h_k\frac{dY_k}{dt}\right) + \sum_{k=1}^{K_g} Y_k h_k \frac{d(\rho V)}{dt}$$

where $\bar{h}$ is the specific enthalpy of the gas mixture equal to the sum of the product of the species mass fraction and the pure species specific enthalpy. Note that in a multi-temperature system, the species enthalpies are evaluated at the species temperature T_k, which may differ from the mean gas temperature. In thermal systems, all T_k equal T, the gas temperature. c_{pk} represents the species specific heat capacity at constant pressure. Expansion of the bulk and surface contributions to *Equation 8-25* yields:

Equation 8-27

If we neglect the time dependence of the bulk- and surface-phase species enthalpies and molecular weights, and make use of *Equation 8-11*, *Equation 8-27* is greatly simplified to:

$$\sum_{m=1}^{M}\sum_{n=N_b^f(m)}^{N_b^l(m)}\frac{dH_n(m)}{dt} =$$
$$\sum_{m=1}^{M}\sum_{n=N_b^f(m)}^{N_b^l(m)}\left\{h_n(m)\overline{W}_{n,m}^b\frac{d}{dt}(A_m L_{n,m} C_{n,m}^b) + A_m L_{n,m} C_{n,m}^b \frac{d}{dt}(h_n(m)\overline{W}_{n,m}^b)\right\} +$$
$$\sum_{m=1}^{M}\sum_{n=N_s^f(m)}^{N_s^l(m)}\sum_{k=K_s^f(n,m)}^{K_s^l(n,m)}\left\{h\frac{d(A_m c_k W_k)}{dt} + A_m c_k W_k \frac{dh_k}{dt}\right\}$$

Equation 8-28

$$\sum_{m=1}^{M}\sum_{n=N_s^f(m)}^{N_b^l(m)}\frac{dH_n(m)}{dt} = \sum_{m=1}^{M}\sum_{n=K_s^f(m)}^{K_b^l(m)} A_m \dot{s}_{k,m} W_k h_k$$

Combining *Equation 8-1*, *Equation 8-2*, *Equation 8-21*, *Equation 8-25*, *Equation 8-26*, and *Equation 8-28* gives the transient energy equation for solving the gas temperature, as follows:

Equation 8-29 Energy Equation

$$(\rho V)^{(j)}\left[\bar{c}_p(1-Y_e)\frac{dT}{dt} + Y_e c_{pe}\frac{dT_e}{dt}\right]^{(j)} =$$
$$\sum_{i=1}^{N_{\text{inlet}}^{(j)}}\dot{m}_i^{(j)}\sum_{k=1}^{K_g} Y_{k,i}^*(h_{k,i}^* - h_k)^{(j)} + \sum_{r=1}^{N_{\text{PSR}}}\dot{m}^{(r)}R_{rj}\sum_{k=1}^{K_g} Y_k^{(r)}(h_k^{(r)} - h_k^{(j)})$$
$$- V^{(j)}\sum_{k=1}^{K_g}(h_k\dot{\omega}_k)^{(j)}W_k - \sum_{m=1}^{M}A_m^{(j)}\sum_{k=1}^{K_{\text{tot}}}(h_k\dot{s}_k)^{(j)}W_k - Q_{\text{loss}}^{(j)} + Q_{\text{source}}^{(j)} + V^{(j)}\frac{dP^{(j)}}{dt}$$

Here we define $\bar{c}_p$ as the mean gas specific heat excluding the contribution of the electrons, since we assume that the electron temperature may be significantly different from the gas temperature. All other species are assumed to be in thermal equilibrium at the gas temperature T. In other words,

Equation 8-30

$$\bar{c}_p = \sum_{k=1;k\neq e}^{K_g} Y_k c_{pk}$$

where the subscript, e, indicates the electron species. When no electrons are present *Equation 8-29* reverts back to the thermal-equilibrium case and the mean specific heat is merely the mass-averaged value of all species components. The actual form of the gas energy equation solved is the result of subtracting the electron energy equation from *Equation 8-29*. This form is presented after the introduction of the electron energy equation in the following section.

Heat release rates from gas-phase and/or surface reactions are calculated from the instantaneous chemical state of the reactor. In many cases, the time history of the heat release rate can be very noisy because of the underlying chemical system or the lack of time resolution during integration. The fluctuations in the heat release rate profile make accurate calculation of the total heat release from chemical reactions extremely challenging. In cases where precise time-profiles of heat release from gas-phase and/or surface reactions are needed, optional heat release equations can be included in the calculation. These heat release equations, one for gas-phase reactions and the other for surface reactions, are only used to provide smoother and more accurate time profiles of heat releases; they are “dummy” equations and should not affect the other equations. The equations used to obtain the accumulated heat release from gas-phase and surface reactions are given respectively in Equation (a) and (b) as:

Equation 8-31 a:

$$\frac{dQ_g^{(j)}}{dt} = -V^{(j)} \times \sum_{k=1}^{K_g} \left(h_k \dot{\omega}_k\right)^{(j)} W_k$$

b:

$$\frac{dQ_s^{(j)}}{dt} = -\sum_{m=1}^{M} \left[A_m^{(j)} \left(\sum_{k=1}^{K_{tot}} h_k \dot{s}_{k,m}{}^{(j)} W_k \right) \right]$$

8.3.7 Heat Exchange Between Reactors in Reactor Clusters

In Chemkin, the reactor cluster capability has been extended to optionally perform reactor-to-reactor and global balancing of heat in the reactor network model. We assume that heat exchange is a combination of convection/conduction and/or radiation. These extensions allow prediction of the net heat release from the reactor-

network system. for example, in modeling a fuel-cell reforming system, one reactor can represent a combustor and the combustor can serve as the heat source for activating the catalytic reactions in another reactor that represents the reformer. Heat balance is a critical issue in the design of many catalytic devices.

Figure 8-3 shows a schematic of a reactor unit or module and the heat flow that may occur into or out of that module in a general reactor network. An individual reactor (e.g., Reactor M in *Figure 8-3*) may be thermally connected to one or more other modules and to the system's external environment. A general heat balance for Reactor M must account for conduction, convection, and radiation heat exchange. Transient simulations must also account for heat capacity effects.

Figure 8-3 Schematic of the thermal communication of a reactor in a network

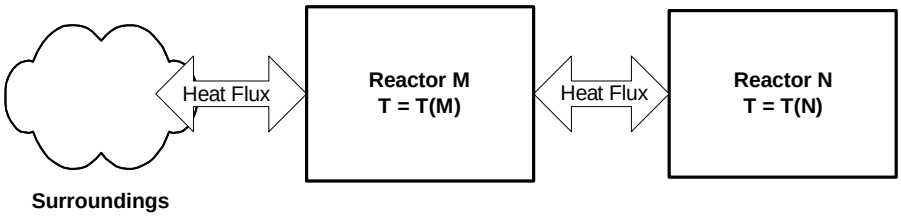

If heat transfer is allowed between Reactor M and Reactor N, (see *Figure 8-3*), the transient energy balance equation for Reactor M becomes:

Equation 8-32 Energy Equation Including Reactor-to-reactor Heat Transfer, for Reactor M

$$(\rho V)^{(M)}\left[\bar{c}_p(1-Y_e)\frac{dT}{dt}+Y_e c_{pe}\frac{dT_e}{dt}\right]^{(M)} =$$

$$\sum_{i=1}^{N_{\text{inlet}}{}^{(M)}} \dot{m}_i^{(M)} \sum_{k=1}^{K_g} Y^*_{k,i}(h^*_{k,i}-h_k)^{(M)} + \sum_{r=1}^{N_{\text{PSR}}} \dot{m}^{(r)} R_{rM} \sum_{k=1}^{K_g} Y_k^{(r)}(h_k^{(r)}-h_k^{(M)})$$

$$-V^{(M)} \sum_{k=1}^{K_g} (h_k \dot{\omega}_k)^{(M)} W_k - \sum_{m=1}^{M} A_m^{(M)} \sum_{k=1}^{K_{\text{tot}}} (h_k \dot{s}_k)^{(M)} W_k + V^{(M)} \frac{dP^{(M)}}{dt}$$

$$-Q^M_{\text{loss}} + Q^{(M)}_{\text{source}} + \sum_{N=1}^{N_{\text{PSR}}} \dot{Q}^{(M)}_{N\to M}$$

where $\dot{Q}^{(M)}_{N\to M}$ is the heat flow coming from Reactor N to Reactor M and is given as:

Equation 8-33 Optional Heat Flow Between Two Reactors

$$\dot{Q}_{N\to M}^{(M)} = (hA_e)_{N\to M}(T^{(N)} - T^{(M)}) + (\varepsilon A_e)_{N\to M}(T^{(N)4} - T^{(M)4})$$

The first term of *Equation 8-33* describes the heat flow caused by localized heat transfer modes such as conduction and convection and the second term is an optically-thin model for thermal radiation heat transfer between the two reactors. The area, A_e, is the "external" surface area that is available for heat transfer, which may be different from the internal surface area available for surface chemistry. Since $(hA_e)_{N\to M} = (hA_e)_{M\to N}$ and $(\varepsilon A_e)_{N\to M} = (\varepsilon A_e)_{M\to N}$, the properties of a "heat exchange matrix" can be obtained from *Equation 8-33*, with the additional relationships:

Equation 8-34

$$\dot{Q}_{M\to N}^{(N)} = -\dot{Q}_{N\to M}^{(M)}$$

and

Equation 8-35

$$\dot{Q}_{M\to M}^{(M)} = 0$$

In this way, the total energy among the reactors is conserved in the absence of any external heat loss. The user input parameters that control this reactor-to-reactor heat transfer are described in the *ANSYS Chemkin Input Manual* (**QXCO** and **QXRA** keywords).

8.3.8 Optional Wall Energy Balance and Heat Capacity Effects

To allow simulation of transient heat effects due to thermal inertia of a reactor wall, or other solid material associated with the reactor, the user now has the option to specify a total heat capacity associated with each reactor module. For transient systems, this heat-capacity effect or thermal inertial will be included in the energy balance of the system. In addition, the possibility for heat exchange between the gas and the wall mass, and between the wall mass and the environment is also optionally included. These extensions allow modeling of the system effects of transient chemical processes or of specifying realistic heating or cooling environments. Such analysis can be critical for determining start-up and cool-down behavior and the effects of varying loads on a reactor system.

The energy equation, *Equation 8-32*, is derived by conserving the thermal energy of an imaginary control volume without considering the presence of a reactor wall. The control volume consists of the gas mixture inside the reactor and the interface between the gas and the reactor wall so that heats of reaction from both gas-phase and surface chemistries are included. A schematic of this control volume is given in *Figure 8-4*. Because of the absence of a reactor wall, all heat fluxes interact directly with the gas mixture in the form of the $\dot{Q}_{loss}^{(M)}$ and $\dot{Q}_{N\to M}^{(M)}$ terms in the gas-energy balance.

Figure 8-4 Schematic of the gas phase control volume in the absence of the reactor wall

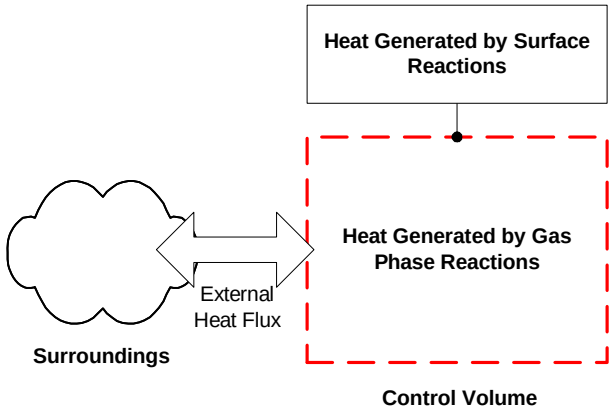

However, when the reactor wall is included in the energy balance, an additional equation is needed to solve for the wall temperature since the wall temperature can be different from the temperature of the gas mixture. To this end, we consider a new reactor-wall control volume, so that the wall energy equation can be established. Furthermore, the original gas-phase control volume is modified to make the gas-wall interface part of the reactor-wall control volume. The new configuration of the control volumes and their thermal energy interactions are shown in *Figure 8-5*.

Figure 8-5 Schematic of the gas-phase and wall control volumes for energy balance

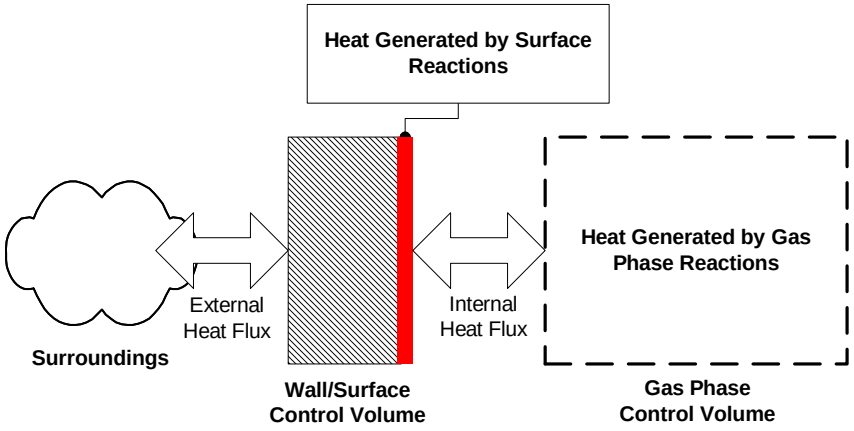

Accordingly, the wall energy-balance equation for Reactor M is given in *Equation 8-36*.

Equation 8-36 Wall Energy Balance for Reactor M

$$(\rho CV)_{\text{wall}}^{(M)}\frac{dT_{\text{wall}}^{(M)}}{dt} =$$

$$-\sum_{m=1}^{M} A_m^{(M)} \sum_{k=1}^{K_{\text{tot}}} (h_k \dot{s}_k)^{(M)} W_k + Q_{\text{gas}\rightarrow\text{wall}}^{M} - Q_{\text{loss}}^{(M)} + \sum_{N=1}^{N_{\text{PSR}}} \dot{Q}_{N\rightarrow M}^{(M)}$$

As a consequence of including the wall-energy balance, the energy-conservation equation for the gas mixture inside the reactor becomes

Equation 8-37 Modified Gas Energy Equation for Reactor M Accounting for Wall-energy Balance

$$(\rho V)^{(M)}\left[\bar{c}_p(1-Y_e)\frac{dT}{dt} + Y_e c_{pe}\frac{dT_e}{dt}\right]^{(M)} =$$

$$\sum_{i=1}^{N_{\text{inlet}}{}^{(M)}} \dot{m}_i^{(M)} \sum_{k=1}^{K_g} Y_{k,i}^{*}(h_{k,i}^{*} - h_k)^{(M)} + \sum_{r=1}^{N_{\text{PSR}}} \dot{m}^{(r)} R_{rM} \sum_{k=1}^{K_g} Y_k^{(r)}(h_k^{(r)} - h_k^{(M)})$$

$$-V^{(M)} \sum_{k=1}^{K_g} (h_k \dot{\omega}_k)^{(M)} W_k - \sum_{m=1}^{M} A_m^{(M)} \sum_{k=1}^{K_{\text{tot}}} (h_k \dot{s}_k)^{(M)} W_k + V^{(M)}\frac{dP^{(M)}}{dt}$$

$$-Q_{\text{gas}\rightarrow\text{wall}}^{M} + Q_{\text{source}}^{(M)}$$

In the above equations, the general term for heat-transfer to the external environment has been replaced by a term accounting for heat-transfer between the gas in the reactor and the wall material, where the wall material now interacts exclusively with the external environment. Since convection is the dominant heat-transfer mechanism between the gas mixture and the reactor wall, the heat flux can be cast into the following form:

Equation 8-38 Heat Transfer Between the Reactor Gas and Wall in Reactor M

$$\dot{Q}_{\text{gas}\rightarrow\text{wall}}^{(M)} = h_{\text{inner}} A (T^{(M)} - T_{\text{wall}}^{(M)})$$

To enable *Equation 8-37* and *Equation 8-38*, the user must supply the gas-to-wall convective heat-transfer coefficient as well as the thermal mass and heat capacity of the reactor wall. These input parameters are provided through the Chemkin Interface.

8.3.9 Treatment of Activities for Bulk Species

The net gas-phase chemical production rate of each species, $\dot{\omega}_k$, results from the competition between all the chemical reactions involving that species. For reactions stated as reversible in the GAS-PHASE KINETICS and SURFACE KINETICS input files, the reverse rate parameters can be determined from the forward rate coefficients and the thermodynamic properties of the species involved in the reaction, via the law of mass action. In these cases, SURFACE KINETICS requires activities to be defined for bulk-phase species, in order to determine the species thermochemistry. In these reactor models, the program sets the bulk activities, a_k^b, equal to their mole fraction in the bulk phase:

Equation 8-39

$$a_k^b(T, P, X_k^b(n, m)) = X_k^b(n, m)$$

More details regarding chemical reaction specifications, reaction-rate determinations, and thermochemical properties, are available in *Chapter 3* and *Chapter 4*.

8.4 Internal Combustion Engine Model

An Internal Combustion Engine (IC HCCI) model simulates a combustion cylinder in an internal combustion (IC) engine under auto-ignition conditions, most relevant to the study of fuel auto-ignition behavior, engine knock, and homogeneous charge compression ignition (HCCI) engines. Heywood[46] provides equations that describe the volume (to first order) as a function of time, based on engine parameters, including compression ratio, crank radius, connecting rod length, speed of revolution of the crank arm, and the clearance or displaced volume. These equations are described briefly below. The engine parameters are specified by the user directly in the Chemkin Interface for the Internal Combustion HCCI Engine Reactor Model.

46. J. B. Heywood, *Internal Combustion Engines Fundamentals*, McGraw-Hill Science/Engineering/Math, New York, 1988.

Figure 8-6 Schematic of an engine cylinder

Schematic of an engine cylinder, used in the ICEN model to determine the volume as a function of time. The dashed rectangle indicates the swept volume, which changes with time as the crank arm (L_A) rotates.

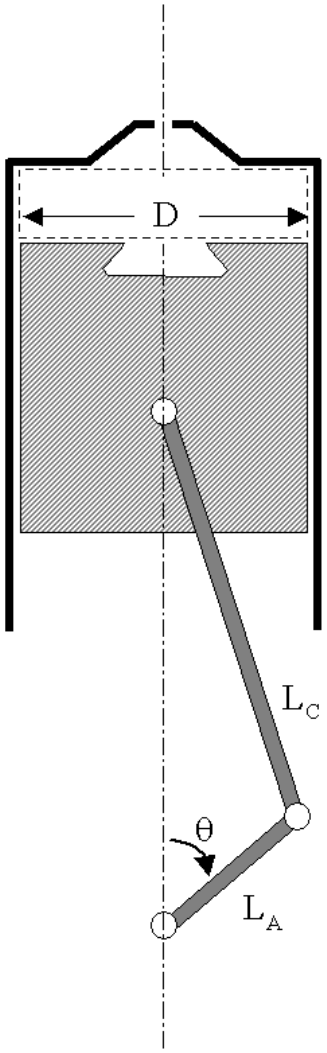

For the time-dependence of the engine cylinder volume, consider the diagram in *Figure 8-6*. The connecting rod length is given by L_C, while the crank arm radius is given by L_A. The volume swept by the piston (cross-hatched area) is represented by the dashed rectangle above the piston. The clearance volume V_c is represented by the open areas above and below the swept volume. The maximum swept or displaced volume is given by:

Equation 8-40

$$V_{s,\,\max} = \frac{\Pi}{2} D^2 L_A$$

where D is the cylinder bore diameter as shown in *Figure 8-6*. The engine compression ratio C is defined as the ratio of the maximum total volume to the clearance volume,

Equation 8-41 Compression Ratio

$$C = \frac{V_{s,\max} + V_c}{V_c}$$

Note that in some cases it is only necessary to define the compression ratio, and it is not strictly necessary to define the clearance volume, since it is only used to scale the calculated volume. However, if the user is interested in performing post-analyses for engine efficiency, for example, or in the case that the IC HCCI Engine heat transfer coefficient correlation is used, the clearance volume should be specified with a physical value. By default, a value of 1.0 is assumed. The other parameter required for the IC HCCI Engine problem is R, the ratio of the connecting rod length L_C to the crank-arm radius L_A:

Equation 8-42 Ratio of Connecting Rod to Crank-arm Radius

$$R = \frac{L_C}{L_A}$$

Finally, the user must specify the rotation rate of the crank arm, where

Equation 8-43

$$\Omega \equiv \frac{d\theta}{dt}$$

With these definitions, one can derive the relationship between the total volume available for combustion in the cylinder as a function of time, scaled by the clearance volume:[46, p. 148]

Equation 8-44

$$\frac{V(t)}{V_c} = 1 + \frac{C-1}{2}\left[R + 1 - \cos\theta - \sqrt{R^2 - \sin^2\theta}\right]$$

while the time derivative of the volume is:

Equation 8-45

Equation 8-40 through *Equation 8-45*) provide the volume and volume-derivative functions of time, which allows solution of the general equations for species and energy conservation discussed in *Section 8.3*.

$$\frac{d(V/V_c)}{dt} = \Omega\left(\frac{C-1}{2}\right)\sin\theta\left[1+\frac{\cos\theta}{\sqrt{R^2-\sin^2\theta}}\right]$$

8.4.1 Piston Offsets

The schematic in *Figure 8-7* shows the configuration of an engine cylinder with the centerline of the piston pin shifted to the left of the crank shaft by an amount of L_D. A negative L_D value means the piston pin is located to the right of the crank shaft center. The crank shaft radius is L_A, the connecting rod length is L_C, and the bore diameter is D. The nominal values of the clearance volume of the cylinder and the compression ratio are V and C, respectively.

The location of the top piston surface above the crank shaft center x can be expressed as a function of crank angle θ:

Equation 8-46

$$\frac{x(\theta)}{L_A} = \cos\theta + \sqrt{\left(\frac{L_C}{L_A}\right)^2 - \left(\sin\theta + \frac{L_D}{L_A}\right)^2}$$

The crank angle (in radians) is a function of time and engine speed N (in rpm) and is given as $\theta(t) = \theta_{IVC} + \Omega t$, in which the angular velocity of the crank shaft is $\Omega = 2\pi N / 60 \cdot$

A positive piston offset will lead to top-dead center (TDC) advance and its effects on piston movement are illustrated by *Figure 8-8*. A “negative” piston offset (i.e., the piston pin is to the right of the crank shaft) will result in retarding TDC.

The actual TDC of an engine with a piston offset of L_D can be found as

Equation 8-47

$$\theta_{TDC} = 2n\pi + \sin^{-1}\left(\frac{-L_D / L_A}{1 + L_C / L_A}\right)$$

And the bottom dead center (BDC) is located at

Equation 8-48

$$\theta_{BDC} = 2n\pi + \pi - \sin^{-1}\left(\frac{-L_D / L_A}{1 - L_C / L_A}\right)$$

The actual stroke can be computed as

Equation 8-49

$$Stroke = x(\theta_{TDC}) - x(\theta_{BDC})$$

Subsequently, the piston velocity can be derived by taking the time-derivative of the piston location $x(\theta)$:

Equation 8-50

$$\frac{v(\theta)}{L_A} = \frac{d\left(x(\theta)/L_A\right)}{d\theta}\frac{d\theta}{dt} = -\Omega\left\{\sin\theta + \frac{\cos\theta\left[\sin\theta + \left(L_D/L_A\right)\right]}{\sqrt{\left(L_C/L_A\right)^2 - \left[\sin\theta + \left(L_D/L_A\right)\right]^2}}\right\}$$

The instantaneous cylinder volume can be found to be:

Equation 8-51

$$\frac{V(\theta)}{V_c} = 1 + \frac{(C-1)}{Stroke}\left[x(\theta_{TDC}) - x(\theta)\right]$$

and the rate of change of the cylinder volume is the time-derivative of the cylinder volume:

Equation 8-52

$$\frac{1}{V_c}\frac{dV}{dt} = \frac{1}{V_c}\frac{dV}{d\theta}\frac{d\theta}{dt} = \frac{-(C-1)}{Stroke}v(\theta)$$

The internal surface area of the cylinder (for wall heat transfer calculations) is

Equation 8-53

$$A(\theta) = \pi D\left(x\left(\theta_{TDC}\right) - x(\theta)\right) + \frac{4V_c}{D} + (AR_{head} + AR_{piston})\frac{\pi D^2}{4}$$

or

Equation 8-54

$$A(\theta) = \frac{4V(\theta)}{D} + (AR_{head} + AR_{piston})\frac{\pi D^2}{4}$$

AR_{head} is the cylinder-head-to-bore area ratio, and AR_{piston} is the piston-head-to-bore area ratio. The default value of the area ratios is 1.

Figure 8-7 Schematic of an engine cylinder with a positive piston offset.

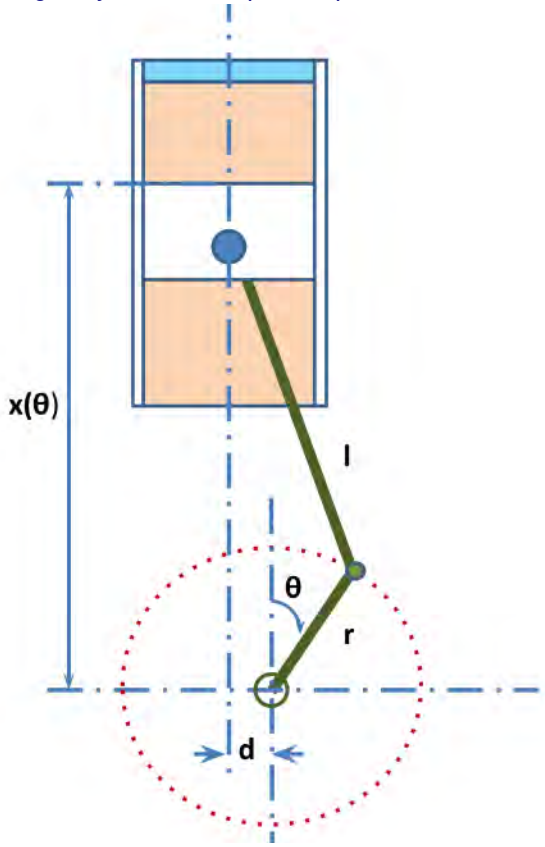

Figure 8-8 Comparison of piston location ($x(\theta)/L_A$) versus crank angle (θ in degree) between engines with positive piston offset and without piston offset (L_C/L_A=3.5 and L_D/L_A=0.4).

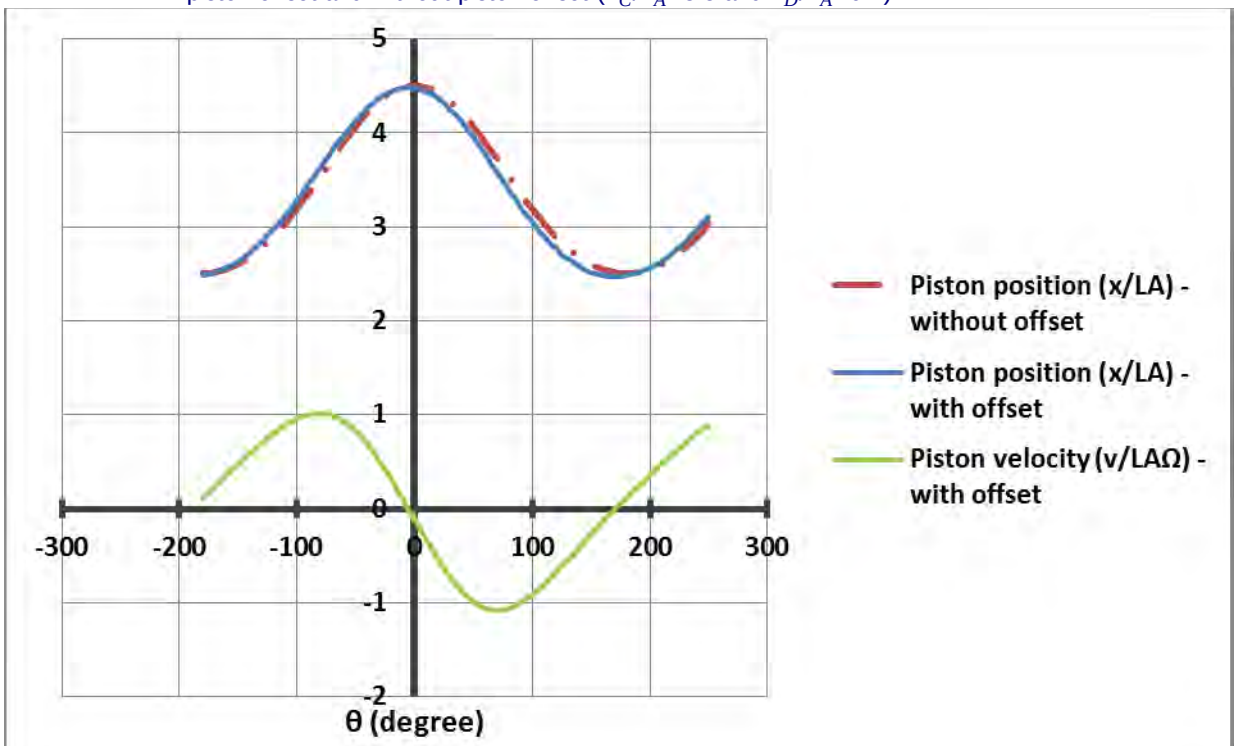

8.4.2 Heat-transfer Options for the IC HCCI Engine Model

An additional option to the Internal Combustion Engine HCCI Engine model is specification of convective heat loss from the gas to the solid walls during the compression and expansion cycle. The heat loss is calculated at each point in time according to:

Equation 8-55

$$Q_{\text{wall}} = hA(T - T_{\text{wall}})$$

where the user specifies T_{wall} and the heat transfer coefficient, h, is obtained from the following generalized heat transfer correlation[46, p. 148] based on user-specified constants a, b, and c:

Equation 8-56 Form of the IC HCCI Engine Heat-transfer Correlation

$$Nu_h = aRe^b Pr^c$$

Nu_h is the Nusselt number for heat transfer, Re is the Reynolds number, and Pr is the Prandtl number. These are defined according to:

Equation 8-57 Nusselt Number Definition

$$Nu_h \equiv \frac{hD}{\lambda}$$

Equation 8-58 Reynolds Number Definition Based on Piston Speed

$$Re \equiv \frac{D\overline{S_p}\rho}{\mu}$$

Equation 8-59 Prandtl Number Definition

$$Pr \equiv \frac{C_p \mu}{\lambda}$$

where λ is the gas conductivity, $\bar{S}_p$ is the mean piston speed ($= 4L_A\omega$), and μ is the gas viscosity. In calculating the heat transfer coefficient using *Equation 8-56*, the gas properties are assumed to be those of air, since, for typical operating conditions, the molar concentrations of fuel and its by-products are relatively dilute. The area available for heat transfer, A, includes the cylinder walls (time-varying) and end surfaces ($\approx 2\pi D^2/4$). Accordingly, when the IC HCCI Engine heat-transfer correlation is invoked, the user must also specify the engine bore diameter, D.

8.4.2.1 Woschni Correlation for IC HCCI Engine Heat Transfer

An extension to the heat-transfer correlation described above, is the use of the Woschni Correlation.[46, p. 148] This option is now provided in the Chemkin IC HCCI Engine model and the parameters that govern the Woschni correlation are described here.

The Woschni Correlation allows a more accurate estimation of the average cylinder gas speed used in the definition of the Reynold's number for the heat-transfer correlation. As stated in *Equation 8-56*, the convective heat transfer coefficient between the gas and cylinder wall can be obtained from the generalized heat transfer correlation in terms of a Nusselt number (defined in *Equation 8-57*). For the Woschni Correlation option, however, the velocity used in the Reynolds number definition is an estimation of the average cylinder gas velocity, w, instead of the mean piston speed, as stated in *Equation 8-60*.

Equation 8-60 Reynolds Number Definition Used in Woschni Correlation

$$Re \equiv \frac{D\bar{w}\rho}{\mu}$$

To obtain the average cylinder gas velocity, Woschni proposed a correlation that relates the gas velocity to the mean piston speed and to the pressure rise due to combustion, $(P - P_{\text{motored}})$, as given in *Equation 8-61*.

Equation 8-61 Woschni Correlation of Average Cylinder Gas Velocity

$$w = \left[\left(C_{11} + C_{12}\frac{v_{\text{swirl}}}{\overline{S_p}}\right)\right]\overline{S_p} + C_2\frac{V_d T_i}{P_i V_i}(P - P_{\text{motored}})$$

Here, C_{11}, C_{12}, and C_2 are modeling parameters, v_{swirl} is the swirl velocity, V_d is the displacement volume, P_{motored} is the motored cylinder pressure, and T_i, V_i, and P_i are the initial temperature, volume and pressure inside the cylinder, respectively.

The motored cylinder pressure is the pressure associated with an isentropic compression, in which the pressure and volume ratios are related by a specific heat ratio γ.

Equation 8-62

$$\frac{P_{\text{Motored}}}{P_i} = \left(\frac{V_i}{V}\right)^{\gamma}$$

8.4.3 Multi-zone HCCI Model

With the absence of flame propagation, the homogeneous charge compression-ignition (HCCI) combustion process is dominated by chemical kinetics. Implementation of a detailed reaction mechanism is therefore generally necessary for HCCI combustion analysis. A comprehensive HCCI combustion model requires the combination of fluid mechanics, heat transfer and detailed kinetics. While computational fluid dynamics (CFD) have been applied to the study of HCCI combustion for simple fuels, it is often too computationally intensive for routine analyses involving practical fuels. Single-zone HCCI combustion models, on the other hand, permit detailed modeling of the chemical kinetics for practical fuels by assuming that the gas in the combustion chamber is homogeneous, with uniform temperature, pressure, and gas composition. A single-zone model can adequately predict ignition in an HCCI engine when the initial conditions (loading) are known. However, because it does not account for low-temperature regions within the thermal boundary layers and crevices, a single zone model tends to under-predict CO and unburned hydrocarbon (UHC) emissions and over-predict peak pressures.

A multi-zone HCCI model serves as a compromise, in that it provides some resolution of temperature and composition inhomogeneities, while still allowing the use of detailed kinetics models for practical fuels. Many multi-zone models proposed for studying HCCI combustion processes have focused on addressing the non-uniformity of temperature. Some have considered both temperature and concentration distributions inside the cylinder.

The Chemkin Multi-zone HCCI model allows the possibility of adopting the hybrid solution approach developed by Aceves et al. The hybrid approach uses a non-reacting fluid-mechanics simulation to compute temperature (and initial concentration) distribution inside the cylinder and then, prior to chemical kinetics becoming significant, employs a multi-zone model to calculate ignition, heat release and emissions while using a detailed reaction mechanism. The computational fluid dynamics (CFD) step provides the multi-zone model with initial in-cylinder temperature and composition distributions, which are important to establishing appropriate zones in the multi-zone model. This approach is especially helpful with high levels of residual gas. Once the initial conditions of each zone are defined, the

Multi-zone HCCI model is able to provide improved predictions of peak pressure and trace-species emissions. Although this hybrid approach is an option, the Multi-zone HCCI model can also be used independently, using specified heat-transfer parameters from the start of simulation after intake valve closing

8.4.3.1 Model Description

Following the multi-zone model approach reported by Aceves et al.[47], a multi-zone homogeneous charge compression-ignition (HCCI) combustion model was developed for use within the Chemkin software framework[48].

The cylinder volume is divided into a number of imaginary zones according to the in-cylinder distribution of a variable, normally gas temperature. The Multi-zone HCCI model treats each zone as a closed homogeneous reactor, where the zone mass is conserved. Pressure is assumed to be the same for all zones and the total volume of all zones is equal to the instantaneous volume of the cylinder. Heat transfer between zones is not considered. The only interaction between zones is through pressure work; if combustion takes place within a zone, it expands to exert work on the other zones. The assumptions pertaining to this model formulation are summarized below

1. All zones have the same pressure.
2. No mass or heat transfer occurs between zones. The only interaction between the zones is compression work.
3. The total volume of the zones must equal the cylinder volume computed by the slider-crank relationship used in the single-zone internal-combustion engine model. This constraint is used to determine the zone/cylinder pressure.

The Chemkin Multi-zone HCCI model accommodates the hybrid or sequential approach for HCCI combustion simulation by allowing the zone temperature to be determined in two ways: constrained with a given temperature versus time profile or solved with the energy equation. This hybrid approach takes advantage of CFD's capabilities of modeling fluid dynamic mixing and heat transfer in complex geometries when heat release from chemical reactions is negligible. If zone temperature profiles extracted from a CFD solution are given, the Multi-zone HCCI model will obtain zone temperatures from the profiles before the simulation reaches the transition crank angle. The transition crank angle is a user-defined model parameter, when the multi-zone model is used in the context of the hybrid approach, to specify the crank angle at which chemical kinetics is considered to become important and the multi-zone model

47. Aceves, M. S., D. L. Flowers, et al. (2001). A Sequential Fluid-Mechanic Chemical-Kinetic Model of Propane HCCI Combustion. SAE Technical Paper 2001-01-1027.
48. CHEMKIN-PRO, Reaction Design: San Diego, CA. 2008.

should start solving zone temperature with the energy equation instead. Transitioning to solving the energy equation too late causes the model to miss some of the early chemistry, which is important for determining ignition timing. By default, the Multi-zone HCCI model solves the energy equation from the starting crank angle specified to obtain zone temperatures.

The total heat-transfer rate between gas mixture and cylinder wall is the sum of individual zone wall heat transfer rates. Zone wall heat transfer rates are determined by zone temperature, zone wall heat transfer coefficient, and zone wall surface area. The wall heat transfer coefficient of each zone is calculated by the Woschni correlation[49] using the same set of parameters. The Multi-zone HCCI model computes zone wall surface area by multiplying the instantaneous cylinder wall surface by a zone surface area fraction which is given by the user and kept constant during the simulation.

8.4.3.2 Governing Equations

Since the zones are treated as variable-volume closed homogeneous reactors, governing equations for species and temperature of individual zones are the same as those employed by the single-zone HCCI engine model:

8.4.3.2.1 Species

Equation 8-63

$$\rho^i \frac{dY_k^i}{dt} = \dot{\omega}_k^i W_k \qquad , \qquad \text{for i = 1,…, } N_{zone}$$

where ρ is zone density and Y_k, W_k and $\dot{\omega}_k$ are the mass fraction, molecular weight, and molar production rate of the kth species. The superscript in the equation denotes the zone index and N_{zone} is the number of zones used by the Multi-zone HCCI model analysis.

8.4.3.2.2 Internal Energy/Temperature

The zone temperature may be determined in two ways. When the crank angle is less than a pre-defined transition crank angle, θ_t, the zone temperature is obtained from a temperature profile extracted from a CFD solution:

49. Heywood, J. B. (1988). *Internal Combustion Engine Fundamentals*, McGraw-Hill.

Equation 8-64

$$T^i = T^i_{\text{profile}}(t), \quad \theta(t) \le \theta_t$$

In the above equation, θ(t) is the crank angle at time t and $T^i_{\text{profile}}(t)$ is the temperature versus time profile for zone i. The temperature profile option allows the Multi-zone HCCI model to take advantage of the more precise zone temperature histories predicted by third-party CFD software when heat release from chemical reactions is not significant. After the transition angle is reached, the zone temperature will be solved by the zone energy equation:

Equation 8-65

$$\rho^i C_v^i \frac{dT^i}{dt} = -\sum_{k=1}^{kgas} \dot{\omega}_k^i W_k u_k^i - \frac{P^i}{V^i}\frac{dV^i}{dt} - \frac{h_w^i \left(T^i - T_w\right) A_w^i}{V^i}, \quad \theta(t) > \theta_t$$

P, T, and V are zone pressure, temperature and volume, respectively. C_v is the constant-volume specific heat capacity of the gas mixture comprising the zone and u_k is the internal energy of the kth species. h_w and A_w are zone wall heat transfer coefficient and zone wall surface area, respectively. The Chemkin Multi-zone HCCI model assumes zone wall surface area is a constant fraction of the total cylinder wall surface area. The wall heat-transfer coefficient is computed by the Woschni heat-transfer correlation.[49, p. 158]

8.4.3.2.3 Volume/Accumulated Volume

In the Multi-zone HCCI model, the cylinder volume is computed by the slider-crank relationship used in the single-zone internal-combustion engine model. Individual zone volume is not known and needs to be solved. Since gas composition and temperature in each zone are solved by their corresponding governing equations, zone pressure and volume are coupled by the equation of state, i.e., ideal gas law.

In order to solve the system of equations more efficiently, a new variable is introduced

Equation 8-66

$$G^i = \sum_{j=1}^{i} P^j V^j$$

Since pressure is the same in all zones, the G variable can be considered as a pressure-weighted accumulated zone volume. The use of pressure as scaling factor helps minimize the variation of G variable during the engine cycle. In addition, by replacing zone volume, V, with the G variable, the Jacobian matrix becomes banded along the diagonal and the system of equation can be integrated more effectively. The zone volume can be converted from the G variable by

Equation 8-67

$$V^i = \frac{G^i - G^{i-1}}{P^i}$$

The governing equation for the new G variable can be derived from the equation of state as

Equation 8-68

$$G^1 = P^1 V^1 = M^1 R T^1 \left(\sum_{k=1}^{kgas} \frac{Y_k^1}{W_k} \right) \quad \text{for i=1,}$$

and, according to the definition of G (*Equation 8-66*),

Equation 8-69

$$G^i = G^{i-1} + P^i V^i = G^{i-1} + M^i R T^i \left(\sum_{k=1}^{kgas} \frac{Y_k^i}{W_k} \right) \quad \text{for i=1,}$$

where R is the universal gas constant and $M^i = \rho^i V^i$ is the gas mass of zone i.

8.4.3.2.4 Cylinder pressure

The assumption of uniform pressure among all zones serves a constraint and provides coupling between the zones

Equation 8-70

$$P^i = P^{i+1}, \text{ for } i = 1,\ldots, N_{zone}-1.$$

To close the pressure equation, the volume constraint

Equation 8-71

$$V_{cylinder} = \sum_{i=1}^{N_{zone}} V^i$$

is used to determine the pressure of the last zone ($i = N_{zone}$). By substituting *Equation 8-70* and *Equation 8-71* into *Equation 8-66* for $i = N_{zone}$, the governing equation for the pressure in the last zone can be obtained

Equation 8-72

$$P^{N_{zone}} = G^{N_{zone}} / V_{cylinder}$$

where $V_{cylinder}$ is the instantaneous cylinder volume.

The Chemkin Multi-zone HCCI model solves *Equation 8-63* - *Equation 8-65*, *Equation 8-68* - *Equation 8-70* and *Equation 8-72* for all zones fully-coupled to obtain zone properties. Average properties such as temperature and species concentrations are derived from their zone values.

8.4.4 SI Engine Zonal Simulator

The Spark Ignition (SI) Engine Zonal model is a multi-zone and zero-dimensional model that can be applied to simulate the evolution of gas composition inside the cylinder between intake valve closing (IVC) and exhaust valve opening (EVO) when the engine cylinder is a closed system.

The SI Engine Zonal Simulator consists of two homogeneous "balloon" zones/reactors. The unburned zone/reactor has no inlet and initially contains a fresh fuel-air gas mixture, which will be extracted from the zone after combustion occurs. The burned zone/reactor is initially empty and will be filled with combustion products after ignition. The burned zone allows gas to enter but no gas can leave the zone. In addition, there is a turbulent premixed flame separating the unburned and the burned zones after ignition. The SI Engine Zonal Simulator model treats the flame as an interface with negligible physical size. The purpose of the flame sheet is solely to transform the fresh fuel-air mixture into combustion products.

The SI Engine Zonal Simulation between IVC and EVO can be divided into three distinct stages depending on the presence of mass exchange and zonal mass. The first stage is the *pre-combustion* stage, which begins at IVC and extends to the start of combustion, θ_c. During the pre-combustion stage, only the unburned zone contains gas and there is no mass exchange. The SI Engine Zonal Simulator model in this stage behaves like a single-zone IC HCCI Engine model.

Figure 8-9 SI Engine Zonal Simulator: Zone I, pre-combustion.

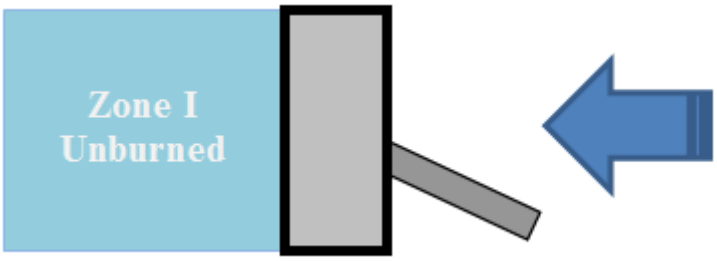

The second stage is the *combustion* stage. The combustion process is initiated by energy and ions released from the spark plug at the start of combustion time. The burned kernel expands as the turbulent premixed flame propagates towards the unburned fuel-air mixture inside the cylinder. The mass fraction of the burned gas at a given crank angle can be obtained from the Wiebe function from which the mass flow rate between the zones can be derived. The length of the combustion stage is

specified by the burn duration, $\Delta\theta_c$, which is a parameter required by the Wiebe function. The SI Engine Zonal Simulator model becomes a true multiple-zone model at this stage because all zones have non-zero mass. Another reason to "isolate" the combustion stage is that the Wiebe function is only valid between θ_c and $\theta_c + \Delta\theta_c$.

The flame sheet exists only during the combustion stage (*Figure 8-10*). By assuming complete and instantaneous combustion, the flame should have zero thickness and be adiabatic. The burned gas composition can then be determined by finding the constant-enthalpy, constant-pressure equilibrium state with respect to the gas mixture currently in the unburned zone.

Figure 8-10 SI Engine Zonal Simulator: Combustion stage.

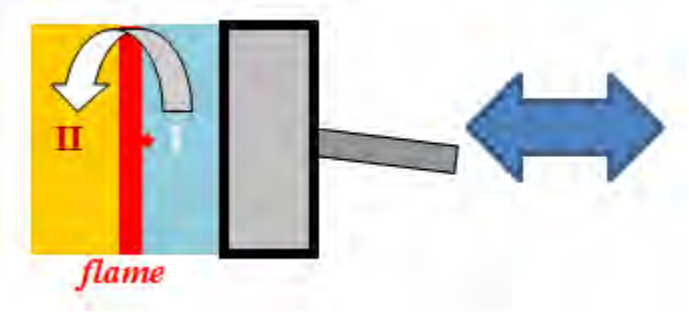

The *post-combustion* (expansion) stage is the last stage (*Figure 8-11*). It spans from the end of combustion to EVO. Since no unburned gas is left after the combustion stage (unless the combustion efficiency is less than 1), the unburned zone has no mass and the SI Engine Zonal Simulator model is again reduced to a single-zone IC HCCI Engine model.

Figure 8-11 SI Engine Zonal Simulator: Post-combustion (expansion) stage.

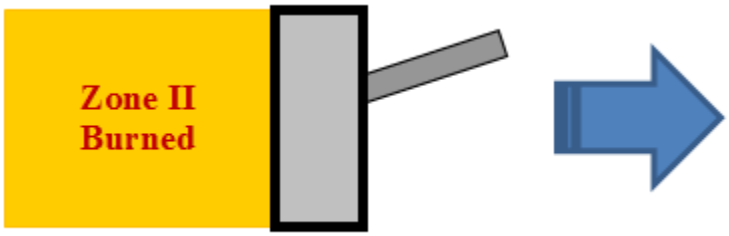

8.4.4.1 Fuel Burn Rate: Mass Exchange Rate Between the Zones

The mass exchange rate between the unburned zone and the burned zone is determined by the Wiebe function, which is commonly used to describe the accumulated burned mass fraction in an SI Engine Zonal Simulator. With a given combustion duration and ignition timing, the Wiebe function is expressed as:

Equation 8-73

$$W_b = \frac{m_b}{m_{total}} = \frac{m_b}{(m_b + m_u)} = f_{combust}\left(1 - e^{-b\left[(\theta-\theta_c)/\Delta\theta_c\right]^{n+1}}\right), \qquad \theta_c \le \theta \le \theta_c + \Delta\theta_c$$

where θ_c and $\Delta\theta_c$ are burn duration and the start of combustion (crank angle), respectively. $f_{combust}$ is the combustion efficiency and is defined as the mass fraction of gas in the cylinder burned. The Wiebe function itself contains two adjustable parameters, b and n ($n \neq -1$), that could be determined by fitting the experimental burned mass curves of a specific engine. By default, b = 5 and n = 2 are used in the SI Engine Zonal Simulator model. The mass flow rate between burned and unburned zones is the time derivative of *Equation 8-74*:

Equation 8-74

$$\dot{m}_b = \frac{dm_b}{dt} = \frac{dm_b}{d\theta}\frac{d\theta}{dt}$$

or

Equation 8-75

$$\dot{m}_b = f_{combust} m_{total}\left[(n+1)\frac{b}{\Delta\theta_c}\left(\frac{\theta-\theta_c}{\Delta\theta_c}\right)^n\right] e^{-b\left[(\theta-\theta_c)/\Delta\theta_c\right]^{n+1}}\frac{d\theta}{dt}, \qquad \theta_c \le \theta \le \theta_c + \Delta\theta_c$$

Figure 8-12 and *Figure 8-13* show typical burned mass fraction and fuel consumption rate profiles given by the Wiebe function and its derivative (with respect to θ) against crank angle, respectively.

The gas mixture entering the burned zone through the flame will be at the adiabatic flame temperature with the equilibrium composition corresponding to the instantaneous gas mixture in the unburned zone (with all NOx species fractions set to zero). The adiabatic flame temperature increases during compression because of the energy gain from the piston work.

Figure 8-12 Burned mass fraction W_b represented by the Wiebe function (θ_c = -10 ATDC, $\Delta\theta_c$ = 50 CA) against crank angle. The effects of the Wiebe function parameters, b and n, on the burned mass fraction profile are also shown.

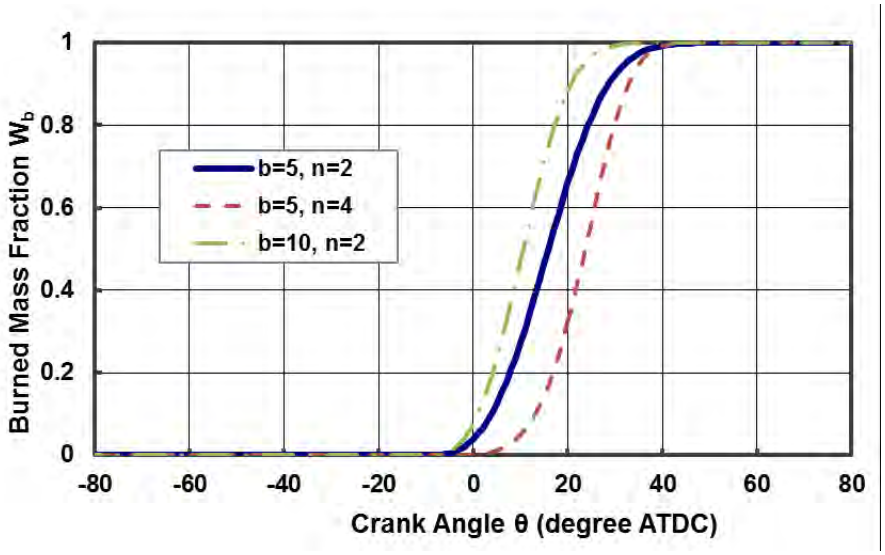

Figure 8-13 Fuel Consumption rate per crank angle (dW_b/d) against crank angle. The effects of the Wiebe function parameters, b and n, on the fuel consumption rate profile are also shown.

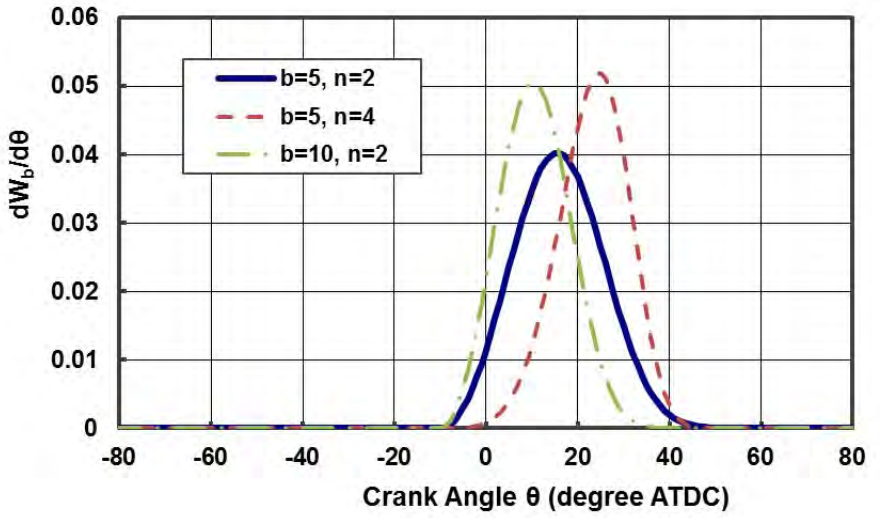

8.4.4.2 Governing Equations for the Combustion Stage

For the pre- and the post- combustion stages, there is no mass exchange between the unburned and the burned zones. Thus, the zones during these two non-combustion stages can be considered as individual closed homogeneous reactors and the governing equations for the IC HCCI Engine model (or the Multi-Zone HCCI Engine model) can be applied to the SI Engine Zonal Simulator model.

Although the gas mass inside the engine cylinder is constant during the combustion stage, the gas mixture is allowed to come out of the unburned zone and enter the burned zone. Therefore, the governing equations must be modified to include the effect of mass exchange on the gas properties in the zones. Moreover, there are some constraints that must be met during the multi-zone combustion stage:

1. Pressure is uniform among the zones.
2. Zone volumes must sum to the cylinder volume.

8.4.4.2.1 Mass Conservation of Zones

The outgoing mass flow rate from the unburned zone must equal to the mass flow rate incoming to the burned zone so that the overall mass inside the engine cylinder can be conserved. The mass conservation equation is the same for both zones; the differences occur for the mass flow rates in and out of the zones:

Equation 8-76

$$\frac{dm}{dt} = \dot{m}_{in} - \dot{m}_{out}$$

The inlet and the outlet mass flow rates of each zone are given in Table 1 where $\dot{m}_{out}$ is the mass exchange rate given by *Equation 8-75*.

Table 8-1 Inlet and outlet mass flow rates for the unburned and the burned zones during the combustion stage.

	Combustion $\theta_c \le \theta \le \theta_c + \Delta\theta_c$	
	$\dot{m}_{in}$	$\dot{m}_{out}$
Unburned Zone (zone I)	0	$\dot{m}_b$
Burned Zone (zone II)	$\dot{m}_b$	0

8.4.4.2.2 Conservation of Species Mass

The mass exchange has no impact gas composition in the unburned zone because gas is only allowed to leave the zone. On the other hand, species concentrations in the burned zone will be affected by the addition of burned gas products from the premixed flame. Therefore, for the burned zone, the gas species equation will have an additional term to account for the inlet gas effect:

Equation 8-77

$$m_{bnd}\frac{dY_{k,\mathrm{bnd}}}{dt}=\rho_{bnd}V_{bnd}\frac{dY_{k,i}}{dt}=\dot{m}_b\left(Y_{k,in}-Y_{k,\mathrm{bnd}}\right)+V_{bnd}\dot{\omega}_{k,\mathrm{bnd}}W_k$$

where $\dot{\omega}_{k,\mathrm{bnd}}$ and W_k are the molar production rate and molecular weight of species k, respectively. The inlet gas mass fractions $Y_{k,in}$ are given by the equilibrium species mass fractions from the flame. The equilibrium calculation uses the unburned gas properties and assumes both pressure and enthalpy are constant. If there are NO_x species in the mechanism, the concentrations of these species are fixed at 0 during the equilibrium calculation.

8.4.4.2.3 Conservation of Energy

The gas temperature of the burned zone will be affected by the mass addition. The energy equation for the burned zone will have to include the contribution of the incoming gas:

Equation 8-78

$$\rho_{bnd}V_{bnd}\overline{Cp}_{bnd}\frac{dT_{bnd}}{dt}=V_{bnd}\frac{dP_{bnd}}{dt}+\dot{m}_b\sum_{k=1}^{kkgas}Y_{k,in}\left(h_{k,in}-h_{k,\mathrm{bnd}}\right)-V_{bnd}\sum_{k=1}^{kkgas}\dot{\omega}_{k,\mathrm{bnd}}W_k h_{k,\mathrm{bnd}}$$

where $h_{k,in}$ is the enthalpy of the k-th species evaluated at the adiabatic flame temperature, which is determined by the equilibrium calculation.

8.4.4.2.4 Zone Volume

The governing equation for zone volume is different for each zone. For the unburned zone, the equation of state is used to compute the zone volume:

Equation 8-79

$$\frac{dV_{ubn}}{dt}=V_{ubn}\left[\frac{1}{T_{ubn}}\frac{dT_{ubn}}{dt}+\bar{W}_{ubn}\sum_{k=1}^{kkgas}\left(\frac{1}{W_k}\frac{dY_{k,\mathrm{ubn}}}{dt}\right)+\frac{1}{m_{ubn}}\frac{dm_{ubn}}{dt}-\frac{1}{P_{ubn}}\frac{dP_{ubn}}{dt}\right]$$

where $\bar{W}_{ubn}$ denotes the mean molar weight of gas mixture in the unburned zone.

For the burned zone, the constraint that the zone volumes must sum to the cylinder volume is applied:

Equation 8-80

$$\frac{dV_{bnd}}{dt}=\frac{dV_{cyl}}{dt}-\frac{dV_{ubn}}{dt}$$

where $V_{cyl}=\sum V_{ubn}+V_{bnd}$ and dV_{cyl}/dt are the cylinder volume and its time derivative, respectively.

8.4.4.2.5 Cylinder Pressure

The governing equation of pressure in the unburned zone is derived from the uniform pressure constraint.

Equation 8-81

$$\frac{dP_{ubn}}{dt} = \frac{dP_{bnd}}{dt}$$

For the burned zone, the equation of state is used as the pressure equation:

Equation 8-82

$$\frac{dP_{bnd}}{dt} = P_{bnd}\left[\frac{1}{T_{bnd}}\frac{dT_{bnd}}{dt} + \bar{W}_{bnd}\sum_{k=1}^{kkgas}\left(\frac{1}{W_k}\frac{dY_{k,\mathrm{bnd}}}{dt}\right) + \frac{1}{m_{bnd}}\frac{dm_{bnd}}{dt} - \frac{1}{V_{bnd}}\frac{dV_{bnd}}{dt}\right]$$

8.5 Plasma Systems

The treatment of plasmas with the Plasma Reactor or Closed Plasma Reactor model requires that power is deposited uniformly into the plasma bulk or, alternatively, that the electrons' diffusion and thermal conduction transport processes are fast relative to the rates of electron-driven chemical kinetics. In addition, we assume that the chemical reaction rate coefficients are independent of reactor conditions. This assumption may be invalid in the case where the electron energy distribution function deviates significantly from Maxwellian conditions.[46, p. 148] However, modeling plasma systems in this manner still provides important insight into the reactor chemistry.[50,51,52,53,54] Finally, the characterization of a quasi neutral bulk plasma depends on a thin-sheath approximation, where the sheath thickness is much smaller than the reactor-chamber dimensions.

In this section we describe the equations and formulations specific to homogeneous plasma reactor models.

50. M. A. Lieberman and R. A. Deutsche, in *Physics of Thin Films*, edited by M. Frenchman and J. Vision Academic Press, New York, 1993.
51. C. Lee, D. B. Graves, M. A. Lieberman, and D. W. Less, *Journal of the Electrochemical Society* **141**:1546 (1993).
52. E. Meeks and J. W. Son, *IEEE Transactions on Plasma Science* **23**:539 (1995).
53. E. Meeks and J. W. Son, *Journal of Vacuum Science and Technology A* **13**:2884 (1995).
54. E. Meeks, R. S. Larson, S. R. Vision, and J. W. Son, *Journal of the Electrochemical Society* **144**:358 (1997).

8.5.1 Electron Energy Equation for Plasma Systems

The transient form of the electron energy balance equates the time-rate-of-change of the electron swarm's internal energy, u_e, to the net flow of electron enthalpy into and out of the reactor, accounting for net chemical production rates, surface losses, collisions losses, and power deposition from externally applied electromagnetic fields. This balance is stated as:

Equation 8-83 Electron Energy Equation

$$\frac{d}{dt}(\rho_e V u_e)^{(j)} = \sum_{i=1}^{N_{\text{inlet}^{(j)}}} \dot{m}_i^{*(j)} Y_{e,i}^{*} h_{e,i}^{*} + \sum_{r=1}^{N_{\text{PSR}}} \dot{m}^{(r)} R_{rj} Y_e^{(r)} h_e^{(r)}$$

$$- \dot{m}^{(j)} Y_e^{(j)} h_e^{(j)} + \dot{\omega}_e W_e \tilde{h}_e V + \sum_{m=1}^{M} (\dot{s}_{e,m} h_e A_m)^{(j)} W_e - Q_{\text{loss}}^{\text{elas}} - Q_{\text{loss}}^{\text{inel}} + Q'_{\text{source}}$$

where ρ_e is the electron mass density (equal to the product of the electron number density and the electron mass). $\tilde{h}_e$ refers to the electron enthalpy of newly created electrons in the gas-phase; when electrons are formed from the ionization of a relatively cold neutral, the electron is assumed to originate close to the neutral temperature. The energy required to thermalize new electrons is therefore taken into account. At the surface, electron losses are assumed to dominate electron emission, so that no equivalent term is included to account for new electrons coming off the surface with thermal energies equal to the surface temperature. The electron enthalpy loss at the surface is therefore calculated from the net production rate of electrons due to surface reactions on each material, $\dot{s}_{e,m}$, and the electron enthalpy, h_e. The second- and third-to-last terms on the right-hand-side refer to the collision energy lost by the electrons both from elastic, momentum-transfer collisions, and from inelastic collisional processes. The inelastic collisions may include both excitation reactions, as well as chemical reactions resulting from electron-impact collisions. The source term Q'_{source} differs from Q_{source} in *Equation 8-29* in that it represents only that power deposited to the electrons, rather than to the plasma as a whole. In particular, some of the deposited power may contribute to heating of ions in the plasma bulk, or accelerating ions through the plasma sheath. We therefore define the electron-energy source term as:

Equation 8-84

$$Q'_{\text{source}} = Q_{\text{source}} - Q_{\text{ions}}^{\text{sheath}} - Q_{\text{ions}}^{\text{plasma}}$$

The internal energy of the electron and electron specific heats are defined by:

Equation 8-85

$$u_e = h_e - \frac{P_e}{\rho_e} = \frac{5}{2}\frac{R}{W_e}T_e - \frac{RT_e}{W_e} = \frac{3}{2}\frac{R}{W_e}T_e; c_{pe} = \frac{5}{2}\frac{R}{W_e}; c_{ve} = \frac{3}{2}\frac{R}{W_e}$$

If we assume $\tilde{h}_e = (5/2)RT/W_e$, substitute *Equation 8-84*, and *Equation 8-85* into *Equation 8-83*, and subtract *Equation 8-2* multiplied by $c_{pe}T_e$, we arrive at:

Equation 8-86

$$(\rho V)^{(j)}\left[Y_e c_{ve}\frac{dT_e}{dt} - \frac{R}{W_e}T_e\frac{dY_e}{dt}\right]^{(j)} = \sum_{i=1}^{N_{\text{inlet}}^{(j)}} \dot{m}_i^{*(j)} Y_{e,i}^{*} c_{pe}(T_e^{*} - T_e) +$$
$$\sum_{r=1}^{N_{\text{PSR}}} \dot{m}^{(r)} R_{rj} Y_e^{(r)} c_{pe}(T_e^{(r)} - T_e^{(j)}) + (\dot{\omega}_e V c_{pe})^{(j)} W_e (T - T_e) - Q_{\text{loss}}^{\text{elas}} - Q_{\text{loss}}^{\text{inel}} + Q'_{\text{source}}$$

Here the second term on the right-hand-side represents the thermalization energy required for newly created electrons. The loss and source terms in *Equation 8-86* and *Equation 8-84* are defined as follows:

Equation 8-87

$$Q_{\text{loss}}^{\text{elas}} = \frac{3VR\rho_e}{W_e}(T_e - T)\sum_{k=1;k\neq e}^{K_g}\frac{W_e}{W_k}\upsilon_{ek}$$

Equation 8-88

$$Q_{\text{loss}}^{\text{inel}} = V\sum_{r=1}^{I_{ei}} \Delta H_r q_r + Q_{\text{other}}(T_e)$$

Equation 8-89

$$Q_{\text{ions}}^{\text{sheath}} = \sum_{m=1}^{M}\sum_{i=1}^{K_i} \dot{s}_{i,m}\varepsilon_i A_m$$

and

Equation 8-90

$$Q_{\text{ions}}^{\text{plasma}} = \sum_{i=1}^{K_i} \dot{\omega}_i (h_i(T_{\text{ion}}) - h_i(T))V$$

In *Equation 8-87*, υ_{ek} is the momentum-transfer collision frequency between the electrons and the *k*th heavy species. The plasma-reactor model calculates the momentum-transfer collision frequencies from momentum-transfer collision cross-sections specified with the input keywords XSEK and XSDF. The first term in *Equation 8-88* represents the summation of electron energy loss per electron-impact reactions as specified in the GAS-PHASE KINETICS input file. The total number of electron-impact (i.e., electron-temperature dependent) reactions I_{ei}, q_r is the net rate

of progress of the *r*th reaction, and ΔH_r is the net enthalpy change of the reaction. ΔH_r can be determined from species' thermochemistry as available in the Chemkin thermodynamic data, or can be input directly through use of the GAS-PHASE KINETICS reaction auxiliary keyword EXCI (*Table 3-6* of the *ANSYS Chemkin Input Manual*). The second term on the right-hand side of *Equation 8-88* represents other loss terms that the user may choose to include separately from the GAS-PHASE KINETICS reaction descriptions (e.g., explicit user specification of electron energy loss in the User Interface). In *Equation 8-89*, ε_i is the energy gained by an ion when traversing the sheath, while K_i is the total number of ionic species. ε_i may be supplied through one of several options: direct specification of ion energy, calculation from the electron temperature and a user-specified multiplication factor (Sheath Loss Factor in the Chemkin Interface, under Materials-specific Data), or through specification of a bias power applied to the material. For the bias power option, the ion energy is determined as the power divided by the total ion current to that material. In *Equation 8-90*, we introduce an ion temperature T_{ion} to capture the source energy that is deposited into the ions, although we are not solving an ion energy equation explicitly. The ion temperature in the plasma bulk is specified directly by the user and assumed to be constant.

8.5.2 Gas Energy Equation Adjusted for Plasma Systems

For plasma systems, the actual gas energy equation solved results from subtracting *Equation 8-86* from *Equation 8-29*. This approach keeps only those terms that directly affect the gas temperature in the gas energy equation. The resulting gas energy equation is then:

Equation 8-91 Gas Energy Equation minus Electron Energy Equation

$$(\rho V)^{(j)}\left[\bar{c}_p(1-Y_e)\frac{dT}{dt}+\frac{R}{W_e}\frac{d(Y_eT_e)}{dt}\right]^{(j)} = \sum_{i=1}^{N_{\text{inlet}}{}^{(j)}}\dot{m}_i^{(j)}\sum_{k=1;k\neq e}^{K_g}Y_k^{*(j)}\left(h_{k,i}^{*}-h_k\right)^{(j)} +$$

$$\sum_{r=1}^{N_{\text{PSR}}}\dot{m}^{(r)}R_{rj}\sum_{k=1;k\neq e}^{K_g}Y_k^{(r)}\left(h_k^{(r)}-h_k^{(j)}\right) - V^{(j)}\sum_{k=1;k\neq e}^{K_g}\left(\tilde{h}_e\dot{\omega}_e\right)^{(j)}W_e$$

$$-\sum_{m=1}^{M}A_m^{(j)}\sum_{k=1}^{K_{\text{tot}}}\left(\dot{s}_{k,m}h_k\right)^{(j)}W_k - Q_{\text{loss}}^{(j)} + Q_{\text{loss}}^{\text{elas}(j)} + Q_{\text{loss}}^{\text{inel}(j)} + Q_{\text{ions}}^{\text{plasma}(j)} + Q_{\text{ions}}^{\text{sheath}(j)}$$

8.5.3 Application of the Bohm Condition for Ion Fluxes to Surfaces

Often, when modeling very low-pressure plasmas, it is reasonable to constrain the ion flux to a surface according to the Bohm criterion. This condition maintains that the maximum net flux of a particular ion to a surface is equal to the product of the ion density and the Bohm velocity, which is defined as:

Equation 8-92

$$U_{\text{Bohm}} = \left(\frac{RT_e}{W_i}\right)^{1/2}$$

For an electronegative gas, this expression must be modified to account for the presence of negative ions and their effect on the plasma sheath behavior. In the limit of a purely electronegative gas, the ion flux to a surface would be limited by the thermal speed of the ion.

To accommodate a large range of conditions, then, we use the correction to the Bohm velocity derived by Braithewaite and Allen,[55] as follows:

55. N. S. J. Braithwaite and J. E. Allen, *Journal of Physics D* **21**:1733 (1988).

Equation 8-93

$$U_{\text{Bohm, mod}} = \left(\frac{RT_e}{W_i}\right)^{1/2}\left[\frac{(c_e + c_{n,\text{tot}})T_i}{(c_{n,\text{tot}}T_e + c_eT_i)}\right]^{1/2}$$

where $c_{n,\text{tot}}$ is the sum over all negative ions of the product of the ion species' concentration and its integer electronic charge.

The Plasma Reactor Models allow the user to specify this constraint in one of two ways. The first way is to use the Plasma Reactor "Bohm factor" setting. This keyword includes the input of a correction factor ξ to the above Bohm velocity. When this option is included, the production rate of each ion by each surface reaction will be scaled, such that the net production rate of the ion on each material is given by

Equation 8-94

$$\dot{s}_{i,m} = \dot{s}_{i,\text{Bohm}} = \xi c_i U_{\text{Bohm, mod}} = \xi c_i\left(\frac{RT_e}{W_i}\right)^{1/2}\left[\frac{(c_e + c_{n,\text{tot}})T_i}{(c_{n,\text{tot}}T_e + c_eT_i)}\right]^{1/2}$$

The second way to apply the modified Bohm criterion, is to use the SURFACE KINETICS BOHM auxiliary keyword. In this case, the individual reaction for which the auxiliary BOHM keyword is included, will have a rate of progress calculated in the SURFACE KINETICS routines as

Equation 8-95

$$q = \xi c_i U_{\text{Bohm, mod}} = \xi c_i\left(\frac{RT_e}{W_i}\right)^{1/2}$$

where, in this case, the correction factor ξ is the first reaction-rate coefficient specified on the reaction line in the SURFACE KINETICS input file. This rate-of-progress of the Bohm reaction will then be modified within the Plasma Reactor Model to account for the presence of any negative ions in the plasma; i.e., each reaction with a BOHM auxiliary keyword ultimately has a rate of progress defined as:

Equation 8-96

$$q_{\mathrm{mod}} = \xi c_i \left(\frac{RT_e}{W_i}\right)^{1/2} \left[\frac{(c_e + c_{n,\,\mathrm{tot}})T_i}{(c_{n,\,\mathrm{tot}}T_e + c_e T_i)}\right]^{1/2}$$

The main difference between these two approaches arises when an ion participates in more than one surface reaction subject to the Bohm criterion. In the first approach, the net ion flux to the surface will be automatically scaled to the Bohm-limiting flux modified for electronegative gases and the user-defined correction factor ξ. In the latter approach, each reaction will be subject to the Bohm limit independently. In that case, it is up to the user to make sure that the reaction coefficients ξ add up to the desired overall correction factor, for all the reactions involving a particular ion. This overall correction factor is often used to account for spatial variations in ion density or transport limitations in the reactor being modeled. For example, the correction factor may be set equal to an estimation of the ratio of the ion density at the sheath edge to the ion density in the bulk of the plasma.[51,52,53]

8.5.4 Summary of Solution Variables for Homogeneous Systems

The total number of species defined in the homogeneous system is

Equation 8-97

$$K = K_g + \sum_{m=1}^{M} [K_s(m) + K_b(m)]$$

where K_g is the number of gas-phase species; $K_s(m)$ and $K_b(m)$ is the number of surface- and bulk-phase species on the *m*th material; and M is the total number of different reacting materials defined in the reactor. The maximum number of unknowns in the problem, J, is therefore given by

Equation 8-98

$$J = \left[L + K + \sum_{m=1}^{M} N_\rho(m)\right] \times N_{\mathrm{PSR}}$$

where, in addition to species fractions and surface phase densities, we will be solving *L* additional equations, which may include gas temperature, electron temperature, and/or surface temperature. These equations are solved simultaneously for all N_{PSR} reactors in the cluster. The equation corresponding to gas-phase species is *Equation 8-1*. The equation corresponding to surface phase site fractions is *Equation 8-9*, while the equation for bulk species is either *Equation 8-18* or *Equation 8-19*, depending on whether or not the bulk species may be etched. The

equations corresponding to site densities, in the case when non-site-conserving reactions are included in the surface mechanism, is *Equation 8-20*. The gas temperature is determined by *Equation 8-91* and the electron energy equation is *Equation 8-85*.

9 Partially Stirred Reactor (PaSR) Model

In this chapter we derive the general equations and discuss the solution methodology for simulation of zero-dimensional systems that are not well mixed. These “partially stirred” systems include both open (with flow) and closed systems and the equations are solved in transient form, using time-integration methods. The following Chemkin reactor models are addressed:

1. Closed Partially Stirred Reactor
2. Partially Stirred Reactor (PaSR)

Many practical applications deviate significantly from an ideally mixed situation, including gas turbines and internal combustion engines. When the turbulent mixing rate is not fast compared to chemical kinetics, the degree of mixing can have a profound impact on the reactor characteristics. The PaSR model allows us to relax the perfectly stirred reactor (PSR) assumption of fast turbulent mixing. Since the most salient feature of a PaSR is the unmixed nature of the reactive fluids at the molecular level, the modeling focuses on the influence of an unmixed state on the reactor properties. The mean thermo-chemical properties inside a PaSR are assumed to be spatially homogeneous, but imperfectly mixed at the molecular level. That is, the reactive fluids are not completely diffused into each other at the molecular level but their mean values are uniform throughout the reactor by turbulent stirring.

The mixing process in the PaSR is characterized by the mixing frequency, which is often modeled by the reciprocal of the turbulence time scale. Because fluid dynamics inside the PaSR are not resolved, the mixing frequency will be prescribed as an input parameter. Therefore, in addition to the mean reactor residence time, the mixing time is another fluid mechanical time scale that controls the properties of the PaSR.

The composition and temperature in the PaSR are described by a probability density function (PDF). This composition PDF is a subset of the joint velocity-composition PDF, because the flow field in the PaSR is assumed to be spatially homogeneous. Velocity fluctuations are also ignored; that is, the PDF is over scalars only, but is not a delta-function in scalar space because reactants, intermediates, and products are not mixed at the molecular level.

The PaSR is related to and bounded by other models commonly used in combustion. When the mixing time scale approaches zero, the mixing process becomes fast enough that the properties inside the PaSR are homogeneously mixed at the molecular level. In this limit, the PaSR becomes a PSR, for which the joint scalar PDF degenerates to a delta function in the composition space and the mean residence time is the sole controlling time scale. In the other extreme limit (large mixing time), there is no mixing among the pockets of gas in the PaSR; consequently, the PaSR consists of segregated reactive mixtures. The average statistics are the sum of the properties of the reactive mixture pockets weighted by the PDF of their ages inside the PaSR. In this case the PaSR acts like a plug-flow reactor, for limit of no mixing and relatively large mean residence times (closed system).

The PaSR may be used as a stand-alone model for studying turbulent combustion or other reactor systems where mass transport may be a rate-limiting factor. Or a PaSR can be used to simulate the sub-grid turbulent mixing and chemical reactions in a computational fluid dynamic (CFD) cell.

One of the important concerns of turbulent reactive flows, especially turbulent flames, is the coupling between chemical reactions and turbulence. The interaction between chemical reactions and fluid dynamics is best described by the Damköhler number, which is defined as the ratio of characteristic flow time and the characteristic chemical reaction time. Due to the large spectrum of chemical times in a multicomponent chemical system, the Damköhler number can also span a large spectrum. As the Damköhler number corresponding to a specific chemical reaction approaches infinity, the reaction responds much faster to the flow so that it approaches equilibrium conditions. On the other hand, if the Damköhler number of a reaction is small, the reaction is considered frozen. Only when the Damköhler number is of the order of unity, are the interactions between the reaction and the fluid dynamics strong. In this case, the reaction becomes one of the “controlling” steps of the process. Depending on the flow time, the same chemical process can be controlled by different sets of reactions.

A PaSR addresses the interaction between chemical reactions and turbulence.[56, 57] The basic assumptions for the PaSR are similar to other zero-dimensional models. The major difference between a PSR and a PaSR lies in the treatment of the molecular mixing inside the reactor. In a PSR, the contents of the reactor are well mixed, by assuming very diffuse conditions, high-intensity turbulent stirring action, or some other active "stirring" mechanism. The only influence of fluid dynamics in a PSR is introduced by the reactor residence time τ_R. Unlike the PSR, a PaSR allows fluid dynamics to control the extent of the molecular mixing and consequently the chemical reactions, by means of an additional parameter: the scalar mixing time, τ_{mix}. The turbulent mixing time scale is often considered to be proportional to the turbulent eddy turnover time as

Equation 9-1 Definition of Mixing Time

$$\tau_{\text{mix}} = C_D \frac{\tilde{\kappa}}{\tilde{\varepsilon}}$$

where C_D is usually treated as a constant but its value varies for different flow configurations. The ratio of turbulent kinetic energy to its dissipation rate, $\tilde{\kappa}/\tilde{\varepsilon}$, represents the time scale of the energy-containing eddies, which characterize the turbulent mixing action.

9.1 The Joint PDF Transport Equation

One of the crucial issues of modeling chemical reaction in turbulent flows is the chemical closure problem. It is well known that in such flows, due to the highly non-linear dependence of chemical reactions on temperature, using the mean temperature and mean species concentrations for calculations of mean chemical reaction rates can cause significant errors.

The closure problem associated with non-linearities in the equations governing turbulent flow can be avoided by considering the joint probability density function (PDF) of the flow variables. The joint PDF of scalars, $P_\phi(\psi;\hat{x},t)$, provides a complete statistical description of the chemical and thermodynamic state. The use of a transport equation for $P_\phi(\psi;\hat{x},t)$ is particularly attractive for reacting flows, since the effects of reactions appear in closed form, irrespective of the complexity and non-linearity of the reaction mechanism. However, reactive flows of practical interest usually involve many species. Consequently the dimensions of the PDF $P_\phi(\psi_1, \psi_1, \ldots, \psi_\sigma;\hat{x},t)$ are large and finite-difference solutions of the PDF transport

56. S.M. Correa, *Combustion and Flame* **93**:41-60 (1993).
57. J.-Y. Chen, *Combustion Science and Technology* **122**:63-94 (1997).

equation are impractical because of the large σ. Pope[58] developed a Monte Carlo algorithm that makes solving the PDF transport equation practical for general turbulent reactive flows. Rather than considering $P_\phi(\psi;\hat{x},t)$ explicitly, the dependent variable in the simulation is represented by an *N*-member ensemble:

Equation 9-2

$$\phi^{(1)}, \phi^{(2)}, \ldots, \phi^{(n)}, \ldots, \phi^{(N)}$$

Here each of the N members of the ensemble is referred to as a "particle". Although each particle is ascribed a unique number, $1 \le n \le N$, no ordering is implied. In fact, operations are performed either on all particles or particles selected at random. Thus, the numbering is a convenience that has no effect on the outcome. The ensemble average of any function $Q(\phi)$ is defined by

Equation 9-3

$$\langle Q(\phi)\rangle \equiv \frac{1}{N}\sum_{n=1}^{N} Q(\phi^{(n)})$$

In the limit of large N, Pope[58, p. 180] showed that the ensemble average $\langle Q(\phi)\rangle$ converges to the corresponding density-weighted average, i.e.,

Equation 9-4

$$\langle Q(\phi)\rangle \to \tilde{Q}(\phi) = \int Q(\psi)\tilde{P}_{\bar{\phi}}(\psi)d(\psi)$$

For the general multiple reactive scalars, the transport equation for the joint PDF in the PaSR is derived by integrating the governing equation of the single-point joint scalar PDF over the reactor volume. The resulting PDF transport equation for the PaSR is

Equation 9-5

$$\frac{\partial \tilde{P}_{\bar{\phi}}(\bar{\psi},t)}{\partial t} = -\sum_{\alpha=1}^{K_{\text{tot}}} \frac{\partial}{\partial \psi_\alpha}\{S_\alpha(\bar{\psi})\tilde{P}_{\bar{\phi}}(\bar{\psi},t)\} + \frac{1}{\tau_R}\sum_{i=1}^{M}\{\tilde{P}_{\bar{\phi},i}(\bar{\psi},t) - \tilde{P}_{\bar{\phi}}(\bar{\psi},t)\} - \sum_{\alpha=1,\beta=1}^{K_{\text{tot}}} \frac{\partial^2}{\partial \psi_\alpha \partial \psi_\beta}\{\langle \varepsilon_{\alpha\beta} | \bar{\phi} = \bar{\psi}\rangle \tilde{P}_{\bar{\phi}}(\bar{\psi},t)\}$$

58. S.B. Pope, *Combustion Science and Technology* **25**:159-174 (1981).

The first two terms on the right hand side of *Equation 9-5* represent the effects of chemical reaction and the through-flow on the joint PDF, respectively. The last term represents the effect of micro-scale mixing on the PDF, which requires the use of a mixing model. The mixing model mimics the finite rate mixing of particles in the stochastic simulations. Two widely used mixing models are employed as options in the current PaSR model.

The simplicity of using a Monte Carlo method and a scalar PDF permits us to carry out simulations with detailed chemistry without significant computing costs.

9.2 Molecular Mixing Models

Two current mixing models are considered: the modified Curl's mixing model[59] and the linear-mean-square-estimation (LMSE) model. Briefly, we summarize the expressions of these mixing models here. Detailed descriptions of these models can be found in the corresponding references.

Equation 9-6 The modified Curl's mixing model

$$-\sum_{\alpha=1,\beta=1}^{K_{\mathrm{tot}}}\frac{\partial^2}{\partial\psi_\alpha\partial\psi_\beta}\{\langle\varepsilon_{\alpha\beta}|\bar{\phi}=\bar{\psi}\rangle\tilde{P}_{\bar{\phi}}(\bar{\psi},t)\}=$$

$$\frac{1}{\tau_{\mathrm{mix}}}\left\{\iint_{\psi',\,\psi''}\tilde{P}_{\bar{\phi}}(\psi',t)\tilde{P}_{\bar{\phi}}(\psi'',t)H(\psi',\,\psi'''|\bar{\psi})d\psi'd\psi''-\tilde{P}_{\bar{\phi}}(\bar{\psi},t)\right\}$$

where H is the transitional probability defined as $H(\psi',\,\psi''|\bar{\psi})=\{1/|\psi''-\psi'|$ for $\psi\in[\psi',\,\psi']$ otherwise 0.

The Interaction-by-Exchange-with-the-Mean (IEM) or the Linear-Mean-Square-Estimation (LMSE) model[60] is shown in *Equation 9-7*

Equation 9-7 IEM or LMSE model

$$-\sum_{\alpha=1,\beta=1}^{K_{\mathrm{tot}}}\frac{\partial^2}{\partial\psi_\alpha\partial\psi_\beta}\{\langle\varepsilon_{\alpha\beta}|\bar{\phi}=\bar{\psi}\rangle\tilde{P}_{\bar{\phi}}(\bar{\psi},t)\}=\frac{C_\phi}{2\tau_{\mathrm{mix}}}\frac{\partial}{\partial\psi_\alpha}\{(\bar{\psi}-\tilde{\phi})\tilde{P}_{\bar{\phi}}(\bar{\psi},t)\}$$

where C_ϕ is a constant parameter for the model.

59. J. Janicka, W. Kolbe and W. Kollmann, *Journal of Non-equilibrium Thermodynamics* **4**:47- (1979).
60. C. Dopazo, *Physics of Fluids* **18**:397- (1975).

Chen[57, p. 179] derived analytical forms of unmixedness as a function of mixing time scale for the two mixing models. These analytical functions serve as a base for validating the PaSR code. The unmixedness or the segregation variable is a parameter used to quantify the unmixed nature, and its definition is given as

$$\text{unmixedness} = \frac{\langle f'' f'' \rangle}{(1 - \langle \tilde{f} \rangle)\langle \tilde{f} \rangle}$$

Where f is the mixture fraction and $\tilde{f}$ and f'' denote density-weighted average and fluctuation, respectively. The definition guarantees that the unmixedness is bounded by zero and one, which corresponds to completely segregated and perfectly mixed states, respectively. The theoretical values of the unmixedness at the statistically stationary state for the two mixing models are:

Equation 9-8 Modified Curl's model

$$\text{unmixedness} = \frac{1}{1 + \tau_{\text{res}} / 3\tau_{\text{mix}}}$$

Equation 9-9 LMSE (IEM) model

$$\text{unmixedness} = \frac{1}{1 + C_\phi \tau_{\text{res}} / \tau_{\text{mix}}}$$

When $C_\phi = 1/3$, the two mixing models should produce identical levels of unmixedness for a given mixing time scale. *Figure 9-1* shows the unmixedness versus mixing frequency from simulations of a pure mixing problem for $\tau_R = 1\text{ms}$. The numerical results of Chemkin show excellent agreement with the theoretical values.

Figure 9-1 Unmixedness vs. mixing frequency for PaSR of stoichiometric H_2/air mixture with 1 ms residence time

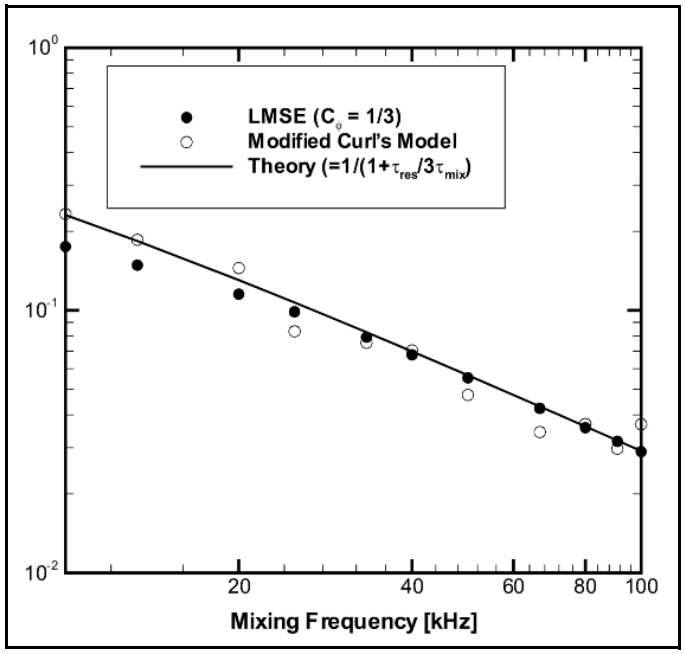

9.3 Reactor Equations

The PaSR consists of an adiabatic chamber having M inlet streams and one outlet. Steady flows of reactants are introduced through the inlets with given gas compositions and temperatures. The reactor pressure is assumed to be constant. Since there is no surface reaction, the mass flow rate at the outlet must be equal to the sum of the mass flow rates of all inlets so that the mass is conserved. In order to represent the evolution of the PDF properly by a stochastic scheme, PaSR addresses all problems in a transient manner. The overall mass balance for the gas mixture inside the PaSR is

Equation 9-10

$$\frac{d\langle M\rangle}{dt} = \frac{d(\langle\rho\rangle V)}{dt} = \sum_{i=1}^{M} \dot{m}_i - \dot{m}_o = 0$$

where $\dot{m}_i$ is the mass flow rate of the *i* th inlet and $\dot{m}_o$ is the through-flow mass flow rate. The average properties of the PaSR are obtained from the ensemble of particles inside the reactor. Each particle is regarded as an independent PSR and interacts with others only through the molecular mixing process. Therefore, the conservation of energy and species is applied to an individual particle rather than to the reactor.

The species equation for a particle is then similar to that of a PSR:

Equation 9-11

$$\frac{dY_k^{(n)}}{dt} = \frac{1}{\dot{m}_o \tau_R} \sum_{i=1}^{M} \{\dot{m}_i (Y_{i,k} - \langle Y_k \rangle)\} + \frac{W_k \dot{\omega}_k^{(n)}}{\rho^{(n)}}$$

and similarly the energy equation for a particle is:

Equation 9-12

$$\frac{dT^{(n)}}{dt} = \frac{1}{C_p^{(n)} \dot{m}_o \tau_R} \sum_{i=1}^{M} \dot{m}_i \left(\sum_{k=1}^{k_g} Y_{i,k} (h_{i,k} - \langle h_k \rangle) \right) - \sum_{k=1}^{k_g} \frac{W_k \dot{\omega}_k^{(n)} h_k^{(n)}}{\rho^{(n)} C_p^{(n)}}$$

In the above equations, the angled bracket ($\langle\ \rangle$) indicates the ensemble average that we use to approximate the density-weighted average in the simulation. The average residence time of the reactor, τ_R, is calculated as

Equation 9-13

$$\tau_R = \frac{\langle \rho \rangle V}{\dot{m}_o}$$

9.4 Stochastic Simulation

A time marching scheme with a time-step size of Δt is used to solve *Equation 9-13* and the stochastic simulation is carried out by the following sequential procedures with N statistical particles:

9.4.1 Through-flow (Convection)

The number of correct particles in a time step is chosen as:

Equation 9-14

$$N_c = N \times \Delta t / \tau_R$$

In the first procedure, we set the properties of these N_c particles from the stochastic ensemble, the properties of the inlet mixture. Property changes of the statistics due to mixing and chemical reaction will be computed by the next two procedures.

9.4.2 Molecular Mixing

With the modified Curl's mixing model,

Equation 9-15

$$N_m = C_m N \times \Delta t / \tau_{\text{mix}}$$

particles are chosen to mix with each other. C_m in *Equation 9-15* is a parameter for the modified Curl's model. If the IEM (LMSE) model is used, *Equation 9-9* is solved to determine the statistics over a period of Δt.

9.4.3 Chemical Reaction

Next, we compute chemical kinetics for each particle by integrating the species and energy equations (*Equation 9-11* and *Equation 9-12*) over a period of Δt.

9.4.3.0.1 These same procedures (*Section 9.4.1* through *Section 9.4.3*) are repeated for the next time step until the end of the simulation time is reached.

9.4.3.0.2

10

10 Plug-flow Assumptions and Equations

In this chapter, we will discuss the governing equations pertaining to plug-flow conditions in an arbitrarily shaped channel, with consideration of gas and surface kinetics. The governing equations and assumptions discussed here pertain to the following Chemkin reactor models:

1. Plug-flow Reactor (PFR)
2. Honeycomb Reactor
3. Plasma Plug-flow Reactor (Plasma PFR)

Tubular flow reactors have long been used throughout the chemical process industries. The tube flow configuration is a natural choice for processes that are carried out in a continuous fashion. For this reason, such reactors are usually operated at steady state. Traditional applications have included both homogeneous reactions (carried out in an empty tube) and fluid-solid heterogeneous reactions in packed beds. More recently, tubular reactors have been used extensively to deposit thin solid films via chemical vapor deposition (CVD). While this is technically a batch process with regard to the solid deposit, the reactor still operates essentially at steady state for extended periods of time. The PFR models describe the steady-state, tube flow reactor that can be used for process design, optimization, and control.

Because the general equations for chemically reacting flow involve transport phenomena in addition to kinetics and thermodynamics, rigorous reactor models are by necessity multidimensional. However, there are often practical as well as mathematical reasons for considering idealized models of reduced dimensionality. In the case of tube flow, the accepted ideal is the plug-flow reactor, in which it is assumed that there is no mixing in the axial (flow) direction but perfect mixing in the direction(s) transverse to this. It can be shown[61] that the absence of axial mixing

61. J. M. Smith, *Chemical Engineering Kinetics*, McGraw-Hill Book Company, New York, 1981.

allows the achievable reactant conversion to be maximized. Likewise, the lack of transverse gradients implies that mass-transfer limitations are absent, once again enhancing the reactor performance. Along with these practical advantages, the plug flow reactor is computationally efficient since it is modeled using first-order ordinary differential equations (ODE's), and no transport properties are needed.

The equations governing the behavior of a plug-flow reactor are simplified versions of the general relations for conservation of mass, energy, and momentum.[62] They can be derived most easily by writing balances over a differential slice in the flow direction x, with the stipulations that (a) there are no variations in the transverse direction, and (b) axial diffusion of any quantity is negligible relative to the corresponding convective term. In this way the overall mass balance (continuity equation) for the gas is found to be

Equation 10-1 Mass Continuity Equation

$$\rho u\frac{dA}{dx} + \rho A\frac{du}{dx} + uA\frac{d\rho}{dx} = \sum_{m=1}^{M} a_{i,m} \sum_{k=1}^{K_g} \dot{s}_{k,m} W_k$$

Here ρ is the (mass) density and u the axial velocity of the gas, which consists of K_g species; W_k is the molecular weight of species k, and $\dot{s}_k$ is the molar production rate of this species by all *surface* reactions. The quantities A and $a_{i,m}$ are the cross-sectional (flow) area and the effective internal surface area per unit length of material m, respectively, in the reactor. Both A and $a_{i,m}$ can change as arbitrary functions of x. *Equation 10-1* simply states that the mass flow rate of the gas can change as a result of generation or consumption by surface reactions on all materials in the reactor. A similar equation can be written for each species individually:

Equation 10-2 Gas-species Conservation Equation

$$\rho uA\frac{dY_k}{dx} + Y_k \sum_{m=1}^{M} a_{i,m} \sum_{k=1}^{K_g} \dot{s}_{k,m} W_k = W_k \left(\sum_{m=1}^{M} \dot{s}_{k,m} a_{i,m} + \dot{\omega}_k A \right)$$

Here Y_k is the mass fraction of species k and $\dot{\omega}_k$ is its molar rate of production by homogeneous *gas* reactions. Such reactions cannot change the total mass of the gas, but they can alter its composition.

62. R. B. Bird, W. E. Stewart, and E. N. Lightfoot, *Transport Phenomena*, John Wiley and Sons, New York, 1960.

Turning now to the energy equation, one finds.

Equation 10-3 Energy Equation

$$\rho u A\left(\sum_{k=1}^{K_g} h_k \frac{dY_k}{dx} + \bar{C}_p \frac{dT}{dx} + u\frac{du}{dx}\right) + \left(\sum_{k=1}^{K_g} h_k Y_k + \frac{1}{2}u^2\right)\sum_{m=1}^{M} a_{i,m}\sum_{k=1}^{K_g} \dot{s}_{k,m} W_k = a_e Q_e - \sum_{m=1}^{M} a_{i,m}\sum_{k=K_b^f}^{K_b} \dot{s}_{k,m} W_k h_k$$

where h_k is the specific enthalpy of species k, $\bar{C}_p$ is the mean heat capacity per unit mass of the gas, T is the (absolute) gas temperature. In the right-hand summation, $\dot{s}_{k,m}$ is the molar production rate of bulk solid species k by surface reactions on material m. The distinction between bulk and surface species is discussed in *Section 1.1* and *Chapter 4* of this manual. *Equation 10-3* states that the total energy (enthalpy plus kinetic) of the flowing gas changes due to the heat flux Q_e from the surroundings to the outer tube wall (whose surface area per unit length is a_e) and also due to accumulation of enthalpy in the bulk solid. It is worth noting that *Equation 10-3* does not involve the enthalpies of the surface site species.

The momentum equation for the gas expresses the balance between pressure forces, inertia, viscous drag, and momentum added to the flow by surface reactions. Thus,

Equation 10-4 Momentum Equation

$$A\frac{dP}{dx} + \rho u A\frac{du}{dx} + \frac{dF}{dx} + u\sum_{m=1}^{M} a_{i,m}\sum_{k=1}^{K_g} \dot{s}_{k,m} W_k = 0$$

where P is the absolute pressure and F is the drag force exerted on the gas by the tube wall, to be discussed below. The pressure is related to the density via the ideal-gas equation of state, as given in *Equation 2-4*.

Since the heterogeneous production rates $\dot{s}_{k,m}$ will depend, in general, on the composition of the surface as well as that of the gas, equations determining the site fractions Z_k of the K_s surface species are now needed. Assuming that these species are immobile, the steady-state conservation equations are simply stated in *Equation 10-5*. The surface species conservation equation is applied to every species in each surface phase n contained on each surface material m.

Equation 10-5 Surface Site Species Conservation Equation

$$\dot{s}_k = 0 \qquad k = K_s^f, \ldots, K_s^l$$

i.e., the net production rate of each surface species by heterogeneous reactions must be zero. However, we also assume that the total site density for each surface phase is a constant. As a result, the algebraic equations represented by *Equation 10-5* are not all independent, and for each phase on each material, one of the equations must be replaced by the condition,

Equation 10-6

$$\sum_{\text{phase}} Z_k = 1$$

In order to minimize errors, *Equation 10-6* is used to replace *Equation 10-5* for the species having the largest site fraction.

The system of governing equations for the reactor is now mathematically closed. However, because the residence time τ of the gas is often a quantity of interest, it is useful to include an equation that computes it automatically. This is simply

Equation 10-7

$$\frac{d\tau}{dx} = \frac{1}{u}$$

Equation 10-1 through *Equation 10-7* provide a total of $5 + K_g + K_s$ differential/algebraic relations involving the dependent variables ρ, u, T, P, τ, Y_k and Z_k. The functions $\overline{W}$, h_k, $\overline{C}_p$, $\dot{\omega}_k$, and $\dot{s}_{k,m}$ can all be expressed in terms of these and are obtained from calls to GAS-PHASE KINETICS and SURFACE KINETICS subroutine libraries. The quantities $A(x)$, $a_{i,m}(x)$, and $a_e(x)$ are fixed by the reactor geometry. This then leaves only Q_e and F to be addressed.

For plug-flow and related reactor models, there are many different options for handling the reactor energy balance:

1. Constrained Temperature. The reactor can be declared to be isothermal, or the (axial) temperature profile can be specified as a user-defined piecewise linear profile, or an arbitrary temperature profile can be specified via a user subroutine; in all constrained-temperature cases, the energy equation (*Equation 10-3*) is not solved.
2. Adiabatic reactor, or ($Q_e = 0$). In this case the energy equation is solved.
3. Specified Heat loss. This can be a constant heat flux or a user-specified piecewise-linear function of heat flux vs. distance, which define $Q_e(x)$.
4. A specified heat-transfer coefficient. For this option, $Q_e(x)$ is defined in terms of the ambient temperature T_∞ and an overall heat transfer coefficient U:

Equation 10-8

$$Q_e = U(T_\infty - T)$$

Both T_∞ and U must be supplied by the user.

The viscous drag force F is written in terms of a friction factor f as follows:

Equation 10-9

$$\frac{dF}{dx} = a_i \cdot \frac{1}{2}\rho u^2 f$$

The friction factor can in turn be expressed as a function of the local Reynolds number

Equation 10-10

$$\mathrm{Re} = \frac{Du\rho}{\mu}$$

where D is the tube diameter (or the mean hydraulic diameter for a conduit with a noncircular cross section) and μ is the gas viscosity. For laminar flow ($\mathrm{Re} = 2100$) the analytical result for round tubes is

Equation 10-11

$$f = \frac{16}{\mathrm{Re}}$$

while for turbulent flow one can use the approximate Blasius formula,[62]

Equation 10-12

$$f = 0.0791\mathrm{Re}^{-0.25}$$

This approach is only approximate, especially for noncircular conduits, but viscous drag is usually of very minor importance in gas-phase reactors. In keeping with this, and in order to avoid having to calculate transport properties, the gas viscosity is computed by scaling the inlet value (supplied by the user) by $(T/T_{in})^{0.5}$ and ignoring the composition dependence.

It remains to specify the initial (inlet) conditions for the reactor. Clearly, values for ρ, u, T, P and Y_k at $x = 0$ should be known or easily obtainable from the problem statement, the ideal gas law, and the reactor geometry, and of course $\tau = 0$ at this point. Since there are no derivatives of the Z_k in the governing equations, it might appear that no initial conditions are needed for them. However, the transient solver employed requires a consistent set of derivatives of the Z_k variables at the reactor inlet. For plug-flow simulations, this is accomplished in a separate preliminary calculation, in which a set of fictitious transient equations are solved, as given in *Equation 10-13* is solved in conjunction with *Equation 10-6* until steady state is reached.

Equation 10-13 Preliminary Surface Site Equation

$$\frac{dZ_k}{dt} = \frac{\dot{s}_k \sigma_k}{\Gamma} \qquad k = K_s^f, \ldots, K_s^l$$

Here σ_k is the site occupancy number for species k and Γ is the total site density of the phase in question. The initial values of Z_k for *Equation 10-13* are essentially arbitrary (unless there are multiple steady states), although better guesses will lead to faster convergence.

10.1 Honeycomb Monolith Reactor Calculations

The Honeycomb Monolith Reactor is a special case of a general plug-flow reactor, where user input parameters describing the honeycomb geometry are used to automatically calculate the available surface area for gas-surface reactions. In the Chemkin User Interface, the Honeycomb Monolith Reactor is represented as a separate reactor icon.

When this reactor model is chosen, Chemkin provides a special parameter-entry panel that allow users to specify parameters that describe the honeycomb monolith and catalyst loading conditions. These parameters are then automatically converted into corresponding plug-flow parameters by the Chemkin Interface utilities. *Table 10-1* shows the parameters with the default units that are entered by the user on the Honeycomb Monolith Reactor Panel tabs.

Table 10-1 Honeycomb Monolith Reactor Parameters

Parameter	***Default Units***
Cells Per Square Inch, $cpsi$	1/in^2
Cell Wall Thickness, t_w	mil or 1/1000 in
Diameter, D_r	cm
Length, L_r	cm
Cell Size, D_{cell} or the width of the individual cell channel for a square channel	cm
Metal Surface Area, A_{cat}	cm^2/g catalyst
Metal Weight, W_{cat}	g catalyst
Metal Dispersion, r_{cat}	%
Pressure Gradient, dP/dx	dyne/cm^3

Using this information, Chemkin performs the following conversions behind the scenes, to set up the PFR model using honeycomb monolith parameters:

1. Calculates the internal surface area of the PFR, A_{int}, where A_{int} is the active internal surface area per unit length of the plug-flow reactor (cm^2/cm):

Equation 10-14

$$A_{\text{int}} = \frac{A_{\text{cat}} W_{\text{cat}} r_{\text{cat}}}{100 \times L_r}$$

2. Calculates the external heat transfer area per unit length (cm^2/cm), A_{ext}:

Equation 10-15

$$A_{\text{ext}} = \pi D_r$$

3. Calculate the cross sectional flow area (cm^2), A_{flow}:

Equation 10-16

$$A_{\text{flow}} = \frac{cpsi}{(2.54)^2}\frac{\pi}{4}D_r{}^2 D_{\text{cell}}{}^2$$

Equation 10-17

$$D_{\text{cell}} = 2.54\left((cpsi)^{-1/2} - \frac{t_w}{1000}\right)$$

4. Set up a pressure profile to represent the user-specified pressure drop. In this case we assume a linear profile from the beginning of the channel to the end of the channel, with the starting point set at the reference pressure specified in the main reactor panel, and the ending pressure set as:

Equation 10-18

$$P_{\text{end}} = P_0 - \left(\frac{dP}{dx}\right)L_r$$

When a user chooses units different from the default, the units conversion will be performed automatically, as with other Chemkin parameters.

Once these parameters have been calculated, the simulation proceeds as described for the general Plug-flow Reactor.

10.2 Plasma Plug-flow Extensions

For the Plasma Plug-flow Reactor Model, an electron energy equation is solved in a manner that is analogous to the implementation discussed for a 0-D homogeneous system, as described in *Section 8.5*. For plug-flow, the electron energy equation will take the form:

Equation 10-19 Plug-flow Electron Energy Equation

$$(\rho uA)\left[Y_e c_{ve}\frac{dT_e}{dx} - \frac{R}{W_e}T_e\frac{dY_e}{dx}\right] = (\dot{\omega}_e A c_{pe})W_e(T - T_e) - Q_{\text{loss}}^{\text{elas}} - Q_{\text{loss}}^{\text{inel}} + Q'_{\text{source}}$$

The loss terms included in *Equation 10-19* are defined in *Equation 10-20* through *Equation 10-23*, where $Q_{\text{other}}(T_e)$ includes $Q_{\text{ions}}^{\text{sheath}}$ and $Q_{\text{ions}}^{\text{plasma}}$, as described in more detail in *Section 8.5* for the homogeneous systems.

Equation 10-20

$$Q_{\text{loss}}^{\text{elas}} = \frac{3AR\rho_e}{W_e}(T_e - T) \sum_{k=1;k\neq e}^{K_g} \frac{W_e}{W_k}\upsilon_{ek}$$

Equation 10-21

$$Q_{\text{loss}}^{\text{inel}} = A\sum_{r=1}^{I_{ei}} \Delta H_r q_r + Q_{\text{other}}(T_e)$$

Equation 10-22

$$Q_{\text{ions}}^{\text{sheath}} = \sum_{m=1}^{M}\sum_{j=1}^{K_i} \dot{s}_{j,m}\varepsilon_j a_{i,m}$$

and

Equation 10-23

$$Q_{\text{ions}}^{\text{plasma}} = \sum_{i=1}^{K_i} \dot{\omega}_i(h_i(T_{\text{ion}}) - h_i(T))A$$

11

11 Boundary-layer Channel Flow

Moving up in complexity from plug-flow assumptions, accounting for the boundary-layer interactions in a channel-flow can be important for many applications. In a boundary-layer approximation, we include the effects of radial diffusion and dispersion for species, mass, and energy. However, convection is assumed to dominate in the axial direction (i.e., along the channel), such that axial diffusion is neglected. These flow conditions can represent laminar flow in cylindrical or planar channels for a variety of applications, including thin film processing in channel-flow reactors, catalytic conversion in a representative pore of a catalyst monolith, or flow within a microchannel reactor, for example. This section describes the governing equations for boundary-layer approximations applied to channel flows. The reactor models addressed here include:

1. Cylindrical Channel Shear-layer Flow Reactor
2. Planar Channel Shear-layer Flow Reactor

The Shear-layer Flow Reactor Models simulate the coupled hydrodynamics, gas-phase chemistry and surface chemistry in laminar-flow channels. Detailed mathematical formulation of this model and a demonstration of its application to chemistry in the chemical vapor deposition (CVD) of silicon from silane have been reported previously in the literature.[63, 64] The model is general, in that it can be applied to any channel-flow system for which gas-phase and surface kinetic mechanisms are known. The model predicts gas-phase temperature and velocity fields, concentration fields for any number of chemical species, deposition or etching rates and surface-species coverage. Results will depend on user-specified flow

63. M. E. Coltrin, R. J. Kee, and J. A. Miller, *Journal of the Electrochemical Society* 131:425 (1984).
64. M. E. Coltrin, R. J. Kee, and J. A. Miller, *Journal of the Electrochemical Society* 133:1206 (1986).

conditions or boundary conditions, such as surface temperature, flow rate, inlet partial pressure of the reactants, total pressure, and reactor dimensions. The models are restricted to two-dimensional geometric representations, using either planar or radial coordinates for Cartesian or axisymmetric flows, respectively.

The Shear-layer Flow Reactor Models require gas transport properties. These are determined using the TRANSPORT Pre-processor and subroutine libraries for calculating thermal diffusion coefficients and for the rigorous calculation of ordinary multicomponent transport properties. The effects of thermal diffusion, which is the separation of species of differing size in a temperature gradient may be included when requested by the user. Thermal diffusion can have an important effect on predicted concentration profiles.[64] The boundary conditions describing chemical reactions at the surface are formulated using the SURFACE KINETICS Pre-processor, while the gas-phase kinetics calculations employ the GAS-PHASE KINETICS Pre-processor.

11.1 Boundary-layer Equations

The boundary-layer equations can again be derived from general conservation equations that govern the fluid flow coupled with species and energy transport. These equations describe chemical species production and destruction, and both convective and diffusive transport. Details of the formulation have been published by Coltrin, *et al*.[63, p. 197,64, p. 197] The applicability of the equations relies on the existence of a principal flow direction in which diffusive transport is negligible compared to convective transport. To simplify the numerical procedure somewhat, we recast the equations using the Von Mises transformation,[65] in which the cross-stream coordinate is replaced by the stream function as an independent variable. We use an additional transformation of the stream function[64, p. 197] that accounts for possible mass loss (or gain) in the gas due to deposition (or etching) at the reacting surfaces.

The set of equations describing the channel-flow models are given as follows:

65. F. K. Moore, in *High Speed Aerodynamics and Jet Propulsion* (Princeton University Press, Princeton, NJ, 1964), Vol. IV.

Equation 11-1 Momentum

$$\rho u\frac{\partial u}{\partial x}-\frac{\rho u}{\dot{m}}\left(\xi\frac{d\dot{m}}{dx}-\frac{d\dot{m}_l}{dx}\right)\frac{\partial u}{\partial \xi}+\frac{dP}{dx}=\frac{\rho u}{\dot{m}^2}\frac{\partial}{\partial \xi}\left(\rho u\mu y^{2\alpha}\frac{\partial u}{\partial \xi}\right)+g(\rho_i-\rho)$$

Equation 11-2 Species

$$\rho u\frac{\partial Y_k}{\partial x}-\frac{\rho u}{\dot{m}}\left(\xi\frac{d\dot{m}}{dx}-\frac{d\dot{m}_l}{dx}\right)\frac{\partial Y_k}{\partial \xi}=\dot{\omega}_k W_k-\frac{\rho u}{\dot{m}}\frac{\partial}{\partial \xi}(y^\alpha \rho Y_k V_{k,y}) \qquad k=1,\ldots,K_g$$

Equation 11-3 Energy

$$\rho u c_p\frac{\partial T}{\partial x}-\frac{\rho u c_p}{\dot{m}}\left(\xi\frac{d\dot{m}}{dx}-\frac{d\dot{m}_l}{dx}\right)\frac{\partial T}{\partial \xi}=\frac{\rho u}{\dot{m}^2}\frac{\partial}{\partial \xi}\left(\rho u\lambda y^{2\alpha}\frac{\partial T}{\partial \xi}\right)-\sum_{k=1}^{K_g}\dot{\omega}_k W_k h_k-\frac{\rho^2 u y^\alpha}{\dot{m}}\sum_{k=1}^{K_g}Y_k V_{k,y}c_{pk}\frac{\partial T}{\partial \xi}$$

Equation 11-4 State

$$P=\frac{\rho RT}{\overline{W}}$$

We provide the option of choosing from two different transport models. In these equations when multicomponent transport is used, the diffusion velocity $V_{k,y}$ is given by

Equation 11-5

$$V_{k,y}=\frac{\rho u y^\alpha}{X_k\overline{W}\dot{m}}\sum_{j\neq k}^{K_g}W_j D_{k,j}\frac{\partial X_k}{\partial \xi}-\frac{D_k^T}{\rho Y_k}\frac{\rho u y^\alpha}{T\dot{m}}\frac{\partial T}{\partial \xi}$$

When mixture-averaged transport is used, the diffusion velocity is:

Equation 11-6

$$V_{k,y}=-\frac{D_{km}\rho u y^\alpha}{X_k\dot{m}}\frac{\partial X_k}{\partial \xi}-\frac{D_k^T}{\rho Y_k}\frac{\rho u y^\alpha}{T\dot{m}}\frac{\partial T}{\partial \xi}$$

The equations represent either cylindrical or cartesian coordinates. For a flow in cylindrical coordinates, the parameter α is 1, and y represents the radius measured from the flow centerline. If α is zero then the equations are in planar coordinates for the flow between two infinitely wide plates, and y is the height above the lower wall. We also allow a third case of cartesian coordinates in which both walls are identical and there is a plane of symmetry. In this case y is the distance above the symmetry plane.

The independent variables x and ξ represent the axial coordinate and the normalized stream function, respectively. (All variables are defined in the Chemkin *Nomenclature* at the end of this manual.) The last term in the momentum equation, *Equation 11-1*, can only be included when the gravity vector is along the principal flow direction, i.e., when the flow is either vertically upward or downward, rather than horizontal.

We define the stream function ψ as

Equation 11-7

$$\psi = \frac{1}{\alpha+1}\int_0^y \rho u dy^{\alpha+1}$$

The stream function is defined such that there is an equal mass flow rate between two lines of constant stream function value (between streamlines, when there is no mass loss). If there is no mass loss to the walls, the reactor walls themselves are streamlines, i.e., lines of constant streamfunction. The independent variable y then ranges from zero at one boundary to the total mass flux $\dot{m}$ at the other. If there is no mass loss at the surfaces, then the total mass flux is evaluated at the initial condition and is constant throughout the computation. In this case, the numerical method can use a mesh in which each mesh point has a specified value of stream function. However, if mass is lost from the gas then the total mass flux changes along the flow direction, and the independent variable changes at each mesh point (i.e., a moving coordinate system). In order to make a new independent variable whose total magnitude is fixed for the entire problem, we define a new stream function that is normalized by the local total mass flux

Equation 11-8

$$\xi = \frac{\psi}{\dot{m}}$$

where $\dot{m}$ is the *local value* of the total mass flux. Therefore, ξ ranges between 0 and 1, and is not dependent on the total mass previously lost (or gained) at the walls.

The relationships between the physical coordinates (y and x) and the transformed coordinates (ξ, ψ and x) are stated in the following equations that define the Von Mises transformation.

Equation 11-9

$$\left(\frac{\partial}{\partial x}\right)_y = \left(\frac{\partial}{\partial x}\right)_\psi - \rho v y^\alpha \left(\frac{\partial}{\partial \psi}\right)_x + \frac{d\dot{m}_l}{dx}\left(\frac{\partial}{\partial \psi}\right)_x$$

Equation 11-10

$$\left(\frac{\partial}{\partial x}\right)_y = \left[\left(\frac{\partial}{\partial x}\right)_\xi - \left(\frac{\xi}{\dot{m}}\frac{d\dot{m}}{dx} - \frac{1}{\dot{m}}\frac{d\dot{m}_l}{dx}\right)\left(\frac{\partial}{\partial \xi}\right)_x\right] - \rho v y^\alpha \frac{1}{\dot{m}}\left(\frac{\partial}{\partial \xi}\right)_x$$

Equation 11-11

$$\left(\frac{\partial}{\partial y}\right)_x = \rho u y^\alpha \left(\frac{\partial}{\partial \psi}\right)_x = \rho u y^\alpha \frac{1}{\dot{m}}\left(\frac{\partial}{\partial \xi}\right)_x$$

The total local mass flux $\dot{m}$ is computed from an equation that accounts for the mass deposited on each boundary

Equation 11-12

$$\frac{d\dot{m}}{dx} = \frac{d\dot{m}_l}{dx} + \frac{d\dot{m}_u}{dx}$$

The mass flux at the lower boundary (in the asymmetric planar case) is determined from the convective (Stefan) mass flux to the boundary

Equation 11-13 (asymmetric, planar case only)

$$\frac{d\dot{m}_l}{dx} = \rho v\Big|_{y=0}$$

(calculation of the transverse velocity at the boundary is discussed in *Section 11.2*). Note that *Equation 11-13* applies only in the asymmetric planar coordinate case (since in cylindrical coordinates or for a symmetric channel in planar coordinates the lower boundary is the centerline, and thus there is no mass change at that boundary). The rate of change of mass flux at the upper boundary (which is the upper wall in planar coordinates or the outer radius in cylindrical coordinates) is similarly defined by

Equation 11-14

$$\frac{d\dot{m}_u}{dx} = -\rho v y^\alpha\Big|_{y=y_{\max}}$$

The initial mass flux entering the channel is defined by

Equation 11-15

$$\dot{m}_0 = \left(\int_0^{y_{\max}} \rho u y^{\alpha} dy \right)_0$$

which serves as the initial condition for *Equation 11-12*.

The system of equations is completed by an equation that relates the cross-stream coordinate y to the normalized stream function

Equation 11-16

$$\frac{1}{\dot{m}} \frac{\partial y^{\alpha+1}}{\partial \xi} = \frac{\alpha+1}{\rho u}$$

This equation comes from differentiating the definition of the streamfunction, *Equation 11-7*.

In addition to including detailed gas-phase chemistry, we include detailed surface reaction chemistry through use of the SURFACE KINETICS Pre-processor. Here we consider M different materials on the solid walls.The number of surface phases (or site types) and the number of surface species on the *m*th material are denoted by $N_s(m)$ and $K_s(m)$, respectively. At each axial position, we solve for the steady-state surface site fractions for each of the N_s surface phases on each material. Thus additional equations, as many as the total number of surface species in the heterogeneous reaction mechanism, have to be solved. The total number of bulk phases is given by $N_b(M)$.We have N_s different surface phases (or site-types), and at each axial position we can solve for the steady-state surface site fractions for each of the surface phases in the form:

$$\sum_{m=1}^{M} N_s(m)$$

Thus, we solve additional equations, where the total number of surface species in the heterogeneous reaction mechanism is:

$$\sum_{M} K_s(m)$$

These equations are shown in *Equation 11-17* and *Equation 11-18* below.

Equation 11-17

$$\dot{s}_{k,\,m} = 0, \quad k = K_s^f(n, m), \ldots, K_s^l(n, m) - 1;\; n = N_s^f\,(m), \ldots, N_s^l\,(m); m = 1, \ldots, M$$

Equation 11-18

$$1 = \sum_{k = K_s^f(n, m)}^{K_s^l(n, m)} Z_{k'} \qquad n = N_s^f\,(m), \ldots, N_s^l\,(m);\; (m = 1, \ldots, M)$$

Here, $K_s^f(n, m)$ and $K_s^l(n, m)$ represent the first and last surface species for surface phase number n on the mth material. This nomenclature is described in more detail in *Section 1.2* and *Section 8.3.2*. For one species in each surface phase, we do not solve the steady state condition given by *Equation 11-17*, but instead use *Equation 11-18*, which requires that the site fractions sum to unity in each phase.

To summarize the system of equations considered for channel-flow, we solve *Equation 11-1* through *Equation 11-4*, *Equation 11-13*, *Equation 11-14*, and *Equation 11-6* at every gas-phase mesh point. In planar coordinates, we also solve *Equation 11-17* and *Equation 11-18* at the upper and lower boundaries. In cylindrical coordinates (or for a symmetric channel in planar coordinates) we solve *Equation 11-17* and *Equation 11-18* only at the upper boundary. This is a parabolic system of equations, where the dependent variables are: P, $y^{\alpha+1}$, u, T, $\dot{m}_l$, $\dot{m}_u$, and Y_k. The equations are subject to a set of algebraic constraints, which are the equations for the surface site fractions, Z_k. This system of equations is solved using the method of lines. We treat the equations as a set of differential/algebraic equations (DAE's),[66] which we solve using the numerical software DASSL.[67, 68]

At the entrance to the reactor channel, the initial profiles of u, T, and Y_k, the pressure, and the surface site fractions z_k must be specified (see *Section 11.3* on species concentration at boundaries). The velocity profile can be either a fully developed parabolic profile or a flat velocity profile, with an optionally specified boundary-layer thickness. If the boundary-layer thickness is specified, then a parabolic profile is assumed only within the boundary-layer. The initial gas temperature across the channel is usually set equal to the initial surface temperature. However, the user may also specify different gas and surface temperatures. As with the velocity profile, if a boundary-layer thickness is specified, the application linearly

66. R. J. Kee and L. R. Petzold, Sandia National Laboratories Report SAND86-8893, 1982.
67. L. R. Petzold, *A Description of DASSL*, Sandia National Laboratories Report SAND82-8637, 1982.
68. K. E. Brenan, S. L. Campbell, and L. R. Petzold, *Numerical Solution of Initial-Value Problems in Differential-Algebraic Equations* North-Holland, New York, (1989).

interpolates the gas-phase temperature between the surface temperature and the gas temperature over the boundary-layer thickness. The initial gas-phase species mass fractions Y_k are taken to be uniform across the channel, with the exception of the mass fractions at reactive walls. These are calculated by the procedure described in *Section 11.3* on species concentrations at boundaries. From the initial profiles we compute the local mass flux $\dot{m}$ and the physical locations of all the mesh points, i.e., a profile of y^{α}.

11.2 Boundary Conditions

For the energy equation, either the temperature, a zero-heat-flux (adiabatic), or a specified heat flux condition is specified at the solid walls. In the transformed equations, ξ is the independent variable and the physical coordinate y is a dependent variable. For the evaluation of y, then, we specify as boundary conditions that $y = 0$ at the lower boundary and $y = y_{\max}$ at the upper boundary (the channel radius in the case of cylindrical coordinates). Notice that there is no explicit equation or boundary condition for the pressure P even though it is a dependent variable. Note also that a boundary value of y is specified at both boundaries even though *Equation 11-16* is only a first-order equation. This apparent over-specification is resolved by the fact that there is no boundary condition for pressure.[63, p. 197]

The boundary conditions for the surface species involve heterogeneous reactions. The convective and diffusive mass fluxes of gas-phase species at the surface are balanced by the production (or depletion) rates of gas-phase species by surface reactions. This relationship is

Equation 11-19

$$\rho Y_k (V_{k,y} + v) = \sum_{m=1}^{M} \dot{s}_{k,m} W_k a_m, \qquad (K = 1, \ldots K_g)$$

where the gas-phase diffusion velocities are given by *Equation 11-5* or *Equation 11-6* and a_m is the surface area fraction of the *m*th material on the solid wall.

In nonreacting flows the fluid velocity normal and tangential to a solid wall is zero. However, if there are chemical reactions at the wall, then the normal velocity can be nonzero. This so-called Stefan flow velocity occurs when there is a net mass flux between the surface and the gas. The Stefan velocity is given by

Equation 11-20

$$v = \frac{1}{\rho} \sum_{m=1}^{M} \sum_{k=1}^{K_g} \dot{s}_{k,m} W_k a_m$$

This expression is easily obtained from the interfacial mass balance, *Equation 11-19*, by summing over all K_g gas-phase species and using the requirement that the mass fractions must sum to one, i.e.,

Equation 11-21

$$\sum_{k=1}^{K_g} Y_k = 1$$

and that the sum of the diffusion fluxes must be zero.

The SURFACE KINETICS input includes the mass densities ρ_k for all bulk species involved in a surface reaction mechanism. These densities are used to convert the surface reaction rate of production of a bulk species (in moles/cm^2/sec) into a growth rate G_k (in cm/sec) for each bulk species. The relationship is given by:

Equation 11-22

$$G_k = \frac{\dot{s}_k W_k a_m}{\rho_k} \qquad (k = K_b^f(m), \ldots, K_b^l(m);\ m) = 1, \ldots, M$$

11.3 Initial Conditions on Species Concentrations at Boundaries

For an arbitrarily complex surface reaction mechanism, it can be difficult to provide an initial set of surface site fractions z_k and gas-phase mass fractions Y_k at the surface, which satisfies *Equation 11-17*, *Equation 11-18*, *Equation 11-19* and *Equation 11-20* at $x = 0$. This self-consistency is necessary because the equations for the surface site fractions and gas-phase mole fractions at the walls are actually algebraic equations, rather than ordinary differential equations. For the solution to begin smoothly, it is necessary to satisfy exactly the algebraic equations at $x = 0$. To this end, a solution is first determined for the correct set of z_k and Y_k that satisfy these

boundary condition equations at the channel inlet. This procedure employs the numerical software TWOPNT to solve for the self-consistent set of gas-phase and surface concentrations at each wall. The user can optionally give the TWOPNT procedure initial guesses for the gas-phase and surface concentrations to aid in the convergence. The initial TWOPNT problem can also be bypassed altogether if the self-consistent values for the z_k and Y_k are supplied by the user.

11.4 Implementation of Multicomponent Transport

Although the mixture-averaged transport approximation is inadequate for some applications (for example, CVD at very low pressures, or when a carrier gas is not used), it has some properties that make it attractive for numerical computation. It is significantly less computationally intensive than the full multicomponent transport formulation (see *Chapter 5* for more information). Also, the mixture-averaged diffusion velocity of species k (*Equation 11-6*) depends explicitly on the concentration gradient of species k, but the multicomponent diffusion velocity of *Equation 11-5* depends on the concentration gradients of all the remaining species. As a result, the Jacobian of the diffusion velocity has a strong diagonal term in the former case, but not in the latter case.

We find that solution of the set of differential/algebraic equations is aided by using a form for the multicomponent diffusion coefficient discussed by Coltrin, *et al.*,[64, p. 197] found by equating *Equation 11-5* and *Equation 11-6* and solving for D_{km},

Equation 11-23

$$D_{km} = \frac{\sum_{j \neq k}^{K_g} W_j D_{k,j} (\partial X_j / \partial \xi)}{\overline{W} \sum_{j \neq k}^{K_g} (\partial X_j / \partial \xi)}$$

The denominator in *Equation 11-23* is found by noting that

Equation 11-24

$$\frac{\partial X_k}{\partial \xi} = -\sum_{j \neq k}^{K_g} \frac{\partial X_j}{\partial \xi}$$

Here, we implement multicomponent transport using the diffusion velocity of the form in *Equation 11-6*, with D_{km} calculated using *Equation 11-23*.

Mass conservation requires that the diffusive mass fluxes sum to zero

Equation 11-25

$$\rho \sum_{k=1}^{K_g} Y_k V_k = 0$$

However, a consequence of using the mixture-averaged transport formulation in *Equation 11-6* to define a diffusion velocity and using the mixture-averaged diffusion coefficients D_{km} is that mass is not always conserved, i.e., the diffusive mass fluxes are not guaranteed to sum to zero. Therefore, at the mixture-averaged level of closure of the transport formulation some corrective measures must be taken. The user has two options. One is to apply an ad-hoc correction velocity,[25, p. 84] defined as

Equation 11-26

$$V_c = -\sum_{k=1}^{K_g} Y_k V_k$$

When this correction velocity (independent of species, k) is added to all the species diffusion velocities as computed from *Equation 11-6*, diffusional mass conservation is assured. This Correction Velocity option can be specified in the User Interface.

Another option to account for the deficiencies of the mixture-averaged closure of the transport problem and to assure mass conservation is to solve only $K_g - 1$ gas-phase species conservation equations and to determine the remaining mass fraction by requiring $\sum_{k=1}^{K_g} Y_k = 1$. (The mixture-averaged transport closure is asymptotically correct in the trace-species limit.) In cases where one species is present in large excess (such as a carrier gas), this is a reasonable option. The carrier-gas composition is conveniently determined as

Equation 11-27

$$Y_{k_m} = 1 - \sum_{\substack{k=1 \\ k \neq k_m}}^{K_g} Y_k$$

Where k_m is the species for which we have chosen to apply the closure constraint. The program will determine k_m as the index of the species with the highest concentration. If the user does not specify use of a correction velocity, it is assumed that the species k_m is the carrier gas and thus a corresponding conservation equation (*Equation 11-2*) for that species is not solved. Instead, for that species, *Equation 11-27* applies.

11.5 Thermal Diffusion

Thermal diffusion is the separation of two species of differing size in the presence of a temperature gradient. Because there can be strong temperature gradients in a reactor, thermal diffusion can significantly influence deposition rates[64, p. 197,69,70] as well as density profiles, as observed by *in situ* measurements.[71,72,73,74] The effect of thermal diffusion is included in the diffusion velocity as the second term on the right side of *Equation 11-5* or *Equation 11-6*. Note that a full multicomponent model is used for the computation of thermal diffusion coefficients, regardless of whether the user has specified the mixture-averaged or the multicomponent option for the calculation of the diffusion velocity. See *Chapter 5* for more details about this formulation.

11.6 Finite Difference Approximations

The governing conservation equations require discretization to allow numerical solution. For channel-flow models, a finite difference approximation is used on a non-uniform grid with points numbered as $j = 1$ at the lower boundary to $j = J$ at the upper boundary. Approximation of the spatial derivatives is accomplished by finite difference representations on a fixed grid in the normalized stream function.

69. J. P. Jenkinson and R. Pollard, *Journal of the Electrochemical Society* **131**:2911 (1984).
70. J. Juza and J. Cermak, *Journal of the Electrochemical Society* **129**:1627 (1982).
71. W. G. Breiland and M. J. Kushner, *Applied Physics Letters* **42**:395 (1983).
72. P. Ho and W. G. Breiland, *Applied Physics Letters* **43**:125 (1983).
73. P. Ho and W. G. Breiland, *Applied Physics Letters* **44**:51 (1984).
74. W. G. Breiland and P. Ho, in *The Electrochemical Society Softbound Proceedings Series*, edited by M. Robinson, C. H. J. v. d. Brekel, G. W. Cullen, J. M. Blocher and P. Rai-Choudhury The Electrochemical Society, New York, 1984.

In the momentum, species, and energy equations, we approximate the second derivatives with conventional central difference formulas as shown in *Equation 11-28*.

Equation 11-28

$$\frac{\partial}{\partial \xi}\left(\alpha \frac{\partial f}{\partial \xi}\right) \approx \left(\frac{2}{\xi_{j+1} - \xi_{j-1}}\right)\left[\alpha_{j+1/2}\left(\frac{f_{j+1} - f_j}{\xi_{j+1} - \xi_j}\right) - \alpha_{j-1/2}\left(\frac{f_j - f_{j-1}}{\xi_j - \xi_{j-1}}\right)\right]$$

Here the subscript j denotes the *j*th grid point. We approximate the first derivatives, as needed in *Equation 11-3*, by central differences as

Equation 11-29

$$\frac{\partial T}{\partial \xi} \approx \frac{T_{j+1} - T_{j-1}}{\xi_{j+1} - \xi_{j-1}}$$

We evaluate terms with no derivatives, such as the chemical production rate in *Equation 11-2*, using the conditions existing at ξ_j. Likewise, the coefficients of derivatives, such as ρu in *Equation 11-1*, are also evaluated at ξ_j.

First-order ODE's, such as *Equation 11-16*, are differenced according to the trapezoidal rule as

Equation 11-30

$$\frac{1}{\dot{m}}\left(\frac{y_j^{\alpha+1} - y_{j-1}^{\alpha+1}}{\xi_j - \xi_{j-1}}\right) = (\alpha+1)\frac{2}{\rho_j u_j + \rho_{j-1} u_{j-1}}$$

It is important to represent the integral equations as first-order differential equations and include the variables such as $y^{\alpha+1}$ in the dependent variable vector. The reason for this choice is associated with the structure of the Jacobian matrix, which is needed to solve the problem. When *Equation 11-30* is used, the number of dependent variables increases, but the Jacobian remains banded (a very desirable feature). On the other hand, if $y^{\alpha+1}$ were to be considered as a coefficient in the transport equations, as defined by the integral of the stream function, then the Jacobian loses its banded property and the required computer storage would increase enormously.

11.7 Non-Uniform Grid

In many reacting flow problems a thin reactive boundary-layer forms near a surface. Many grid mesh points may be needed to resolve the important chemical species concentration profiles. However, further away from the surface there may be no need for such a finely resolved mesh. A non-uniform grid may be specified by the user, through the “Stretch” parameter, s. This parameter can be used to include a mesh that is finer near a surface and more widely spaced as distance from the surface increases.

For cartesian coordinates, if the user has specified N mesh points, then the *j*th grid point will be placed at a distance $y(j)$ from the lower wall

Equation 11-31

$$y(j) = \frac{H}{(N-1)^s}(j-1)^s$$

where H is the channel height. If $s = 1$, a uniform grid is produced. For $s > 1$, the grid is more tightly spaced at the lower boundary. In cylindrical coordinates, the grid will be made finer at the outer boundary through use of an analogous formula.

12

12 1-D Premixed Laminar Flames

The equations governing steady, isobaric, quasi-one-dimensional flame propagation are discussed in this chapter. These equations pertain to the following two Chemkin Reactor Models:

1. Premixed Laminar Burner-stabilized Flame
2. Premixed Laminar Flame-speed Calculation

Many practical combustors, such as internal combustion engines, rely on premixed flame propagation. Moreover, burner-stabilized laminar premixed flames are often used to study chemical kinetics in a combustion environment. Such flames are effectively one-dimensional and can be made very steady, facilitating detailed experimental measurements of temperature and species profiles. Also, laminar flame speed is often used to characterize the combustion of various fuel-oxidizer combinations and in determining mixture flammability limits. Therefore, the ability to model chemical kinetics and transport processes in these flames is critical to flammability studies, interpreting flame experiments, and to understanding the combustion process itself. Examples of the use of flame modeling to interpret experimental observations and to verify combustion chemistry and pollution formation can be found in Miller, *et al*.[75,76,77]

75. J. A. Miller, R. E. Mitchell, M. D. Smooke, and R. J. Kee, in *Proceedings of the Nineteenth Symposium (International) on Combustion*, The Combustion Institute, Pittsburgh, Pennsylvania, 1982, p. 181.
76. J. A. Miller, M. D. Smooke, R. M. Green, and R. J. Kee, *Combustion Science and Technology* **34**:149 (1983).
77. J. A. Miller, M. C. Branch, W. J. McLean, D. W. Chandler, M. D. Smooke, and R. J. Kee, in *Proceedings of the Twentieth Symposium (International) on Combustion*, The Combustion Institute, Pittsburgh, Pennsylvania, 1985, p. 673.

The Premixed Flame Models solve the set of governing differential equations that describe the flame dynamics using implicit finite difference methods, as well as, a combination of time-dependent and steady-state methods. The solver algorithm employed automates coarse-to-fine grid refinement as a means to enhance the convergence properties of the steady-state approach and as a means to provide optimal mesh placement.

The Burner-stabilized Flame Model is the one most often used for analyzing species profiles in flame experiments, where the mass flow rate through the burner is known. The user has two options for the burner-stabilized flame—one where the temperature profile is known and one in which the temperature profile is determined by the energy conservation equation. Often the temperatures are obtained from experiment. In this case, only the species transport equations are solved. In many flames there can be significant heat losses to the external environment, which are of unknown or questionable origin and thus are difficult to model. However, since the chemistry depends strongly on temperature, it is essential to know the temperatures accurately in order to draw conclusions about the chemical kinetics behavior. If a temperature profile can be measured accurately, it is often better to use this measurement than the temperature profile obtained by solving an energy conservation equation. For cases where the heat losses are known to be negligible, the application can solve a burner-stabilized flame problem in which the temperatures are determined from the energy conservation equation. Comparing these two problem types for the burner-stabilized model may also provide some indication of the heat losses.

The Flame-speed Calculation Model involves a freely propagating flame. This configuration is used to determine the characteristic flame speed of the gas mixture at specified pressure and inlet temperature. In this case there are no heat losses (by definition) and thus the temperatures should be computed from the energy equation. Flame speed depends, in part, on the transport of heat, and predicting the temperature distribution is an integral part of the flame speed calculation.

12.1 1-D Flame Equations

For these equations, we assume 1-dimensional flow with uniform inlet conditions. The governing conservation equations reduce to:

Equation 12-1 Continuity

$$\dot{M} = \rho u A$$

Equation 12-2 Energy

$$\dot{M}\frac{dT}{dx} - \frac{1}{c_p}\frac{d}{dx}\left(\lambda A\frac{dT}{dx}\right) + \frac{A}{c_p}\sum_{k=1}^{K}\rho Y_k V_k c_{pk}\frac{dT}{dx} + \frac{A}{c_p}\sum_{k=1}^{K}\dot{\omega}_k h_k W_k + \frac{A}{c_p}\dot{Q}_{rad} = 0$$

Equation 12-3 Species

$$\dot{M}\frac{dY_k}{dx} + \frac{d}{dx}(\rho A Y_k V_k) - A\dot{\omega}_k W_k = 0 \qquad (k = 1, \ldots, K_g)$$

Equation 12-4 Equation of State

$$\rho = \frac{P\overline{W}}{RT}$$

In these equations x denotes the spatial coordinate; $\dot{M}$ the mass flow rate (which is independent of x); T the temperature; Y_k the mass fraction of the *k*th species (there are K_g gas species); P the pressure; u the velocity of the fluid mixture; ρ the mass density; W_k the molecular weight of the *k*th species; $\overline{W}$ the mean molecular weight of the mixture; R the universal gas constant; λ the thermal conductivity of the mixture; c_p the constant-pressure heat capacity of the mixture; c_{pk} the constant pressure heat capacity of the *k*th species; $\dot{\omega}_k$ the molar rate of production by chemical reaction of the *k*th species per unit volume; h_k the specific enthalpy of the *k*th species; V_k the diffusion velocity of the *k*th species; $\dot{Q}_{rad}$ the heat loss due to gas and particle radiation; and A the cross-sectional area of the stream tube encompassing the flame (normally increasing due to thermal expansion) normalized by the burner area. The user may provide an area profile (`APRO`) or alternatively a subroutine to specify the area as a function of the spatial coordinate. By default, the stream tube area is taken to be constant and equal to unity.

The net chemical production rate $\dot{\omega}_k$ of each species results from a competition between all the chemical reactions involving that species. We presume that each reaction proceeds according to the law of mass action and the forward rate coefficients are in the modified Arrhenius form,

Equation 12-5

$$k_f = AT^{\beta}\exp\left(\frac{-E_A}{RT}\right)$$

The details of the chemical reaction equations and the thermochemical properties are found in *Chapter 3* and *Chapter 2*, which discuss the evaluation of these expressions.

In addition to chemical reaction rates, we must also be concerned with the transport properties of the species, i.e., thermal conductivities and diffusion coefficients. Stockmayer potentials are used throughout in evaluating transport properties, as described in *Chapter 5*. The user has the option of evaluating transport properties using mixture-averaged formulas or a multicomponent diffusion model. Although details of the calculation of transport properties are available in *Chapter 5*, a brief description is also provided here.

12.2 Mixture-averaged Transport Properties

For the mixture-averaged formula, we assume the diffusion velocity V_k to be composed of three parts:

Equation 12-6

$$V_k = V_k + W_k + V_c$$

V_k is the ordinary diffusion velocity and is given in the Curtiss-Hirschfelder[26, p. 84] approximation by

Equation 12-7

$$V_k = -D_{km}\frac{1}{X_k}\frac{dX_k}{dx}$$

where X_k is the mole fraction, and where the mixture-averaged diffusion coefficient D_{km} is given explicitly in terms of the binary diffusion coefficients D_{kj}

Equation 12-8

$$D_{km} = \frac{1 - Y_k}{\sum_{j \neq k} X_j / D_{kj}}$$

A non-zero thermal diffusion velocity is included only for the low molecular weight species H, $\mathrm{H_2}$, and He. The trace, light-component limit is employed in determining W_k, i.e.,

Equation 12-9

$$W_k = \frac{D_{km}\Theta_k}{X_k}\frac{1}{T}\frac{dT}{dx}$$

where Θ_k is the thermal diffusion ratio.[37, p. 96] The sign of Θ_k makes the lower molecular weight species diffuse from low to high temperature regions.

The correction velocity V_c (independent of species but a function of the distance x) is included to insure that the mass fractions sum to unity or equivalently

Equation 12-10

$$\sum_{k=1}^{K} Y_k V_k = 0$$

The formulation of the correction velocity is the one recommended by Coffee and Heimerl[25, p. 84, 78] in their extensive investigation of approximate transport models in hydrogen and methane flames and discussed further in *Section 5.5* (*Equation 5-85*).

12.3 Multicomponent Transport Properties

For the multicomponent option, the transport property evaluation follows the method described by Dixon-Lewis.[21, p. 83] Multicomponent diffusion coefficients, thermal conductivities and thermal diffusion coefficients are computed through the solution of a system of equations involving the binary diffusion coefficients, the species mole fractions, and the thermodynamic and molecular properties of the species. Details of the matrix of equations, the solution algorithms, and the subsequent determination of multicomponent transport properties are provided in *Chapter 5*. These equations result in the determination of ordinary multicomponent diffusion coefficients, $D_{k,j}$, for species k diffusing in species j, as well as species thermal diffusion coefficients and thermal conductivities.

For the multicomponent formulation, the correction velocity, V_c, is not required and the diffusion velocity is defined as:

Equation 12-11

$$V_k = V_k + W_k$$

Now, the ordinary diffusion velocity term is given in *Equation 12-12*.

78. T. P. Coffee and J. M. Heimerl, *Combustion Science and Technology* **34**:31 (1983).

Equation 12-12

$$V_k = \frac{1}{X_k \overline{W}} \sum_{j \neq k}^{K} W_j D_{k,j} \mathbf{d_j}$$

Here $\overline{W}$ is the mean molar mass, W_j is the molar mass of species j, and $\mathbf{d_j}$ is defined as:

$$\mathbf{d_j} = \nabla X_k + (X_k - Y_k)\frac{1}{P}\nabla P$$

The thermal diffusion velocity is given as:

Equation 12-13

$$W_k = \frac{D_k^T}{\rho Y_k}\frac{1}{T}\nabla T$$

where D_k^T is the thermal diffusion coefficient for species k. We strongly recommend using the multicomponent option when thermal diffusion effects are important, as this is considerably more accurate than the mixture-averaged approach.

12.4 Gas and Particulate Thermal Radiation Model for Flames

The radiation heat-transfer model assumes that the radiation transport is through "optically thin" media. In the optically thin limit, the local gas does not re-absorb radiation emitted from other parts of the gas, such that the radiation does not need to be considered as a separate source of energy in the energy balance. The radiation heat loss, then, is due to exchange between the gas and the surroundings and between the particles and the surroundings. The optically-thin model is computationally efficient and allows quick assessment of the effects of radiation heat loss on flame structure and emissions.

The radiation model is provided as an option to calculate radiation heat loss from gas and particulate matter in unconfined, lightly sooting flames, for all Chemkin Flame simulators, including flat-flame burner and opposed-jet flow configurations.

The optically-thin radiation heat loss from a mixture of gas and particulates is given as

Equation 12-14

$$\dot{Q}_{rad} = 4\sigma\left((T^4 - T_{amb}^4)\left[\sum_i p(X_i a_i) + \kappa_{particle}\right]\right)$$

where σ is the Stefan-Boltzmann constant, T is the gas temperature, T^{amb} is the ambient temperature, p is the gas pressure, X_i is the mole fraction of species i, a_i is the Planck mean absorption coefficient for species i, and $\kappa_{particle}$ is the mean absorption coefficient for the particles.

Equation 12-14 assumes that locally gas and particles locally have the same temperature, since the energy balance of the particulate phase is not solved. The mean absorption coefficients of gas species and particles are treated as thermodynamic properties and are therefore required inputs to the radiation model.

Detailed information on how gas-phase radiation absorption coefficient data should be provided to the model is also described in *Section 2.1.4* in the *ANSYS Chemkin Input Manual*. Handling of particulate absorption is described below. The input parameter controlling particulate absorption behavior is also described in the *ANSYS Chemkin Input Manual*.

12.4.1 Particulate Absorption Coefficient

The spectral absorption coefficient of a particle cloud can be modeled by the Mie solution reformulated in terms of moments of particle size distribution[79]. The absorption coefficient of an ensemble of spherical particles is defined as

Equation 12-15

$$K_{abs}(\lambda) = \sum_i \frac{\pi d_i^{\,2}}{4} Q_{abs,i}(\lambda) N_i$$

Using the Penndorf expansion of the Mie solution for scattering and extinction efficiencies[79], the absorption coefficient takes the form

Equation 12-16

$$K_{abs}(\lambda) = L_1(\lambda)M_1 + L_2(\lambda)M_{5/3} + L_3(\lambda)M_2 + L_4(\lambda)M_{7/3} + L_5(\lambda)M_{8/3}$$

where

79. Frenklach, M. and Wang, H., "Detailed Mechanism and Modeling of Soot Particle Formation", Soot Formation in Combustion: Mechanisms and Models, (H. Bockhorn, Editor), Springer-Verlag, Berlin, 1994, p. 165.

$$L_1(\lambda) = K_1\frac{\pi}{4}\left(\frac{\pi}{\lambda}\right)\left(\frac{6m_0}{\pi\rho_B}\right) = K_1\frac{\pi}{4}\left(\frac{\pi}{\lambda}\right)d_0$$

$$L_2(\lambda) = K_3\frac{\pi}{4}\left(\frac{\pi}{\lambda}\right)^3 d_0^{5/3}$$

$$L_3(\lambda) = (K_3 - 6K_6)\frac{\pi}{4}\left(\frac{\pi}{\lambda}\right)^4 d_0^2$$

$$L_4(\lambda) = K_5\frac{\pi}{4}\left(\frac{\pi}{\lambda}\right)^5 d_0^{7/3}$$

$$L_5(\lambda) = K_8\frac{3\pi}{2}\left(\frac{\pi}{\lambda}\right)^6 d_0^{8/3}$$

and the K's are the optical coefficients given in Frenklach and Wang[79].

For the absorption coefficients of agglomerates, the equivalent-sphere model[80] is employed. For this model, we let $\bar{j}_{p,ag}$ be the average class of the primary particle in the , which is assumed to be constant throughout the particle population. The equivalent effective diameter for a class i agglomerate is given as

Equation 12-17

$$d_{eff,i} = d_p n_{p,i}^{1/3} = d_0 j_{p,ag}^{-1/3}\left(\frac{i}{\bar{j}_{p,ag}}\right)^{1/3} = d_0 i^{1/3}$$

Substituting the effective diameter into the expression for $K_{abs}(\lambda)$ (*Equation 12-15*) yields the same formulation in terms of moments (*Equation 12-16*).

The total emissivity of the particle ensemble can be obtained by integrating the spectral radiation as

Equation 12-18

$$\kappa_{particle} = \int_0^\infty K_{abs}(\lambda)B_\lambda(T)d\lambda/\sigma T^4$$

where the Planck function is given as

80. Drolen, B.L. and Tien, C.L., "Absorption and Scattering of Agglomerated Soot Particulate", J. Quant. Spectrosc. Radiat. Transfer **37**:433-448 (1987).

Equation 12-19

$$B_\lambda(T) = \frac{2hc^2}{\lambda^5}\frac{1}{e^{hc/\lambda\kappa_B T}-1}$$

Since computing the overall absorption (or emission) coefficient of a particle cloud is computationally expensive, a semi-empirical model can be derived by dropping terms of high-order d_0 in *Equation 12-16*:

Equation 12-20

$$K_{abs}(\lambda) \cong K_1\frac{\pi}{4}\left(\frac{6m_0}{\pi\rho_B}\right)M_1 = \frac{3}{2}K_1\left(\frac{\pi}{\lambda}\right)\left(\frac{m_0 M_1}{\rho_B}\right) = \frac{3K_1}{2}\left(\frac{\pi}{\lambda}\right)f_v$$

where f_v is the volume fraction of the particle ensemble.

Accordingly, the overall emissivity of a particle cloud can be expressed as a function of temperature T and particle volume fraction f_v:

Equation 12-21

$$\kappa_{particle} = c_{part} f_v T$$

The model parameter c_{part} is a user input and has dimensions of [length * temperature]$^{-1}$. (See the EMPAR keyword in the *ANSYS Chemkin Input Manual.*)

12.5 Boundary Conditions

We consider two different types of flames: burner-stabilized flames and adiabatic, freely propagating flames. The conservation equations governing the two are the same, but the boundary conditions differ. In both cases the appropriate boundary conditions may be deduced from the early work of Curtiss and Hirschfelder.[26, p. 84] For burner-stabilized flames $\dot{M}$ is a known constant, the temperature and mass flux fractions ($\varepsilon_k = Y_k + \rho Y_k V_k A/\dot{M}$) are specified at the cold boundary, and vanishing gradients are imposed at the hot boundary.

For freely propagating flames $\dot{M}$ is an eigenvalue and must be determined as part of the solution.[81] Therefore, an additional constraint is required, or alternatively one degree of freedom must be removed from the problem. We choose to fix the location of the flame by specifying and fixing the temperature at one point. This is sufficient to allow for the solution of the flame speed eigenvalue $\dot{M}$. The user must select this point in such a way as to insure that the temperature and species gradients "nearly" vanish at the cold boundary. If this condition is not met then the resultant $\dot{M}$ will be too low because some heat will be lost through the cold boundary. More details on boundary conditions are described in *Section 12.5.1*.

12.5.1 Boundary Condition Details

The boundary conditions are relatively easily implemented. At the cold boundary we specify the mass flux fractions and the temperature, i.e., we solve

Equation 12-22

$$\varepsilon_{k,1} - Y_{k,1} - \left(\frac{\rho A Y_k V_k}{\dot{M}}\right)_{j=1\frac{1}{2}} = 0$$

and

Equation 12-23

$$T_1 - T_b = 0$$

where $\varepsilon_{k,1}$ is the inlet reactant fraction of the *k*th species and T_b is the specified burner temperature. At the hot boundary we specify that all gradients vanish, i.e.,

Equation 12-24

$$\frac{Y_{k,J} - Y_{k,J-1}}{x_J - x_{J-1}} = 0$$

and

Equation 12-25

$$\frac{T_J - T_{J-1}}{x_J - x_{J-1}} = 0$$

The boundary conditions for $\dot{M}$ depend on whether the given problem is a burner-stabilized or a freely propagating flame. The boundary conditions for each case are discussed in *Section 12.5*.

81. M. D. Smooke, J. A. Miller, and R. J. Kee, *Combustion Science and Technology* **34**:79 (1983).

12.6 Finite Difference Approximations

The first task in solving the flame problem is to discretize the governing conservation equations. We use finite difference approximations on a non-uniform grid with points numbered from 1 at the cold boundary to J at the hot boundary. On the convective terms the user has the choice of using either first order windward differences or central differences. Both cases are illustrated using the convective term in the energy equation. The windward difference is given as

Equation 12-26

$$\left(\dot{M}\frac{dT}{dx}\right)_j \approx \dot{M}_j\left(\frac{T_j - T_{j-1}}{x_j - x_{j-1}}\right)$$

where the index j refers to the mesh point. The central difference formula is

Equation 12-27

$$\left(\dot{M}\frac{dT}{dx}\right)_j \approx \dot{M}_j\left(\frac{h_{j-1}}{h_j(h_j + h_{j-1})}T_{j+1} + \frac{h_j - h_{j-1}}{h_j h_{j-1}}T_j - \frac{h_j}{h_{j-1}(h_j + h_{j-1})}T_{j-1}\right)$$

where $h_j = x_{j+1} - x_j$. The windward difference formula introduce artificial diffusion on a coarse mesh; this has the effect of spreading out the solution and making the convergence of Newton's method less sensitive to the starting estimate. However, because the mesh is refined in regions of high gradient, the artificial diffusion becomes relatively unimportant after the solution has progressed to the fine meshes. Nevertheless, for a given mesh, the windward difference approximation is less accurate than the central difference formula. Therefore, the user may want to select the central difference formula on finer meshes or in cases where the solution is converging without difficulty.

The first derivative in the summation term in the energy *Equation 12-2* is always approximated by a central difference formula,

Equation 12-28

$$\left(\frac{dT}{dx}\right)_j \approx \left(\frac{h_{j-1}}{h_j(h_j + h_{j-1})}T_{j+1} + \frac{h_j - h_{j-1}}{h_j h_{j-1}}T_j - \frac{h_j}{h_{j-1}(h_j + h_{j-1})}T_{j-1}\right)$$

and the coefficients in the summation are evaluated at j.

The second derivative term in the energy equation is approximated by the following second order central difference:

Equation 12-29

$$\frac{d}{dx}\left((\lambda A)\frac{dT}{dx}\right)_j \approx \left(\frac{2}{x_{j+1}-x_{j-1}}\right)\left[(\lambda A)_{j+\frac{1}{2}}\left(\frac{T_{j+1}-T_j}{x_{j+1}-x_j}\right)+\left(-(\lambda A)_{j+\frac{1}{2}}\right)\left(\frac{T_j-T_{j-1}}{x_j-x_{j-1}}\right)\right]$$

The coefficients in this formula (at $j \pm 1/2$) are evaluated using the averages of the dependent variables between mesh points.

The diffusive term in the species conservation equation is approximated in a similar way, but it appears to be different because we have written it using diffusion velocities. The ordinary (*Equation 12-7*) and thermal (*Equation 12-9*) diffusion velocities are approximated at the $j \pm 1/2$ positions as illustrated by the following mixture-averaged evaluation:

Equation 12-30

$$(Y_k V_k)_{j+1/2} \approx -\left(\frac{W_k D_{km}}{\overline{W}}\right)_{j+1/2}\left(\frac{X_{k,j+1}-X_{k,j}}{x_{j+1}-x_j}\right)$$

and

Equation 12-31

$$(Y_k W_k)_{j+1/2} \approx -\left(\frac{W_k D_{km}\Theta_k}{\overline{W}T}\right)_{j+1/2}\left(\frac{T_{j+1}-T_j}{x_{j+1}-x_j}\right)$$

Since the mole fraction of a species can be zero, we avoid difficulties by forming $Y_k V_k$, which is the expression needed in *Equation 12-3*, rather than V_k itself ($Y_k = X_k W_k / \overline{W}$). After the diffusion velocities are computed at all the mesh midpoints, the correction velocity V_c is computed at the midpoints from

Equation 12-32

$$V_c = \sum_{k=1}^{K} (V_k + W_k)$$

Upon forming the full diffusion velocities $V_k = V_k + W_k + V_c$ the diffusion term is evaluated with the following difference approximation.

Equation 12-33

$$\frac{d}{dx}(\rho A Y_k V_k)_j \approx \frac{(\rho A Y_k V_k)_{j+1/2} - (\rho A Y_k V_k)_{j-1/2}}{x_{j+1/2} - x_{j-1/2}}$$

All the non-differentiated terms, such as the chemical production rate terms, are evaluated at the mesh points j. Coefficients not appearing within derivatives are also evaluated at the mesh points.

12.7 Transient Forms of the Equations

As discussed in *Section 15.2*, even though the Premixed Flame models are solved as steady-state problems, the steady-state solution algorithm sometimes requires pseudo time-stepping to condition the solution iterate. For this reason, we extend the discussion of the governing equations presented in *Section 12.1* to include the transient terms used in time-stepping procedures. The transient equations are obtained by adding the time derivatives to *Equation 12-2* and *Equation 12-3*, obtaining,

Equation 12-34

$$\rho A \frac{\partial T}{\partial t} + \dot{M} \frac{\partial T}{\partial x} - \frac{1}{c_p} \frac{\partial}{\partial x}\left(\lambda A \frac{\partial T}{\partial x}\right) + \frac{A}{c_p} \sum_{k=1}^{K} \rho Y_k V_k c_{pk} \frac{\partial T}{\partial x} + \frac{A}{c_p} \sum_{k=1}^{K} \dot{\omega}_k h_k W_k = 0$$

and

Equation 12-35

$$\rho A \frac{\partial Y_k}{\partial t} + \dot{M} \frac{\partial Y_k}{\partial x} + \frac{\partial}{\partial x}(\rho A Y_k V_k) - A \dot{\omega}_k W_k = 0 \qquad (k = 1, \ldots, K)$$

The full system now becomes a system of parabolic partial differential equations, rather than an ordinary differential equation boundary value system. Solution is obtained via the backward-Euler method. In this method, the time derivatives are approximated by finite differences as illustrated by

Equation 12-36

$$\rho A \frac{\partial T}{\partial t} \approx \rho_j^{n+1} A_j \left(\frac{T_j^{n+1} - T_j^n}{h} \right)$$

where the superscript n indicates the time level and h represents the size of the time step. All other terms are approximated with finite differences as before, but at time level $n+1$. Since all variables are known at time level n, the discretized problem is just a system of nonlinear algebraic equations for the dependent variable vector ϕ at time level $n+1$.

13

13 Opposed-flow and Stagnation Flames

In this chapter, we describe the conservation equations and assumptions that govern the behavior of opposed-flow and stagnation flames, which may result from impinging separate fuel and oxidizer streams or from two premixed streams, or from a premixed stream impinging on a solid surface. The governing equations rely on a similarity transformation that reduces the three-dimensional nature of the flow to a one-dimensional (axial) dependence of the governing equations. This discussion pertains to the Chemkin Reactor Models: Diffusion or Premixed Opposed-flow Flame and Premixed Burner-Stabilized Stagnation Flame.

13.1 Axisymmetric and Planar Diffusion

For the Opposed-flow Flame model, a steady-state solution is computed for either axisymmetric or planar diffusion flames between two opposing nozzles. The opposed-flow geometry makes an attractive experimental configuration, because the flames are flat, allowing for detailed study of the flame chemistry and structure. The two or three-dimensional flow is reduced mathematically to one dimension by assuming that the y - or radial velocity varies linearly in the y - or radial direction, which leads to a simplification in which the fluid properties are functions of the axial distance only. The one-dimensional model then predicts the species, temperature, and velocity profiles in the core flow between the nozzles (neglecting edge effects). Both premixed and non-premixed flames can be simulated.

The axisymmetric geometry consists of two concentric, circular nozzles directed towards each other, as in *Figure 13-1*. This configuration produces an axisymmetric flow field with a stagnation plane between the nozzles. The planar geometry consists of two concentric linear nozzles directed towards each other as shown in *Figure 13-2*. This configuration produces a 2-D planar flow field with a stagnation line between the two nozzles. The location of the stagnation plane (line) depends on the momentum balance of the two streams. When the streams are premixed, two premixed flames

exist, one on either side of the stagnation plane. When one stream contains fuel and the other oxidizer, a diffusion flame is established. Since most fuels require more air than fuel by mass, the diffusion flame usually sits on the oxidizer side of the stagnation plane; fuel diffuses through the stagnation plane to establish the flame in a stoichiometric mixture.

Our Opposed-flow Flame Simulator is derived from a model that was originally developed by Kee, *et al*.[82] for premixed opposed-flow flames. The reduction of the three-dimensional stagnation flow is based upon similarity solutions advanced for incompressible flows by von Karman,[83] which are more easily available in Schlichting.[84] The use of the similarity transformation is described in more detail in *Chapter 14*. Note that the Chemkin impinging and stagnation-flow models are based on a finite domain, where the user specifies the nozzle separation. For this approach, an eigenvalue must be included in the solution of the equations and the strain rate varies, such that a characteristic strain rate must be determined from the velocity profile. Following the analysis of Evans and Grief,[85] Kee, *et al*.[82] showed that this formulation allowed more accurate predictions of the extinction limits for premixed flames than other approaches.

The geometry and axes for the axisymmetric and planar configurations are sketched in *Figure 13-1* and *Figure 13-2*, respectively. In the following equations, ξ represents either the radial direction r for the axisymmetric case, or the perpendicular direction y for the planar case. The coordinate parameter n allows us to present one set of equations for both cases, with $n = 3$ for the 3-D axisymmetric flow and $n = 2$ for the 2-D planar case. A more detailed derivation of the governing equations for the opposed-flow geometry is provided by Kee, et al.[82, p. 226]

At steady-state, conservation of mass in cylindrical or planar coordinates is

Equation 13-1

$$\frac{\partial(\rho u)}{\partial x} + \frac{1}{\xi^{n-2}}\frac{\partial(\rho v_\xi \xi^{n-2})}{\partial \xi} = 0$$

where u and v_ξ are the axial and radial (or cross-flow) velocity components, and ρ is the mass density.

82. R. J. Kee, J. A. Miller, and G. H. Evans, in *Proceedings of the Twenty-Second Symposium (International) on Combustion*, The Combustion Institute, Pittsburgh, Pennsylvania, 1988, p. 1479.
83. T. V. Karman, A. Angew. *Math. Mech.* **1**:233 (1921).
84. H. Schlichting, *Boundary Layer Theory*, McGraw-Hill, New York, 1979.
85. G. H. Evans and R. Greif, *Numerical Heat Transfer* **14**:373 (1988).

Figure 13-1 Geometry of the axisymmetric opposed-flow diffusion flame

The dashed line represents the stagnation plane; the shaded region suggests the flame.

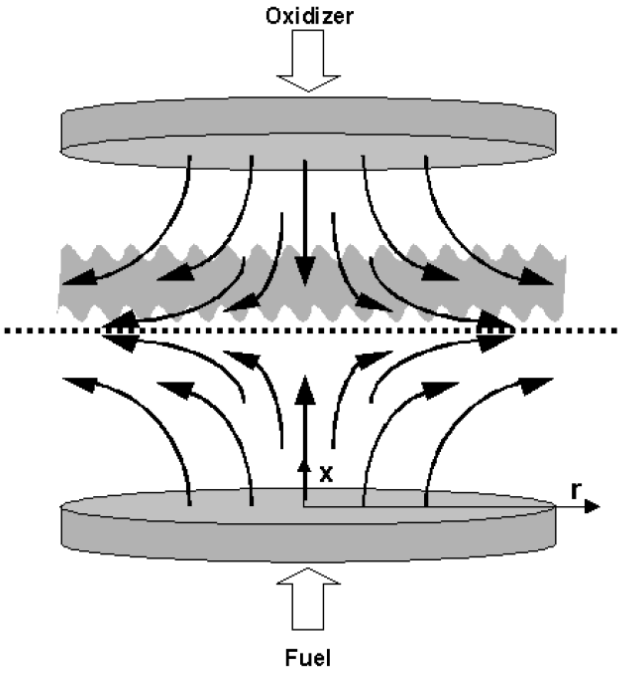

Figure 13-2 Geometry of the planar opposed-flow diffusion flame

The dashed line represents the stagnation line; the shaded region suggests the flame.

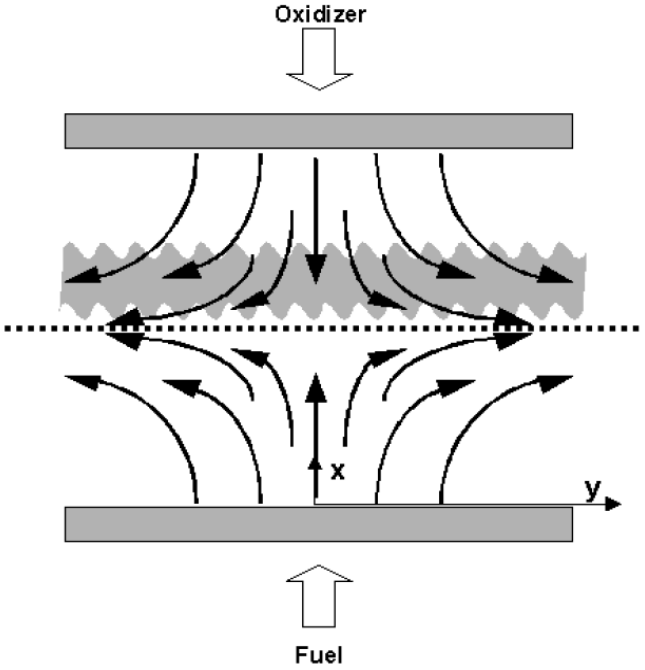

Following von Karman,[83, p. 226] who recognized that v_ξ/ξ and other variables should be functions of x only, we define

$$G(x) = \frac{-(\rho v_\xi)}{\xi} \qquad F(x) = \frac{\rho u}{(n-1)}$$

for which the continuity *Equation 13-1* reduces to

Equation 13-2

$$G(x) = \frac{dF(x)}{dx}$$

for the axial velocity u. Since F and G are functions of x only, so are ρ, u, T and Y_k.

The perpendicular momentum equation is satisfied by the eigenvalue

Equation 13-3

$$H = \frac{1}{\xi^{n-2}}\frac{\partial p}{\partial \xi} = \text{constant}$$

The perpendicular momentum equation is

Equation 13-4

$$H - (n-1)\frac{d}{dx}\left(\frac{FG}{\rho}\right) + \frac{nG^2}{\rho} + \frac{d}{dx}\left[\mu\frac{d}{dx}\left(\frac{G}{\rho}\right)\right] = 0$$

Energy and species conservation are

Equation 13-5

$$\rho u\frac{dT}{dx} - \frac{1}{c_p}\frac{d}{dx}\left(\lambda\frac{dT}{dx}\right) + \frac{\rho}{c_p}\sum_k c_{pk}Y_k V_k\frac{dT}{dx} + \frac{1}{c_p}\sum_k h_k\dot{\omega}_k + \frac{1}{c_p}\dot{Q}_{rad} = 0$$

where $\dot{Q}_{rad}$ is the heat loss due to gas and particle radiation which is described in *Section 12.4*.

Equation 13-6

$$\rho u\frac{dY_k}{dx} + \frac{d}{dx}(\rho Y_k V_k) - \dot{\omega}_k W_k = 0 \qquad k = 1, \ldots, K$$

where the diffusion velocities are given by either the multicomponent formulation

Equation 13-7

$$V_k = \frac{1}{X_k \overline{W}} \sum_{j \neq k}^{K} W_j D_{k,j} \frac{dX_j}{dx} - \frac{D_k^T}{\rho Y_k} \frac{1}{T} \frac{dT}{dx}$$

or the mixture-averaged formulation

Equation 13-8

$$V_k = -\frac{1}{X_k} D_{km} \frac{dX_k}{dx} - \frac{D_k^T}{\rho Y_k} \frac{1}{T} \frac{dT}{dx} \qquad \text{where} \qquad D_{km} = \frac{1 - Y_k}{\sum_{j \neq k}^{K} \frac{X_j}{D_{jk}}}$$

and $D_{k,j}$, D_{km}, D_{jk} and D_k^T are the multicomponent, mixture-averaged, binary, and thermal diffusion coefficients, respectively.

The boundary conditions for the fuel (F) and oxidizer (O) streams at the nozzles are

Equation 13-9

$$x = 0: \qquad F = \frac{\rho_F u_F}{(n-1)}; \quad G = 0; \quad T = T_F; \quad \rho u Y_k + \rho Y_k V_k = (\rho u Y_k)_F$$

$$x = L: \qquad F = \frac{\rho_O u_O}{(n-1)}; \quad G = 0; \quad T = T_O; \quad \rho u Y_k + \rho Y_k V_k = (\rho u Y_k)_O$$

Note that the inflow boundary condition (*Equation 13-9*) specifies the total mass flux, including diffusion and convection, rather than the fixing species mass fraction $Y_k = Y_{k,F}$. If gradients exist at the boundary, these conditions allow diffusion into the nozzle.

The differential *Equation 13-2* through *Equation 13-6* and boundary conditions *Equation 13-9* form a boundary value problem for the dependent variables (F, G, H, T, Y_k). The GAS-PHASE KINETICS Subroutine Library provides the reaction rates and thermodynamic properties, while the TRANSPORT package evaluates the transport properties for these equations.

13.2 Pre-mixed Burner-stabilized Stagnation Flame

The governing equations for the stagnation-flame reactor model are identical to those used in the Opposed-Flow Flame Simulator, described in *Section 13.1*. Only the boundary conditions at one boundary are changed. Specifically, there is only one inlet while the other boundary is a wall. The inlet is therefore assumed to be a pre-mixed blend of fuel and oxidizer.

The reactor model fixes the burner inlet at $x = 0$ and is the same as that given in *Equation 13-9*. The boundary conditions at the wall ($x = L$) are replaced by *Equation 13-10*.

Equation 13-10

$$T = T_{\text{Wall}}$$
$$u = 0$$
$$\rho Y_k (u + V_k) = 0$$

This reactor model does not solve for the surface chemistry at the wall, but instead assumes a no-slip convective velocity condition and assumes that the species convective and diffusive fluxes balance. In the absence of thermal diffusion, the wall boundary condition for the species equation implies that the species concentration gradient goes to zero.

13.3 Emission Indices

Emission indices are important flame properties that can be used to compare flame characteristics in different flow fields. They are usually given as the mass of pollutant generated per kilogram fuel consumed, g/kg-fuel. Chemkin flame models, the Premixed Laminar flame model and Opposed-flow flame model, use formulations derived by Takeno and Nishioka[86] to evaluate emission indices. Brief descriptions of emission index calculations are provided below. For a detailed derivation of the formulations, see the cited paper.

86. Takeno, D. and Nishioka, M., "Species Conservation and Emission Indices for Flames Described by Similarity Solutions", *Combustion and Flame* **92**:465-468 (1993).

Since emission indices are reported per kilogram of fuel consumed, it is important to identify fuel components in the inlets. The flame codes assume fuel is introduced to the system only through the fuel boundary at x = 0. Any species containing a C or H element in the fuel inlet will be treated as a fuel species, except CO_2 and H_2O. The total fuel-mass flow rate coming into the system can then be obtained from fuel inlet properties as

Equation 13-11

$$\dot{m}_{fuel} = \rho_F \left(u_F + V_{fuel,F}\right) Y_{fuel,F} = \left(\rho u Y_{fuel}\right)_F$$

where subscript F and $fuel$ denote fuel boundary and all fuel species of the system, respectively. The fraction of fuel consumed at a given location x can be computed by the ratio of accumulated fuel consumption and total fuel mass flow rate as

Equation 13-12

$$I_f(x) = \frac{-\int_0^x \dot{\omega}_{fuel}(l) W_{fuel} dl}{\dot{m}_{fuel}}$$

and the fraction of unburned fuel is $1 - I_f(x)$.

The emission index of a pollutant, for example NO, can be calculated as

Equation 13-13

$$EI_{NO}(x) = \frac{\int_0^x \dot{\omega}_{NO}(l) W_{NO} dl}{I_f(x) * \dot{m}_{fuel}} \times 1000 \quad \text{[g-NO/kg-fuel].}$$

and the total NO emission index from the flame is

Equation 13-14

$$EI_{NO}(L) = \frac{\int_0^L \dot{\omega}_{NO}(l) W_{NO} dl}{I_f(L) * \dot{m}_{fuel}} \times 1000 \quad \text{[g-NO/kg-fuel].}$$

The NOx emission index is reported as grams of NO_2-equivalent formed per kilogram of fuel consumed, that is,

Equation 13-15

$$EI_{NO_x}(x) = \frac{W_{NO_2}}{W_{NO}} \times EI_{NO}(x) + EI_{NO_2}(x)$$

Emission indices of CO (EICO), NO (EINO), and NOx (EINOx) are available in the Chemkin Post-Processor for selected reactor models.

13.4 Finite-difference Approximations

Discretization of the differential equations uses conventional finite differencing techniques for non-uniform mesh spacing. Diffusive terms use central differences, with truncation error that is second-order in the mesh spacing. For better convergence, convective terms use upwind differencing, which uses the sign of the velocity to choose which direction the spatial difference will go. If $u_j = 0$, for example, then the convective term in the energy equation is differenced as:

Equation 13-16

$$\rho u \frac{dT}{dx} \approx \rho_i u_j \left(\frac{T_j - T_{j-1}}{x_j - x_{j-1}} \right)$$

The truncation error of this approximation is first-order in the mesh spacing, leading to what is often called “artificial diffusion”, but this form avoids unwanted oscillations during the solution on a coarse mesh. Alternatively, the convective terms can be centrally differenced, but the default windward differencing is recommended.

13.5 Regrid Operation

A Regrid operation is specified by supplying a new number of grid points during a restart or continuation, which allow a new flame solution to begin from an initial guess based on the solution of a previous flame.

The steady-state solver, TWOPNT, automatically refines the grid by adding points in regions where they are needed to resolve the first and second derivatives of the solution, using criteria controlled by the Gradient and Curvature grid parameters. However, TWOPNT does not move or remove points. If it reaches a maximum number of points (internally defined by the dimensions), a warning message is printed and the adaptation is terminated. In some cases, then, it may be necessary to reduce the number of points when starting a new solution from a previous result. The Regrid operation redefines the solution guess on the user-specified number of mesh points.

The Regrid operation is different from the grid-point insertion operation performed by TWOPNT. Both operations attempt to resolve the gradient and curvature in the solution, except that TWOPNT considers all solution components, whereas Regrid only considers the temperature profile. TWOPNT only adds points, leaving the old points as they were, but Regrid alters the location and solution of all the points interior to the boundaries. Regrid computes new locations for exactly the given number of points, and then interpolates the solution from the previous grid to obtain a new approximation of the solution. Regrid does not conserve any properties of the solution; in fact, it tends to smooth the solution by the error inherent in the interpolation.

Regrid redistributes a weighting function of the first and second derivatives of the temperature. The profiles of the other dependent variables are ignored on the assumption that the temperature profile defines the flame location well enough for the purposes of realigning the mesh for an initial condition. The redistribution uses a transformation from the physical coordinate x to a new coordinate η

Equation 13-17

$$\frac{dx}{d\eta}W(x, T) = C$$

with the weighing function,

Equation 13-18

$$W(x, T) = 1 + b_1\left|\frac{dT}{dx}\right| + b_2\left|\frac{d^2T}{dx^2}\right|$$

Integration over the entire domain defines the constant

Equation 13-19

$$C = \frac{1}{N-1}\int_O^L W(x, T)dx$$

Integrating over a portion of the domain gives an expression for the point locations in η-space

Equation 13-20

$$\eta = 1 + \frac{1}{C}\int_0^x W(x, T)dx$$

The new grid locations x come by interpolation between the computed values of η defined using the old mesh, onto a uniform mesh in η-space. Since $d\eta$ is constant on this uniform mesh, the solution to *Equation 13-17* states that $W(x, T)dx$ is constant, so the new values of x will be concentrated where the weighting function is large.

Below is a sample set of parameters that would direct the Opposed-flow Flame Model to perform the Regrid operation during a restart:

Table 13-1 Parameter Examples

Parameter	*Value*
Number of Grid Points for Regrid	**20**
Percent of Grids for Regrid	**0.6**
Ratio of Gradient to Curvature Adaptation	**1.0**

These parameters are specified in the Cluster Properties Panel, when Restart problem-type is chosen. This sequence will create a new solution guess on 20 points, devoting 60 percent of the points to resolving gradients, with equal weighting of gradient and curvature in the temperature profile. From experience, we recommend a value greater than or equal to 1 for the gradient to curvature adaptation ratio. Depending on the resolution of the existing solution, the percent of grids used in the regrid process should be in the neighborhood of 50%. Note that using 0 percent grids for regrid results in a uniform mesh.

13.6 Simulation of Flame Extinction

The Flame Extinction Simulator solves the same set of equations for a 1-D strained flame as the Opposed-flow Flame Simulator, as described in *Section 13.1*. However, this model is used to determine the extinction strain rate for the non-premixed or premixed flame conditions, through an iterative series of opposed-flow flame simulations. As flame strain rate is varied, the Flame-Extinction Simulator will predict an S-curve response for the flame temperature as a function of strain rate. The lower and upper branches of the temperature vs. strain-rate S-curve represent weak and strong solutions, respectively, while the middle branch represents unstable solutions. The lower and upper turning points are interpreted as the ignition and extinction points, respectively.

Figure 13-3 Flame response curve showing extinction (turning) for premixed stoichiometric methane-air flame. The inlet temperature is 296 K and ambient pressure is 1 atm. The calculated extinction strain rate is 550 /s.

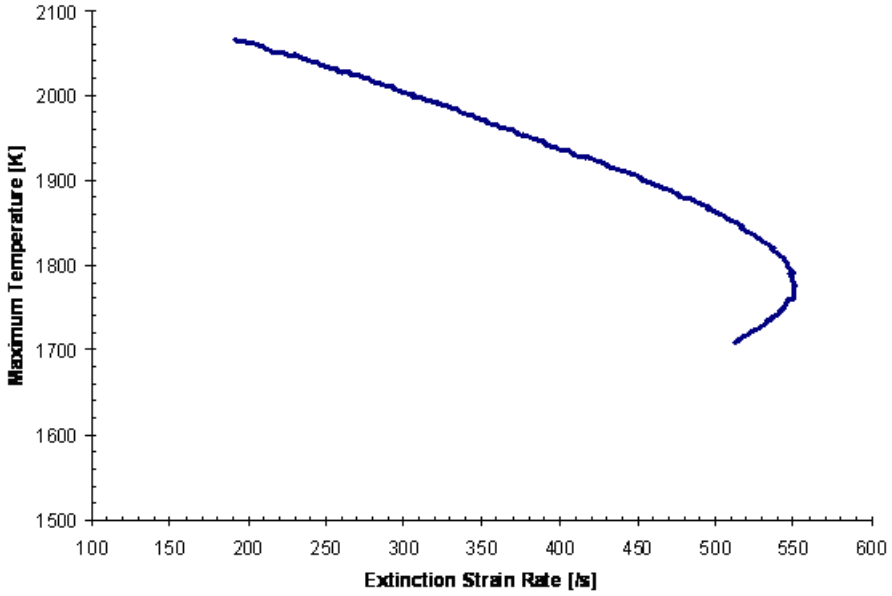

Since the Jacobian matrix is singular at the turning points, a special technique called arc-length continuation[87] is used to compute the solutions through the turning points. In theory, one can calculate the solutions up to the turning point using successive continuations on velocity. Such a technique requires smaller and smaller changes in the velocity, accompanied by more computational difficulty to get a solution, as the extinction point is approached.

As described in *Section 13.1*, the Opposed-flow Flame Simulator solves for the variables $T, F, G, H,$ *and* Y_k. For the purpose of this discussion, while T is the temperature and Y_k is the species mass fraction of the k^{th} species, F and G can be considered to represent the x and y velocities, respectively. H is the eigenvalue of the problem and represents the pressure curvature. This system of equations constitutes a two-point boundary value problem. The governing equations for $T, G,$ *and* Y_k are second-order and hence require two (boundary) conditions. For the continuation analysis, the F and H equations are relevant and these are re-written here:

Equation 13-21

$$\frac{dF}{dx} - G = 0$$

87. Miller, J.A., *Rich Methane/Air Flames: Burning Velocities, Extinction Limits, and Flammability Limits*, Sandia National Laboratory.

Equation 13-22

$$\frac{dH}{dx} = 0$$

As two first-order differential equations, these two equations require two boundary conditions. *Table 13-2* shows a summary of the equations and associated boundary conditions used in the Opposed-Flow Flame Simulator.

Table 13-2 Summary of Boundary Conditions in the Opposed-flow Flame simulator

Equation	***Left (Fuel) Boundary***	***Right (Oxidizer) Boundary***
T	T_f	To
F	$\rho_f U_f/(n-1)$	--
G	G_f	G_o
H	--	$\rho_o U_o/(n-1)$ ***
Y_k	$Yk,_f$	$Yk,_o$

As shown in *Table 13-2*, the Opposed-flow Flame Simulator uses the oxidizer inlet velocity as the boundary condition for the eigenvalue equation. Thus, effectively, information about F propagates from fuel to oxidizer inlet locations while "shooting" for the correct value at the oxidizer side. The corrective measure for the shooting is supplied by the H value propagating from oxidizer to fuel locations.

In principle, by swapping the roles of the response and control variables, it is possible to calculate all points along the full response curve for flame-extinction calculations. The Flame-Extinction Simulator uses a flame-controlling continuation as described in Takeno et al.[88] Instead of performing continuations with the velocity from either nozzle, an additional constraint, in this case a fixed temperature at a particular grid point, is specified. This additional constraint means one boundary condition must be relaxed. The natural choice, in this case, would be the oxidizer velocity (U_o) or fuel velocity (U_f), such that the oxidizer (or fuel) velocity is obtained as a part of the solution. In theory, any number of such *internal* constraints can be specified on any solution variable: temperature, species mass fraction, etc. Depending upon the number, M, of constraints specified, the flame-controlling technique can be termed as M-point controlling.

88. Takeno, T., M. Nishioka, and C.K. Law, *A Flame-Controlling Continuation Method for Generating S-curve Responses with Detailed Chemistry*. Combustion and Flame, 1996. **104**: p. 328-342

It may be difficult or in some cases even impossible to go though the extinction point with one-point control. This is the case if the response variable of the continuation problem itself shows a turning-point behavior. In the case of the Flame-Extinction Simulator, the response variable is the oxidizer velocity or the pressure eigenvalue. Although one-point continuation is adequate for most of the cases, the Flame-Extinction Simulator can perform both one-point and two-point control. In the former case, temperature at a point on the fuel side is specified while in the latter temperature is specified at one point on both fuel and oxidizer sides.

13.6.1 One-point Control

For one-point control, the oxidizer boundary condition is relaxed and temperature at some internal point is specified. As a result, the H equation is modified, as shown in *Equation 13-23*.

Equation 13-23

$$\frac{dH}{dx} = 0;\ j \neq J_{Fix}$$
$$T = T_{given};\ j == J_{Fix}$$

It can be noted that the above treatment is similar to the one used for fixing temperature at a point employed in the Flame-speed Calculator (*Section 12.5*). The H information then propagates from the fixed point to either inlet. At the oxidizer boundary the mass flux term ($\rho_o U_o$) appears as boundary value F_o in the Y_k equations, instead of as a condition for the *H* equation.

In addition, it is also possible to introduce some condition on the fuel inlet velocity, such as $U_f = g(U_o)$. This is useful in matching experimental conditions such as equal velocities or momentum of the jets. In such cases, another boundary condition must be relaxed and the natural choice is the fuel (or oxidizer) velocity boundary condition. The Flame-Extinction Simulator model adds an extra equation for U_f. This equation merely copies U_F at each grid point as is done for the pressure eigenvalue. At the oxidizer boundary, the F_o condition is imposed on the equation for U_f using $U_f = g(U_o)$. Thus,

Equation 13-24

$$\frac{dU_f}{dx} = 0$$
$$\rho_o U_o = \rho_o g^{-1}(U_f)$$

The species conservation equations are then recast to use the oxidizer mass flux in terms of U_f at the oxidizer boundary.

If the fuel velocity is fixed and the fixed temperature value is chosen on the fuel side of the flame then a decrease in the fixed temperature results in a decrease in the global strain rate, whereas if fixed temperature is chosen on the oxidizer side then a decrease in the fixed temperature results in an increase in the strain rate (for the upper branch solutions).

13.6.2 Two-point Control

When employing two-point control, we need an additional equation. This can be the same as the U_f equation except that the $U_f = g(U_o)$ constraint is replaced by a fixed temperature value.

Equation 13-25

$$\frac{dU_f}{dx} = 0;\ j \neq J_{Fix}$$
$$T = T_{given};\ j == J_{Fix}$$

Similar to *Equation 13-23*, U_f also "propagates" from the fixed point to either side. The fixed locations are chosen on either side of the flame.

The two-point control method may facilitate computing solutions through the extinction turning point or may "jump" from the upper branch to the middle branch. In the latter case, one can use one-point control once a solution on the middle branch is obtained to trace back to the extinction point.

13.6.3 Extinction Strain Rate

Once the extinction point is captured, the extinction strain rate can be defined in several ways. Some commonly used methods are global strain rate (average velocity from the nozzle divided by the separation distance) or maximum axial velocity gradient (dU/dx) on the oxidizer side of the flame.

14

14 Stagnation-Flow and Rotating-Disk CVD

The equations governing reacting flow impinging on a static or rotating surface are discussed in this chapter. The surface is assumed to be a reactive surface, where chemical vapor deposition (CVD) may occur. Such configurations (i.e., shower-head, single-wafer reactors) are commonly used in semiconductor wafer processing. The governing equations and assumptions described in this chapter pertain to the following two Chemkin Reactor Models:

1. Stagnation Flow CVD Reactor
2. Rotating Disk CVD Reactor

In a rotating-disk reactor a heated substrate spins (at typical speeds of 1000 rpm or more) in an enclosure through which the reactants flow. The rotating disk geometry has the important property that in certain operating regimes[89] the species and temperature gradients normal to the disk are equal everywhere on the disk. Thus, such a configuration has great potential for highly uniform chemical vapor deposition (CVD),[90,91,92] and commercial rotating disk reactors are common, particularly for materials processing in the microelectronics industry.

In certain operating regimes, the equations describing the complex three-dimensional spiral fluid motion can be solved by a separation-of-variables transformation[92, p. 239, 83, p. 226] that reduces the equations to a system of ordinary differential equations. Strictly speaking, the transformation is only valid for an unconfined infinite-radius disk and buoyancy-free flow. Furthermore, only some boundary conditions are consistent with the transformation (e.g., temperature, gas-phase composition and approach velocity all specified to be independent of radius at some distance above the disk).

89. G. Evans and R. Greif, *Journal of Heat Transfer ASME* **109**:928 (1987).
90. D. R. Olander, *I. and E. C. Fund.* **6**:178 (1967).
91. M. L. Hitchman, B. J. Curtis, H. R. Brunner, and V. Eichenberger, in *Physicochemical Hydrodynamics*, edited by D. B. Spalding Advanced Publications, London, 1977, Vol. 2.
92. R. Pollard and J. Newman, *Journal of the Electrochemical Society* **127**:744 (1980).

Fortunately, however, the transformed equations still provide a very good practical approximation to the flow in a finite-radius reactor over a large fraction of the disk (up to ~90% of the disk radius) when the reactor operating parameters are properly chosen, i.e., high rotation rates.[89, p. 239]

In the limit of zero rotation rate, the rotating disk flow reduces to a stagnation-point flow, for which a similar separation-of-variables transformation is also available. Such flow configurations ("pedestal reactors") also find use in CVD reactors.

This chapter reviews the rotating-disk/stagnation-point flow equations. An infinite-radius disk rotating below a fluid medium is a classic problem in fluid mechanics.[83, p. 226,84, p. 226,93] Under these ideal conditions this problem has a solution that is an exact solution of the Navier-Stokes equations. Consequently, the heat and mass transfer near an infinite-radius rotating disk have been extensively studied.[94,95] For CVD applications, Olander[96] used a rotating disk to study deposition in the germanium-iodide system. Pollard and Newman[92, p. 239] performed a theoretical study of the deposition of Si from $SiCl_4$ on a rotating-disk susceptor. They extended the von Karman similarity solution for isothermal flow[83, p. 226] by adding energy and species equations and incorporating temperature-dependent fluid properties to obtain an ordinary differential equation boundary-value problem for the heat, mass and momentum transfer. Hitchman, *et al*.[97] studied epitaxial Si deposition from $SiCl_4$ in a rotating-disk reactor and analyzed their results in terms of the infinite-disk solution.

Consider a solid rotating surface of infinite extent in the r, θ plane (*Figure 14-1*) separated from a facing, parallel, porous, non-rotating surface by a distance $x = L$. A forced flow with purely axial velocity emerges from the porous surface and is directed toward the rotating one. The flow at $x = L$ approximates the inlet flow conditions in a cylindrical, rotating-disk CVD reactor. The finite x domain in the present case results in a nonzero value of the radial pressure gradient.

Analysis by Evans and Greif[89, p. 239] combined the stagnation and rotating disk flows for the situation of an infinite-radius, porous, non-rotating disk separated by a distance L from an infinite-radius, nonporous, heated, rotating disk. This combination of flows provides a good approximation to the flow field in a rotating disk reactor. The Evans and Greif analysis was used as a foundation for the Chemkin stagnation-flow and

93. F. M. White, *Viscous Fluid Flows*, McGraw-Hill, New York, 1974.
94. W. G. Cochran, *Proc. Cambridge Phil. Soc.* **30**:365 (1934).
95. E. M. Sparrow and J. L. Gregg, *Journal of Heat Transfer ASME* **82**:294 (1960).
96. D. R. Olander, *I. and E. C. Fund.* 6:178 (1967)
97. M. L. Hitchman, B. J. Curtis, H. R. Brunner, and V. Eichenberger, in *Physicochemical Hydrodynamics*, edited by D. B. Spalding Advanced Publications, London, 1977, Vol. 2

rotating-disk transport model. However, the Chemkin model also incorporates a species conservation equation for each species that occurs in the gas phase, with GAS-PHASE KINETICS and SURFACE KINETICS contributions. These equations account for convective and diffusive transport of species, as well as production and consumption of species by elementary chemical reactions.

14.1 Impinging-flow Conservation Equations

The conservation equations defining the boundary-value system that we solve are stated below.

Equation 14-1 Mixture continuity

$$\frac{1}{\rho}\frac{\partial \rho}{\partial t} = \frac{\partial u}{\partial x} - 2V - \frac{u}{\rho}\frac{\partial \rho}{\partial x} = 0$$

Equation 14-2 Radial momentum

$$\rho\frac{\partial V}{\partial t} = \frac{\partial}{\partial x}\left(\mu\frac{\partial V}{\partial x}\right) - \rho u\frac{\partial V}{\partial x} - \rho(V^2 - W^2) - \frac{1}{r}\frac{dp_m}{dr} = 0$$

Equation 14-3 Circumferential momentum

$$\rho\frac{\partial W}{\partial t} = \frac{\partial}{\partial x}\left(\mu\frac{\partial W}{\partial x}\right) - \rho u\frac{\partial W}{\partial x} - 2\rho VW = 0$$

Equation 14-4 Thermal energy

$$\rho c_p\frac{\partial T}{\partial t} = \frac{\partial}{\partial x}\left(\lambda\frac{\partial T}{\partial x}\right) - \rho c_p\frac{\partial T}{\partial t} - \sum_{k=1}^{K_g}\left(c_{pk}\rho Y_k V_k\frac{\partial T}{\partial x} + \dot{\omega}_k h_k M_k\right) + S_q(x) = 0$$

Figure 14-1 Sketch of the infinite-radius disk and inlet boundary conditions

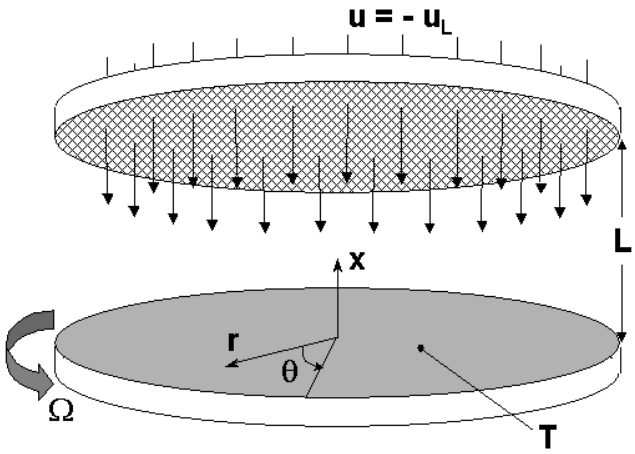

Equation 14-5 Species continuity

$$\rho\frac{\partial Y_k}{\partial t} = -\frac{\partial \rho Y_k V_k}{\partial x} - \rho u\frac{\partial Y_k}{\partial x} + M_k\dot{\omega}_k = 0 \qquad (k = 1, K, K_g)$$

Equation 14-6 Equation of state

$$P = \frac{\rho RT}{\overline{M}}$$

Equation 14-7 Surface-species conservation

$$\frac{dZ_k}{dt} = \frac{\dot{s}_k}{\Gamma_n} = 0 \qquad (k = 1, K, K_s)$$

The above equations can be solved as either a steady-state problem or time-accurate transient. For a steady-state solution, the solution is sought to the above equations where the transient terms on the left-hand side of the equations are zero. The steady-state algorithm is discussed further in the *Chapter 15*.

In the governing equations the independent variables are x, the distance normal to the disk surface, and t, time. The dependent variables are the velocities, the temperature T, the gas-phase species mass fractions Y_k, and the surface-species site fractions Z_k. The axial velocity is u, and the radial and circumferential velocities are scaled by the radius as $V = v/r$ and $W = w/r$, respectively. The mass density is given by ρ and the specific heats by c_p. The molecular weight and specific enthalpy for species k are given by M_k and h_k. The viscosity and thermal conductivity are given by μ and λ. The universal gas constant is R. The chemical production rate of species by the gas-phase reaction is resumed to result from a system of elementary chemical reactions that proceed according to the law of mass action. The chemical production rate of species $\dot{\omega}_k$ by surface reaction is given by $\dot{s}_k$. K_g is the number of gas-phase species and K_s is the number of surface species, not including bulk-phase species. The factor Γ_n is the surface site density for site type n. The details of the chemical reaction rate formulation can be found in *Chapter 3* and *Chapter 4*. Details of the transport property (i.e., viscosities, thermal conductivities and diffusion coefficients) formulation can be found in *Chapter 5*.

The term $(1/r)(dp_m/dr) \equiv \Lambda$ in the radial momentum equation is taken to be constant and its value is computed as an eigenvalue of the problem. The pressure is assumed to be composed of two parts: an average thermodynamic pressure P that is taken to be constant, and a spatially varying component p_m that appears in the radial momentum equation, see *Equation 14-2* (c.f. Paolucci[98]).

98. S. Paolucci, Sandia National Laboratories Report SAND82-8257, 1982.

The “surface-species conservation” equation states simply that in steady state the surface composition does not change. In some sense it could be considered a (possibly complex) boundary condition on the gas-phase system. However, because the surface composition is determined as part of the solution, *Equation 14-7* should be considered part of the system of governing equations.

Provisions are made for dealing with the transport properties at the mixture-averaged (Fickian) level or at the full multicomponent level. At the mixture-averaged level, each species diffusion velocity is calculated in terms of a diffusion coefficient and a species gradient,

Equation 14-8

$$V_k = -\frac{1}{X_k} D_{km} \frac{dX_j}{dx} - \frac{D_k^T}{\rho Y_k} \frac{1}{T} \frac{dT}{dx}$$

where,

Equation 14-9

$$D_{km} = \frac{1 - Y_k}{\sum_{j \neq k}^{K} X_j / D_{kj}}$$

At the multicomponent level, the diffusion velocities are given as

Equation 14-10

$$V_k = \frac{1}{X_k \overline{M}} \sum_{j=1}^{K_g} M_j D_{k,j} \frac{dX_j}{dx} - \frac{D_k^T}{\rho Y_k} \frac{1}{T} \frac{dT}{dx}$$

Both formulations have an ordinary diffusion component and may have a thermal diffusion component (Soret effect). In these expressions, X_k is the mole fraction for the *k*th species, D_{kj} is the binary diffusion coefficient matrix, $D_{k,j}$ is the matrix of ordinary multicomponent diffusion coefficients, and D_k^T is the thermal diffusion coefficient for the *k*th species. Thermal diffusion often plays an important role in CVD problems. In the presence of strong temperature gradients, thermal diffusion causes high molecular-weight species in a low molecular-weight carrier to diffuse rapidly toward the low-temperature region.[26, p. 84] The multicomponent and mixture transport properties are evaluated from the pure species properties using the averaging procedures as discussed in *Chapter 5*.

Mass conservation requires that $\sum_{k=1}^{K_g} Y_k V_k = 0$. However, a consequence of using the Fickian mixture-averaged diffusion coefficient defined in *Equation 14-9* to define a diffusion velocity in *Equation 14-8* is that mass is not always conserved, i.e., $\sum_{k=1}^{K_g} Y_k V_k \neq 0$. Therefore, at this level of closure of the transport formulation, some corrective measures must be taken. The user has several options. One is for the program to apply an *ad hoc* Correction Velocity, defined as

Equation 14-11

$$V_c = -\sum_{k=1}^{K_g} Y_k V_k$$

When this correction velocity (independent of species k) is added to all the species diffusion velocities as computed from *Equation 14-8*, mass conservation is assured.

Another option is to account for the deficiencies of the mixture-averaged closure of the multicomponent transport problem and to assure mass conservation is to solve only $K_g - 1$ gas-phase species conservation equations and determine the remaining mass fraction by requiring $\sum_{k=1}^{K_g} Y_k = 1$ (Trace option). The mixture-averaged transport closure is asymptotically correct in the trace-species limit. In cases where one species is present in large excess (such as a carrier gas in a CVD reactor), this is a reasonable option.

The carrier gas composition is conventionally determined as

Equation 14-12

$$Y_{k_g} = 1 - \sum_{k=1}^{K_g - 1} Y_k$$

The default for this option is to consider the last-named gas-phase species in the GAS-PHASE KINETICS input (K_g) as the species for which a conservation equation is not solved. Since the last species may not always be the most abundant species, a further option provides for dynamically determining the largest species concentration at each mesh point and removing its conservation equation from the system of equations (Reorder option in the User Interface).

The source term in the thermal energy equation $S_q(x)$ is a spatially distributed thermal energy source that we assume is in the form of a Gaussian:

Equation 14-13

$$S_q(x) = \dot{q}\frac{1}{w_s}\sqrt{\frac{3}{\pi}}\exp\left[\frac{-3(x-x_s)^2}{w_s^2}\right]$$

To use this expression, the user is expected to specify three parameters: $\dot{q}$, w_s and x_s. The parameter $\dot{q}$ is the total energy integrated over its full spatial extent. Implicit in *Equation 14-13* is the fact that

Equation 14-14

$$\dot{q} = \int_{-\infty}^{\infty} S_q(x)dx$$

The distribution is centered at $x = x_s$ and w_s is the 2σ half-width of the distribution. (The integral of $S_q(x)$ from $-w_s$ to w_s includes 95% of the total added energy $\dot{q}$.)

The disk boundary condition becomes relatively complex in the presence of heterogeneous surface reactions. The gas-phase mass flux of each species to the surface j_k is balanced by the creation or depletion of that species by surface reactions, i.e.,

Equation 14-15

$$j_k = \dot{s}_k M_k \qquad (k = 1, \ldots, K_g)$$

The gas-phase mass flux of species k at the surface is a combination of diffusive and convective processes,

Equation 14-16

$$j_k = \rho Y_k u + \rho Y_k V_k \qquad (k = 1, \ldots, K_g)$$

where u is the bulk normal fluid velocity at the surface and V_k is the diffusion velocity of the *k*th species. The bulk normal fluid velocity at the surface is computed from the surface reaction rates summed over all the gas-phase species K_g,

Equation 14-17

$$u = \sum_{k=1}^{K_g} \frac{\dot{s}_k M_k}{\rho}$$

Even though the susceptor surface is solid, there is a bulk fluid velocity into the surface (the Stefan velocity) that accounts for the mass of solids deposited. This bulk velocity at the surface is usually small, and thus the boundary movement due to the deposition is neglected. That is, the problem is solved in a fixed spatial domain. While the surface growth rate is predicted, the computational domain is not adjusted to account for small changes resulting from surface growth.

There are two options for treating the thermal-energy boundary condition on the deposition surface. The first is to simply specify the surface temperature. If the temperature is controlled or measured directly, this option is usually the one of choice. However, some problems require that the surface temperature be predicted as part of the solution. The appropriate boundary condition is derived from a surface energy balance. Exothermicity (or endothermicity) of surface reactions contributes to the energy balance at an interface. Diffusive and convective fluxes in the gas-phase are balanced by thermal radiative and chemical heat release at the surface. This balance is stated as

Equation 14-18

$$\lambda\frac{\partial T}{\partial x} - \sum_{k=1}^{K_g} \rho Y_k (V_k + u) h_k = \sigma\varepsilon(T^4 - T_w^4) + \sum_{k=K_s^f}^{K_b^l} \dot{s}_k M_k h_k + \dot{P}$$

In the radiation term, σ is the Stefan-Boltzmann constant, ε is the surface emissivity, and T_w is the temperature to which the surface radiates. The summation on the right-hand side runs over all surface and bulk species. K_b^l and K_s^f are the SURFACE KINETICS notations for the indices that identify the first surface species and the last bulk species. By substituting *Equation 14-15* and *Equation 14-16* into *Equation 14-18*, the energy balance can be written in a more compact form as

Equation 14-19

$$\lambda\frac{\partial T}{\partial x} = \sigma\varepsilon(T^4 - T_w^4) + \sum_{k=1}^{K} \dot{s}_k M_k h_k + \dot{P}$$

The reaction-rate summation on the right-hand side runs over all species, including the gas-phase species. The term $\dot{P}$ presents an energy source in the surface itself, such as might be generated by resistance heating.

The SURFACE KINETICS Pre-processor requires as input the mass densities ρ_k of the bulk species. These densities are used to convert the rate of production of a bulk species (in moles/cm^2/sec) into a thickness growth rate G (in cm/sec). The needed relationship is

Equation 14-20

$$G = \sum_{k=K_s^f}^{K_b^l} \frac{\dot{s}_k M_k}{\rho_k}$$

When solving for the flow induced by the rotation of a disk in an infinite, otherwise quiescent fluid, the axial velocity u at $x = L$ is part of the solution. However, for the case corresponding to injection of the gas through a non-rotating porous surface, u is the specified inlet velocity at height $x = L$. This gives us the flexibility of either "forcing" or "starving" the inlet flow compared to the natural flow induced by the spinning disk itself. It is always necessary to specify the inlet velocity in the case of a stagnation-point flow.

The other boundary conditions on the fluid flow fields are relatively simple. The temperature at $x = L$ (the reactor inlet) is specified. Normally, the radial and circumferential velocities are zero at $x = L$. A linearly varying radial velocity or a specified spin rate may also be specified at $x = L$. In these cases, $V = v/r = a_i$ or $W = w/r = o_i$, where a_i and o_i are specified parameters. The radial velocity on the disk is zero, and the circumferential velocity is determined from the spinning rate $W = \Omega$. For the species composition at the inlet boundary, the default formulation is to solve the following flux balance:

Equation 14-21

$$\rho u \varepsilon_k = \rho u Y_k + \rho Y_k V_k$$

where ε_k is the species mass fraction specified for the inflow. The user may also opt to fix the species composition (i.e., $Y_k = \varepsilon_k$), by specifying the option in the User Interface to fix the inlet composition rather than the inlet flux.

14.2 Finite Difference Approximations

The first task in solving the deposition problem is to discretize the governing conservation equations. We use finite difference approximations on a non-uniform grid with points numbered by j from 1 at the disk boundary to J at the inlet boundary.

The "convective" terms, such as $\rho u \partial V / \partial x$ in *Equation 14-2* are approximated by first-order upwind formulas, as

Equation 14-22

$$\rho u \frac{\partial V}{\partial x} \approx \rho_j u_j \left(\frac{V_{j+1} - V_j}{x_{j+1} - x_j} \right)$$

The u velocity is always negative in these problems (flowing from the inlet at large values of x toward the substrate at $x = 0$), so the upwind differencing calls for the derivative to be formed between $j+1$ and j. Upwind differences cause substantial artificial diffusion, especially on coarse mesh networks. However, we have found that they lead to much more reliable convergence on coarse meshes early in the iteration procedure. Ultimately, because the meshes are adaptively refined, the artificial diffusion is very small in the final solution.

The first derivative in the summation term in the energy *Equation 14-4* is always approximated by a central difference formula,

Equation 14-23

$$\left(\frac{\partial T}{\partial x} \right)_j \approx \left(\frac{h_{j-1}}{h_j (h_j + h_{j-1})} T_{j+1} + \frac{h_j - h_{j-1}}{h_j h_{j-1}} T_j - \frac{h_j}{h_{j-1} (h_j + h_{j-1})} T_{j-1} \right)$$

where the mesh intervals $h_j = x_{j+1} - x_j$. The coefficients in the summation are evaluated at j.

The second-derivative diffusion terms, such as that in the energy equation, are approximated by the following second order central difference:

Equation 14-24

$$\frac{\partial}{\partial x} \left(\lambda \frac{\partial T}{\partial x} \right)_j \approx \left(\frac{2}{x_{j+1} - x_{j-1}} \right) \left[\lambda \left(\frac{T_{j+1} - T_j}{x_{j+1} - x_j} \right) - \lambda \left(\frac{T_j - T_{j-1}}{x_j - x_{j-1}} \right) \right]$$

The coefficient λ in this formula (at $j \pm 1/2$) are evaluated using the averages of the dependent variables between mesh points.

The diffusive terms in the species conservation equations are analogous to the diffusive term in the energy equation. However, because we express them in terms of diffusion velocities, they at first appear different. In *Equation 14-5*, the diffusive term is approximated as

Equation 14-25

$$\frac{\partial \rho Y_k V_k}{\partial x} \approx \frac{\rho_{j+1/2} Y_{k,j+1/2} V_{k,j+1/2} - \rho_{j-1/2} Y_{k,j-1/2} V_{k,j-1/2}}{x_{j+1/2} - x_{j-1/2}}$$

The ordinary multicomponent diffusion and thermal diffusion fluxes (*Equation 14-10*) are approximated at the $j \pm 1/2$ positions as illustrated by

Equation 14-26

$$(\rho Y_k V_k)_{j+\frac{1}{2}} = \left(\frac{\rho \dot{m}_k}{\overline{M}^2}\right)_{j+\frac{1}{2}} \sum_{l=1}^{K_g} (\dot{m}_l D_{k,l})_{j+\frac{1}{2}} \left(\frac{X_{l,j+1} - X_{l,j}}{x_{j+1} - x_j}\right) + \left(\frac{D_k^T}{\rho Y_k T}\right)_{j+\frac{1}{2}} \left(\frac{T_{j+1} - T_j}{x_{j+1} - x_j}\right)$$

An analogous finite-difference expression is used for the mixture-averaged approximation to the diffusion fluxes. Since the mole fraction of a species can be zero, we avoid difficulties by forming $\rho Y_k V_k$, which is the expression needed in *Equation 14-4*, rather than V_k itself ($Y_k = X_k \dot{m}_k / \overline{M}$).

All the non-differentiated terms, such as the chemical production rate terms, are evaluated at the mesh points j. Coefficients not appearing within derivatives are also evaluated at the mesh points.

15

15 Numerical Solution Methods

In this chapter we describe in some detail the solution algorithms used to solve steady-state and transient problems for the reactor types described in previous chapters. The proprietary steady-state solver, TWOPNT, is described in more detail, while the transient solvers have been primarily developed by 3rd-party organizations and are documented elsewhere in order to provide insight into the diagnostic messages and solution procedure. Several of the transient solvers employed by Chemkin are available in the public domain. In such cases, the source code is included in the Chemkin installation and this code usually includes detailed explanation of the solver usage as comments in the FORTRAN code. A discussion of which transient solver is used for each class of reactor models and references to those solvers are generally included in the previous reactor-model chapters. For steady-state problems, however, some common characteristics of the solver approach are discussed here.

15.1 Steady-state Solver for Homogeneous Systems

For steady-state problems, the 0-D homogeneous systems described in *Chapter 8* employ Reaction Design's numerical solver, TWOPNT, to determine a solution to the set of algebraic equations governing these Reactor Models. TWOPNT solves the system of algebraic equations by first applying a damped modified Newton algorithm to the set of J nonlinear algebraic equations represented by the steady-state versions of *Equation 8-1*, *Equation 8-9*, *Equation 8-18*, *Equation 8-19*, *Equation 8-20*, *Equation 8-91*, and *Equation 8-85*. However, in the event that the Newton algorithm fails to converge during the iteration, the solution estimate will automatically be conditioned by integration of the time-dependent version of the equations over a fixed number of time steps. This time-stepping procedure provides a new starting estimate for the Newton algorithm that is closer to the steady-state solution, increasing the

likelihood of convergence for the Newton method. After time-stepping, the Newton algorithm tries again for convergence and, if this fails, TWOPNT takes additional time steps on the transient solution to further improve the initial iterate. Ultimately, the Newton iteration converges on the steady-state solution.

15.1.1 Starting Estimates

The use of a Newton iteration algorithm for solution of the governing equations requires the user to provide initial estimates of the solution variables. It may sometimes be difficult to obtain good initial estimates of species composition, especially when one is not familiar with the chemistry system being studied. In such cases, it may be necessary to approach the problem from points that are more intuitive. For example, in a thermal problem, a good initial estimate of gas species is often the thermodynamic equilibrium composition at the initial temperature. For this purpose, an optional equilibrium calculation (used by default if no initial guess is provided), minimizes the Gibb's free energy of the system in order to determine the equilibrium gas mole fractions. This method of determining the initial estimate of the gas-phase composition is automatically initiated when the user does not supply any initial estimates for the gas-phase species' mole fractions. If equilibrium composition does not provide immediate convergence for the reactor conditions of interest, the user may increase the residence time (thereby driving the conditions closer to equilibrium) from the target conditions until a solution is reached. This solution can then be used as the initial estimate for the desired residence time. Such gradual approach to a desired solution is facilitated by the Continuation capability, and generally requires very little computational time. For a plasma system, a similar approach could be used to obtain a solution where the initial guess is difficult to obtain. In this case, the user might assume an initial guess for the gas-phase composition close to that of the reagent gases entering the reactor, and set the power deposition level very low. Then gradually increasing the reactor power using the continuation capability can lead to the desired solution.

Initial estimates of surface site fractions are often more difficult, but also have less impact on the ability of the Newton algorithm to reach a solution. A general rule of thumb for all species types is to provide an estimate for every species in the system, even if these numbers are small. An initial guess of 1×10^{-7}, for example, is generally much better than allowing the application to set the initial fraction to zero. All initial estimates will be normalized, such that the sums of gas mole fractions, surface site fractions, and bulk species fractions are all equal to one.

The user has an option to either solve the gas energy equation or to keep the temperature fixed at the initial specified value. There are some cases when the user may choose not to solve the gas energy equation. For example, the reactor temperature may have been accurately measured, while heat losses are difficult to estimate. In cases where the energy equation is solved, the user has an option to solve the system of equations in one or two steps. The default is to use two steps: first solve for the species composition at the fixed temperature estimate provided by the user, and then solve simultaneously the energy equation and the species composition using the first solution as the initial guess. This two-stage method provides more robust convergence for thermal systems, where the reaction rates' exponential dependence on the gas temperature is the primary source of equation stiffness and nonlinearities. For plasma systems, when one is solving for the electron energy equation, convergence is usually most expedient with the one-step option with no fixed-temperature iteration.

15.1.2 Modified Damped Newton's Method for 0-D Reactors

Newton's method determines a sequence of iterations or approximate solutions that approach the true solution. For the sake of notation simplicity, we call these approximate solution vectors, ϕ. When an arbitrary ϕ is substituted into the governing equations, the equations generally do not equal zero unless ϕ also represents the true solution; in general the equations equal a residual vector F. The goal then is to find ϕ such that

Equation 15-1

$$F(\phi) = 0$$

For 0-D homogeneous reactors, this vector ϕ may be, for example:

Equation 15-2

$$\phi = \{\zeta_j, \ldots, \zeta_{N_{\mathrm{PSR}}}\}^T$$

where:

Equation 15-3

$$\zeta_j = \left\{ T, T_e, Y_1, \ldots, Y_{K_g}, Z_{K_s^f(1)}, \ldots, Z_{K_s^l(1)}, X^b_{K_b^f(1)}, \ldots, X^b_{K_b^l(1)}, \rho_{N_\rho^f(1)}, \ldots, \rho_{N_\rho^l(1)}, Z_{K_s^f(M)} \right.$$

$$\left. Z_{K_s^f(M)}, \ldots, Z_{K_s^l(M)}, X^b_{K_b^f(M)}, \ldots, X^b_{K_b^l(M)}, \rho_{N_\rho^f(M)}, \ldots, \rho_{N_\rho^l(M)} \right\}^T$$

where T and T_e are the gas and electron temperatures, the Y's are the gas species mass fractions, the Z's are the surface site fractions within each surface phase, the X's are the mole fractions of species in the bulk phases, and the ρ's are the surface site densities of those surface phases whose site densities are allowed to change. The exact components of the solution vector may vary depending on problem type and reactor model. The total number of unknowns, J, is defined by *Equation 8-97*. The corresponding vector F is composed of a corresponding set of residuals of the gas energy equation, the electron energy equation, the species equations, and the continuity equation for the surface site densities.

Provided the initial estimate $\phi^{(0)}$ of the solution is sufficiently good, Newton's method produces a sequence of iterates $\{\phi^{(n)}\}$ that converges to the solution of the nonlinear equations $F(\phi^{(n)}) = 0$. The purest form of the Newton algorithm,

Equation 15-4

$$\phi^{(n+1)} = \phi^{(n)} - \left(\frac{\partial F}{\partial \phi}\right)^{-1}_{\phi^{(n)}} F(\phi^{(n)})$$

is usually difficult to implement in practice. Evaluating the Jacobian matrices, $\partial F / \partial \phi$, is time consuming, and convergence typically requires a very good initial estimate $\phi^{(n)}$. TWOPNT employs the usual remedies for these problems. First, TWOPNT retains the Jacobian matrix through several iteration steps, rather than updating at every iteration as indicated in *Equation 15-10*. Thus, the Jacobian used at the current iteration, $J^{(n)}$, may be based on a solution that is several iterations old. The user can specify in the input the maximum number of iterations TWOPNT performs before calculating a new Jacobian. Second, the advancement of the iterate $\phi^{(n)}$ to $\phi^{(n+1)}$ is damped by a factor $\lambda^{(n)}$. The modified Newton algorithm is then,

Equation 15-5

$$\phi^{(n+1)} = \phi^{(n)} - \lambda^{(n)} (J^{(n)})^{-1} F(\phi^{(n)})$$

where $0 < \lambda^{(n)} \leq 1$, and

Equation 15-6

$$J^{(n)} = \left(\frac{\partial F}{\partial \phi}\right)_{\phi^{(m)}} \qquad 1 < m \leq n$$

Internally, TWOPNT will generate a new Jacobian whenever convergence with the old Jacobian fails. While *Equation 15-7* correctly indicates the relation between the new and the old iterate, TWOPNT does not compute the inverse of the Jacobian matrix, but rather solves a system of linear equations, $J^{(n)}\Delta\phi^{(n)} = F(\phi^{(n)})$, for the undamped vector, $\Delta\phi^{(n)}$.

The TWOPNT algorithm determines the damping parameter $\lambda^{(n)}$ and the need for a new Jacobian based on several criteria designed to keep the iteration stable and within solution bounds. To accept a new solution iterate $\phi^{(n+1)}$, TWOPNT requires that the undamped steps decrease in magnitude,[99] i.e.,

Equation 15-7

$$\left|(J^{(n)})^{-1}F(\phi^{(n+1)})\right| < \left|(J^{(n)})^{-1}F(\phi^{(n)})\right|$$

If the solution $\phi^{(n+1)}$ fails this criterion, TWOPNT rejects it and retries the step with half the damping parameter or a new Jacobian matrix. TWOPNT adjusts the damping parameter to ensure that the evolving solution always remains within the solution bounds. Examples of physical bounds that are imposed on the solution are: the temperature(s) must be positive and the species mass fractions must be between zero and one. For the steady-state solver, it is actually possible to modify the lower bounds placed on the species mass fractions to be slightly negative (species “floor” value). Allowing some species mole fractions to become slightly negative during iteration sometimes enhances the convergence rate, especially when the solution composition has species mass fractions that vary over many orders of magnitude.

The Newton iteration procedure continues along these lines until the user-defined convergence criteria are met. Convergence requires that the maximum norm of the undamped correction vector $\Delta\phi^{(n)}$ has been reduced to within user-defined absolute and relative tolerances, i.e.,

Equation 15-8

$$|\Delta\phi| \leq \max(A, R \times |\phi|)$$

where A is the absolute tolerance and R is the relative tolerance. The relative tolerance roughly indicates the number of significant digits in the converged solution, and the absolute tolerance serves to exclude solution components smaller than A from the relative convergence criterion. Typically, the absolute tolerance A should be

99. P. Deuflhard, *Numerical Mathematics* **22**:289 (1974).

smaller than the maximum mass fraction of any species of interest. The user should be particularly careful in specifying A for plasma solutions, since the small electron mass will result in a much smaller mass fraction for electrons than for other important species. The relative tolerance should generally be in the range of 10^{-3} to 10^{-4}.

If damping does not produce a suitable correction vector, TWOPNT computes a new Jacobian. In the case when a new Jacobian has just been computed, and a damped Newton step still cannot produce a suitable correction vector, TWOPNT begins to take time steps. The time-stepping procedure is described in the section following the description of the Jacobian Matrix below.

15.1.3 Jacobian Matrix

The Jacobian Matrix is a dense $J \times J$ matrix. Rather than derive and evaluate analytic expressions for the Jacobian elements, we form the elements of the Jacobian numerically, through finite difference perturbations. This approach is justified since the accuracy of analytic Jacobians is not required for the modified Newton method described above. This is demonstrated by the successful use of old (and therefore inaccurate) Jacobians. We evaluate the numerical Jacobian elements from a one-sided finite difference formula as follows:

Equation 15-9

$$J_{i,j} \approx \frac{F_i(\phi_j + \delta) - F_i(\phi_j)}{\delta}$$

where

Equation 15-10

$$\delta = r \times \phi_j + a$$

We choose the relative and absolute perturbations, r and a, to be the square root of the computer's unit round-off.

15.1.4 Pseudo Time-Stepping Procedure

The steady-state solution that we seek could be obtained through pure time-stepping using the transient equations described in *Section 8.5.3*. Such a procedure is very reliable but also very slow. However, because the time-stepping is robust, we employ this procedure to condition the initial iterate in cases when the Newton's method is not converging. When the modified Newton's method fails, TWOPNT solves the transient

equations for a given number of time steps, and then returns to the Newton method using the result of the time-stepping as the new initial iterate. This trial solution will be closer to the steady-state solution, and thus it is more likely to be within Newton's convergence domain.

The transient equations are given in *Chapter 8*. We solve this system of ordinary differential equations using the backward-Euler method. In this method, the time derivatives are approximated by first-order, backwards finite differences. For example, dT/dt is approximated as

Equation 15-11

$$\frac{dT}{dt} \approx \frac{T_j^{n+1} - T_j^n}{\Delta t}$$

where here the subscript n indicates the time step index and Δt represents the size of the time step. All other terms in the governing equation are evaluated at time level n. The time-discretized problem is then another system of nonlinear algebraic equations for the dependent variable vector ϕ at time level $n+1$.

To solve the system of equations for each time step we use the same Newton method as we employ in the steady-state problem. However, the transient problem is much more likely to converge; it should always converge for a sufficiently small time step. The objective, then, is to choose a time step that is sufficiently large to make progress toward the steady solution, yet not so large as to introduce convergence difficulties in the transient solution method. Typical time steps range from 1-10 microseconds, although in plasma systems it is often necessary to choose time steps much smaller than this (10-100 nanoseconds).

After solving the specified number of time steps, TWOPNT again attempts to solve the steady problem by Newton's method. If the steady solution fails again the application reverts to time stepping, beginning where it left off at the last time-stepping procedure. Clearly the better the user's initial estimate of the solution, the less likely the application will have to resort to time stepping. If the application fails to converge in time-stepping, then, the user may either choose smaller time steps, or try a new starting estimate.

The time-stepping solution procedure described here is not particularly sophisticated, since we are neither interested in the accuracy of the transient path nor in solving the transient problem all the way to steady state. We chose to use a method that is relatively inexpensive per step and employs the same Newton algorithm that is used in the steady-state solution. The transient solution therefore serves only to condition the starting estimates for the Newton algorithm, but does not provide accurate solution of the transient process.

15.2 Steady-state 1-D Solution Methods

The following reactor models include one-dimensional grids for steady-state solution:

1. Premixed Laminar Burner-stabilized Flame
2. Premixed Laminar Flame-speed Calculation
3. Opposed-flow Diffusion Flame
4. Premixed Burner-Stabilized Stagnation Flame
5. Flame-Extinction Simulator
6. Stagnation-flow CVD Reactor
7. Rotating-disk CVD Reactor

The numerical solution procedure begins by making finite difference approximations to reduce the boundary value problem to a system of algebraic equations. The initial approximations are usually on a very coarse mesh that may have as few as five or six points. After obtaining a solution on the coarse mesh, new mesh points are added in regions where the solution or its gradients change rapidly. We obtain an initial guess for the solution on the finer mesh by interpolating the coarse mesh solution. This procedure continues until no new mesh points are needed to resolve the solution to the degree specified by the user. This continuation from coarse to fine meshes has several important benefits that are explained later in this chapter. We attempt to solve the system of algebraic equations by the damped modified Newton algorithm in TWOPNT. However, if the Newton algorithm fails to converge, the solution estimate is conditioned by integration in time. This provides a new starting point for the Newton algorithm that is closer to the solution, and thus more likely to be in the domain of convergence for Newton's method. As the mesh becomes finer we normally find that the estimate interpolated from the previous mesh is within the domain of convergence of Newton's method. This point is key to the solution strategy.

15.2.1 Starting Estimates

The 1-D steady-state reactor models require a starting estimate of the solution from which to begin its iteration. The general form of this estimate is shown in *Figure 15-1*. For this estimate, we presume that there is a reaction zone in which reactants are specified at one end of the reaction zone and the reactants change from their unreacted values to the products that are found on the far-end of the flow domain. The user can provide estimates for the location and thickness of this reaction zone. The user may also provide estimates of the product species fractions, or the species composition that is expected at the far-end of the domain.

For Premixed Laminar 1-D Flame, Flame-speed Calculator, Stagnation-flow, and Rotating-Disk models, if no product species estimates are given, Chemkin will calculate an equilibrium composition to be used as the product estimate. When equilibrium is used to estimate the product concentrations, the user can also provide a minimum value to be applied to all species when creating the product estimates. For Opposed-flow Flames, the “product” and “reactant” are represented by the two inlet streams compositions (e.g., fuel and oxidizer compositions for diffusion flames) that provide the boundary conditions for the flow domain.

Within the reaction zone straight lines are used between the initial and final values for both the reactants and products. On the reactant side of the reaction zone the reactant species profiles are flat at the reactant values. On the product side, the product species are flat at the estimated product values. Note that any given species can be both a reactant and a product species. For example, the nitrogen in a hydrocarbon-air flame will be both a reactant and a product. The excess fuel in a rich flame will also be both a reactant and a product. Species can also be identified as “intermediates.” Intermediates, such as short-lived radical species, are assumed to have a Gaussian profile that peaks in the center of the reaction zone. The peak height is specified in the input to the model, and the Gaussian width is such that the profile is at 1/10 of its peak value at the edges of the reaction zone.

Figure 15-1 The general form of the starting estimate

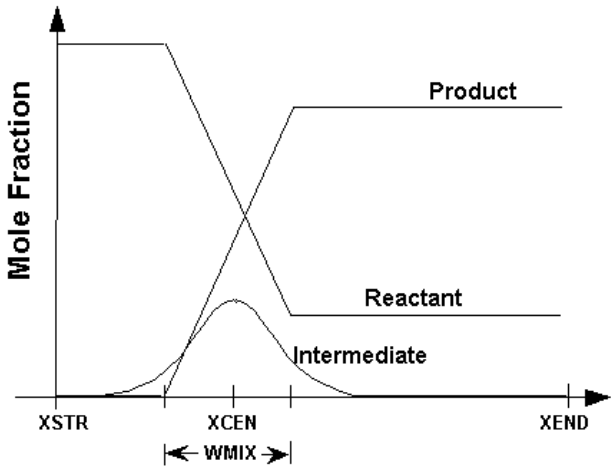

The shape of the assumed species profiles is not too important. Smoother functions, such as cubic polynomials and hyperbolic tangents for the reactant and product species, have no apparent effect on the convergence properties of the method. Since the starting profiles are typically evaluated on a very coarse mesh, it makes little difference whether the underlying function is smooth or not. Therefore, simple linear starting profiles are used.

15.2.2 Continuation Start-up Procedure and User-Specified Temperature Profile

It is often preferable from a physical point of view to model a system with a known temperature profile. Doing so eliminates the need to model heat losses in the energy equation, but it does require that the user be able to provide the temperature profile. There are also computational advantages to using a known temperature profile, rather than solving an energy equation. The most severe nonlinearities in chemical kinetics come from the exponential dependence of the reaction rates on temperature. Thus, eliminating temperature changes from the iteration may make the problem considerably easier to solve.

Even if the energy equation is being solved for the temperature distribution, the iteration often converges more reliably if the species profiles are first computed using a fixed temperature profile. Chemkin, therefore, provides for a two-stage or three-stage procedure to solve the fully coupled reacting-flow and energy equations, depending on the Reactor Model. For Premixed and Opposed-flow Flames, a two-stage procedure is used, where the first solution uses the initial temperature profile as a fixed-temperature constraint and only solves for the species composition and velocity profile. For Stagnation-flow and Rotating-disk CVD reactors, a three-stage procedure is used, where the first stage solves for velocity and temperature profiles,

the second stage solves for species and velocity using a fixed temperature profile, and the third stage solves the fully coupled problem. In all cases, the preliminary stages can be skipped by using appropriate Solver Parameters (e.g., Skip Non-reacting Problem, Skip Intermediate Fixed-Temperature Solution) if desired. This multi-stage continuation procedure, however, is usually more efficient than attempting to solve the fully coupled problem directly.

The user input for the temperature profiles is in the form of position-temperature pairs, which can be created using the Chemkin Profile tool in the User Interface. In general, the mesh used by does not have to correspond to the one on which the given temperature estimate is defined. A linear interpolation of the given temperatures onto the current mesh is used. In the case where the energy equation is not included, it is therefore important for the user to provide enough temperature points that the profile is well resolved and relatively smooth.

15.2.3 Modified Damped Newton's Method

The method by which TWOPNT arrives at a solution to the 1-D governing equations is described here in detail. After discretization on a given mesh, we have a system of nonlinear algebraic equations that TWOPNT attempts to solve by a damped Newton's method. Newton's method determines a sequence of iterations or approximate solutions that approach the true solution. For the sake of notational ease we call these approximate solution vectors ϕ. When any arbitrary ϕ is substituted into the finite difference analog of *Equation 12-2* and *Equation 12-3*, they do not equal zero as they would if the true solution were substituted; in general, they equal a residual vector that we will call F. The objective is to find a vector ϕ that satisfies

Equation 15-12

$$F(\phi) = 0$$

In our case the vector ϕ is composed as follows:

Equation 15-13

$$\phi = (T_1, Y_{1,1}, \ldots, Y_{K,1}, \dot{M}_1, \ldots, T_j, \ldots, Y_{k,j}, \ldots, \dot{M}_j, \ldots, T_J, Y_{1,J}, \ldots, Y_{K,J}, \dot{M}_J)^T$$

The corresponding F vector is composed of the residuals of the energy equation, the species equation, and an equation specifying that $d\dot{M}/dx = 0$. The final equation is included for purposes of maintaining a banded Jacobian structure. The ordering of the F vector corresponds to the order of the ϕ vector; it begins with the residuals of the left boundary condition $j = 1$, followed by the residuals at the interior mesh points, and finally the residuals at the right boundary, $j = J$.

Provided the initial estimate $\phi^{(0)}$ of the solution is sufficiently good, Newton's method produces a sequence $\{\phi^{(n)}\}$ that converges to the solution of the nonlinear equations $F(\phi)$. The purest form of the algorithm

Equation 15-14

$$\phi^{(n+1)} = \phi^{(n)} - \left(\frac{\partial F}{\partial \phi}\right)^{-1}_{\phi^{(n)}} F(\phi^{(n)})$$

is too expensive and delicate to be used in practice. On the one hand, evaluation of the Jacobian matrices $\partial F / \partial \phi$ is time consuming, and on the other hand, convergence usually requires a very good initial estimate $\phi^{(0)}$. Chemkin employs the usual remedies. First, the Jacobian matrix is replaced by one, $J^{(n)}$, inherited from a previous step of the algorithm. Second, the full step from $\phi^{(n)}$ to $\phi^{(n+1)}$ may be cut short by a damping parameter $\lambda^{(n)}$. In this way the iteration becomes

Equation 15-15

$$\phi^{(n+1)} = \phi^{(n)} - \lambda (J^{(n)})^{-1} F(\phi^{(n)})$$

where, $0 < \lambda^{(n)} \leq 1$, and

Equation 15-16

$$J^{(n)} = J^{(n-1)}$$

$$J^{(n)} = \left(\frac{\partial F}{\partial \phi}\right)_{\phi^{(n)}}$$

The inverse Jacobian matrix in *Equation 15-15* is not actually computed; instead a system of linear equations is solved for the undamped correction vector $\Delta\phi^{(n)}$.

Our selection of the matrix $J^{(n)}$ and of the parameter $\lambda^{(n)}$ is governed by a look-ahead procedure that forces certain behavior upon the algorithm. Thus, having tentatively chosen $\phi^{(n+1)}$ the program looks ahead to the calculation of $\phi^{(n+2)}$. The criterion[99, p. 255] for accepting $\phi^{(n+1)}$ is that the undamped steps decrease in magnitude,

Equation 15-17

$$\left|(J^{(n)})^{-1} F(\phi^{(n+1)})\right| < \left|(J^{(n)})^{-1} F(\phi^{(n)})\right|$$

This prevents the iteration from stepping away from the region where there is good reason to believe a solution lies. Should $\phi^{(n+1)}$ fail this criterion, the application rejects it and retries the step with a halved damping parameter or a new Jacobian matrix. The damping parameter $\lambda^{(n)}$ is initially chosen to be as large as possible so

that $\phi^{(n+1)}$ does not violate various bounds that are set on the solution variables. We know, for example, that the temperature and mass flow rate must be positive, and that the species mass fractions must be between zero and one. The concentrations of many species, such as fuels downwind of a flame, are close to zero and frequently threaten to place the solution out of bounds.

The Newton iteration continues until the maximum norm of the undamped correction vector $\Delta\phi$ is reduced to within a user-specified tolerance. Specifically, the criteria for Newton iteration convergence is when the solution correction vector satisfies

Equation 15-18

$$|\Delta\phi| \leq \max(A, R \times |\phi|)$$

The relative R and absolute A tolerances are parameters that govern the convergence criteria for the Newton iteration. Roughly speaking the relative tolerance indicates how many significant digits the converged solution should contain, and the absolute tolerance serves to exclude solution components smaller than A from the relative convergence criteria. Typically, the absolute tolerance A should be smaller than the maximum mass fraction of any species of interest. The relative tolerance should be in the range of 10^{-3} to 10^{-4}, which will serve to provide 3 to 4 digits of accuracy.

If damping cannot produce a suitable correction, then a new Jacobian is computed. If, after computing a new Jacobian, a damped Newton step still cannot produce a suitable correction, then the application begins to take pseudo time steps. This strategy is described further in *Section 15.1.4*.

15.2.4 Adaptation

We have found that starting the iteration on a coarse mesh has several important advantages. One is that the Newton iteration is more likely to converge on a coarse mesh than on a fine mesh. Moreover, the number of variables is small on a coarse mesh and thus the cost per iteration is relatively small. Since the iteration begins from a user-specified “guess” at the solution, it is likely that many iterations will be required. Ultimately, of course, to be accurate, the solution must be obtained on a fine mesh. However, as the solution is computed on each successively finer mesh, the starting estimates are better, since they come from the converged solution on the previous coarse mesh. In general, the solution on one mesh lies within the domain of convergence of Newton’s method on the next finer mesh.[100] Thus, even though the cost per iteration is increasing, the number of required iterations is decreasing.

100. M. D. Smooke and R. M. M. Mattheij, *Appl. Numer. Math.* **1**:463 (1985)

The adaptive placement of the mesh points to form the finer meshes is done in such a way that the total number of mesh points needed to represent the solution accurately is minimized. Specifically, we place the mesh points in the following way. To resolve the gradients we bound the variation in the solution components between mesh points as

Equation 15-19

$$\left|\phi_{n,j} - \phi_{n,j-1}\right| \leq \delta(\max\phi_n - \min\phi_n)$$

and to resolve the curvature in the solution we bound the variation in the solution's derivatives between mesh points by

Equation 15-20

$$\left|\left(\frac{d\phi_n}{dx}\right)_j - \left(\frac{d\phi_n}{dx}\right)_{j-1}\right| \leq \gamma\left(\max\frac{d\phi_n}{dx} - \min\frac{d\phi_n}{dx}\right)$$

We evaluate the above expressions between each of the mesh points. In each of the subintervals where the inequality is not satisfied, a new mesh point is placed at the midpoint of the subinterval. The parameters δ and γ are user-specified input parameters (Gradient and Curvature ratios, respectively). We exclude variables that are below a certain floor value from consideration in the adaptation. This avoids adapting on variables that are essentially zero, but due to rounding errors may show locally high derivatives. The starting estimate for the dependent variable vector ϕ is determined by a linear interpolation of the coarse mesh solution onto the new finer mesh. After determining a converged solution on this new fine mesh, the adaptation procedure is performed once again. A sequence of solutions on successively finer meshes is computed until the inequalities in *Equation 15-19* and *Equation 15-20* are satisfied between all mesh points.

15.3 Transient Solution Method

The system of ordinary differential equations described for the Reactor Models is generally stiff, which means that there is a large disparity in time scales for evolution of different species in the reactor system. Such systems are most efficiently solved by implicit techniques for time integration. For transient cases, a modified version of a software package called DASPK[101, 102] performs the time integration, as well as the

101. S. Li and L.R. Petzold, "Software and algorithms for sensitivity analysis of large-scale differential algebraic systems." *Journal of Computational and Applied Mathematics*, 2000, vol. 125, no. 1/2, pp. 131.

first-order sensitivity analysis. We employ the direct-solution method in DASPK, which uses backwards-differencing methods for the time integration. Details of the DASPK solver are discussed by Li and Petzold.[101, p. 264] The Reactor Models that employ the DASPK solver for time-accurate transient simulations are:

1. Closed Homogeneous Reactor
2. IC HCCI Engine
3. Closed Plasma Reactor
4. Perfectly Stirred Reactor (PSR)
5. Plasma Reactor
6. Plug-flow Reactor (PFR)
7. Honeycomb Reactor
8. Plasma Plug-flow Reactor (Plasma PFR)
9. Closed Partially Stirred Reactor (Closed PaSR)
10. Partially Stirred Reactor (PaSR)
11. Stagnation Flow CVD Reactor
12. Rotating Disk CVD Reactor

In the case of the PaSR models, several solver options are provided.

102. L. Petzold, R. Serban, S. Li, S. Raha, and Y. Cao, in *Proceedings of the NATO Advanced Research Workshop on Computational Aspects of Nonlinear Structural Systems with Large Rigid Body Motion*, 1999.

16

16 Sensitivity Analysis

Sensitivity analysis of a problem solution allows quantitative understanding of how the solution depends on the various parameters contained in a model.[103] Sensitivity analysis is often an invaluable tool in interpreting the results of stirred reactor[104] and flame experiments.[105,25, p. 84,106]

In Chemkin, we consider the first-order sensitivity coefficients of the gas temperature, species fractions, and, where appropriate, the bulk-phase growth rates, with respect to the reaction rate coefficients. The computationally efficient sensitivity analysis methods exploit the fact that the differential equations describing the sensitivity coefficients are linear, regardless of any non-linearities in the model problem itself. Rate-of-production analysis provides complementary information on the direct contributions of individual reactions to species net production rates.

Sensitivity analysis results are normalized and included in the XML Solution File (e.g. *XMLdata.zip*) for post-processing. In addition, results may be printed to the diagnostic output file. Here we describe the methods used for calculating sensitivity coefficients, for both steady-state and transient solutions, and for normalizing the resulting quantities.

103. J. A. Miller, M. C. Branch, W. J. McLean, D. W. Chandler, M. D. Smooke, and R. J. Kee, in *Proceedings of the Twentieth Symposium (International) on Combustion*, The Combustion Institute, Pittsburgh, Pennsylvania, 1985, p. 673

104. P. Glarborg, R. J. Kee, and J. A. Miller, *Combustion and Flame* **65**:177 (1986).

105. J. A. Miller, M. C. Branch, W. J. McLean, D. W. Chandler, M. D. Smooke, and R. J. Kee, in *Proceedings of the Twentieth Symposium (International) on Combustion*, The Combustion Institute, Pittsburgh, Pennsylvania, 1985, p. 673.

106. Y. Reuven, M. D. Smooke, and H. Rabitz, *Sensitivity Analysis of Boundary Value Problems: Application to Nonlinear Reaction-Diffusion Systems*, Yale University Mechanical Engineering Department Report ME-104-85, 1985.

16.1 Sensitivity Analysis for Steady-state Solutions

The steady-state numerical method described in *Section 15.1* and *Section 15.2* facilitates sensitivity analysis by having already computed the solution Jacobians. Once the Jacobian has been computed for the purposes of solving the nonlinear equations, the sensitivity coefficients are easily calculated. These techniques have been developed over many years and reported in the chemical engineering literature.[107,108,109]

To specify the sensitivity coefficients for steady-state computations, we begin by rewriting *Equation 15-8*, which represents the vector of governing equations, as

Equation 16-1

$$F(\phi(\alpha);\alpha) = 0$$

Here, we have introduced the idea that the equation may depend not only on the solution variables but also on a set of model parameters, α. The residual vector F depends, both explicitly and implicitly, on the solution vector ϕ. For reaction-rate sensitivity, we consider the α's to represent the pre-exponential "A-factors" in the Arrhenius reaction-rate expressions. For heat-of-formation sensitivity, α represents the vector of heats of formation for all the species in the system (available for Premixed Laminar Flame, Flame-speed Calculator, Opposed-flow Flames, Stagnation-flow and Rotating-disk CVD reactor models). By differentiating *Equation 16-1* with respect to an α we obtain a matrix equation for the sensitivity coefficients:

Equation 16-2

$$\frac{\partial F}{\partial \phi}\frac{\partial \phi}{\partial \alpha} + \frac{\partial F}{\partial \alpha} = 0$$

The matrix $\partial F/\partial \phi$ is the Jacobian of the original system and $\partial F/\partial \alpha$ is the matrix of partial derivatives of F with respect to the parameters. The sensitivity coefficients are defined as $\partial \phi/\partial \alpha$. It is helpful to think of the $\partial F/\partial \alpha$ matrix column by column, with each column indicating the dependence of the residual vector F on each parameter. There are as many columns as there are parameters, i.e., the number of gas-phase and surface reactions. The sensitivity coefficient matrix $\partial \phi/\partial \alpha$ contains quantitative

107. R. A. Brown, L. E. Scriven, and W. J. Silliman, in *Nonlinear Problems in Dynamics*, edited by P. Holmes (SIAM, Philadelphia 1980), Vol. p. 289.
108. H. Saito and L. E. Scriven, *Journal of Computational Physics* **42**:53 (1981).
109. W. E. Stewart and J. P. Sørensen, in *Proceedings of the 4th International / 6th European Symposium on Chemical Reactor Engineering*, Dechema, Frankfurt, 1976.

information on how each reaction-rate coefficient affects the temperature(s) and species fractions. The sensitivity coefficient matrix has a structure similar to that of the $\partial F / \partial \alpha$ matrix. That is, each column contains the dependence of the solution vector on a particular chemical reaction.

The Jacobian and its LU factorization are already available from the solution of the original system by Newton's method. Parameter derivatives are computed in a manner similar to the computation of the Jacobian. We can therefore readily solve the linear system of equations represented by *Equation 16-2* for each column of the sensitivity coefficient matrix corresponding to the sensitivities of the solution vector to each of the reaction rates in the GAS-PHASE KINETICS and SURFACE KINETICS mechanisms. TWOPNT employs the LINPACK[110] software to perform these computations. We factor the Jacobian only once, and compute each column of the sensitivity coefficient matrix by back substitution, such that the calculation is relatively inexpensive computationally.

16.2 Sensitivity Analysis For Transient Solutions

The method used for transient sensitivity analysis (for 0-D Homogeneous and Plug-flow models) also takes advantage of the fact that the sensitivity equations are described in terms of the Jacobian of the model problem. For backwards-differencing methods, such as that used in DASPK,[101, p. 264,102, p. 265] the Jacobian is required for solution of the model problem, so it is available for the sensitivity computation. In Reaction Design's modified version of DASPK, the sensitivity equations described below are solved simultaneously with the dependent variables of the solution itself.

The system of ordinary differential equations that describe the physical problem are of the general form

Equation 16-3

$$\frac{d\varphi}{dt} = F(\varphi, t; \alpha)$$

where, in our case, φ is the vector of temperature(s), mass fractions, surface site fractions, and bulk activities, as given for example in *Equation 15-3* of *Section 15.1.2*. Here, the parameter vector α is defined as in *Equation 16-1*.

The first-order sensitivity coefficient matrix is defined as

110. J. J. Dongarra, C. B. Moler, J. R. Bunch, and G. W. Stewart, "LINPACK Users' Guide", *Society of Industrial and Applied Mathematics*, 1979.

Equation 16-4

$$w_{j,i} = \frac{\partial \varphi}{\partial \alpha_i}$$

where the indices j and i refer to the dependent variables and reactions, respectively. Differentiating *Equation 16-4* with respect to the parameters α_i yields

Equation 16-5

$$\frac{dw_{j,i}}{dt} = \frac{\partial F}{\partial \varphi} \cdot w_{j,i} + \frac{\partial F_j}{\partial \alpha_i}$$

Note that this equation for the sensitivity coefficients is linear, even though the model problem may be nonlinear. Of course, when coupled with a nonlinear model problem, the whole system is still nonlinear. Nevertheless, when solved via the same backwards-differentiation formula method as the model problem, the sensitivity solution is efficient because of the linearity. The Newton iteration for the corrector step converges in one iteration.

The Jacobian matrix $\partial F / \partial \varphi$ that appears in *Equation 16-5* is exactly the one that is required by the backwards-differentiation formula method in solving the original model problem, so it is readily available for the sensitivity computation. Each column corresponds to the sensitivities with respect to one of the reaction pre-exponential constants. The solution proceeds column by column. Note that the Jacobian matrix is the same for each column of the $w_{j,i}$. However, since the $\partial F_j / \partial \alpha_i$ matrix describes the explicit dependence F on each of the reaction parameters α_i, each of its columns must be formed prior to solving for a column of $w_{j,i}$.

In addition to determining time-integrated sensitivity of solution variables to reaction rate coefficients, derived sensitivity of growth or etch rates to the reaction parameters can also be calculated. Growth-rate sensitivity analysis for the transient calculations uses the same local-sensitivity calculations described for the steady-state calculations, as described in *Section 16.1*. In this case, the sensitivities are not integrated over time but are instead based only on local conditions at each time-step.

16.3 Normalization of Sensitivity Coefficients

Chemkin further manipulates the raw sensitivity coefficients to make them more useful. First, we compute normalized sensitivity coefficients in the form of logarithmic derivatives, i.e.,

Equation 16-6

$$\left.\frac{\partial \ln Y_k}{\partial \ln \alpha_i}\right|_F = \left.\frac{\alpha_i}{Y_k}\frac{\partial Y_k}{\partial \alpha_i}\right|_F$$

or

Equation 16-7

$$\left.\frac{\partial \ln T}{\partial \ln \alpha_i}\right|_F = \left.\frac{\alpha_i}{T}\frac{\partial T}{\partial \alpha_i}\right|_F$$

Second, although the gas-phase species solution variables are mass fractions, the sensitivity coefficients are computed in terms of mole fractions, as follows:

Equation 16-8

$$\left.\frac{\alpha_i}{X_k}\frac{\partial X_k}{\partial \alpha_i}\right|_F = \left.\frac{\alpha_i}{Y_k}\frac{\partial Y_k}{\partial \alpha_i}\right|_F - \alpha_i \overline{W} \sum_{j=1}^{K_g} \frac{1}{W_j}\left.\frac{\partial Y_k}{\partial \alpha_i}\right|_F$$

where X_k are the gas-phase mole fractions, W_j are the species molecular weights, and $\overline{W}$ is the mean molecular weight of the gas-phase mixture.

Normalized sensitivity coefficients for the surface-site fractions and bulk-phase mole fractions are computed as:

Equation 16-9

$$\left.\frac{\partial \ln Z_k}{\partial \ln \alpha_i}\right|_F = \left.\frac{\alpha_i}{Z_k}\frac{\partial Z_k}{\partial \alpha_i}\right|_F$$

and

Equation 16-10

$$\left.\frac{\partial \ln X_k^b}{\partial \ln \alpha_i}\right|_F = \left.\frac{\alpha_i}{X_k^b}\frac{\partial X_k^b}{\partial \alpha_i}\right|_F$$

where Z_k is the site fraction of surface species k, and X_k^b is the mole fraction of the bulk species k.

In some cases, it can be argued that sensitivity coefficients are more useful when they are normalized by the maximum value of each dependent variable (e.g., the maximum value over the solution time or the maximum value over a spatial profile). For such cases, Chemkin allows the option for users to obtain sensitivity coefficients normalized as:

Equation 16-11

$$\frac{\alpha_i}{X_k^{\max}} \frac{\partial X_k}{\partial \alpha_i}$$

where $X_k^{\max}$ is the maximum mole fraction of the species in the relevant domain. This normalization avoids artificially high sensitivity coefficients in regions where the mole fractions are approaching zero, and thus subject to numerical errors. The implementation of this “maximum” normalization option is performed during post-processing as a “units” option in Chemkin Graphical Post-Processor.

16.4 Sensitivity of Bulk Growth or Etch Rates

In addition to the gas, surface, and bulk species sensitivity coefficients, sensitivity coefficients for the growth (or etch) rates of the bulk phases with respect to the reaction rate coefficient parameters α_i may also be computed where applicable. As the growth rates are derived quantities, the local sensitivity calculation method described in this section is used for both steady-state and for transient simulations.

First, the linear growth rate (units of cm/sec) of the bulk phase n can be expressed by:

Equation 16-12

$$G_{n,m} = \sum_{k=K_b^f(n,m)}^{K_b^l(n,m)} \frac{W_k}{\rho_k} \dot{s}_{k,m}$$

The derivative with respect to the parameters is then,

Equation 16-13

$$\left.\frac{dG_{n,m}}{d\alpha_i}\right|_F = \sum_{k=K_b^f(n,m)}^{K_b^l(n,m)} \frac{W_k}{\rho_k}\left.\frac{d\dot{s}_{k,m}}{d\alpha_i}\right|_F$$

Equation 16-14

$$= \sum_{k=K_b^f(n,m)}^{K_b^l(n,m)} \frac{W_k}{\rho_k}\left[\sum_{l=1}^{J}\left.\frac{\partial\dot{s}_{k,m}}{\partial\phi_l}\right|_{\alpha_i,\,\phi_{p\neq l}}\left.\frac{\partial\phi_l}{\partial\alpha_i}\right|_F + \left.\frac{\partial\dot{s}_{k,m}}{\partial\alpha_i}\right|_{\phi_p}\right]$$

The vector, $\left.(\partial\phi_l/\partial\alpha_i)\right|_F$ is the vector of raw sensitivity coefficients computed by solution of *Equation 16-8*. $\left.(\partial\dot{s}_{k,m}/\partial\phi_l)\right|_{\alpha_i,\,\phi_{p\neq l}}$ is a matrix representing the derivative of the bulk species production rates from surface reaction with respect to the solution variables. W_k and ρ_k are the molecular weight and mass density of the *k*th bulk-phase species, respectively. The normalized growth rate sensitivity coefficients are computed as:

Equation 16-15

$$\left.\frac{\partial \ln G_{n,m}}{\partial \ln \alpha_i}\right|_F = \frac{\alpha_i}{|G_{n,m}|}\left.\frac{\partial G_{n,m}}{\partial\alpha_i}\right|_F$$

Note that, in general, $G_{n,m}$ can be either positive (growth) or negative (etch). Therefore, the absolute value of $G_{n,m}$ on the right-hand-side of *Equation 16-15* is necessary to correctly normalize the sensitivity coefficients.

17

17 Rate-of-production Analysis

Another useful tool in understanding reacting-flow calculations is rate-of-production analysis. Rate-of-production analysis determines the contribution of each reaction to the net production or destruction rates of a species. Rate-of-production analysis is particularly useful for 0-D and plug-flow systems, where the computational expense for the added calculations is small and it is possible to consider data from a large reaction set. For this reason, rate-of-production tables are printed to the diagnostic output file for these types of models (based on user requests), to allow quick identification of dominant reaction paths. For all other reactor models in Chemkin, rate of production data can be obtained through the Graphical Post-Processor. This data option can be selected at the time that the solution file data is being imported into the Post-Processor.

17.1 0-D Homogeneous and Plug-flow Systems

For a 0-D homogeneous system, the molar production of a species per unit volume, P_k, is given by

Equation 17-1

$$P_k = \dot{\omega}_k + \sum_{m=1}^{M} \frac{A_m}{V} \dot{s}_{k,m} = \sum_{i=1}^{I} \upsilon_{ki} q_i + \sum_{m=1}^{M} \frac{A_m}{V} \sum_{i=1}^{I_s} \upsilon_{ki}^s q_i^s$$

where υ_{ki} and υ_{ki}^s are the stoichiometric coefficients for the gas and surface reactions, respectively, and q_i and q_i^s are the rate of progress of the I gas-phase reactions and the I_s surface reactions. The contribution to the rate of production of species k from gas-phase reaction i is therefore

Equation 17-2

$$C_{ki} = \upsilon_{ki} q_i$$

and for a surface reaction,

Equation 17-3

$$C^s_{ki} = \frac{A_m}{V} \upsilon^s_{ki} q^s_i$$

where A_m is the surface area of the material m with which the reaction i is associated. Further details about how the reactions contribute to net species production rates are found in *Chapter 3* and *Chapter 4*. The reactor model computes normalized values of the reaction contributions to the species production and destruction rates. The normalized production-contributions for gas-phase reactions are given by:

Equation 17-4

$$\overline{C}^p_{ki} = \frac{\max(\upsilon_{ki}, 0) q_i}{\sum_{i=1}^{I} \max(\upsilon_{ki}, 0) q_i + \sum_{m=1}^{M} \frac{A_m}{V} \sum_{i=1}^{I^s} \max(\upsilon^s_{ki}, 0) q^s_i}$$

and the normalized destruction values for the gas-phase reactions is given by:

Equation 17-5

$$\overline{C}^d_{ki} = \frac{\min(\upsilon_{ki}, 0) q_i}{\sum_{i=1}^{I} \min(\upsilon_{ki}, 0) q_i + \sum_{m=1}^{M} \frac{A_m}{V} \sum_{i=1}^{I^s} \min(\upsilon^s_{ki}, 0) q^s_i}$$

The normalized production values for the surface reactions are given by:

Equation 17-6

$$\overline{C}^p_{ki^s} = \frac{\frac{A_m}{V} \max(\upsilon^s_{ki}, 0) q^s_i}{\sum_{i=1}^{I} \max(\upsilon_{ki}, 0) q_i + \sum_{m=1}^{M} \frac{A_m}{V} \sum_{i=1}^{I^s} \max(\upsilon^s_{ki}, 0) q^s_i}$$

and the normalized destruction values for surface reactions are given by:

Equation 17-7

$$\overline{C}^{d}_{ki^s} = \frac{\frac{A_m}{V}\min(\upsilon^s_{ki}, 0)q^s_i}{\sum_{i=1}^{I}\min(\upsilon_{ki}, 0)q_i + \sum_{m=1}^{M}\frac{A_m}{V}\sum_{i=1}^{I^s}\min(\upsilon^s_{ki}, 0)q^s_i}$$

Thus, the normalized contributions to production and destruction sum to one, as follows:

Equation 17-8

$$\sum_{i=1}^{I}\overline{C}^{p}_{ki} + \sum_{i=1}^{I^s}\overline{C}^{p}_{ki^s} = 1$$

and

Equation 17-9

$$\sum_{i=1}^{I}\overline{C}^{d}_{ki} + \sum_{i=1}^{I^s}\overline{C}^{d}_{ki^s} = 1$$

In transient simulations, when rate-of-production analysis is requested, the above calculations are performed at every time step.

18

18 Particle Size-Distribution Tracking

Within several of the Chemkin reactor models, there is an option to use the Particle Tracking feature. This option allows inclusion of dispersed, condensed-phase material in the form of particles, in conjunction with the gas-phase reactor models. The Particle Tracking feature accounts for particle formation and destruction, and can be used to determine global properties about the amount of particulates in the system as well as information about size-distribution function.

To describe some of the theory behind the Particle Tracking feature, we first need to define particles in this context. Like gaseous species, each type of particle corresponds to a symbolic representation in the chemistry set and has properties associated with it. To form particles from the gas-phase, one or more nucleation events need to be defined to identify the particle properties at inception. Chemical composition and thermodynamic properties of the particle are defined in this way. The definition of the particle and its properties are described in *Chapter 6: Description and Properties of Particles [CHEMKIN-PRO Only]* in the *ANSYS Chemkin Input Manual*.

The nucleation “reaction” is used to define how the particle (or nucleus) is created from gas phase species. The nucleation reaction is an irreversible reaction that provides the particle inception rate and defines the size and the surface coverage of the nucleus. After the nuclei are formed, they start to interact with each other as well as with the gas mixture around them. While particle-particle interactions such as coagulation are non-chemical processes, interactions between particles and the surrounding gas mixture can result in chemical processes taking place on the particle surface. These surface processes might result in mass growth or reduction of the particle or might just simply recondition the particle surface. To include the effects from all these surface processes, a surface mechanism is needed to describe all surface reactions and associated surface species on the particle. The Particle Tracking feature then determines the impact of individual surface reactions on the particle sizes from the expression of the surface reactions

The sections below describe the concept and theory behind the Particle Tracking computations along with implementation and numerical solution considerations. Examples are available in the *ANSYS Chemkin Tutorials Manual* to illustrate how required information is entered and how the Particle Tracking option is enabled for different Chemkin reactor models.

There are two options for tracking particle size-distribution information within the Particle Tracking module. One is the Moment Method, which uses less computational resources but provides only statistical information about the size distribution. The second option is the Sectional Method, which typically takes more compute time, but directly outputs size-distribution function. *Section 18.1* below describes the Moment Method, while *Section 18.2* describes the Sectional Method. *Section 18.3* draws on many of the same definitions provided in *Section 18.1*.

18.1 Description and Properties of a Particle Population

18.1.1 Moments of Particle-Size Distribution Functions

The application of the method of moments to soot-particle formation was first reported by Frenklach and coworkers.[111,112,113] This method describes the average properties of a particle population. The method of moments tracks the evolution of an aerosol system by moments of its particle-size distribution function. The use of moments rather than the actual form of the particle-size distribution function overlooks variations among individual particles in the aerosol system. Also, the actual particle-size distribution function cannot be derived from its moments unless an assumption is made regarding the form of the distribution function. Since in many practical applications only the average properties of the aerosol system are sought, the history and properties of individual particles may not be important such that this approximation can still be quite useful. The loss in details of the particle-size distribution function due to the use of method of moments is compensated by computational speed with which the moments are calculated, which reduces the demand for computing resources. Detailed descriptions of the method of moments are reported elsewhere by Frenklach et al.[111,112,113].

111. M. Frenklach and H. Wang, in *Soot Formation in Combustion: Mechanisms and Models*, H. Bockhorn (Ed.), Springer-Verlag, pp. 165-192 (1994).
112. J. Appel, H. Bockhorn, and M. Frenklach, *Combust. and Flame*, **121**:122-136 (2000).
113. M. Frenklach and S.J. Harris, *J. of Colloid and Interface Sci.*, **118**:252-261 (1987).

Without making any assumptions about the form of the particle-size distribution function, the method of moments can provide overall properties of a particle system such as number density, total particle volume fraction, total particle surface area density, and average particle size. To express these overall properties in terms of particle-size moments, we first define the particle-size moments.

Given a particle-size distribution function $n(j)$, where $0 \le j < \infty$ represents a measure of particle size, e.g., particle mass or particle diameter, the *r*-th moment of this particle-size distribution function is defined in *Equation 18-1*.

Equation 18-1

$$M_r = \int_0^\infty j^r \times n(j) \times dj \quad r = 0, 1, 2, \ldots$$

The Particle Tracking module uses particle class, which is defined as the number of bulk species molecules in a particle core, as the measure of particle size. Both particle mass, and particle volume, are proportional to particle class. Because particle classes are discrete numbers, the number of class j particles can be represented by a discrete function N_j and *Equation 18-1* is equivalent to *Equation 18-2*.

Equation 18-2

$$M_r = \sum_{j=0}^{\infty} j^r \times N_j$$

In the following sections, the summation notation of *Equation 18-2* will be used in formulation expressions and derivations.

18.1.2 Total Particle Number of a Particle Population

From *Equation 18-1* we see that the zero-th moment is the total particle number of the particle population, as shown in *Equation 18-3*.

Equation 18-3

$$N_\Sigma = M_0 = \int_0^\infty n(j) \times dj = \sum_{j=0}^{\infty} N_j$$

18.1.3 Total and Average Particle Mass

Since the mass of a particle is proportional to its class, the total mass of a particle population can be calculated as:

$$m_{p,\Sigma} = \sum_{j=0}^{\infty} (j \times m_0) \times N_j$$

Note that m_0 is the mass of a bulk species molecule comprising the particle core and is constant. The total mass of a particle population can be expressed in a simple form as *Equation 18-4*.

Equation 18-4

$$m_{p,\mathbf{\Sigma}} = m_0 \times M_1$$

Here,

$$M_1 = \sum_{j=0}^{\infty} j^1 \times N_j$$

is the first moment of the discrete particle-size distribution function N_j. The average particle mass of the population can be obtained by dividing the total particle mass by the number of particles and is given in *Equation 18-5*,

Equation 18-5

$$\bar{m}_p = \frac{m_{p,\Sigma}}{N_\Sigma} = m_0 \times \frac{M_1}{M_0} = m_0 \times \bar{j}$$

where $\bar{j}$ is the average particle class of the population.

18.1.4 Total and Average Geometric Properties of a Particle Population

Similarly, the total particle volume is found to be

Equation 18-6

$$V_{p,\mathbf{\Sigma}} = \frac{m_0}{\boldsymbol{\rho}_B} M_1$$

where $\rho_{\boldsymbol{B}}$ [g/cm^3] is the bulk density of the particle core. By assuming that the particles are spherical, an average particle diameter can be obtained as

Equation 18-7

$$\bar{d}_p = \frac{1}{N_\Sigma} \sum_{j=0}^{\infty} d_0 \times j^{1/3} \times N_j = d_0 \times \frac{M_{1/3}}{M_0}$$

The total sphere-equivalent surface area of a particle population is given as

Equation 18-8

$$A_{s,\Sigma} = \sum_{j=0}^{\infty} A_{s,0} \times j^{2/3} \times N_j = A_{s,0} \times M_{2/3}$$

With these equations, all basic properties of a particle population are defined for the moment method. In *Section 18.4* through *Section 18.7*, we introduce the kinetics models used by the Particle Tracking feature to describe formation, growth, reduction, and interaction of the particles.

18.2 Sectional Model for Tracking Particle-Size Distribution

As described in the previous section, the method of moments can be used as one option in the Particle Tracking feature to determine statistics of the particle-size distribution. The method of moment calculates total particle number density and volume fraction. Average properties of distribution such as average particle diameter can be estimated. Although the method of moments has advantages over other methods in terms of computational efficiency, one limitation it has is that only statistics of the size distribution are predicted, rather than the size distribution itself. This becomes an issue when trying to quantitatively compare predictions of the shape of the distribution against experimental data, especially when the size distribution form is complex. Such quantitative predictions can be important in understanding and formulating particle-gas kinetics mechanisms.

To address this issue, an alternative approach is available with the Particle Tracking module for a subset of the Chemkin models that can use the moment method. The sectional model approach provides more direct prediction of the size-distribution shape. It is available for the Chemkin Closed 0-D and Open 0-D reactors models (without plasma), Plug-flow, the Pre-mixed Burner-stabilized Stagnation Flame model, Premixed Burner-stabilized Flame, Premixed Laminar Flame Speed Calculator, and Opposed-flow Diffusion Flame model. For the sectional-model approach, the number density is computed as a function of different “bins” that are defined for different particle sizes. The disadvantage of this approach is that it requires relatively more computational resources, due to the need to add one equation per bin that would be considered. In this way, the more resolved the distribution is, the more computationally expensive the calculation.

18.2.1 Sectional Model Details

Sectional models divide the particle-size domain into a finite number of sections.The particle size-distribution, i.e., number density of particles, within a section can then approximated by some function, such as delta, piecewise polynomial, etc. In principle, particles of various sizes (can) reside in a given section. The complexity and the overall cost of a sectional method are influenced by the choice of approximation for in-section size-distribution. The resulting formulation is referred to as a discretized population balance. The sectional models thus avoid excessive computational requirements of the discrete model and also avoid oversimplification imposed by the moment models.

The classical population balance equation for the discrete spectrum is called the Smoluchowski equation[114]. Using this equation, the net rate of generation of particles of size k (N_k) is written as:

Equation 18-9

$$\frac{dN_k}{dt} = \frac{1}{2}\sum_{i+j=k}\beta(i,j)N_iN_j - N_k\sum_{i=1}^{\infty}\beta(i,j)N_i$$

The first term on the right-hand side is the rate of formation of particles of size k by the collision of particles of size i and j. A factor of ½ is introduced since each collision is counted twice. The second term is the rate of loss of particles of size k by collisions with all other particles. The collision frequency function (β) depends on the physical model employed for coagulation.

Aggregation and coagulation are the internal processes that modify the particle-size distribution of a particulate system. The driving force behind these processes is collision among the particles. While the term *aggregation* is used for non-coalescing collisions, in the case of *coagulation*, it is assumed that the colliding particles coalesce immediately after the collision and a new (spherical) particle is formed. Coagulation can be thought of as starting from an aggregate-particle that eventually forms a fully coalesced particle. Coagulation and aggregation decrease the total number of particles and the total surface area, while increasing the average particle size. For a chemically reacting flow system, the collision frequency function is a function of the sizes of the colliding particles, the flow field, and gas properties such as temperature and pressure, and viscosity.

114. Smoluchowski, M. (1917). *Z. Phys. Chem.* **92**(129).

Except for a very few idealized cases, finding an analytical solution for the Smoluchowski equation is impossible and numerical techniques must be employed. A number of approximate solution techniques have been proposed. These techniques may be broadly classified as either moment models or section models.

Discretized population balance approaches have been developed by quite a few researchers, e.g., Gelbard and Seinfeld[115], Marchal et al.[116], and Landgrebe and Pratsinis[117]. These models vary in their choice of discretization (linear, geometric, etc.), their assumption about the shape of the size distribution in each interval, and their choice of average value of properties for each interval. Hounslow [118] showed that some of these methods gave significant errors in their prediction of either the total volume or the total number of particles. Hounslow et al.[118] and Litster et al.[119], developed a discretized-population-balance (DPB) that ensures correct prediction of the total particle number and volume. They use geometric, adjustable discretization as follows:

Equation 18-10

$$\frac{V_{i+1}}{V_i} = 2^{1/q}, \qquad 2^{i/q} < V_i \le 2^{i+1/q}$$

In the above equation, q is a positive integer and thus the discretization is adjustable, V is the volume/size, and subscript i is the section index. The higher the value of q is, the finer the resolution. Wynn [120] corrected the formulation of Litster et al.[119, p. 285] and the population balance for aggregation is written as

115. Gelbard, F. and J. H. Seinfeld (1980). "Simulation of multicomponent Aerosol Dynamics." *Journal of Colloid Interface Science* **78**(2): 485-501.
116. Marchal, P., R. David, et al. (1988). "Crystallization and Precipitation Engineering I: An effective Method for Solving the Population Balance for Crystallization with Agglomeration." *Chemical Engineering Science* **43**(1): 59-67.
117. Landgrebe, J. D. and S. E. Pratsinis (1990). "A Discrete-Sectional Model for Powder Production by Gas-Phase Chemical Reaction and Aerosol Coagulation in the Free-Molecular Regime." *Journal of Colloid Interface Science* **139**(1): 63-86.
118. Hounslow, M. J., R. L. Ryall, et al. (1988). "A Discretized Population Balance for Nucleation, Growth, and Aggregation." *AICHE Journal* **34**(11): 1821-1832.
119. Litster, J. D., D. J. Smit, et al. (1995). "Adjustable Discretized Population Balance for Growth and Aggregation." *AICHE Journal* **41**(3): 591-603.
120. Wynn, E., J. W. (1996). "Improved Accuracy and Convergence of Discretized Population Balance of Litster et al." *AICHE Journal* **42**(7): 2084-2086.

Equation 18-11

$$\frac{dN_i}{dt} = \sum_{j=1}^{i-S_1} \beta_{i-1,j} N_{i-1} N_j \frac{2^{(j-i+1)/q}}{2^{1/q}-1} + \sum_{p=2}^{q} \sum_{j=i-S_{p-1}}^{i-S_p} \beta_{i-p,j} N_{i-p} N_j \frac{2^{(j-i+1)/q} - 1 + 2^{-(p-1)/q}}{2^{1/q}-1}$$

$$+ \frac{1}{2} \beta_{i-q,i-q} N_{i-q}^2 + \sum_{p=1}^{q-1} \sum_{j=i+1-S_{p+1}}^{i+1-S_p} \beta_{i-p,j} N_{i-p} N_j \frac{-2^{(j-i)/q} + 2^{1/q} - 2^{-p/q}}{2^{1/q}-1}$$

$$- \sum_{j=1}^{i-S_1+1} \beta_{i,j} N_i N_j \frac{2^{(j-i)/q}}{2^{1/q}-1} - \sum_{j=i-S_1+2}^{\infty} \beta_{i,j} N_i N_j$$

The above equation guarantees number density and volume (mass) conservation. To capture nucleation, the corresponding rate term is simply added to the appropriate section. Hounslow also proposed a discretization for the growth term that correctly predicts the zeroth, first, and second moment.

Kumar and Ramkrishna[121] proposed a general discretization technique to preserve any two properties (for example, mass and number density) of particle-size distribution. In addition, they more rigorously tackled numerical issues related to growth rate in addition to nucleation and aggregation. They also formulated techniques such as moving pivots and selective refinement. The discretization (without growth) is written as:

121. Kumar, S. and D. Ramkrishna (1996). "On the solution of population balance equations by discretization-- III. Nucleation, growth and aggregation of particles." *Chem. Eng. Sci.* **52**(24): 4659-4679.

Equation 18-12

$$\frac{dN_i}{dt} = \sum_{X_{i-1} \le (X_j + X_k) \le X_i}^{i \ge j \ge k} \eta \left(1 - \frac{\delta_{jk}}{2}\right) \beta_{i,j} N_j N_k - N_i \sum_{k=1}^{M} \beta_{i,k} N_i N_k + \int_{V_i}^{V_{i+1}} S(v) dv$$

Equation 18-13

$$V = X_j + X_k$$

Equation 18-14

$$\eta = \frac{V^\theta X_{i+1}^\psi - V^\psi X_{i+1}^\theta}{X_i^\theta X_{i+1}^\psi - X_i^\psi X_{i+1}^\theta}; X_i \le V \le X_{i+1}$$

Equation 18-15

$$\eta = \frac{V^\theta X_{i-1}^\psi - V^\psi X_{i-1}^\theta}{X_i^\theta X_{i-1}^\psi - X_i^\psi X_{i-1}^\theta}; X_{i-1} \le V \le X_i$$

In *equations 18-13* through *18-15*, X_i indicates the pivot size within the size range V_i to V_{i+1}, δ_{jk} is the Kronecker delta function, $S(v)$ is the function representing nucleation, and θ and ψ are the powers of any two power-law properties of the PSD that are conserved. (For example, 0 and 1 for number density and volume (mass)). For the cases when the size distribution within a section is far from being uniform, it is possible to consider the pivot $X_i = X_i(t)$. The rate of movement of the pivot is proportional to the growth rate.

In ANSYS Chemkin, the fixed pivot technique by Kumar and Ramkrishna[121, p. 286] is used considering its computational efficiency. It can be noted that, using this technique, only the particles of certain “representative” size are thought to exist in the system.

18.2.2 Creation/Selection of Sections

Figure 18-1 shows a screen capture of the relevant input panel related to creation of sections as it appears in the ANSYS Chemkin User Interface. As shown in *Figure 18-1*, the sections are based on the number of monomers (and therefore volume) in a particle and spaced in a geometric series defined by the spacing factor. Note that the term *monomer* is used here instead of *atom*. This is done so that it includes cases where the basic unit of particles to be modeled is a molecule, for example, titania (TiO_2).

Figure 18-1 Dispersed Phase panel to input parameters for sections.

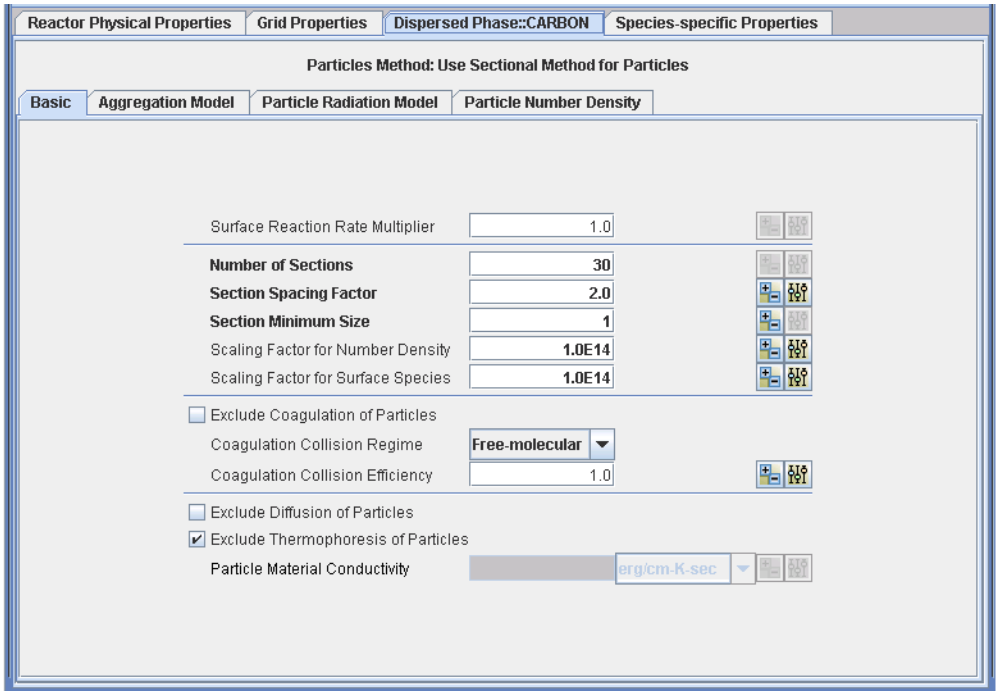

To consider a concrete example, as shown in *Figure 18-1*, the first section corresponds to particles with 1 monomer as given in the section minimum size (on the input panel). With a spacing factor of 2, the second section's representative particle has 2 monomers, whereas the third section's representative particle has 4 monomers, and so on. The section minimum size allows omission of sections with representative particles having fewer than a certain number of monomers. This can be useful, for example, when there is no particle depletion so that the minimum number of monomers in a particle is always greater than or equal to the monomers in a nucleation reaction.

If a spacing factor of less than 2 is used, some of the initial sections will have representative particles that cannot exist. For example, if the spacing factor in the previous example is 1.414, then the second section's representative particle has 1.414 monomers in it and such a particle cannot physically exist. The solution of sectional model equations will return zero or a computationally negligible number for such sections as there will be no processes contributing to number density change in such sections. Note that although such spacing factors give sections corresponding to non-physical particles, it can be useful to resolve number density in larger size ranges.

It should be noted that the actual unknown that is solved for is the number density of the representative-size particles. The post-processor also gives dN/dLog$D$ distribution as the experimental data is typically in this form. When writing this output it is assumed that the section volume boundaries are mid-way between the representative values. For the first and the last section, it is assumed that the representative volume is located mid-way between the bounding volumes. Thus, if there are 4 sections with representative volumes of 1, 2, 4, and 8 then the volume boundaries will be 0.5, 1.5, 3, 6, and 10. Since the actual number density data is available to the user, any other procedure could be used to compute dN/dLog$D$. Since the logarithm of diameter appears in the denominator, the partitioning used does not have a big influence.

18.2.2.1 Validation of the Sectional Model in the Particle Tracking Facility

A test matrix was applied to validate each component of the sectional model. Presented below are the results of two such tests.

18.2.2.2 Sample Results

As mentioned earlier, only a handful of analytical solutions of the population-balance equation are available. For the case of an aggregation-only problem with a size-independent coagulation kernel with exponential initial distribution, the number density function is given as:

Equation 18-16

$$n(V,\tau) = \frac{4N_0}{V_0(\tau+2)^2} Exp\left(-\frac{2V}{V_0(\tau+2)}\right)$$

Equation 18-17

$$\tau = N_0 \beta_0 t$$

In the simulation results reported, the values of N_0 and B_8 are set to 1000 and 0.05, respectively. The minimum volume of the first section is set to V_0/100 and the volume (size) spacing follows $V_{i+1} = 2*V_i$. The numerical solution computed using Equations 18-12 to 18-15 is plotted along with the analytical solution in *Figure 18-2* and *Figure 18-3*. It can be seen in these figures that agreement is excellent.

Shown in *Figure 18-4* are the results of simultaneous nucleation and agglomeration. The nucleation is assumed to happen in the first section and its rate is set to 1000*Exp(-t). The collision frequency is size-independent and is set to unity. At small values of t, the particle size distribution (PSD) is dominated by the nucleation. At moderate values of t a bimodal distribution is obtained. Although not shown in the figure, a similar PSD will evolve as in *Figure 18-2* when the nucleation rate becomes vanishingly small and only agglomeration takes place.

These results demonstrate that the initial implementation of the sectional model is working as expected for the Plug-Flow model. Future versions of the model will be extended to include the effects of growth and oxidation from surface chemistry.

Figure 18-2 Comparison of analytical and numerical solutions for exponential distribution. (Aggregation only, N_0 = 1000, B_0 = 0.05, plotted on linear scale for Y-axis).

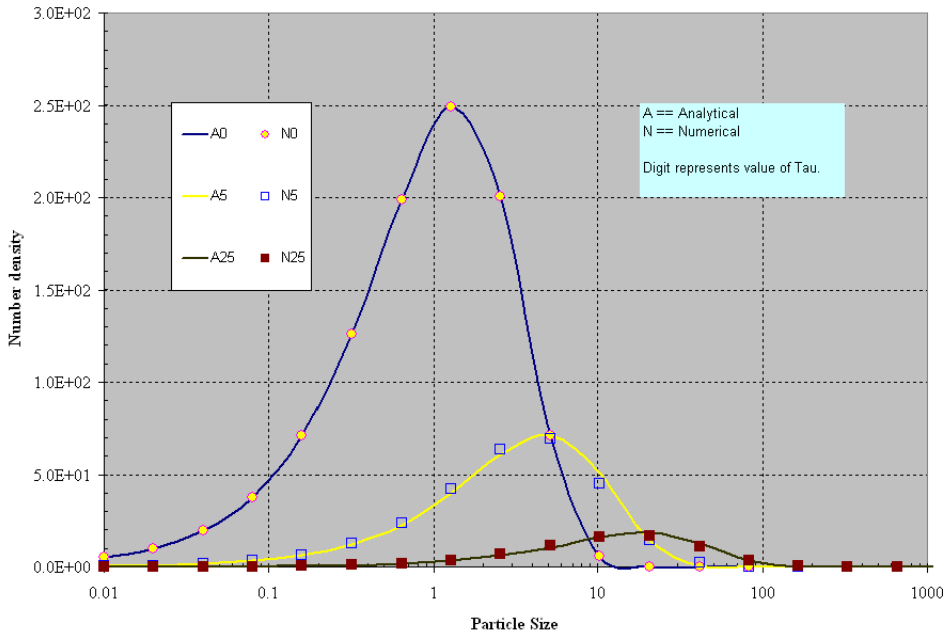

Figure 18-3 Comparison of analytical and numerical solutions for exponential distribution. (Aggregation only, N_0 = 1000, B_0 = 0.05, plotted on logarithmic scale for Y-axis).

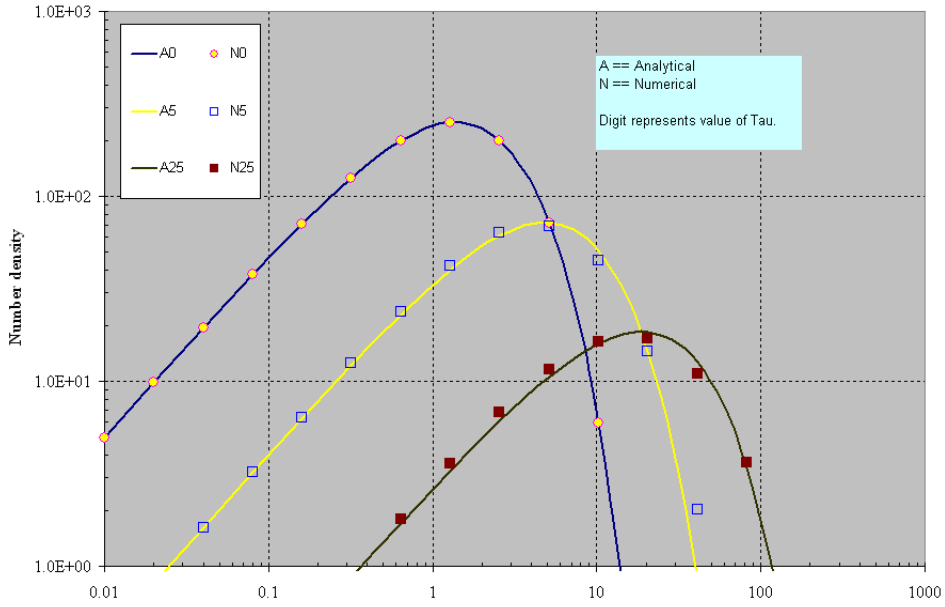

Figure 18-4 Evolution of particle-size distribution for simultaneous nucleation and aggregation.

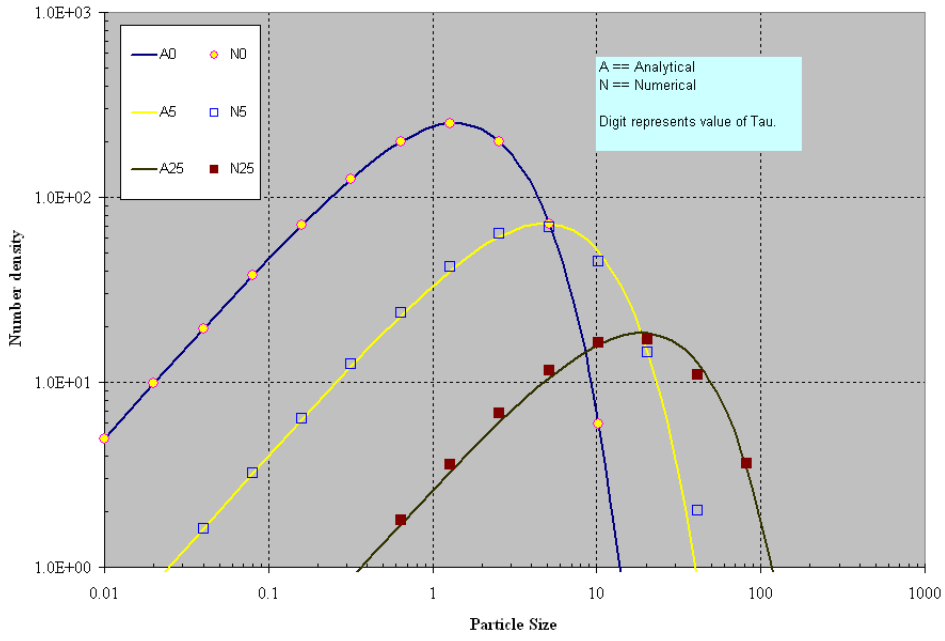

18.3 Particle Inception

Nucleation is the process of forming new condensed-phase particles from a continuous phase, such as gas and vapor. The Particle Tracking feature only considers particles generated via homogeneous nucleation (or self-nucleation); that is, no foreign nucleus is involved in the nucleation process. This constraint is important since we assume that the particle core is made up entirely of one chemical compound, i.e., the bulk species. Note that creation of particles by multiple nucleation reations is allowed.

18.3.1 Nucleation Reaction Description

Particle inception is modeled by a nucleation reaction. A nucleation reaction is a special type of surface reaction detailing the formation and the properties of the new particles. It is irreversible and all reactants must be gas phase species. These gas phase reactants are the precursors; they can be different gas species, i.e., hetero-molecular nucleation, or the same gas species, i.e., homo-molecular nucleation. Because new surface area is created when new particles are formed, the nucleation reaction need not conserve surface sites.

The use of a reaction form to represent particle inception has several advantages. Because the reaction data of the nucleation process are presented in text format, they are easy to comprehend and to transfer. The gas phase precursors from which the new particles are created can be easily identified in the reaction. The chemical composition of the particle core is defined by the bulk product of nucleation reaction, and the particle class of the nuclei is given by the stoichiometric coefficient of the bulk product. The initial coverage on the new particle surface, i.e., species/atoms that bond to the particle core, is indicated by the ratio of the stoichiometric coefficients of surface species products. Moreover, since the nucleation reaction is given as part of the surface reaction mechanism, conservation of element and mass is checked by the interpreter.

18.3.2 Nucleation Reaction Data

To make certain that all information needed to model particle inception is properly presented by the reaction data, certain rules and syntax for the nucleation reaction must be followed.

Figure 18-5 Syntax for nucleation reaction

```
<gas_reactants> -> jnuc<core_bulk>+<surface_products>+<gas_products>A_nucB_nucE_nuc
                NUCL
```

Rules:

1. Auxiliary keyword NUCL must be used to denote a nucleation reaction.
2. The reaction must be irreversible. Any possible reverse reaction must be presented as a separate reaction.
3. Only gas-phase species can appear on the reactant side.
4. There must be one and only one bulk species on the product side. This bulk species represents the composition of the particle core.
5. The particle class of the new particle created by the nucleation reaction is given by the stoichiometric coefficient of the bulk species product, i.e., j_{nuc}.
6. At least one surface species product has to be specified so surface coverage of the new particle can be properly initialized.
7. The gas phase product is optional and its purpose is to balance the reaction.
8. A_{nuc}, B_{nuc}, and E_{nuc} are the Arrhenius rate coefficients. As part of the surface mechanism, their format and default units must be compatible with the defaults or those specified for the reaction in the SURFACE KINETICS input file.
9. More than one nucleation reaction is allowed for one dispersed material. These must describe the formation of the same bulk species.

Units:

Rate of progress and species production rates of nucleation reactions are given in [mole/cm^3-sec].

Example:

The nucleation reaction below describes the formation of particles from gas species $C_{16}H_{10}$:

Figure 18-6 Formation of particles from gas species $C_{16}H_{10}$

```
2 C16H10 => 32 C(B) + 20 H(SE) + 28.72 OPEN(SE)9.0E+090.50.0
     NUCL
```

The new particle core consists of 32 C(B) molecules. About 40% of the new particle surface is initially covered by surface species H(S) and the rest of the surface is covered by another surface species, OPEN(S), which in this case are open sites. No gas-phase product is generated by this nucleation process.

18.3.3 Site Density and Surface Species on Nuclei

The Particle Tracking feature introduces two new concepts to Chemkin's SURFACE KINETICS options: particle surface site density and initial surface coverage. Surface site density Γ is the number of active chemical sites per surface area where adsorption, desorption, and chemical reaction can take place. The value of surface site density is specified in the site data section of the surface mechanism. Besides the site density, surface species that can exist on the particle surface site must be declared in the site data section. These surface species are defined as either elements or fractions of molecular structure, from the precursors, that are neither made into the particle core nor released into the gas phase. More information about syntax and rules regarding site data is provided in *Section 4.2* of the *ANSYS Chemkin Input Manual*.

The following example declares a surface site named "EDGE" on the dispersed (or particle) material "SOOT". The site density of "EDGE" is given as 3.341 x 10^{-9} [mole/cm^2]. Two surface species H(SE) and OPEN(SE) are declared on site "EDGE". According to the thermodynamic data, H(SE) represents a surface-bonded hydrogen atom and OPEN(SE) is an open (or empty) surface site.

Figure 18-7 Declaration of surface site on dispersed material

```
MATERIAL SOOT
! declare dispersed material
DISPERSED
END
! declare name, site density, and surface species
SITE/EDGE/    SDEN/3.341E-9/
   H(SE)
   OPEN(SE) /NATIVE/
END
! declare bulk species that comprises the particle core
BULK/GRAPHITE/ C(B) /1.8/
END
! thermodynamic data for surface and bulk species
THERMO
OPEN(SE)          102903C   0               I  0300.00   5000.00  1000.00      1
 0.14901664E+01 0.16621256E-02-0.06687204E-05 0.12908796E-09-0.09205334E-13    2
-0.07074018E+04-0.08717785E+02-0.06705661E+01 0.07181499E-01-0.05632921E-04    3
 0.02142298E-07-0.04168562E-11-0.07339498E+03 0.02601595E+02                   4
H(SE)             121286C   0H   1          I  0300.00   5000.00  1000.00      1
 0.14901664E+01 0.16621256E-02-0.06687204E-05 0.12908796E-09-0.09205334E-13    2
-0.07074018E+04-0.08717785E+02-0.06705661E+01 0.07181499E-01-0.05632921E-04    3
 0.02142298E-07-0.04168562E-11-0.07339498E+03 0.02601595E+02                   4
C(B)              121286C   1               S  0300.00   5000.00  1000.00      1
 0.14901664E+01 0.16621256E-02-0.06687204E-05 0.12908796E-09-0.09205334E-13    2
-0.07074018E+04-0.08717785E+02-0.06705661E+01 0.07181499E-01-0.05632921E-04    3
 0.02142298E-07-0.04168562E-11-0.07339498E+03 0.02601595E+02                   4
!
END
REACTIONS
!
!   nucleation
!
2A4 => 32C(B) + 20 H(SE) + 28.72 OPEN(SE)        9.0E+09   0.5     0.0
    NUCL
!
END
```

18.3.4 Determination of Stoichiometric Coefficients

When a new particle is created, its surface can be covered by elements or fractional structures from the precursors. The initial surface coverage of new particles is given by the stoichiometric coefficients of surface species products in the nucleation reaction. Determination of the initial surface coverage (or stoichiometric coefficients) is somewhat arbitrary. For example, the initial coverage of new soot particles can be obtained from the hydrogen-to-carbon ratio observed in experiments. However, because nucleation reactions have to conserve surface sites on particles and elements, the values of stoichiometric coefficients are subjected to some limitations. In this section, a pseudo nucleation reaction is used as an example to illustrate how these limitations can be derived from conservation laws.

Consider a pseudo nucleation reaction:

$$C_{x1}H_{y1}+C_{x2}H_{y2} => \upsilon_{C(B)}C(B)+ \upsilon_{C(S)}C(S)+ \upsilon_{H(S)}H(S)+ \upsilon_{(S)}(S)+ \upsilon_{H}H+ \upsilon_{CH}CH$$

The particle core is represented by the only bulk species product C(B), which is a single carbon atom. The inception particle class is equal to the stoichiometric coefficient of C(B), $\upsilon_{C(B)}$. C(S) and H(S) are respectively elementary carbon and hydrogen on the particle surface. (S) denotes an empty surface site. Both H and CH are gas phase products from the nucleation process.

Conservation of element C sets the relation among stoichiometric coefficients of carbon-containing products

Equation 18-18

$$\upsilon_{C(B)} + \upsilon_{C(S)} + \upsilon_{CH} = x1 + x2$$

Similarly, the relationship of stoichiometric coefficients of H-containing products can be obtained by conserving the element H

Equation 18-19

$$\upsilon_{H(S)} + \upsilon_{H} + \upsilon_{CH} = y1 + y2$$

The connection between stoichiometric coefficients of the nucleation reaction and site density of the dispersed material is established via the conservation of surface sites on new particles. Because all particles created by this nucleation reaction are exactly the same, they have the same particle class $j_{\text{nuc}} = \upsilon_{C(B)}$, thus the same surface area, $A_{s,\text{nuc}} = A_{s,0} \times \upsilon_{C(B)}^{2/3}$. Accordingly, if the nucleation rate is r_{nuc} [mole/cm^3-sec], the production rate of new surface area can be calculated as

Equation 18-20

$$\frac{dA_s}{dt} = r_{nuc} \times N_{avo} \times A_{s,0} \times \upsilon_{C(B)}^{2/3} \qquad [\mathrm{cm}^2/\mathrm{cm}^3\text{-sec}]$$

Because the site density on the particle surface is Γ [mole/cm^2], the production rate of new surface sites where new surface species can be accommodated is given by

Equation 18-21

$$\frac{d\Gamma}{dt} = \Gamma \times \frac{dA_s}{dt} = \Gamma \times r_{nuc} \times N_{avo} \times A_{s,0} \times \upsilon_{C(B)}^{2/3} \qquad [\mathrm{mole}/\mathrm{cm}^3\text{-sec}]$$

On the other hand, the production rate of all new surface species on the particles is

Equation 18-22

$$\sum_{ks} \dot{s}_{ks} = r_{nuc} \times \left(\upsilon_{C(S)} + \upsilon_{H(S)} + \upsilon_{(S)} \right) \qquad [\mathrm{mole/cm}^3\text{-sec}]$$

Since each surface site has to be occupied by a surface species, production rate of new surface sites must match that of all surface species, that is,

$$\frac{d\Gamma}{dt} = \sum_{ks} \dot{s}_{ks}$$

or

Equation 18-23

$$\upsilon_{C(S)} + \upsilon_{H(S)} + \upsilon_{(S)} = \Gamma \times N_{avo} \times A_{s,0} \times \upsilon_{C(B)}^{2/3}$$

Equations *18-25*, *18-26* and *18-30* serve as general constraints on the stoichiometric coefficients in the nucleation reaction. Note that there are 6 stoichiometric coefficients but there are only 3 constraints. This means, given the same set of precursors, the nucleation reaction can have more than one set of products that can satisfy the conservation of elements and surface sites. The final form of the nucleation reaction will be determined by additional information such as size and hydrogen-carbon ratio of the new particles and gas phase products detected in experiments.

For the pseudo nucleation reaction under consideration, assume that all carbon atoms in the precursors become the particle core, that is,

$$j_{nuc} = \upsilon_{C(B)} = x1 + x2$$

and

$$\upsilon_{C(S)} = \upsilon_{CH} = 0$$

Consequently, *Equation 18-19* and *Equation 18-23* are reduced to

Equation 18-24

$$\upsilon_{H(S)} + \upsilon_H = y1 + y2$$

and

Equation 18-25

$$\upsilon_{H(S)} + \upsilon_{(S)} = \Gamma \times N_{avo} \times A_{s,0} \times \upsilon_{C(B)}^{2/3}$$

Furthermore, if the hydrogen-to-carbon ratio R_{H-C} of the new particle is known, the stoichiometric coefficients can be obtained as

Equation 18-26

$$\upsilon_{H(S)} = R_{H-C} \times \upsilon_{C(B)}$$

Equation 18-27

$$\upsilon_H = (y1 + y2) - \upsilon_{H(S)} = (y1 + y2) - R_{H-C} \times \upsilon_{C(B)}$$

and

Equation 18-28

$$\upsilon_{(S)} = \Gamma \times N_{avo} \times A_{s,0} \times \upsilon_{C(B)}^{2/3} - R_{H-C} \times \upsilon_{C(B)}$$

Since both must be non-negative, a constraint on the particle hydrogen-to-carbon ratio is obtained

Equation 18-29

$$R_{H-C} \le \min\left[\frac{y1 + y2}{\upsilon_{C(B)}}, \Gamma \times N_{avo} \times A_{s,0} \times \upsilon_{C(B)}^{-1/3}\right]$$

When

$$R_{H-C} \times \upsilon_{C(B)} \le \left(\Gamma \times N_{avo} \times A_{s,0} \times \upsilon_{C(B)}^{2/3}\right) \le (y1 + y2)$$

gas phase H species is generated from the nucleation reaction. If, on the other hand,

$$R_{H-C} \times \upsilon_{C(B)} \le (y1 + y2) \le \left(\Gamma \times N_{avo} \times A_{s,0} \times \upsilon_{C(B)}^{2/3}\right)$$

some surface sites on the new particles will be open. However, the determination of $\upsilon_{(S)}$ also depends on the availability of surface site density Γ data. If a reliable value of Γ is known, the stoichiometric coefficient of open surface site `(S)` is computed from *Equation 18-28*. Alternatively, if $\upsilon_{H(S)}$ and υ_S values are better known, Γ can be derived from

Equation 18-30

$$\Gamma = \frac{\upsilon_{H(S)} + \upsilon_{(S)}}{N_{avo} \times A_{s,0} \times \upsilon_{C(B)}^{2/3}}$$

If $R_{H-C} \times \upsilon_{C(B)} < (\Gamma \times N_{avo} \times A_{s,0} \times \upsilon^{2/3}{}_{C(B)}) < (y1 + y2)$ and data are known, the final form of the pseudo nucleation becomes

$C_{x1}H_{y1}+C_{x2}H_{y2}$ =>

(x1+x2) C(B)
+(R_{H-C}*(x1+x2)) H(S)
+ (G*N_{avo}*$A_{s,0}$*u$^{2/3}{}_{C(B)}$-R_{H-C}*(x1+x2))(S)
+((y1+y2)-R_{H-C}*(x1+x2)) H

18.3.5 Native Surface Sites

The C(S) sites in the preceding section are commonly considered as “open sites” in many nucleation reactions. These are essentially empty sites on the particle surface at which other surface species can reside. For example, consider the following reaction:

2A4 => 32C(B) + *x*Open(S) + 20H(S)

A4 is the pyerene molecule, containing 10 hydrogen (H) atoms and 16 carbon (C) atoms. The above reaction says that all 20 H atoms reside as surface species on the nucleated particle, which contains 32 C atoms. The number of open/empty sites, denoted by *x* in the above reaction, must satisfy the surface site balance (*Equation 18-30*). This number is usually a floating-point number so its consistent calculation (to the precision of computer arithmetic) is essential for site conservation. When such a site is flagged as a “native” site, then Chemkin automatically calculates the value of *x*. You can specify the native site by using the `/NATIVE/` tag in the surface-chemistry input. If no `NATIVE` tag is included, then the first surface species listed for the dispersed-phase material will be assumed to be the native site.

The native surface species is used not only in a nucleation reaction but also when the net surface area of the particle increases. For example, consider the following surface reaction:

Open(S) + C2H2 => H(S) + 2C(B) + H

In this reaction, acetylene (C_2H_2) finds an open site on the particle surface and deposits 2 carbon atoms on the particle. One H atom is also added to the surface while one open site is consumed. The addition of bulk species, however, also creates new surface area and therefore new open sites. While the reaction has the correct

element balance and sets one open site covered by one surface H atom, the reaction does not specify the number of new open sites formed due to new surface area. This number is internally computed by Chemkin. Note that the number of new open sites generated is dependent on the class of the particle on which this reaction happens. For example, suppose the above reaction happens on a particle of class j. After the reaction is completed, the new particle is of class (j+2). Since the particles are considered to be spherical, the surface areas of these two particles are $A_j = A_0 * j^{2/3}$ and $A_{j+2} = A_0 * (j+2)^{2/3}$, respectively. Correspondingly, the total number of surface species before and after reaction are $A_j * \Gamma$ and $A_{j+2} * \Gamma$, where Γ is the surface site density. Since the reaction correctly accounts for the open site occupied by H(S), the total number of new open sites formed is $(A_{j+2} - A_j) * \Gamma$.

Particle surface area is destroyed when particles coagulate and when surface reactions etch particles. When particle area is destroyed, it means that fewer surface sites remain after the reaction. However, it may not necessarily mean that only native sites are destroyed. Therefore, during the net production rate calculation, Chemkin first computes the net rate of surface area generation by all surface reactions and coagulation. If this rate is positive then the rate of generation of native species is computed, as described in the previous paragraph. When the net area generation rate is negative, the rate of generation (which also will be negative) of all surface species (including the native) is considered to be proportional to the activity of each species. In other words, when new area is formed, new native species are formed and when area is destroyed all surface species are destroyed in correct proportion. Note that the destroyed surface species can be considered to be trapped or buried in the bulk and thus lost from the system.

18.3.6 Nucleation Rates

The nucleation rate is expressed in the Arrhenius form as given in *Equation 18-31*,

Equation 18-31

$$r_{nuc} = A_{nuc} \times T^{B_{nuc}} \times e^{-E_{nuc}/RT} \times \prod_k [\chi_k]^{\upsilon_k}$$

where χ_k and υ_k are the chemical symbols for the k-th gas reactant and the stoichiometric coefficient of the k-th gas reactant in the nucleation reaction, respectively.

Because the nucleation process affects only the number density of class j_{nuc} particle, the change of the number density of each discrete particle class “bin” in the size distribution, can be expressed as

Equation 18-32

$$\frac{dN_{j_{nuc}}}{dt} = r_{nuc} \times N_{avo}$$

and

Equation 18-33

$$\frac{dN_j}{dt} = 0 \qquad j = 0,1,2,\ldots; j \neq j_{nuc}$$

18.3.6.1 Implementation for Method of Moments

Using the definition of particle size moments given by *Equation 18-2*, the change in size moment M_r due to nucleation can be obtained as

Equation 19

$$\begin{aligned} R_r &= \frac{d}{dt}\left(\sum_{j=0}^{\infty} j^r N_j\right) \\ &= \sum_{j=0}^{\infty} j^r \times \frac{dN_j}{dt} = j_{nuc}^r \times \frac{dN_{j,nuc}}{dt} \\ &= r_{nuc} \times N_{avo} \times j_{nuc}^r \qquad\qquad r = 0,1,2,\ldots \end{aligned}$$

18.3.6.2 Implementation for Section Method

Depending on the sections specified by the user, this size may or may not coincide with the representative size. The nucleated particle is then split into the adjacent sections such that total number density and mass are conserved. For example, consider the input as in *Figure 18-1* on page 288. If the nucleation reaction creates a particle with 20 monomers in it, then that particle is split as (20-32)/(16-32) = 0.75 particles in the 5th section that has a representative particle with 16 monomers, and 0.25 particles in the 6th section that has representative a particle with 32 monomers. The total particle number density and mass are thus conserved.

18.3.6.3 A General Guideline for the Nucleation Rate Parameters

In the case of soot nucleation, the soot particles are assumed to be formed by coalescence of two poly-aromatic hydrocarbon (PAH) precursors. Therefore, the nucleation rate is equal to the collision rate of the two precursors. In the free-molecular regime, the PAH collision rate takes the form

Equation 18-1

$$r_{coll}^{PAH} = r_{nuc} \times N_{avo} = \frac{1}{2}\sum_{i=1}^{\infty}\sum_{j=1}^{\infty}\beta_{i,j}^{PAH} N_i^{PAH} N_j^{PAH}$$

The free-molecule collision frequency is given as

Equation 18-2

$$\beta_{i,j}^{PAH} = \beta \times \sqrt{\frac{8\pi\kappa_B}{\mu_{i,j}}} \times \sqrt{T} \times \left(\frac{d_i^{PAH}}{2} + \frac{d_j^{PAH}}{2}\right)^2$$

where β is the collision efficiency and $\mu_{i,j}$ is the reduced mass of the collision pair.

If the two precursors are the same PAH species, i.e., $i = j = j_{\mathrm{PAH}}$ and $d_i^{\mathrm{PAH}} = d_j^{\mathrm{PAH}} = d_{\mathrm{PAH}}$, the collision rate becomes

Equation 18-3

$$r_{coll}^{PAH} = r_{nuc} \times N_{avo} = \beta \times \sqrt{\frac{4\pi\kappa_B}{j_{PAH} \times m_0}} \times \sqrt{T} \times d_{PAH}^2 \times \left([PAH] \times N_{avo}\right)^2$$

Consequently, the nucleation rate can be expressed as

Equation 18-4

$$r_{nuc} = \beta \times \sqrt{\frac{4\pi\kappa_B}{j_{PAH} \times m_0}} \times N_{avo} \times d_{PAH}^2 \times T^{1/2} \times [PAH]^2$$

The Arrhenius rate parameters of the nucleation rate can be obtained by comparing *Equation 18-4* against the Arrhenius form:

Equation 18-5

$$A_{nuc} = \beta \times \sqrt{\frac{4\pi\kappa_B}{j_{PAH} \times m_0}} \times N_{avo} \times d_{PAH}^2$$

Equation 18-6

$$B_{nuc} = 1/2$$

Equation 18-7

$$E_{nuc} = 0$$

18.4 Particle Coagulation

The constant interaction among particles in an aerosol system can affect the particle distribution. Agglomeration is the process in which particles collide with one another and adhere to form larger particles. As mentioned in *Section 18.2.2*, we use the term *aggregation* when two particles collide and stick to each other and the term

coagulation when, after forming an aggregate, the particles fuse completely to form a spherical particle. This is described in more detail in *Section 18.8*. In the current discussion, the term coagulation is used as a generic term in the sense of agglomeration.

The Particle Tracking feature considers only the thermal coagulation of the particles or coagulation due to Brownian motion. Since coagulation simply re-distributes the particle size population, it does not affect the total particle mass of the aerosol system.

ANSYS Chemkin uses the frequency or kernel of collision (beta) based on the Knudsen number (Kn) regime of particles, which is defined as $\mathrm{Kn_j} = 2\lambda/\mathrm{D_j}$ where λ is the mean free path of the surrounding gas and $\mathrm{D_j}$ is the diameter of the particle. ANSYS Chemkin offers three choices to the user: free-molecular ($\mathrm{Kn_j} >> 1$), continuum ($\mathrm{Kn_j} << 1$), and transition ($\mathrm{Kn_j} \approx 1$). The first two have relatively simple expressions and are written as

Equation 18-8

$$\beta_{i,j}^{FM} = \sqrt{\frac{\pi K_B T}{2\rho_p}} \sqrt{\frac{1}{V_i} + \frac{1}{V_j}} \left(D_i + D_j\right)^2$$

Equation 18-9

$$\beta_{i,j}^{CN} = \frac{2K_B}{3} \frac{\left(D_i + D_j\right)^2}{D_i D_j} \frac{T}{\eta}$$

An interpolating polynomial that is supposed to be valid in the entire Knudsen number regime, ranging from continuum to free molecular, can be used for the transition regime. It is written as

Equation 18-10

$$\beta_{i,j}^{TR} = 2\pi\left(\delta_{ij}\right)\left(D_{ij}\right)\left(\frac{D_{ij}}{D_{ij} + 2H_{ij}} + 8\frac{\delta_{ij}}{C_{ij} D_{ij}}\right)^{-1}$$

Various terms appearing in the above equations are given below:

$$D_{ij} = D_i + D_j$$

$$H_{ij} = \sqrt{H_i^2 + H_j^2}$$

$$C_{ij} = \sqrt{C_i^2 + C_j^2}$$

$$C_i = \sqrt{\frac{8K_B T}{\pi m_i}}$$

$$\delta_{ij} = \delta_i + \delta_j$$

$$\delta_i = \frac{K_B T}{3\pi\mu D_i} F(\alpha_i)$$

$$\alpha_i = \frac{2\lambda}{D_i}$$

$$\lambda = \frac{\mu}{\rho}\sqrt{\frac{\pi\bar{M}}{2K_B T N_{av}}}$$

$$F(\alpha) = \frac{5 + 4\alpha + 6\alpha^2 + 18\alpha^3}{5 - \alpha + (8+\pi)\alpha^2}$$

$$H_i = \frac{\left(D_i + \xi_i\right)^3 - \left(D_i^2 + \xi_i^2\right)^{3/2}}{3D_i\xi_i} - D_i$$

Equation 18-11

$$\xi_i = \frac{8\delta_i}{\pi C_i}$$

In the equations *Equation 18-8* through *Equation 18-11*, K_B is the Boltzmann constant, D is particle (collision) diameter, V is particle volume, ρ_P is particle material's bulk density, and N_{av} the Avogadro's number along with T, η, ρ, $\overline{M}$ indicating temperature, viscosity, density, and molecular mass of the surrounding gas, respectively. C_j is the mean speed, δ_j is the diffusivity, F is the slip correction factor, α_j is the Knudsen number, and λ is the mean free path of the surrounding gas.

It can be seen that although equation *Equation 18-10* is most general, it is also complicated and hence computationally expensive. Moreover, its form is too involved for effective use with the method of moments. Therefore, for the method of moments ANSYS Chemkin uses the harmonic mean of the two limiting values and employs equation *Equation 18-10* for the sectional method. For typical systems modeled using ANSYS Chemkin, the particles for which the collision kernel in the free-molecular regime is applicable are less than 200 nm in sphere-equivalent diameter.

18.4.1 Implementation for Method of Moments

Assuming spherical particles, equation *Equation 18-8* can be written as

Equation 18-12

$$\beta_{i,j}^{coag,\,free} = C^{coag} \times \sqrt{\frac{i+j}{i \times j}} \left(i^{1/3} + j^{1/3} \right)^2$$

where

Equation 18-13

$$C^{coag} = \beta \sqrt{\frac{6\kappa_B T}{\rho_B}} \left(\frac{3m_0}{4\pi\rho_B} \right)^{1/6}$$

and κ_B is the Boltzmann constant.

Following Method II proposed by Frenklach and Harris[113], the coagulation effect on the *r*-th size moment is defined as

Equation 18-14

$$G_r^f = \frac{1}{2} M_0^2 \sum_{l=0}^{r-1} \binom{r}{l} \sum_{i=1}^{\infty} \sum_{j=1}^{\infty} \beta_{i,j}^{coag,\,free} \frac{i^{r-l} N_i^{soot} j^l N_j^{soot}}{M_0^2}$$

$$= \frac{1}{2} C^{coag} M_0^2 \sum_{l=0}^{r-1} \binom{r}{l} \sum_{i=1}^{\infty} \sum_{j=1}^{\infty} b_{i,j,r,l} \frac{N_i^{soot} N_j^{soot}}{M_0^2} \qquad r > 1$$

where

Equation 18-15

$$b_{i,j,r,l} = \sqrt{\frac{i+j}{i \times j}} \left(i^{1/3} + j^{1/3} \right)^2 i^{r-l} j^l = (i+j)^{1/2} \frac{\left(i^{1/3} + j^{1/3} \right)^2}{\sqrt{i \times j}} i^{r-l} j^l$$

Or, by lumping all the terms inside the summation, the coagulation terms for the *r*-th moment can be rewritten as

Equation 18-16

$$G_r^f = \frac{1}{2} C^{coag} M_0^2 \sum_{l=0}^{r-1} \binom{r}{l} \left\langle {}^{1/2} f_{r,r-l} \right\rangle$$

where

Equation 18-17

$$\left\langle {}^{r}f_{x,y}\right\rangle = \sum_{i=1}^{\infty}\sum_{j=1}^{\infty}(i+j)^{r}\frac{\left(i^{1/3}+j^{1/3}\right)^{2}}{\sqrt{i\times j}}i^{x}j^{y}\frac{N_{i}N_{j}}{M_{0}^{2}} \qquad r=0,1,2,\ldots$$

Note that by definition the function $\langle {}^{r}f_{x,y}\rangle$ is symmetric, i.e., $\langle {}^{r}f_{x,y}\rangle = \langle {}^{r}f_{y,x}\rangle$. The summations in $\langle {}^{r}f_{x,y}\rangle$ can be resolved in terms of the particle size moments, whole and fractional, positive and negative as

Equation 18-18

$$\begin{aligned}
\left\langle {}^{r}f_{x,y}\right\rangle &= \sum_{i=1}^{\infty}\sum_{j=1}^{\infty}(i+j)^{r}\frac{\left(i^{1/3}+j^{1/3}\right)^{2}}{\sqrt{i\times j}}i^{x}j^{y}\frac{N_{i}N_{j}}{M_{0}^{2}}\\
&= \sum_{i=1}^{\infty}\sum_{j=1}^{\infty}(i+j)^{r}\left(i^{2/3}+2\times i^{1/3}\times j^{1/3}+j^{2/3}\right)i^{x-1/2}j^{y-1/2}\frac{N_{i}N_{j}}{M_{0}^{2}}\\
&= \sum_{i=1}^{\infty}\sum_{j=1}^{\infty}(i+j)^{r}\left(i^{x+1/6}j^{y-1/2}+2i^{x-1/6}j^{y-1/6}+i^{x-1/2}j^{y+1/6}\right)\frac{N_{i}N_{j}}{M_{0}^{2}}\\
&= \sum_{i=1}^{\infty}\sum_{j=1}^{\infty}\sum_{l=0}^{r-1}\binom{r}{l}i^{r-l}j^{l}\left(i^{x+1/6}j^{y-1/2}+2i^{x-1/6}j^{y-1/6}+i^{x-1/2}j^{y+1/6}\right)\frac{N_{i}N_{j}}{M_{0}^{2}}\\
&= \sum_{i=1}^{\infty}\sum_{j=1}^{\infty}\sum_{l=0}^{r-1}\binom{r}{l}\left(i^{r-l+x+1/6}j^{l+y-1/2}+2i^{r-l+x-1/6}j^{l+y-1/6}+i^{r-l+x-1/2}j^{l+y+1/6}\right)\frac{N_{i}N_{j}}{M_{0}^{2}}\\
&= \sum_{l=0}^{r-1}\binom{r}{l}\left(\mu_{r-l+x+1/6}\mu_{l+y-1/2}+2\mu_{r-l+x-1/6}\mu_{l+y-1/6}+\mu_{r-l+x-1/2}\mu_{l+y+1/6}\right)
\end{aligned}$$

where

Equation 18-19

$$\mu_{r}=\frac{M_{r}}{M_{0}}$$

The whole-order positive moments are obtained by solving their own transport equations, that is, the equations of size moments. The fractional-order positive moments are determined by logarithmic interpolation between the whole positive moments, i.e.,

$$\mu_{p} = L_{p}(\mu_{0}\equiv 1, \mu_{1}, \mu_{2}, \mu_{3}, \mu_{4}, \mu_{5}) \qquad \text{for } p<0.$$

The fractional-order negative moments, on the other hand, are computed by logarithmic extrapolation from the whole positive moments

$$\mu_p = L_p(\mu_0 \equiv 1, \mu_1, \mu_2) \qquad \text{for } p < 0.$$

Derivation and evaluation of G_r^f and $\langle {}^r f_{x,y} \rangle$ are described in detail in references[112,113]. The final forms of the free-molecular coagulation source terms for the equations of moments are

Equation 18-20

$$G_0^f = \frac{-1}{2} C^{coag} \left\langle {}^{1/2} f_{0,0} \right\rangle M_0^2$$

$$G_1^f = 0$$

Equation 18-21

$$G_2^f = C^{coag} \left\langle {}^{1/2} f_{1,1} \right\rangle M_0^2$$

$\ldots,$

and

Equation 18-22

$$G_r^f = \frac{1}{2} C^{coag} M_0^2 \sum_{k=1}^{r-1} \binom{r}{k} \left\langle {}^{1/2} f_{k,r-k} \right\rangle$$

With an assumption of a spherical particle, the collision kernel for the continuum regime as given by *Equation 18-9* on page 302 can be written in terms of particle class i and j. Additionally, while retaining the Cunningham slip correction factor[122], the following expression is written.

Equation 18-23

$$\beta_{i,j}^{coag,cont} = \left(\frac{2\kappa_B T}{3\eta} \right) \left(\frac{C_i}{i^{1/3}} + \frac{C_j}{j^{1/3}} \right) \left(i^{1/3} + j^{1/3} \right)$$

The slip correction factor is written as $C_i = C_j = 1 \mathrel{+}= Kn$. The source terms for the moments equations for collisions in the continuum regime then become

122. A. Kazakov and M. Frenklach, *Combust. And Flame*, **114**:484-501 (1998).

Equation 18-24

$$G_r^c = \frac{1}{2}\sum_{k=1}^{r-1}\binom{r}{k}\left(\frac{2\kappa_B T}{3\eta}\right)\left(\frac{C_k k^{1/3}(r-k)^{1/3} + C_k(r-k)^{2/3} + C_{r-k}k^{2/3} + C_{r-k}k^{1/3}(r-k)^{1/3}}{k^{1/3}(r-k)^{1/3}}\right)$$

$$k^k (r-k)^{r-k} N_k N_{r-k}$$

$$= \frac{1}{2}\left(\frac{2\kappa_B T}{3\eta}\right)\sum_{k=1}^{r-1}\binom{r}{k}\left(C_k + C_{r-k} + C_k k^{-1/3}(r-k)^{1/3} + C_{r-k}k^{1/3}(r-k)^{-1/3}\right)$$

$$k^k (r-k)^{r-k} N_k N_{r-k}$$

$$= \frac{1}{2}\left(\frac{2\kappa_B T}{3\eta}\right)\sum_{k=1}^{r-1}\binom{r}{k}\left\{2 + k^{-1/3}(r-k)^{1/3} + k^{1/3}(r-k)^{-1/3} + \right.$$

$$1.257\times 2\lambda\left(\frac{\pi\rho_B}{6m_0}\right)^{1/3}\left(k^{-1/3} + (r-k)^{-1/3} + k^{-2/3}(r-k)^{1/3} + k^{1/3}(r-k)^{-2/3}\right)$$

$$\left. k^k (r-k)^{r-k} N_k N_{r-k}\right\}$$

$$= \frac{1}{2}\left(\frac{2\kappa_B T}{3\eta}\right)\sum_{k=1}^{r-1}\binom{r}{k}\left\{2M_k M_{r-k} + M_{k-1/3}M_{r-k+1/3} + M_{k+1/3}M_{r-k-1/3} + \right.$$

$$\left. 2.514\lambda\left(\frac{\pi\rho_B}{6m_0}\right)^{1/3}\left(M_{k-1/3}M_{r-k} + M_k M_{r-k-1/3} + M_{k-2/3}M_{r-k+1/3} + M_{k+1/3}M_{r-k-2/3}\right)\right\}$$

Details of the derivation of coagulation source terms in the continuum regime can be found in the paper by Kazakov and Frenklach[122].

As mentioned earlier, the collision frequency in the transition regime is approximated by the harmonic mean of the two limiting values[123].

Equation 18-25

$$\frac{1}{G_r^t} = \frac{1}{G_r^f} + \frac{1}{G_r^c} \qquad r = 0, 2, 3, \cdots$$

Note that G_1 is always zero. That is, the total number of bulk species molecules in particles (or total particle mass) is not affected by coagulation although the total number of particles decreases.

123. J.A. Marr, PhD. Thesis, Dept. of Chemical Engineering, MIT (1993).

18.4.2 Implementation for Section Method

For the sectional method the coagulation rate expression is simply that given by *Equation 18-13* through *Equation 18-16*. The collision kernels as given by equation *Equation 18-8*, *Equation 18-9*, and *Equation 18-10* are directly used by ANSYS Chemkin, with sizes i and j corresponding to representative particles for the sections under consideration.

18.4.3 Validation of Coagulation Model

The free-molecular coagulation model has been validated against one of the examples given by Frenklach and Harris[113].

Consider a population of soot particles in a closed batch reactor. Initially the particles have the same size, i.e., are mono-dispersed, and the number density of the particles is 10^{12} cm^{-1}. The pressure and temperature of the reactor are kept constant at 1 atm and 1500 K, respectively. The bulk species comprising the soot particle is carbon atom (m_0 = 3.18 x 10^{-21} g) and the bulk density of the particle core, ρ_B, is 1.8 g/cm^3.

The simulations were performed with Chemkin's homogeneous, closed reactor with Particle Tracking Feature. The chosen gas-phase mechanism and thermodynamic data are from Appel et al.[112] and the surface chemistry is created by Chou et al. of Reaction Design.

The time profiles of particle number density and average particle diameter squared predicted by Chemkin using Particle Tracking are plotted in *Figure 18-8* together with the ones computed and published by Frenklach and Harris[113]. Good agreements between the two models validate the coagulation model implementation.

Figure 18-8 Evolutions of number density, ND, and ensemble average of diameter squared from the method of moments by Frenklach and Harris[113] (solid lines) and from Chemkin with Particle Tracking (dashed lines).

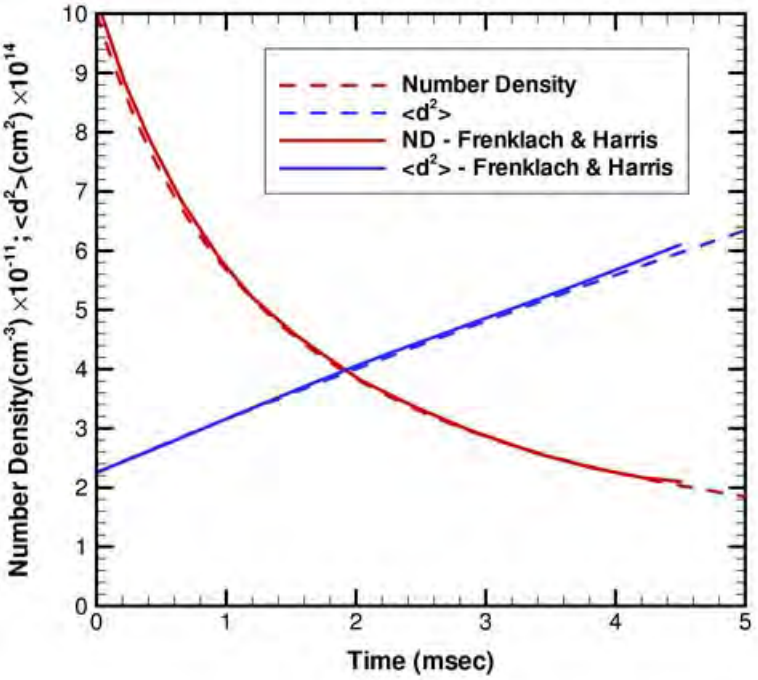

18.5 Chemical Processes on Particle Surfaces

Since particles are in a condensed phase, interactions between particles and a surrounding gas mixture must take place on the particle surface. These particle-gas interactions include adsorption of gas species onto the particle surface, desorption of surface species into the gas, growth of the particle by deposition of bulk species, consumption of the particle by gasification of bulk species, and chemical reactions between surface species. Particle Tracking treats all chemical processes involving particles as surface reactions. This surface chemistry concept reflects the fact that net rates of these particle-gas interactions are proportional to the total active particle surface area. Thus all chemical processes on particle surfaces can be limited by the availability of particle surface area. For example, if there is no particle present in the system, the net rate of particle mass growth by surface reactions is zero. Moreover, Chemkin SURFACE KINETICS has many special formulations, such as sticking coefficients and coverage-dependent activation energy that can provide flexibility in defining the particle-gas processes. Furthermore, since they are incorporated into the surface mechanism, contributions of individual surface processes to particle properties can be determined using standard rate-of-production and sensitivity analyses.

Because there are typically many particles in the system, it is impossible to track the surface condition of individual particles. Particle Tracking instead employs a statistical approach to describe the surface condition of a particle population. The particles are assumed to have the same surface coverage and surface temperature if they are exposed to the same gas mixture locally. When particles from other locations are added, the local surface coverage and surface temperature will change to reflect the new “average” local gas values.

In this section, the connection between particle-gas reactions and particle size distribution (or size moments) is described in detail. In addition, a special surface reaction keyword is introduced. This new keyword allows the size, i.e., diameter, of a gas-phase species to be taken into account when the reaction rate between the gas species and particles is calculated.

18.5.1 Surface Reaction and Particle Size Distribution Function

For a surface reaction to affect the distribution of particle sizes, it must be involved in the production or consumption of the bulk species representing the particle core. A surface reaction can increase the total particle mass if it results in a net gain of the bulk species, and its effect on the particle size distribution function will be to shift the distribution profile to the right (towards the direction of large particle sizes). The surface source terms for the r-th size moment due to the net effect from all surface reactions can be written as

Equation 18-26

$$S_r = \sum_{is=1}^{iisur} S_{r,is} \qquad r = 1, 2, 3, \ldots$$

where $S_{r,\,is}$ represents the contribution of the is-th surface reaction to the r-th moment of the particle size distribution. The units of the source term are [cm^{-3}-sec^{-1}]. Derivations of surface source term for various types of surface reactions are described in the following sections.

18.5.2 Rates of Gas-Particle Reactions

Consider a surface reaction that can represent deposition or condensation of gas species on particle C(B):

Figure 18-9 Surface reaction for deposition/condensation of a gas species

$$\chi + \text{<surface\_reactants>} \rightarrow Dj_{C}\ C(B) + \text{<surface\_products>} + \text{<gas\_products>}$$
$$A_{is} \quad B_{is} \quad E_{is}$$

The rate of this deposition reaction is given in Arrhenius form as

Equation 18-27

$$r_{is} = A_{is} \times T^{B_{is}} \times e^{-E_{is}/RT} \times [\chi] \times \prod [\chi(S)]^{\upsilon_{\chi(S)}} \qquad [\text{mole/cm}^2\text{-sec}]$$

where $\chi(S)$ is the symbol for surface reactants and $\upsilon_{\chi(S)}$ is the stoichiometric coefficient for the surface reactants, and Π implies product over all surface species.

18.5.2.1 Implementation for Method of Moment

In principle, the same reaction rate as given by *Equation 18-27*, above, can also be calculated from the collision rate between the gas species and the particle. Its contribution to the number density of a class *j* particle can be obtained from

Equation 18-28

$$\frac{dN_j}{dt} = \beta_{\chi,i} \times N_\chi \times N_i - \beta_{\chi,j} \times N_\chi \times N_j$$

where $i = j - \Delta j_\chi$. The collision frequency between χ and a class *j* particle is given by

Equation 18-29

$$\beta_{\chi,j} = \beta \times \sqrt{\frac{8\pi\kappa_B}{\mu_{\chi,j}}} \times \sqrt{T} \times \frac{\left(d_\chi + d_j\right)^2}{4} \times \prod \left(\Theta_{\chi(S)}\right)^{\upsilon_{\chi(S)}}$$

where $\Theta_{\chi(S)}$ is the site fraction of surface species $\chi(S)$ and d_χ and d_j are, respectively, the collision diameters of gas species χ and the class *j* particle. By assuming that the particle mass is much greater than that of a gas χ molecule, the reduced mass can be approximated by

Equation 18-30

$$\mu_{\chi,j} = m_\chi = \frac{W_\chi}{N_{avo}}$$

where W_χ is the molar weight of gas species χ.

Hence the collision frequency given by *Equation 18-29* becomes

Equation 18-31

$$\beta_{\chi,j} = \beta \times \sqrt{\frac{\pi \kappa_B}{2m_\chi}} \times \sqrt{T} \times \left(d_\chi + d_j\right)^2 \times \prod \left(\Theta_{\chi(S)}\right)^{v_{\chi(S)}}$$

$$= C_\chi^{surf} \times \sqrt{T} \times \left(d_\chi + d_j\right)^2 \times \Pi_\chi^{surf}$$

With the collision frequency given above, the contribution of χ deposition to the surface-chemistry source term for the *r*-th moment takes the form

$$S_{r,is} = S_{r,\chi} = \sum_{j=0}^{\infty} j^r \times \frac{dN_j}{dt}$$

$$= C_\chi^{surf} \times \sqrt{T} \times \Pi_\chi^{surf} \times \left\{ \sum_{j=0}^{\infty} N_\chi \times j^r \times \left[\left(d_\chi + d_i\right)^2 \times N_i - \left(d_\chi + d_j\right)^2 \times N_j \right] \right\}$$

$$= C_\chi^{surf} \times \Pi_\chi^{surf} \times N_\chi \times \left\{ \sum_{i=0}^{\infty} \left(i + \Delta j_\chi\right)^r \times \left(d_\chi + d_i\right)^2 \times N_i - \sum_{j=0}^{\infty} j^r \times \left(d_\chi + d_j\right)^2 \times N_j \right\}$$

$$= C_\chi^{surf} \times \Pi_\chi^{surf} \times N_\chi \times \left\{ \sum_{i=0}^{\infty} \left(d_\chi + d_i\right)^2 \times \left(1 + \frac{\Delta j_\chi}{i}\right)^r \times i^r \times N_i - \sum_{j=0}^{\infty} \left(d_\chi + d_j\right)^2 \times j^r \times N_j \right\}$$

By assuming $i \gg \Delta j_{is}$, the above equation becomes

Equation 18-32

$$= C_{\chi}^{surf} \times \Pi_{\chi}^{surf} \times N_{\chi} \times \left\{ \sum_{i=0}^{\infty} \sum_{l=0}^{r} \binom{r}{l} \left(d_{\chi} + d_i \right)^2 \times 1^l \times \left(\frac{\Delta j_{\chi}}{i} \right)^{r-l} \times i^r \times N_i \right.$$

$$\left. - \sum_{j=0}^{\infty} \left(d_{\chi} + d_j \right)^2 \times j^r \times N_j \right\}$$

$$= C_{\chi}^{surf} \times \sqrt{T} \times \Pi_{\chi}^{surf} \times N_{\chi} \times$$

$$\left\{ \sum_{i=0}^{\infty} \left[\sum_{l}^{r-1} \binom{r}{l} \left(d_{\chi} + d_i \right)^2 \times \left(\Delta j_{\chi} \right)^{r-l} \times i^l \times N_i - \left(d_{\chi} + d_i \right)^2 \times i^r \times N_i \right] \right.$$

$$\left. - \sum_{j=0}^{\infty} \left(d_{\chi} + d_j \right)^2 \times j^r \times N_j \right\}$$

$$= C_{\chi}^{surf} \times \sqrt{T} \times \Pi_{\chi}^{surf} \times N_{\chi} \times$$

$$\left\{ \sum_{i=0}^{\infty} \sum_{l=0}^{r-1} \binom{r}{l} \left(d_{\chi} + d_i \right)^2 \times \left(\Delta j_{\chi} \right)^{r-l} \times i^l \times N_i - \sum_{i=0}^{\infty} \left(d_{\chi} + d_i \right)^2 \times i^r \times N_i \right.$$

$$\left. - \sum_{j=0}^{\infty} \left(d_{\chi} + d_j \right)^2 \times j^r \times N_j \right\}$$

$$= C_{\chi}^{surf} \times \sqrt{T} \times \Pi_{\chi}^{surf} \times N_{\chi} \times \left\{ \sum_{i=0}^{\infty} \sum_{l=0}^{r-1} \binom{r}{l} \left(d_{\chi} + d_i \right)^2 \times \left(\Delta j_{\chi} \right)^{r-l} \times i^l \times N_i \right\}$$

$$= C_{\chi}^{surf} \times \sqrt{T} \times \Pi_{\chi}^{surf} \times N_{\chi} \times \left\{ \sum_{i=0}^{\infty} \sum_{l=0}^{r-1} \binom{r}{l} \left(d_{\chi}^2 + 2 d_{\chi} d_i + d_i^2 \right) \times \left(\Delta j_{\chi} \right)^{r-l} \times i^r \times N_i \right\}$$

$$= C_{\chi}^{surf} \times \sqrt{T} \times \Pi_{\chi}^{surf} \times N_{\chi} \times \left\{ \sum_{l=0}^{r-1} \binom{r}{l} \left(\Delta j_{\chi} \right)^{r-l} \times \left[d_{\chi}^2 \times \left(\sum_{i=0}^{\infty} i^l \times N_i \right) \right. \right.$$

$$\left. \left. + 2 d_{\chi} d_0 \left(\sum_{i=0}^{\infty} i^{1/3} \times i^l \times N_i \right) + d_0^2 \left(\sum_{i=0}^{\infty} i^{2/3} \times i^l \times N_i \right) \right] \right\}$$

$$= C_{\chi}^{surf} \times \sqrt{T} \times \Pi_{\chi}^{surf} \times N_{\chi} \times$$

$$\left\{ \sum_{l=0}^{r-1} \binom{r}{l} \left(\Delta j_{\chi} \right)^{r-l} \times \left(d_{\chi}^2 \times M_l + 2 d_{\chi} d_0 \times M_{l+1/3} + d_0^2 \times M_{l+2/3} \right) \right\}$$

Equation 18-32 can be rearranged to make a one-to-one mapping between it and the Arrhenius rate expression given by *Equation 18-27* can be made. Since the surface site concentration is related to surface site fraction via:

Equation 18-33

$$[\chi(S)] = \frac{\Gamma \times \Theta_{\chi(S)}}{\sigma_{\chi(S)}}$$

the parameter Π_{χ}^{surf} in *Equation 18-32* can be rewritten as

Equation 18-34

$$\Pi_{\chi}^{surf} = \prod\left(\Theta_{\chi(S)}\right)^{\upsilon_{\chi(S)}} = \frac{\prod\left(\sigma_{\chi(S)} \times [\chi(S)]\right)^{\upsilon_{\chi(S)}}}{\Gamma^{\Sigma\upsilon_{\chi(S)}}} = \frac{\prod\left(\sigma_{\chi(S)}\right)^{\upsilon_{\chi(S)}}}{\Gamma^{\Sigma\upsilon_{\chi(S)}}} \times \prod[\chi(S)]^{\upsilon_{\chi(S)}}$$

$\sigma_{z(s)}$ in the above equations is the site occupancy of surface species $\chi(S)$. The site occupancy of a surface species is assigned when surface species are declared in the mechanism file. A surface species by default has a site occupancy of 1. Definition of surface site occupancy is given in the *ANSYS Chemkin Input Manual*.

By substituting *Equation 18-34* into *Equation 18-32* and by applying the fact that

$$N_{\chi} = [\chi(S)] \times N_{avo}$$

the surface source term due to deposition of gas species χ becomes

Equation 18-35

$$S_{r,is} = \frac{C_{\chi}^{surf}}{\pi} \times \frac{\prod\left(\sigma_{\chi(S)}\right)^{\upsilon_{\chi(S)}}}{\Gamma^{\Sigma\upsilon_{\chi(S)}}} \times N_{avo} \times \sqrt{T} \times [\chi] \times \left(\prod[\chi(S)]^{\upsilon_{\chi(S)}}\right) \times$$
$$\pi \times \left\{\sum_{l=0}^{r-1}\binom{r}{l}\left(\Delta j_{\chi}\right)^{r-l} \times \left(d_{\chi}^2 \times M_l + 2d_{\chi}d_0 \times M_{l+1/3} + d_0^2 \times M_{l+2/3}\right)\right\}$$
$$= r_{is} \times N_{avo} \times$$
$$\pi \times \left\{\sum_{l=0}^{r-1}\binom{r}{l}\left(\Delta j_{\chi}\right)^{r-l} \times \left(d_{\chi}^2 \times M_l + 2d_{\chi}d_0 \times M_{l+1/3} + d_0^2 \times M_{l+2/3}\right)\right\}$$

Hence the Arrhenius rate parameters for the χ deposition reaction can be expressed as

Equation 18-36

$$A_{is} = \frac{\beta}{\pi} \times \sqrt{\frac{\pi\kappa_B}{2m_0}} \times \frac{\prod\left(\sigma_{\chi(S)}\right)^{\upsilon_{\chi(S)}}}{\Gamma^{\Sigma\upsilon_{\chi(S)}}}$$

Equation 18-37

$$B_{is} = 1/2$$

and

Equation 18-38

$$E_{is} = 0$$

It should be noted that *Equation 18-36* through *Equation 18-38* give a guideline for what the reaction rate parameters should be. The actual rate parameters do not have to be these values and can be any general fit. Particle tracking calculates the rate r_{is}

as given by *Equation 18-27* using the specified rate parameters and then computes the source terms for moments from the right-most side of *Equation 18-35*.

18.5.2.2 Implementation for Sectional Method

The sectional method can directly use the reaction rate given by equation *Equation 18-27* to compute the creation and destruction of particles of a certain size. Thus, when a reaction happens on a particle of size k, the corresponding change in number density is calculated as

$$\left.\frac{dN_k}{dt}\right|_{is} = -r_{is} A_k N_k$$

In the above equation, A_k denotes the surface area of a particle of size k. Note that the reaction creates a particles of size j and therefore

$$\left.\frac{dN_j}{dt}\right|_{is} = +r_{is} A_k N_k$$

Three things can be noted about the representation of reaction i:

a. The rate equation applies to particles of “all” sizes.

b. It involves surface composition of the particle under consideration.

c. The etching/oxidation reaction may take out more monomers than the particle of given size holds

In ANSYS Chemkin these are addressed as follows:

1. The particles of size k become the representative particles from section k. As in the case of coagulation, the new particle of size j formed due to the growth/etching reaction may not exactly coincide with the representative particle size from any section. The resulting particle is then split such that two properties of the distribution are conserved as indicated by *Equation 18-13*. CHEMKIN-PRO conserves total particle number density and mass.
2. The surface state of all particles is assumed to be identical. That is, all particles have same surface species coverage. Effectively, ANSYS Chemkin considers the rate-of-progress q_i to be independent of the particle size.
3. When the number of monomers in the particle of a given size are smaller than those etched out by a surface reaction, ANSYS Chemkin proportionately decreases the number density of that size.

18.5.3 Collision Diameter Data for Gas Species

The reaction rate involving a gas species and the particle cloud is proportional to the collision frequency between the gas molecule and the particle surface. When the size of gas molecule is comparable to the particle size, the collision diameter of the gas molecule should be included in the collision frequency calculation. Chemkin permits the collision diameter to be input as part of the reaction data via the DCOL keyword. Syntax and rules of the DCOL keyword are described below.

Figure 18-10 Syntax for DCOL keyword

```
<gas_reactants>+<surface_reactants>   jis<core_bulk>+<products>AisBisEis
         DCOL/diameter_in_cm/
```

Rules:

1. Auxiliary keyword DCOL must be used in conjunction with a surface reaction.
2. The surface reaction must be irreversible. If a reverse reaction is possible, the reverse reaction should be described by a separate irreversible reaction.
3. The surface reaction must have only one gas species on the reactant side. The collision diameter given by the DCOL keyword corresponds to the collision diameter of this gas reactant.
4. There must be at least one surface/bulk species appearing on the reactant side. This is to indicate the particle with which the gas molecules are colliding. The particle is identified by the core bulk species or unique species on its surface.
5. The default value is 0 [cm], which assumes that the size of gas species is much smaller than the particle size.
6. Like regular surface reactions, conservation of surface sites is desirable.

Units:

The reaction rate is given in [mole/cm^2-sec] and the collision diameter is in [cm].

Example:

The surface reaction below describes the deposition of gas species C6H6 on a carbon particle whose core is represented by C(B):

Figure 18-11 Deposition of gas species C6H6 on a particle

```
C6H6 + 4(S) => 6C(B) + 4H(S) + H2          0.1   0.0  0.0
     DCOL/2.41E-8/
     FORD/(S)   2.0/
     STICK
```

The collision diameter for gas species C6H6 is 2.41E-8 [cm]. The parameters given in the reaction line are the sticking coefficient and the reaction rate is second-order with respect to (S) instead of the default fourth-order. Note that, when the sticking coefficient is used to specify the kinetic constant, the $\sqrt{T}$ dependence is embedded in the rate formulation.

18.5.4 Reaction Rate Between Surface Species on Particles

Consider a surface reaction in which all reactants are surface species, such as:

<surface_reactants> $\rightarrow \Delta j_{is}$ <core_bulk> + <products> A_{is} B_{is} E_{is}

This surface reaction will affect the particle size distribution because it increases the particle class, i.e., the number of bulk molecules, by

$$\dot{\omega}_{B,\,is} = r_{is} \times (\Delta j_{is}) \times N_{\text{avo}} \qquad [\text{cm}^{-2}\text{-sec}^{-1}],$$

where $\dot{\omega}_{B,\,is}$ is the production rate of bulk species due to the is-th surface reaction. Also, r_{is} is the rate of progress of the surface reaction in [mole/cm^2-sec] and is evaluated by Chemkin from the Arrhenius coefficients given in the reaction data, i.e.,

Equation 18-39

$$r_{is} = A_{is} \times T^{B_{is}} \times e^{(-E_{is}/RT)} \times \prod [\chi(S)]^{\upsilon_{\chi(S)}}$$

where $\chi(S)$ is the symbol for surface species participating in the surface reaction.

18.5.4.1 Implementation for Method of Moments

As in the case of reactions involving gas and particles, the change of number density of particle class j in the size distribution can be computed as

Equation 18-40

$$\frac{dN_j}{dt} = r_{is} \times N_{avo} \times N_i \times A_{s,i} - r_{is} \times N_{avo} \times N_j \times A_{s,j}$$

in which $i = j - \Delta j_{is}$ and $A_{s,i}$ and $A_{s,i}$ are the surface area for particle class i and j, respectively. Accordingly, the change in the r-th size moment due to this surface reaction is found to be

$$S_{r,is} = \sum_{j=0}^{\infty} j^r \frac{dN_j}{dt}$$
$$= \sum_{j=0}^{\infty} \left[j^r \times r_{is} \times N_{avo} \times \left(N_i \times A_{s,i} - N_j \times A_{s,j} \right) \right]$$
$$= r_{is} \times N_{avo} \times A_{s,0} \times \left\{ \left(\sum_{j=0}^{\infty} j^r \times N_i \times i^{2/3} \right) - \left(\sum_{j=0}^{\infty} j^r \times N_j \times j^{2/3} \right) \right\}$$
$$= r_{is} \times N_{avo} \times A_{s,0} \times \left\{ \left(\sum_{i=0}^{\infty} \left(1 + \frac{\Delta j_{is}}{i} \right)^r \times N_i \times i^{r+2/3} \right) - \left(\sum_{j=0}^{\infty} j^{r+2/3} \times N_j \right) \right\}$$

By assuming $i \gg \Delta j_{is}$, the above equation becomes

Equation 18-41

$$= r_{is} \times N_{avo} \times A_{s,0} \times \left\{ \left(\sum_{i=0}^{\infty} \sum_{i=0}^{r} \binom{r}{l} 1^l \times \left(\frac{\Delta j_{is}}{i} \right)^{r-l} \times N_i \times i^{r+2/3} \right) - M_{r+2/3} \right\}$$
$$= r_{is} \times N_{avo} \times A_{s,0} \times$$
$$\left\{ \left[\sum_{i=0}^{\infty} \sum_{l=0}^{r-1} \binom{r}{l} \left(\Delta j_{is} \right)^{r-l} \times i^{r+2/3-(r-l)} \times N_i \right] + \left(\sum_{i=0}^{\infty} i^{r+2/3} \times N_i \right) - M_{r+2/3} \right\}$$
$$= r_{is} \times N_{avo} \times A_{s,0} \times \left\{ \left[\sum_{i=0}^{\infty} \sum_{l=0}^{r-1} \binom{r}{l} \left(\Delta j_{is} \right)^{r-l} \times i^{l+2/3} \times N_i \right] + M_{r+2/3} - M_{r+2/3} \right\}$$
$$= r_{is} \times N_{avo} \times A_{s,0} \times \left\{ \sum_{l=0}^{r-1} \binom{r}{l} \left(\Delta j_{is} \right)^{r-l} \times \left(\sum_{i=0}^{\infty} i^{l+2/3} \times N_i \right) \right\}$$
$$= r_{is} \times N_{avo} \times A_{s,0} \times \left\{ \sum_{l=0}^{r-1} \binom{r}{l} \left(\Delta j_{is} \right)^{r-l} \times M_{l+2/3} \right\}$$
$$= r_{is} \times N_{avo} \times \pi \times \left\{ \sum_{l=0}^{r-1} \binom{r}{l} \left(\Delta j_{is} \right)^{r-l} \times d_0^2 \times M_{l+2/3} \right\}$$

Note that the surface source term for the r-th moment is proportional to the total particle surface area.

18.5.4.2 Implementation for Sectional Method

The sectional method can directly use the rate expressions for each particle size. Thus, the treatment is identical to that in section *Section 18.5.2.2*.

18.6 Particle Depletion

While the implementation of particle etching/oxidation is relatively straightforward for the sectional method as described in *Section 18.5.2.2*, it needs somewhat special treatment for the method of moments. The particle depletion model included with Particle Tracking is a phenomenological one that mimics the decrease in particle number density and in particle size during reduction (e.g., during soot-particle oxidation). When a particle population undergoes oxidation or gasification, the particles start shrinking in size and the particle population loses mass. Because the particle population covers a wide size range, two different outcomes can be expected for the particles, depending on their sizes. If the particle is large enough, it will primarily decrease in size during the reduction. On the other hand, the smallest particles will disintegrate into gas species as they cannot shrink any further. Of course, in reality, some large-size particles can break down into smaller particles. However, this particle breakdown process is too complicated for our purposes, because it depends on factors related to the structure of the particle and the fluid dynamic forces.

The particle depletion model instead aims to capture the essence of the particle reduction process to the extent possible, given the statistical nature of the problem. The basic concept of the depletion model is that, when the average particle class is above a critical value, the number density of the population remains the same and the particles only undergo size/class reduction. Once the average particle class reaches a minimum value, the smallest particles stop shrinking and begin to disintegrate into gaseous species, i.e., the number density of the particle population decreases.

18.6.1 Particle-Depletion Model Details

During the particle formation phase, surface reactions only affect the size distribution of the particles but not the total number of the particles. However, during the reduction phase, the particle number density has to be decreased when the smallest possible particles (size class = j_{min}) are gasified. The particle-depletion model assumes that the particle-reduction process consists of two distinct steps. When the average particle size is large enough, the size-reduction process will reduce the mean particle diameter first without affecting the particle number density. Once the mean particle class $\dot{j}$ reaches a critical value (size class = j_{crit}), reduction of the total particle number will occur when the smallest particles start disintegrating into gaseous products. Three important model parameters are required in this depletion model: minimum particle class, critical particle class to activate the sink term for the zero-th size moment, i.e., the number density, and the functional form of the sink term. The minimum particle class is assumed to be equal to the smallest inception class of the particle, that is,

Equation 18-42

$$j_{min} = \underset{INUCL}{MIN}\left(j_{nuc}\right)$$

The smallest particles are assumed to begin to disappear when the mean particle size drops below a pre-determined critical size class, j_{crit}. By default, the critical size class is computed by

Equation 18-43

$$j_{crit} = j_{min} + \underset{iisur}{MAX}\left[\Delta j_{is}\right]$$

This parameter can also be specified on the input panel for the Dispersed Material options of the reactor model in the Chemkin Interface. The sink term for the zero-th size moment will be activated when the condition

Equation 18-44

$$\bar{j}_{mean} \le j_{crit}$$

is satisfied. The functional expression of the sink term, S_0, can be easily obtained when the average size class is equal to the minimum size class

Equation 18-45

$$S_0 = \frac{S_1}{j_{min}} = \frac{\sum_{is=1}^{iisur} S_{1,is}}{j_{min}}$$

If the average size class is between j_{crit} and j_{min}, a transition function is needed to describe how S_0, increases from 0 to S_1/j_{min}. For simplicity, a sine function is implemented

Equation 18-46

$$S_0 = \frac{S_1}{j_{min}}\left\{1 - \sin\left[\frac{\pi}{2}\left(\frac{\bar{j} - j_{min}}{j_{crit} - j_{min}}\right)\right]\right\}$$

Other functional forms such as linear and exponential are also possible candidates for the transition function in the particle depletion model. An appropriate functional form can be derived from measurements of particle number density profiles in the particle reduction region.

18.6.2 Soot Burnout Example

The performance of the particle depletion model is demonstrated by an example in which a mono-dispersed soot particle population is oxidized in air inside an isothermal closed perfectly stirred reactor (PSR). The reactor initially contains 30% O2, 70% Ar, and 10” soot particles. The initial particle volume fraction is 10^{-8}. The reactor

temperature is 2500 K and the pressure is maintained at 1 atm. The soot oxidation mechanism, developed by Chou et al.[124], is used here. The minimum particle class is 32 and the critical particle class is set to 142. *Figure 18-12* shows the particle size and number density profiles during soot burnout. Initially, only the particle size is affected by the oxidation process. After the average particle diameter (or size) is reduced to the pre-set minimum level, the number density starts to decrease as further oxidation will cause the soot particle to disintegrate into gas species. Note that particle coagulation is turned off (by setting the collision efficiency to zero) in this example to manifest the effects of soot burnout on particle size and number density. The time profiles of soot volume fraction and gas phase combustion products are given in *Figure 18-13* and *Figure 18-14*, respectively. All soot particles are consumed in 5 msec.

Figure 18-12 Time evolution of soot particle number density and average particle diameter. The particle coagulation is turned off in the simulation to reveal the performance of the particle depletion sub-model.

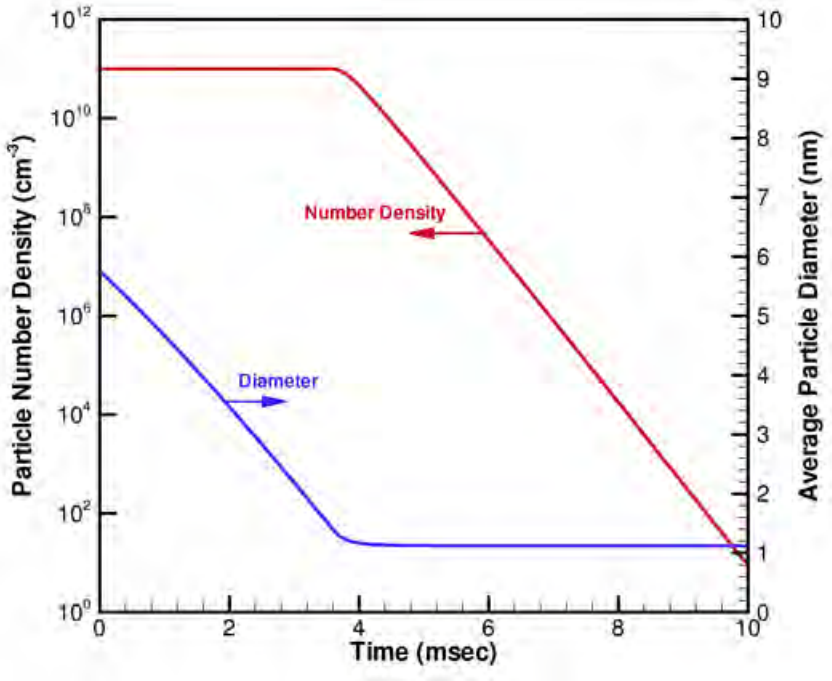

124. C.-P. Chou, P. Ho, and E. Meeks, 30th International Symposium on Combustion, July 25-30, 2004, Work-In-Progress Poster Section, 2F1-22

Figure 18-13 Time evolution of soot volume fraction. Most of the soot mass is consumed in 0.5 msec. The particle coagulation is turned off in the simulation to reveal the performance of the particle depletion sub-model.

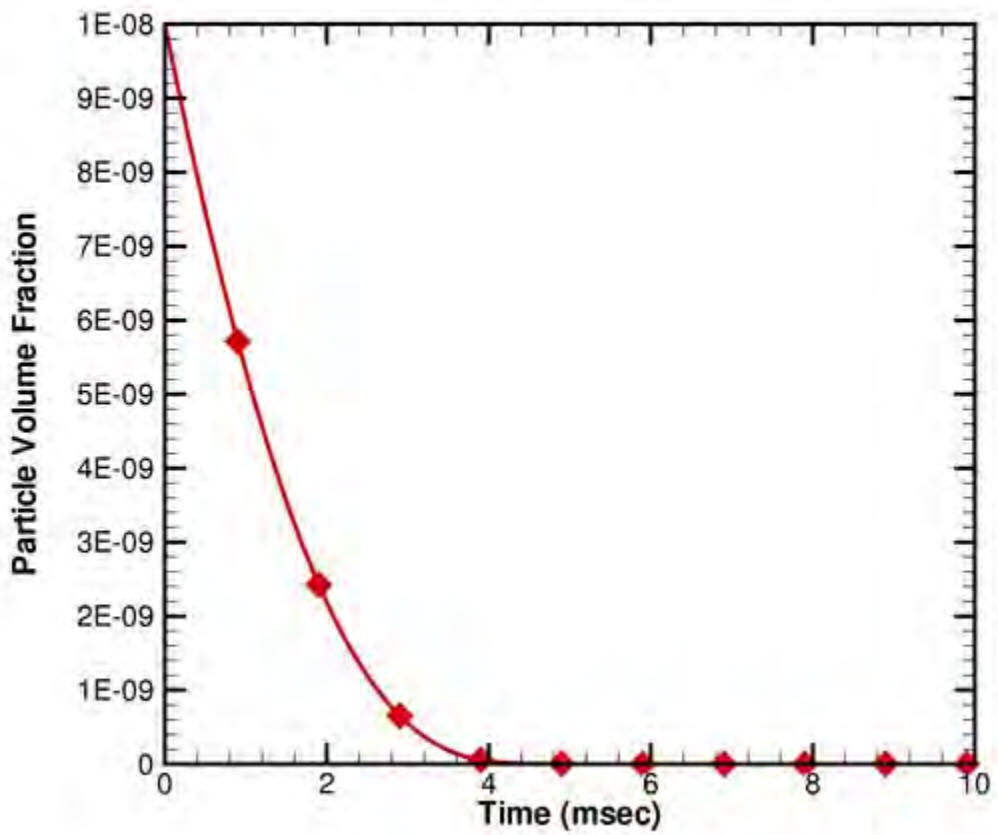

Figure 18-14 Profiles of gas phase products, CO and CO_2, during soot oxidation. The gas mixture inside the PSR is nearly in equilibrium after about 5 msec. The particle coagulation is turned off in the simulation to reveal the performance of the particle depletion sub-model.

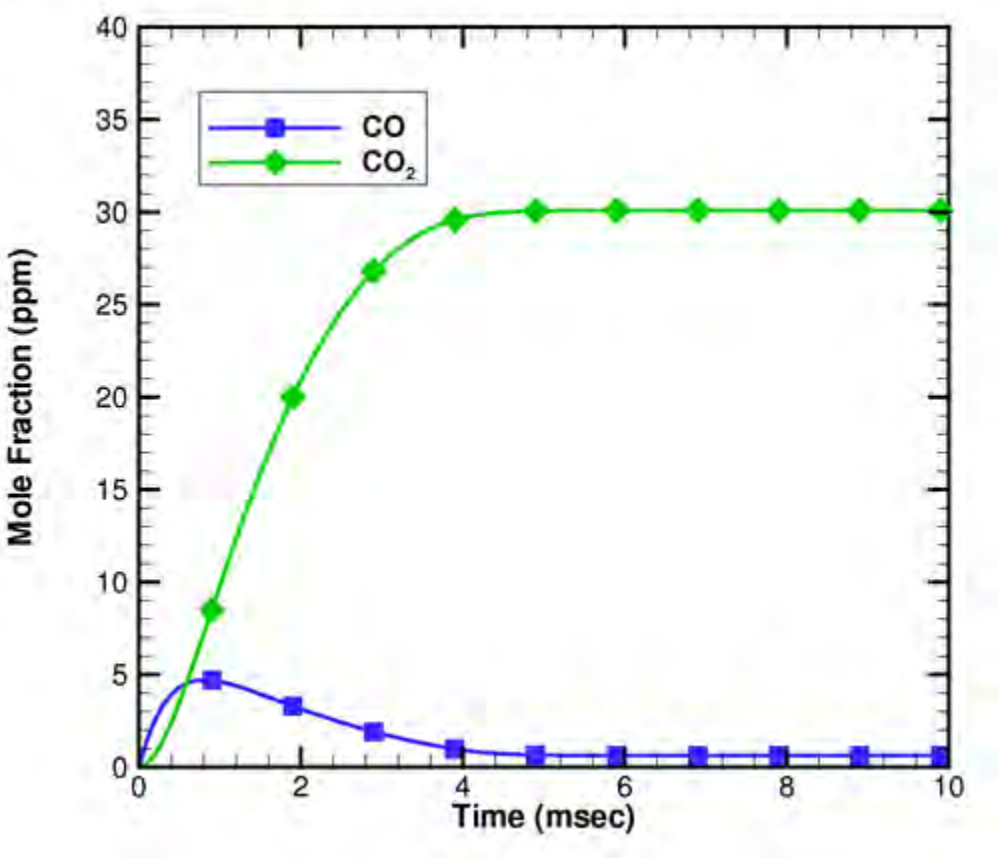

18.7 Particle Transport Equations

The general transport equation for particles of size j can be written as

Equation 18-47

$$\frac{\partial N_j}{\partial t} + \nabla.\left(N_j U_j\right) = \dot{N}_j$$

In the above equation, the right-hand side represents the net generation rate of particles of size j due to processes such as nucleation, collisions leading to coagulation, and gas-particle interactions as described in *Section 18.3* through *Section 18.6*. The particle velocity U_j is considered to be sum of the velocities due to gas flow, particle diffusion, and thermophoresis and is written as

Equation 18-48

$$U_j = u + V_j^D + V_j^T$$

The particle diffusion and thermophoretic velocities, denoted by V^D and V^T respectively in *Equation 18-48*, are expressed as a function of particle number density and gas temperature gradient, respectively. Thus,

Equation 18-49

$$N_j V_j^D = -\delta_j \nabla N_j$$

$$N_j V_j^T = -\theta_j \frac{\eta}{\rho T} \nabla \mathrm{T}$$

In the above equations, δ_j and θ_j are diffusivity and thermophoretic coefficient of particle of size j whereas η and ρ are viscosity and density of the surrounding gas. The diffusivity and thermophoretic coefficients are, in general, functions of the Knudsen number regime. The general expressions for these can be written as

Equation 18-50

$$\delta_j = \frac{K_B T}{3\pi\mu D_j} S(\alpha_j)$$

Where the slip correction factor S is given by

Equation 18-51

$$S(\alpha) = 1 + \alpha\left(A_1 + A_2 Exp\left(-\frac{2A_3}{\alpha}\right)\right)$$

In the above equation α is the Knudsen number = $2\lambda/D_j$ and the gas mean free path is written as

Equation 18-52

$$\lambda = \frac{\eta}{\rho}\sqrt{\frac{\pi\bar{M}}{2K_B N_{avo} T}}$$

ANSYS Chemkin uses values of 1.257, 0.4, and 0.55 for constants A_1, A_2, and A_3, respectively.

The thermophoretic coefficient is written as

Equation 18-53

$$\theta_j = -\frac{2C_S\left(C_R + C_T\alpha_i\right)S\left(\alpha_i\right)}{\left(1+3C_M\alpha_i\right)\left(1+2C_R+2C_T\alpha_i\right)}$$

In the above equation, C_R represents the ratio of gas to particle thermal conductivity. Values of constants C_S, C_T, and C_M used by ANSYS Chemkin are 1.17, 2.18, and 1.14, respectively.

The exact form of transport equation for particles depends on the reactor model. For example, for the closed and open 0-D reactors and Plug-flow reactor, diffusion and thermophoresis are not applicable. On the other hand, for flame simulators all terms are retained. Additionally, while the sectional method uses the complete forms of various terms described above, some simplifying approximations are invoked when the method of moments is used. These are explained in the following section.

18.7.1 Transport Equations for Size Moments

In order to solve the moments of the particle size distribution function, transport equations (or conservation equations) of the size moments are required. The transport equations of the moments for the moments of the particle size distribution function can be derived from those for the discrete number density function.

According to the size moment definition given by *Equation 18-2*, the transport equation of the r-th size moment can be derived by applying $\sum_{j=0}^{\infty} j^r \times$ to each term of *Equation 18-76*. The result of this operation leads to the transport equation for M_r

Equation 18-54

$$\frac{\partial M_r}{\partial t} + \nabla\cdot\left(\vec{u}\times M_r\right) = \nabla\cdot\left[-\vec{u}_T\times M_r + \sum_{j=0}^{\infty} j^r \times D_{p,j}\times\nabla N_j\right] + \left(R_r + G_r + S_r\right)$$

R_r, G_r, and S_r are the production terms of the r-th particle size moment contributed by nucleation, coagulation, and surface reactions, respectively. The definitions of these terms are given in *Equation 19*, *Equation 18-23* – *Equation 18-25*, and *Equation 18-26*. As mentioned earlier, somewhat simplified expressions are used for particle diffusivity and the thermophoretic coefficient when using the method of moments. Specifically, the particle diffusivity given in *Equation 18-54* can be rewritten in terms of the particle size class as

Equation 18-55

$$D_{p,j} = \frac{3}{2}\times\left(1+\frac{\pi\alpha}{8}\right)^{-1}\times\frac{\kappa_B T}{\rho\sqrt{\frac{2\pi\kappa_B N_{avo} T}{\bar{W}}}}\times\frac{1}{\left(d_0\times j^{1/3}\right)^2}$$
$$= \frac{3}{2}\times\left(1+\frac{\pi\alpha}{8}\right)^{-1}\times\frac{\kappa_B T}{\rho\sqrt{\frac{2\pi\kappa_B N_{avo} T}{\bar{W}}}}\times\frac{1}{d_0^2}\times j^{-2/3}$$
$$= D_{p,0}\times j^{-2/3}$$

Similarly, thermophoretic velocity is expressed as

Equation 18-56

$$\bar{u}_T = -\frac{3}{4}\times\left(1+\frac{\pi\alpha}{8}\right)^{-1}\times\left(\frac{\eta}{\rho}\right)\times\frac{1}{T}\nabla T \quad \text{[cm/sec]}$$

Now *Equation 18-54* can be expressed entirely in terms of size moments and the final form of the *r*-th size moment equation becomes

Equation 18-57

$$\frac{\partial M_r}{\partial t}+\nabla\cdot\left(\bar{u}\times M_r\right)$$
$$= \nabla\cdot\left[-\bar{u}_T\times M_r + D_{p,0}\times\nabla\left(\sum_{j=0}^{\infty} j^{-2/3}\times j^r\times N_j\right)\right]+\left(R_r+G_r+S_r\right)$$
$$= \nabla\cdot\left[-\bar{u}_T\times M_r + D_{p,0}\times\nabla M_{r-2/3}\right]+\left(R_r+G_r+S_r\right)$$

18.7.2 Transport Equations for Particle Surface Species

The molar concentration of surface species χ_{ps} in a particle population can be calculated by

Equation 18-58

$$Z_{ps} = \left[\chi_{ps}\right]\sum_j A_{s,j} N_j$$

where $[\chi_{ps}]$ is the surface molar concentration of χ_{ps} in [mole/cm^2] and the summation corresponds to the total particle surface area. Conservation of surface species χ_{ps} leads to the transport equation for Z_{ps} as

Equation 18-59

$$\frac{\partial Z_{ps}}{\partial t} + \nabla.\left(\left[\chi_{ps}\right] A_{s,j} N_j U_j\right) = \dot{Z}_{ps}$$

Note that because surface species only exist on the particle surface, transport of surface species is solely due to the relocation of particles. The production rate term on the right-hand side consists of contributions due to surface chemistry that does not involve particle area change and the processes that modify particle surface area—nucleation, gas-particle interaction (growth/etching), and particle coagulation.

Equation 18-60

$$\dot{Z}_{ps} = \dot{Z}_{ps}\Big|_{SURF} + \dot{Z}_{ps}\Big|_{NUCL} + \left\{ \dot{Z}_{ps}\Big|_{GRET} + \dot{Z}_{ps}\Big|_{COAG} \right\}$$

The surface chemistry contribution due to reactions that do not involve particle area change (i.e., no growth or etching) is simply net production rate due surface reactions and is computed as the product of surface molar production rate and the existing particle surface area.

Equation 18-61

$$\dot{Z}_{ps}\Big|_{SURF} = \left[\dot{\chi}_{ps}\right] \sum_j A_{s,j} N_j$$

Nucleation adds new surface area and correspond surface species are specified by the nucleation reaction. The rate of surface species production can be simply computed using the reaction rate of progress and stoichiometry.

Equation 18-62

$$\dot{Z}_{ps}\Big|_{NUCL} = \dot{\omega}_s\Big|_{NUCL}$$

Notice that this will be exactly the same if computed from the net area production rate due to nucleation. Thus

Equation 18-63

$$\dot{Z}_{ps}\Big|_{NUCL} = \dot{A}_s\Big|_{NUCL}\frac{Y_S}{\sigma_s}\Gamma$$

In the above equation, Y_S and σ_s are the site fraction and occupancy of the surface species, respectively, and Γ is the surface site density. For example, for the nucleation reaction shown in *Figure 18-6*, $Y_{H(s)}$ = 20/48.72. Note that this number will be more exact than this due to the native site stoichiometry computation internally done by ANSYS Chemkin and as explained in *Section 18.3.5*, The area production rate due to nucleation can be computed as

Equation 18-64

$$\dot{A}_s\Big|_{NUCL} = \dot{r}_{NUCL}N_{avo}a_{NUCL} = \dot{r}_{NUCL}N_{avo}A_0 j_{NUCL}^{2/3}$$

In the above equation $\dot{r}_{NUCL}$ is the rate of progress of the nucleation reaction and j_{NUCL} is the size of the nucleated particle.

The growth/etching reactions and particle coagulation modify the total particle surface area. As shown in *Equation 18-65* the corresponding contribution to surface species production is grouped together as indicated by the curly brackets. When the net area generation due to these processes is positive, ANSYS Chemkin considers that this area is occupied by the native species (see *Section 18.3.5*). (Note that for correct elemental balance, the native sites should be “empty” sites.) On the other hand, when the net area generation due to growth/etching reactions and coagulation is negative, ANSYS Chemkin assumes that all surface species are “destroyed” in an amount proportional to their surface coverage. The destroyed species are considered to be “trapped” in the bulk particle and are not released in the gas phase.

18.7.2.1 Implementation for Method of Moments

Using the expressions for particle diffusivity and thermophoretic velocity described in *Section 18.7.1*, *Equation 18-58* is written as

Equation 18-65

$$\begin{aligned}
&\frac{\partial Z_{ps}}{\partial t}+\nabla\cdot\left(\vec{u}\times Z_{ps}\right)\\
&\qquad=\nabla\cdot\left\{\vec{u}_T\times Z_{ps}-\sum_{j=0}^{\infty}\left(D_{p,j}\times\nabla N_j\times\left[\chi_{ps}\right]\times A_{s,j}\right)\right\}+\dot{Q}_{ps}\\
&\qquad=\nabla\cdot\left\{\vec{u}_T\times Z_{ps}-\sum_{j=0}^{\infty}\left(D_{p,0}\times j^{-2/3}\times\nabla N_j\times\left[\chi_{ps}\right]\times A_{s,0}\times j^{2/3}\right)\right\}+\dot{Q}_{ps}\\
&\qquad=\nabla\cdot\left\{\vec{u}_T\times Z_{ps}-D_{p,0}\times A_{s,0}\times\left[\chi_{ps}\right]\times\nabla\left(\sum_{j=0}^{\infty}N_j\right)\right\}+\dot{Q}_{ps}\\
&\qquad=\nabla\cdot\left\{\vec{u}_T\times Z_{ps}-D_{p,0}\times A_{s,0}\times\frac{Z_{ps}}{A_{s,\Sigma}}\times\nabla M_0\right\}+\dot{Q}_{ps}\\
&\qquad=\nabla\cdot\left\{\vec{u}_T\times Z_{ps}-D_{p,0}\times\frac{Z_{ps}}{M_{2/3}}\times\nabla M_0\right\}+\dot{Q}_{ps}\\
&=\nabla\cdot\left\{\left(\vec{u}_T-\frac{D_{p,0}}{M_{2/3}}\times\nabla M_0\right)\times Z_{ps}\right\}+\dot{Q}_{ps}
\end{aligned}$$

18.7.3 Implementation Considerations for Different Reactor Models

Transport equations of particles and particle-bonded surface species for representative reactor models are given in the following sections.

18.7.4 0-D Closed and Open Reactors

In 0-D closed (batch) and open (PSR) reactor models all gas-particle properties are assumed to be uniform throughout the reactor. That is convection, diffusion, and thermophoresis of the properties are ignored. Therefore, the governing equation for particle number density of size *j* is

Equation 18-66

$$\frac{d\left(N_jV\right)}{dt}=N_j\dot{Q}\Big|_{IN}-N_j\dot{Q}\Big|_{OUT}+V\dot{N}_j$$

In the above equation, V is the reactor volume and Q indicates the volumetric flow rate. The last term on right hand side is the net production rate of particles of size *j* per unit volume per unit time computed using expression developed in previous sections.

Accordingly, the *r*-th size moment equation and particle-bound surface species equations are

Equation 18-67

$$\frac{d\left(M_r V\right)}{dt} = M_r \dot{Q}\Big|_{IN} - M_r \dot{Q}\Big|_{OUT} + V\dot{M}_r$$

Equation 18-68

$$\frac{d\left(Z_s V\right)}{dt} = Z_s \dot{Q}\Big|_{IN} - Z_s \dot{Q}\Big|_{OUT} + V\dot{Z}_s$$

18.7.5 Plug-Flow Reactor

A plug-flow reactor operates under steady state conditions. All properties are assumed to be well-mixed on the cross-flow plane, that is, no mass or energy transfer in the transverse direction. Moreover, the gas velocity u is assumed to be large enough so that diffusion and thermophoresis fluxes in the flow direction x are insignificant and can be neglected. Consequently, the transport equation for particles of size j is

Equation 18-69

$$\frac{d}{dx}\left(N_j uA\right) = A\dot{N}_j$$

The equations for M_r moment and surface species are

Equation 18-70

$$\frac{d}{dx}\left(M_r uA\right) = A\dot{M}_j$$

Equation 18-71

$$\frac{d}{dx}\left(Z_s uA\right) = A\dot{Z}_s$$

18.7.6 Flame Simulators

Flame simulators use the full form of the transport equation for the particles and surface species as given by *Equation 18-47* and *Equation 18-59*.

18.8 Particle Aggregation Model

Soot particle samples collected from the exhaust of practical combustion devices are found to be mostly fractal aggregates rather than spherical primary particles. This is also true for other industrial processes such as production of titania (TiO_2) in a tubular reactor. The omnipresence of particles as aggregates, regardless of where and from which processes they are formed, creates the necessity of an aggregation model for use with the Particle Tracking feature.

The particle-particle aggregation process can be modeled as a sequence of collision, sticking, and complete coalescence by fusion, which is also called *sintering*. After a collision of two particles that results in particles sticking to each other, we assume that the contact between the particles is initially a point contact. The individual particles are then called primary particles of a single aggregate. (In the literature, an aggregate is sometimes also referred to as an agglomerate.) The total mass and the total surface area are both conserved at this stage. For a constant material density for the particles, the total volume is also conserved. As a result of processes such as grain-boundary diffusion, the particles that are stuck together proceed to *sinter* or *fuse* together and eventually completely coalesce to form a single particle. Thus, at the end of the coalescence process, the total mass (volume) is conserved but surface area is not. *Figure 18-15* illustrates this process.

Figure 18-15 Schematic showing correlations of the final collision states and measurable aggregate properties.

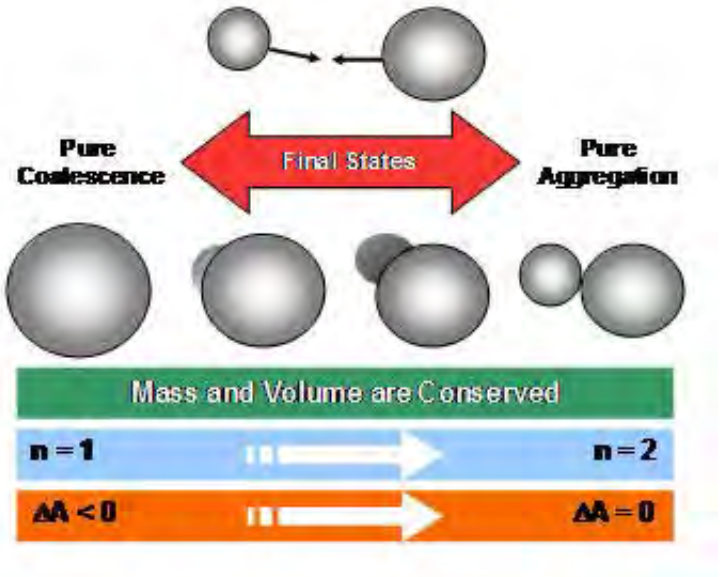

It can be noted that the colliding aggregates may not completely coalesce for a given time scale, i.e., two particles colliding may not become a single sphere. In general, not all primary particles from a given aggregate are of the same size and not all primary particles are truly spherical. However, this approximation is necessary for a computationally feasible representation. Aggregates may also contain different numbers of primary particles. *Figure 18-16* illustrates the case where two colliding aggregates have four and two primary particles, respectively, leading to a new aggregate formed after the collision that initially has six primary particles. After complete coalescence, however, a single spherical (primary) particle is formed from the aggregate similar to the final particle in *Figure 18-15*. *Table 18-1* summarizes changes in various quantities caused by the process illustrated in *Figure 18-16*.

Figure 18-16 Aggregation and coalescence of two particles (general case).

Table 18-1 Size distribution property changes due to aggregation. NP, A, and V indicate the number of primary particles, the surface area, and the volume (directly related to mass), respectively.

State	*Number of Aggregate*	*Number of Primary Particles*	*Surface Area*	*Volume (mass)*
Before collision	2	$= (NP_1 + NP_2)$	$= (A_1 + A_2)$	$= (V_1 + V_2)$
After collision	1	$= (NP_1 + NP_2)$	$= (A_1 + A_2)$	$= (V_1 + V_2)$
After coalescence	1	1	$< (A_1 + A_2)$	$= (V_1 + V_2)$

18.8.1 Driving Force for Fusion/Sintering

The minimum energy state of an aggregate may be considered as the completely coalesced spherical particle. The rate of approach to this state is then considered to be dictated by how much surplus surface area the aggregate has compared to the corresponding spherical particle. Thus,

Equation 18-72

$$\frac{da}{dt} = -\frac{(a - a_s)}{\tau_f}$$

Equation 18-72 can be derived from the simple two-sphere neck growth model[125]. In the above equation, a is the surface area of the aggregate, a_s is the corresponding surface area of the completely coalesced spherical particle, and τ_f is the characteristic fusion (sintering) time.

The characteristic fusion time can be formulated in terms of physical properties of the aggregate bulk material, such as surface tension and viscosity.

The fusion time scale τ_f is the time required for complete coalescence of two individual particles after being brought into contact. For example, τ_f =0 implies an instantaneous coalescence of two colliding particles. The fusion time can be defined as[129, p. 337]:

Equation 18-73

$$\tau_f = \frac{\eta(T)\bar{d}_p}{\sigma(T)}$$

where η and σ are, respectively, the viscosity and the surface tension of the bulk species in liquid phase and $\bar{d}_p (= d_0 M_{1/3} / M_0)$ is the "would-be" particle diameter if coagulation takes place. Surface tension σ is a function of temperature and is given as[126]:

Equation 18-74

$$\sigma \propto (1 - T_r)^{4m}$$

where m varies from 0.25 to 0.31. For $0.4 \le T_r \le 0.7$, $d\sigma/dT$ is almost constant, and the surface tension can be expressed as a linear function of temperature[126]:

Equation 18-75

$$\sigma = A_\sigma + B_\sigma T$$

where the value of A_σ is on the order of 10 and on the order of -10^{-1} for B_σ.

The temperature dependence of liquid viscosity η can be approximated by the Andrade equation[126]:

125. W. Koch and S. K. Friedlander, "The effect of particle coalescence on the surface area of a coagulating aerosol," Journal of Colloid and Interface Science, 140: 419-427, 1990.
126. Reid, R.C., Prausnitz, J.M., and Poling B.E., "The Properties of Gases and Liquids", 4th Edition, McGraw-Hill, New York, 1987.

Equation 18-76

$$\ln \eta = A_\eta + \frac{B_\eta}{T}$$

where the value of A_η is generally on the order of -10 and the value of B_η is between 2000 and 4000.

By combining *Equations 18-75* and *18-76* into *Equation 18-73*, the particle fusion time scale takes the form

Equation 18-77

$$\tau_f = \frac{A_\tau e^{B_\tau / T} \bar{d}_p}{C_\tau + D_\tau T}$$

While the characteristic fusion time is given by *Equation 18-73*, the collision time scale τ_c is already computed by the coagulation model of the Particle Tracking feature and is given as

Equation 18-78

$$\tau_f = A\, T^{\beta} exp\left(-\frac{E}{T}\right) {d_p}^n$$

In *Equation 18-78*, T is the temperature of the aggregate and d_p is the diameter of the primary particle. Note that the above expression tacitly assumes that all the primary particles in an aggregate are spheres although this is not strictly true once the process of fusion starts. The value of the power n typically is 4.

If the characteristic fusion time is shorter than the time required for collisions, then particle coalescence dominates and most of the particles are spheres. At the other extreme, where collisions occur faster than coalescence, a collection of attached primary particles (aggregates) is formed. As expressed by *Equation 18-78*, the fusion time depends on particle temperature and diameter of the primary particles. At high temperatures, the aggregates with smaller primary particles are more likely to coalesce completely.

18.8.2 Aggregate Geometry and Collisions

When a given aggregate is not completely coalesced to a sphere, the apparent collision diameter of the aggregate is different from that of the sphere of the same mass. Consequently, modifications to the collision frequency formulation are required to account for the difference in collision diameter. In general, all aggregates of the same mass (or volume) do not necessarily have the same number of primary particles. Not only can the primary particles that make up an aggregate have different

diameters, they can also have different shapes as well. In addition, a given aggregate can have differing apparent collision diameters that depend on the direction vector along which the aggregate collides. (For example, consider the case of an aggregate consisting of a straight chain of primary particles.)

From a modeling perspective, accounting for such effects would require resolution in another coordinate dimension. The computational cost of such resolution would be prohibitive. It is also quite likely that the physical insight obtained would not be of high fidelity to justify the added expense, due to the uncertainties and further assumptions/sub-models that would be required to capture these effects.

Two simplifying assumptions are therefore made in the aggregation model implemented in the Chemkin Particle Tracking feature as a result of the above considerations. These are:

1. All primary particles are spherical, and
2. All primary particles in an aggregate are of the same size.

For correctly capturing first-order particle aggregate properties (i.e., aggregate area and volume or equivalently number density of primary particles and number density of aggregates), these two simplifying assumptions are appropriate.

With these assumptions, the following quantities can be defined:

Equation 18-79

$$\text{Number of primary particles per aggregate of class } j = n_{p_j} = \frac{N_{p_j}}{N_j}$$

Equation 18-80

$$\text{Volume of each primary particle of aggregate of class } j = v_{p_j} = \frac{N_j}{N_{p_j}} V_j$$

Equation 18-81

$$\text{Diameter of each primary particle of aggregate of class } j = d_{p_j} = \left(\frac{6 * v_{p_j}}{\pi} \right)^{1/3}$$

Equation 18-82

$$\text{Collision diameter of each aggregate of class } j = D_{C_j} = d_{p_j} * \left(\frac{N_{p_j}}{N_j} \right)^{1/D_f}$$

In *Equation 18-79* through *Equation 18-82*, subscript p and j indicate primary particle and the class (i.e., the number of atoms of the bulk material) of the aggregate, respectively, while N is the number density and V denotes the volume. The number of primary particles in the aggregate changes as the aggregate coalesces. The collision diameter of the aggregate depends on the primary particle size and the mass fractal dimension, D_f.

The collision diameter of the aggregates influences the frequency of collision and thus evolution of the particle system. The collision diameter of an aggregate is larger than the corresponding (volume-equivalent) sphere. Thus, there is a more pronounced scavenging effect, i.e., the larger aggregate "consumes" a smaller one, when larger particles are aggregates rather than completely coalesced spheres.

The fractal dimension can be considered as a measure of how densely packed the primary particles are in an aggregate. Its value varies from 3 for completely fused spheres to about 1.7 for cluster-cluster aggregation[127] in Brownian collisions. In principle, the evolution of the fractal dimension may also be modeled as a function of physical processes, such as particle collision frequency and fusion time. However, little fundamental work has been done in this area. Therefore, at present, the Particle Tracking feature assumes that the fractal dimension is fixed and specified by the user.

127. C. Artelt, H.-J. Schmid, and W. Peukert, "On the relevance of accounting for the evolution of the fractal dimension in aerosol process simulations," *J. Aerosol Sci.*, **34**: 511-534, 2003.

18.8.3 Aggregation Model for the Moment Method

Kazakov and Frenklach[128] developed an aggregation model to work in conjunction with the moments method to obtain the distribution of the number of primary particles forming aggregates. While the particle aggregation model of Kazakov and Frenklach allows the prediction of both the average number of primary particles in the aggregates and its variation (standard deviation), this aggregation model does have drawbacks. To obtain the moments of the distribution of the number of primary particles in aggregates, Kazakov and Frenklach's model needs to solve at least two additional moments equations, which are known to be difficult to converge. The additional hard computational work does not provide added benefits, as their aggregation model does not consider the correlation between the size of primary particles and the size of (or the number of primary particles in) the aggregates. The other major issue of the Kazakov-Frenklach aggregation model is the omission of the particle sintering effect[129]. The particle sintering model addresses the competition between coalescence and aggregation, when the particles are brought in contact, and determines the outcome of the collision: a larger primary particle or an aggregate formed by the colliding particles. Without a sintering model, the Kazakov-Frenklach aggregation model would treat all collisions as either strictly coalescent or strictly aggregate.

Building on the method of moments of Frenklach and Harris[130], Mueller et al. implemented a soot aggregation model based on the volume-surface correlation of aggregates. Rather than tracking the moments of aggregate size distribution and moments of primary particle distribution among the aggregates, the joint volume-surface aggregate model solves moments of volume and surface area of aggregates. This aggregate model does allow the inclusion of the particle sintering effect. However, because only aggregate volume and surface area are utilized by this model, it is not straightforward to incorporate physical parameters that actually govern the particle sintering process. Average aggregate properties such as collision diameter and number of primary particles can be computed from aggregate volume and surface area according to the fractal geometry relationship. This aggregate model requires at least 5 moments to properly track the joint volume-surface moments and the authors recommend solving 6 moments.

---

128. Kazakov, A.and Frenklach, M., "Dynamic Modeling of Soot Particle Coagulation and Aggregation: Implementation with the Method of Moments and Application to High-Pressure Laminar Premixed Flames", *Combustion and Flame*, **114**:484-501 (1998).
129. Koch, W. and Friedlander, S.K., "The Effect of Particle Coalescence on the Surface Area of a Coagulating Aerosol", *J. of Colloid and Interface Science*, **140**(2):419-427 (1990).
130. Frenklach M. and Harris, S.J., "Aerosol Dynamics Modeling Using the Method of Moments", *J. of Colloid and Interface Science*, **118**:252-261 (1987).

The relatively simple particle aggregation model implemented with the Particle Tracking feature is also compatible with the moments method. However, it attempts to amend problems associated with the aggregation models of Kazakov and of Mueller, while still providing aggregate properties such as average number of primary particles and average surface area. The aggregation model addresses those disadvantages of other moments-based aggregation models by the inclusion of a particle surface-area equation. By finding connections between average aggregate surface area and the fractal geometry relationship, this aggregation model solves only one additional equation and does not require solution of additional moments. A particle sintering model is incorporated into the surface area equation so that the particle-sintering effect, yielding aggregates in various degrees of fusion, is reflected by the change in particle surface area after collision. The particle-sintering model determines the extent of fusion by comparing the time scales of particle collision and particle fusion.

The aggregation model is capable of providing average aggregate properties such as number of primary particles in an aggregate, aggregate collision diameter, and diameter of the primary particle in addition to overall aerosol characteristics (number density, surface area density, and volume fraction). The only information available from the other aggregation models but not from this model is the variance of the number of primary particles among aggregates.

The moments method implemented in the Particle Tracking feature models the aggregation process by keeping track of the particle surface area. Thus, the total particle surface area (per volume) is solved by a surface area equation, which assumes that particle area is modified by aggregation, as well as by nucleation, coagulation and mass growth/reduction due to surface reactions. This model is designed to be easily solved alongside the particle size moments. Because both mass growth and coagulation effects are included in the moment equations, the surface area equation needs to consider only the difference in area growth when the collision does not result in coagulation (or fusion) but instead by aggregation. The transport equation for total particle surface area per volume $A_{s,\Sigma}$ (cm^2/cm^3) is given as

Equation 18-83

$$\frac{dA_{s,\Sigma}}{dt} + \nabla\bullet\left(\vec{u}A_{s,\Sigma}\right) = -\nabla\bullet\left\{\vec{u}_T A_{s,\Sigma} - D_{p,0}A_{s,0}\nabla M_0\right\} + \dot{A}_{\Sigma}$$

$D_{p,0}$ is the portion of particle diffusion coefficient that is independent of particle size and is given as

Equation 18-84

$$D_{p,0} = \frac{3}{2}\left(1+\frac{\pi\alpha}{8}\right)^{-1} \frac{\kappa_B T}{\rho\sqrt{2N_{avo}\kappa_B T/\bar{W}}} \frac{1}{d_0^2}$$

$\dot{A}_\Sigma$ [cm^2/cm^3-sec] is the total particle surface area production rate and consists of contributions from three sources: nucleation, surface growth, and the combined effect of coagulation and aggregation, i.e.,

Equation 18-85

$$\dot{A}_\Sigma = \dot{A}_{\Sigma,nuc} + \dot{A}_{\Sigma,surf} + \dot{A}_{\Sigma,agg/coag}$$

If the nucleation rate is r_{nuc} [mole/cm^3-sec] and the inception class of the particle is j_{nuc}, the surface area production rate due to nucleation can be calculated as

Equation 18-86

$$\dot{A}_{\Sigma,nuc} = r_{nuc} N_{avo} A_{s,0} j_{nuc}^{2/3}$$

or, in general form, as

Equation 18-87

$$\dot{A}_{\Sigma,nuc} = \sum_{inuc} r_{inuc} j_{inuc}^{2/3} A_{s,0} N_{avo}$$

The surface area production due to the particle mass growth surface reactions can be obtained from the surface growth contribution to the two-third moment:

Equation 18-88

$$\dot{A}_{\Sigma,surf} = A_{s,0} \sum_{is=1}^{nsurf} S_{2/3,is}$$

where $S_{r,is}$ is the contribution of the *is*-th surface reaction to the production of the two-third size moment.

When only particle aggregation is considered, the particle surface area production rate (or actually destruction rate) is interpolated from the production rates of the whole moments:

Equation 18-89

$$\dot{A}_{\Sigma,coag} = A_{s,0} G_{2/3}$$

On the other hand, in the absence of particle coagulation, the pure aggregation process yields no surface area change if the contact surface areas between primary particles in the aggregate are assumed to be negligible; that is,

Equation 18-90

$$\dot{A}_{\Sigma,agg} = 0$$

If both particle coagulation and aggregation are considered, the actual surface area production rate due to these two processes should lay between $\dot{A}_{\Sigma,coag}$ and $\dot{A}_{\Sigma,agg}$. To determine the weight between contributions from these two processes, a measure of their relative importance is considered. Since the final particle structure after collision depends on two characteristic time scales: the characteristic collision time τ_c and the characteristic fusion time τ_f, the ratio of these two characteristic time scales serve as the weighting parameter.

Equation 18-91

$$\tau_c = \frac{M_0}{-G_0}$$

M_0 is the zero-th particle size moment and G_0 is the coalescent coagulation contribution to the production (destruction) of the zero-th size moment.

Now we define a parameter β_a to represent the relative importance of coalescence over aggregation as

Equation 18-92

$$\beta_a = \begin{cases} 0 & \text{if } \tau_c/\tau_f < \beta_{a,crit} \\ \tau_c/\tau_f & \\ 1 & \text{if } \tau_c/\tau_f \geq 1 \end{cases}$$

And the surface area production rate due to the combined effect of particle coagulation and aggregation can be written as

Equation 18-93

$$\dot{A}_{\Sigma,agg/coag} = \beta_a \dot{A}_{\Sigma,coag} + (1-\beta_a)\dot{A}_{\Sigma,agg} = \beta_a \dot{A}_{\Sigma,coag} = \beta_a A_{s,0} G_{2/3}$$

By combining *Equations 18-77* and *18-91* into *Equation 18-93*, the particle surface production rate from coagulation and aggregation can be expressed as

Equation 18-94

$$\dot{A}_{\Sigma,agg/coag} = A_{agg} T^{B_{agg}} e^{-E_{agg}/T} \frac{A_{s,0} M_0}{\bar{d}_{agg}} \frac{G_{2/3}}{-G_0}$$

The average primary particle diameter $\bar{d}_p$ in *Equations 18-73* and *18-77* is replaced by $\bar{d}_{agg}$ in *Equation 18-94,* because collisions can occur between primary particles as well as aggregates. $\bar{d}_{agg}$ is the diameter of the sphere whose volume is the same as the average volume of the aggregates and is given as

Equation 18-95

$$\bar{d}_{agg} = d_0 \frac{M_{1/3}}{M_0}$$

18.8.3.1 Aggregate Properties

For use of the aggregation model, the concept of "particle class" in the Particle Tracking module is extended from being "the number of bulk species in a primary particle" to being "the total number of bulk species in primary particles forming the aggregate". Let n denote the number of primary particles in an aggregate. A class j "particle" without aggregation always indicates a spherical primary particle consisting of j bulk species; i.e., n is always equal to 1. The same j-class "particle" could have many different configurations when aggregation is present, depending on the value of n, as shown schematically in *Figure 18-17*.

Figure 18-17 Depending on the value of n, an aggregate of given class can have various configurations.

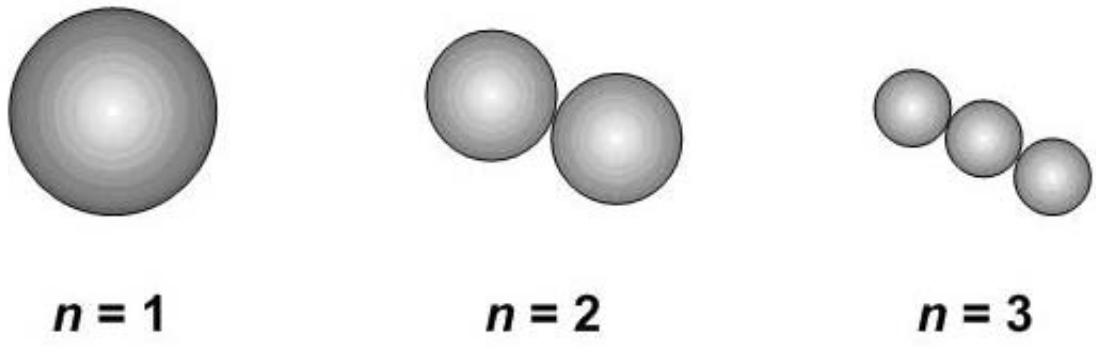

The average number of primary particles in aggregates, $\bar{n}$, is obtained from the total particle surface area, $A_{s,\Sigma}$, which is solved by *Equation 18-83*. Assuming the primary particles in an aggregate are spherical and are connected with each other at one point; then the contact surface area is almost zero. The total surface area of an average aggregate is computed by

Equation 18-96

$$\bar{A}_{s,ag} = \pi \bar{d}^2_{p,ag} \bar{n}$$

Alternatively, the same average aggregate surface area can be obtained from the total particle surface area as

Equation 18-97

$$\bar{A}_{s,ag} = \frac{A_{s,\Sigma}}{M_0}$$

where M_0 is the zero-th moment of the particle size distribution which represents the particle number density of the aerosol population. By combining *Equations 18-96* and *18-97*, an equation for $\bar{n}$ is derived to be

Equation 18-98

$$\bar{d}^2_{p,ag} \bar{n} = \frac{A_{s,\Sigma}}{\pi M_0}$$

Since the average class of primary particle in the aggregate $\bar{j}_{p,ag}$ is derived from the size moments as

Equation 18-99

$$\bar{j}_{p,ag} = \frac{M_1 / M_0}{\bar{n}}$$

the average primary particle diameter in the aggregate, $\bar{d}_{p,ag}$, is expressed in terms of the size distribution moments[131]:

Equation 18-100

$$\bar{d}_{p,ag} = d_0 \bar{j}^{1/3}_{p,ag} = d_0 \left(\frac{M_1 / M_0}{\bar{n}} \right)^{1/3}$$

Therefore, the average number of primary particles in aggregates is obtained by substituting *Equation 18-100* into *Equation 18-98*:

Equation 18-101

$$\bar{n} = \left(\frac{A_{s,\Sigma}}{\pi d_0^2 \left(M_1^2 M_0 \right)^{1/3}} \right)^3$$

Note that $\bar{n}$ should have a value between 1 and M_1/M_0. The collision diameter of the aggregate is then computed by[128, p. 337]:

131. Theory Manual, CHEMKIN, Reaction Design, San Diego, CA, USA, 2009.

Equation 18-102

$$d_{c,ag} = \bar{d}_{p,ag}\bar{n}^{1/D_f} = d_0\left(\frac{M_1}{M_0}\right)^{1/3}\bar{n}^{1/D_f-1/3}$$

where D_f is the fractal dimension of the aggregate. Typically, D_f is about 1.8 for soot aggregates in flame environments[128, p. 337].

18.8.3.2 Collision Frequency of Aggregates in the Moments Method

For a spherical particle of class j, its collision diameter can be easily calculated as[131, p. 342]:

Equation 18-103

$$d_{c,sphere}(j) = d_j = d_0 j^{1/3}$$

The collision diameter of a non-spherical aggregate of the same class can be obtained from *Equation 18-102*, with the help of the singe-size primary particle assumption, as

Equation 18-104

$$d_{c,agg}(j) = \bar{d}_{p,ag}n(j)^{1/D_f} = d_0\bar{j}_{p,ag}^{1/3}\left(\frac{j}{\bar{j}_{p,ag}}\right)^{1/D_f} = d_0\bar{j}_{p,ag}^{1/3-1/D_f}j^{1/D_f}$$

By comparing *Equations 18-103* and *18-104*, the collision frequency formulation can be systematically modified by replacing all one-third moments with the $1/D_f$-th moment and by scaling the unit diameter d_0 by a factor of $\bar{j}_{p,ag}^{1/3-1/D_f}$.

Accordingly, for collision frequency in the free-molecular regime, the collision frequency coefficient becomes

Equation 18-105

$$C^{agg} = C^{coag}\left(\bar{j}_{p,ag}^{1/3-1/D_f}\right)^{3/2} = \beta\sqrt{\frac{6\kappa_B T}{\rho_B}}\left(\frac{3m_0}{4\pi\rho_B}\right)^{1/6}\left(\bar{j}_{p,ag}^{1/3-1/D_f}\right)^{3/2}$$

and the function $\left\langle {}^{r}f_{x,y}\right\rangle$ becomes

Equation 18-106

$$\left\langle {}^{r}f_{x,y}\right\rangle = \sum_{l=0}^{r-1}\binom{r}{l}\left(\mu_{r-i+x+2/D_f-1/2}\mu_{l+y-1/2} + 2\mu_{r-l+x+1/D_f-1/2}\mu_{l+y+1/D_f-1/2} + \mu_{r-l+x-1/2}\mu_{l+y+2/D_f-1/2}\right)$$

where

$$\mu_r = \frac{M_r}{M_0}.$$

The production rate of the r-th moment due to free-molecular aggregation can be expressed as

Equation 18-107

$$G_r^f = \frac{1}{2} C^{agg} M_0^2 \sum_{k=1}^{r-1} \binom{r}{k} \left\langle {}^{1/2} f_{k,r-k} \right\rangle$$

The free-molecular coagulation rates given by *Equation 18-107* are in general valid for $D_f > 2$. That is, highly non-spherical particles can sometimes pass through each other without collision because of the large empty space within the collision diameter. However, this deficiency can be amended by using a smaller collision efficiency β.

Similarly, for collisions in the continuum regime, the production rate of the r-th due to aggregation can be rewritten as:

Equation 18-108

$$G_r^c = \frac{1}{2}\left(\frac{2\kappa_B T}{3\eta}\right)\sum_{k=1}^{r-1}\binom{r}{k}\left\{2M_k M_{r-k} + M_{k-1/D_f} M_{r-k+1/D_f} + M_{k+1/D_f} M_{r-k-1/D_f} + 2.514\lambda\left(\frac{\pi\rho_B}{6m_0}\right)^{1/3}\left(M_{k-1/D_f} M_{r-k} + M_k M_{r-k-1/D_f} + M_{k-2/D_f} M_{r-k+1/D_f} + M_{k+1/D_f} M_{r-k-2/D_f}\right)\right\}$$

18.8.4 Aggregation Model for the Sectional Method

In the sectional method implemented in Particle Tracking, the “sections” along the particle-size coordinate represent a range of masses and therefore volumes since the density of the bulk material is assumed to be constant. In this way, the section to which an aggregate belongs is determined by the volume-based diameter of the corresponding completely coalesced sphere. With the two assumptions mentioned on page 335, the sectional method then tracks the number density of aggregates and the number density of primary particles in each section.

The collision frequency kernels for the aggregates are given by *Equation 18-8*, *Equation 18-9*, and *Equation 18-10* in *Section 18.4*. Along with the dependence of the collision kernel on the collision diameter as the collisions diameter evolves through time, the particle dynamics of aggregates is different from that of completely coalesced spherical particles. For pure coalescence, meaning that the aggregation model is not used, the collision diameter is fixed for each representative aggregate from a section; it is the volume-averaged diameter.

The aggregation model is implemented according to the discretized population balance of Kumar and Ramkrishna[132]. Thus, the aggregation rate of the aggregates is given by

Equation 18-109

$$\beta_{j,k}^{FM} = \sqrt{\frac{8k_B T}{\pi}} \left(\frac{m_j + m_k}{m_j m_k} \right)^{1/2} \frac{\pi}{4} \left(D_{C_j} + D_{C_k} \right)^2$$

Equation 18-110

$$\beta_{j,k}^{CN} = \frac{2k_B T}{3\mu} \frac{\left(D_{C_j} + D_{C_k} \right)^2}{D_{C_j} D_{C_k}}$$

In equations *Equation 18-109* and *Equation 18-110*, m_j is the mass of aggregate of class j, T is the gas temperature, μ is the gas viscosity, k_B is the Boltzmann constant, and superscripts FM and CN indicate free-molecular and continuum regimes. The collision kernel, which is valid in all three collision regimes (i.e., free-molecular, continuum, and transition) is obtained by Fuch's interpolation function and also depends on the collision diameter of the aggregates. It is written as

Equation 18-111

$$\beta_{j,k}^{INT} = 2\pi \left(\mathfrak{D}_{f_j} + \mathfrak{D}_{f_k} \right) \left(D_{C_j} + D_{C_k} \right) \left[\frac{D_{C_j} + D_{C_k}}{D_{C_j} + D_{C_k} + 2G_{j,k}} + \frac{8\left(\mathfrak{D}_{f_j} + \mathfrak{D}_{f_k} \right)}{\phi_{jk} \left(D_{C_j} + D_{C_k} \right)} \right]^{-1}$$

In the above equation, G_{jk} is the so-called transition parameter, Φ_{jk} is the speed parameter, and D_f is the diffusivity of the aggregate. All of these depend on the collision diameter.

Thus, along with the dependence of the collision kernel on the collision diameter given by *Equation 18-109*, *18-110*, and *18-111*, as the collision diameter evolved through time, the particle dynamics of aggregates is different from that of completely coalesced spherical particles. For pure coalescence, meaning that the aggregation model is not used, the collision diameter is fixed for each representative aggregate from a section; it is the volume-averaged diameter.

The aggregation model is implemented according to the discretized population balance of Kumar and Ramkrishna[133]. Thus, the aggregation rate of the aggregates is given by

132. Kumar, S. and D. Ramkrishna (1997). "On the solution of population balance equations by discretization-- III. Nucleation, growth and aggregation of particles." *Chemical Engineering Science* **52**(24): 4659-4679.

Equation 19

$$\left.\frac{dN_i}{dt}\right|_{AGG} = \sum_{X_{i-1}\le(X_j+X_k)\le X_i}^{i\ge j\ge k} \eta\left(1-\frac{\delta_{jk}}{2}\right)\beta_{j,k}N_jN_k - N_i\sum_{k=1}^{M}\beta_{i,k}N_k$$

Equation 20

$$V = X_j + X_k$$

Equation 21

$$\eta = \frac{V^\theta X_{i+1}^\psi - V^\psi X_{i+1}^\theta}{X_i^\theta X_{i+1}^\psi - X_i^\psi X_{i+1}^\theta};\ X_i \le V \le X_{i+1}$$

Equation 22

$$\eta = \frac{V^\theta X_{i-1}^\psi - V^\psi X_{i-1}^\theta}{X_i^\theta X_{i-1}^\psi - X_i^\psi X_{i-1}^\theta};\ X_{i-1} \le V \le X_i$$

In *Equation 18-109* through *Equation 18-2*, X_i indicates the pivot size within the size range V_i to V_{i+1}; δ_{jk} is the Kronecker delta function; and θ and ψ are the powers of any two power-law properties of the particle size distribution (PSD) that are conserved. In this implementation, aggregate number density and volume (mass) are conserved. The collision frequency kernel $\beta_{j,k}$ depends on the collision diameters of representative aggregates from sections *j* and *k*. The primary particle aggregation rate is given by

Equation 23

$$\left.\frac{dN_{pi}}{dt}\right|_{AGG} = \sum_{X_{i-1}\le(X_j+X_k)\le X_i}^{i\ge j\ge k} \eta_p\eta\left(1-\frac{\delta_{jk}}{2}\right)\beta_{j,k}N_jN_k - N_{p_i}\sum_{k=1}^{M}\beta_{i,k}N_k$$

Similar to the aggregates, the distribution factor η_p is determined such that the primary particle size is conserved. Thus,

133. Kumar, S. and D. Ramkrishna (1997). "On the solution of population balance equations by discretization-- III. Nucleation, growth and aggregation of particles." *Chemical Engineering Science* **52**(24): 4659-4679.

Equation 24

$$\eta_p = \frac{V_i}{V_j + V_k}\left(n_{p_j} + n_{p_k}\right)$$

18.8.4.1 Sintering

Using *Equation 18-72* on page 333 and noting that the number of aggregates does not change due to sintering, we can write

Equation 18-1

$$\left.\frac{dN_i}{dt}\right|_{SINT} = 0$$

Equation 18-2

$$\left.\frac{dN_{p_i}}{dt}\right|_{SINT} = -\frac{3N_i}{\tau_f}\left(n_{p_i} - n_{p_i}^{2/3}\right)$$

The total generation rates of aggregates and primary particles are given by the addition of the aggregation rate and sintering rate.

18.8.4.2 Simple Aggregation Model

The parameters for the characteristic fusion time are available for only a few particle materials. Examples where the parameter data are available are typically metals or metal-oxides such as titania (TiO_2), silicon (Si), silica (SiO_2), etc. For other particulate systems of practical importance, especially carbon soot, such data are not typically available. This difficulty hinders usage of the aggregation model presented above. However, as noted in *Section 18.8*, the expression given by *Equation 18-73* indicates a power law dependence on primary particle diameter and the power exponent is typically 4. Such strong dependence indicates that aggregates with small primary particles coalesce quickly while those with large primary particles take a long time to fuse. Although the definitions of small and large are relative, it means that the size (diameter) of primary particles in an aggregate can be limiting, depending on the rate of collisions. The primary particles above this limiting diameter are very slow to fuse. Indeed, for soot particles obtained from flame experiments, the limiting size of primary particles is on the order of 20 to 30 nm.

In addition to difficulty in obtaining reliable sintering data, two equations are solved per section when the complete aggregation model is used in contrast to one equation per section when aggregation is not modeled. Moreover, the system of equations is stiffer due to the sintering rate. When combined, this may make the total computational cost substantially higher with the complete aggregation model.

Considering the above issues, one way to include the effect of aggregation without invoking the full aggregation model is to make use of the limiting primary particle size concept. The aggregates with primary particles less than the limiting value can be thought of as completely coalesced spheres while those with larger primary particles are pure aggregates in which primary particles of the limiting size are in point contact with each other. The corresponding two-parameter model is called the *simple aggregation model* and is available with the sectional method in the Particle Tracking feature. The two user-specified parameters for this model are the limiting diameter for primary particle and the fractal dimension.

In the simple aggregation model for the sectional method, the sections that have a representative aggregate diameter (i.e., the volume-averaged diameter) that is less than the user-specified fixed primary-particle diameter will have aggregates that are coalesced spheres while the sections with larger representative diameter will have pure aggregates. Thus, the number of primary particles per aggregate in any section is known *a priori*. Consequently, the collision diameter and surface area of aggregates are also known *a priori*.

Although the simple aggregation model is less rigorous, it is computationally efficient and captures the essential physics of the aggregation process. Its usage is recommended especially for soot systems. Due to the computational expense of the complete aggregation model, only the simplified model is available for flame simulations.

18.9 Solution Technique

In general, there are two important things to consider when solving equations for a gas-particle system: (a) keeping the numbers well-behaved, and (b) computational efficiency. The following sections describe how ANSYS Chemkin particle tracking feature addresses these.

18.9.1 Keeping the Numbers Well-behaved

During the course of simulation, the particle number density can assume values that span several orders of magnitude. For example, starting from 0 initial particles/cm^3 there can be 10^{12} particles/cm^3 during a nucleation burst and then 10^6 particles/cm^3 when agglomeration or oxidation dominate. There is no intrinsic/natural scale (such as usage of mole fractions for gas-phase species) to “normalize” these numbers. Choice of division by Avogadro number and using mole/cm^3 for number density can

result in small numbers that may not get resolved to sufficient precision. For example, if the number density is 10^{12} particles/cm^3, usage of mole/cm^3 would mean that the value of the variable solved for is 10^{-11}. This is too small for typical “double precision” numbers.

ANSYS Chemkin therefore solves for “scaled molar density”. That is, the variable solved for is phi*molar number density where phi is a user-prescribed scaling factor. For a typical ANSYS Chemkin gas-particle simulation the particle number density is roughly of the order of 10^{12}. Hence, the default value of the scaling factor is 10^{12} which makes the variable solved for of the order of 10.

For the method of moments, in addition to the scaling factor ANSYS Chemkin solves for $(M_r - M_{r-1})$ for $r > 0$. The corresponding equations can be derived using equation 18-88.

18.9.2 Computational Efficiency

When equations for particles are solved in a reactor model, the total number of variables can be written as

$$NC = NC\_gas + NC\_particles$$

and

$$NC\_particles = \{number\ of\ Moments\ or\ Number\ of\ sections\} + Number\ of\ surface\ species$$

Note that when the aggregation model is used, there are additional variables to solve for. For the method of moments, there is one extra variable corresponding to the particle surface area. For the sectional method, the additional number of variables is equal to the number of sections and corresponds to the primary particle number density.

For 0-D closed and open reactor models and for the Plug-Flow reactor, the Particle Tracking feature in ANSYS Chemkin solves the coupled system of equations.

For the flame simulators, the total number of variables becomes $NC*NP$ where NP is the number of grid points. Since a typical gas-phase reaction mechanism contains hundreds of species, the number of variables in the gas phase is typically much larger than the number of variables for the particles. Effectively, the solution of the gas-phase equations consumes the larger portion of the overall computational time. This technique iteratively solves the two (gas and particle) problems separately. Doing so

allows the use of advanced solution techniques for the gas-phase problem. As long as the coupling between the gas phase and the particles is relatively weak, the iterations converge rapidly, such that the overall convergence time is reduced. A relaxation factor can be used in cases where the coupling is strong.

The iteration algorithm is as follows:

1. Initialize all source terms due to particles as zero
2. Compute the gas-phase flame solution using the saved source terms due to particles
3. Use the gas-phase field to compute the solution of the particle-moments or section number density and surface species equations
4. Calculate new source terms for the gas phase due to particles.
5. Compute the effective source term as
   (1 - phi)*$NewSourceTerm$ + phi*$OldSourceTerm$
   where phi is the relaxation factor.
6. Repeat Steps *2* through *5* above until convergence.

Convergence is determined when the change in the computed gas-phase solution is below a user-specified tolerance.

Figure 19 Flowchart of segmented solver.

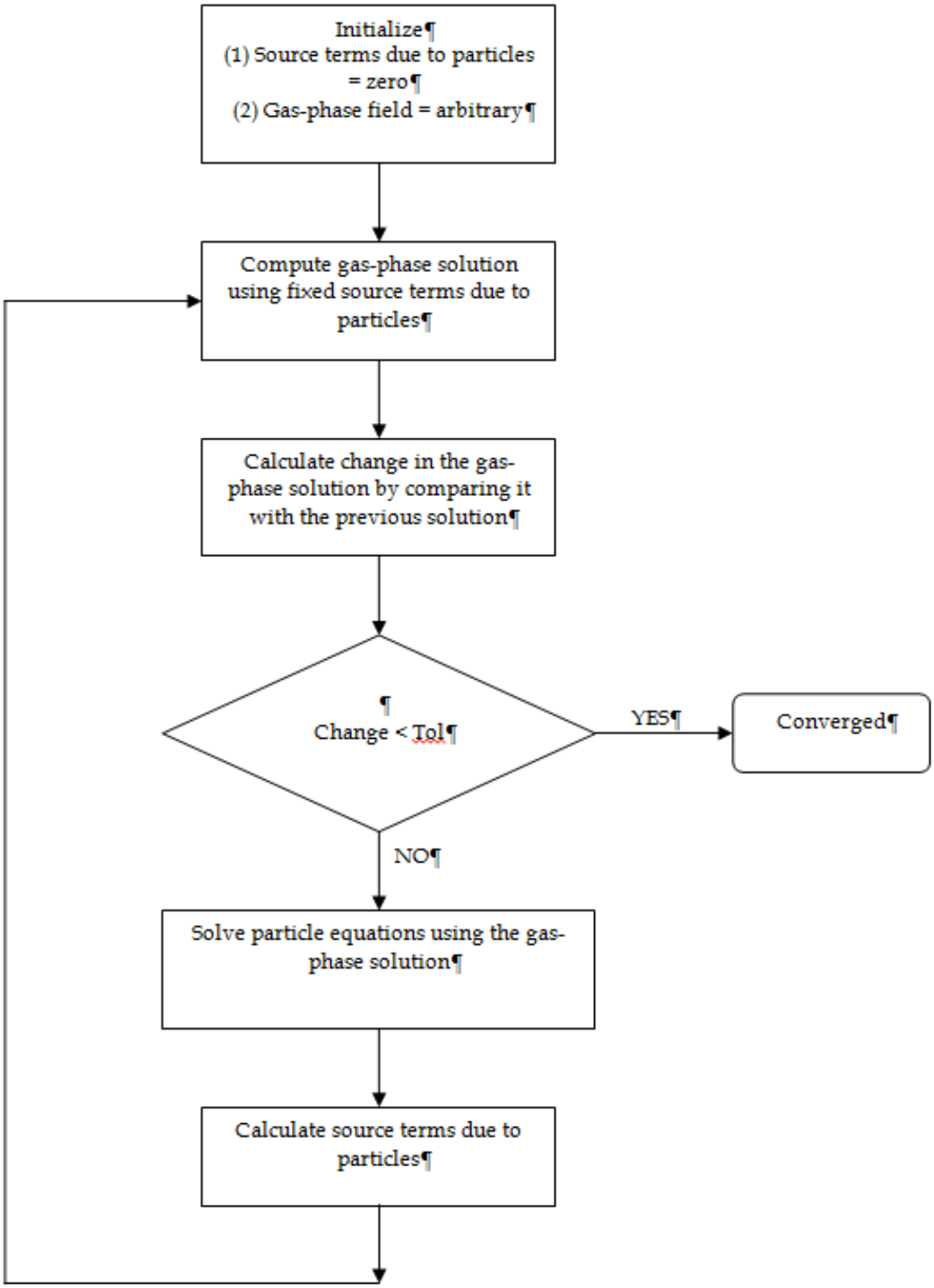

Figure 20 Steps in solution for particle equations for sectional model in flame simulations.

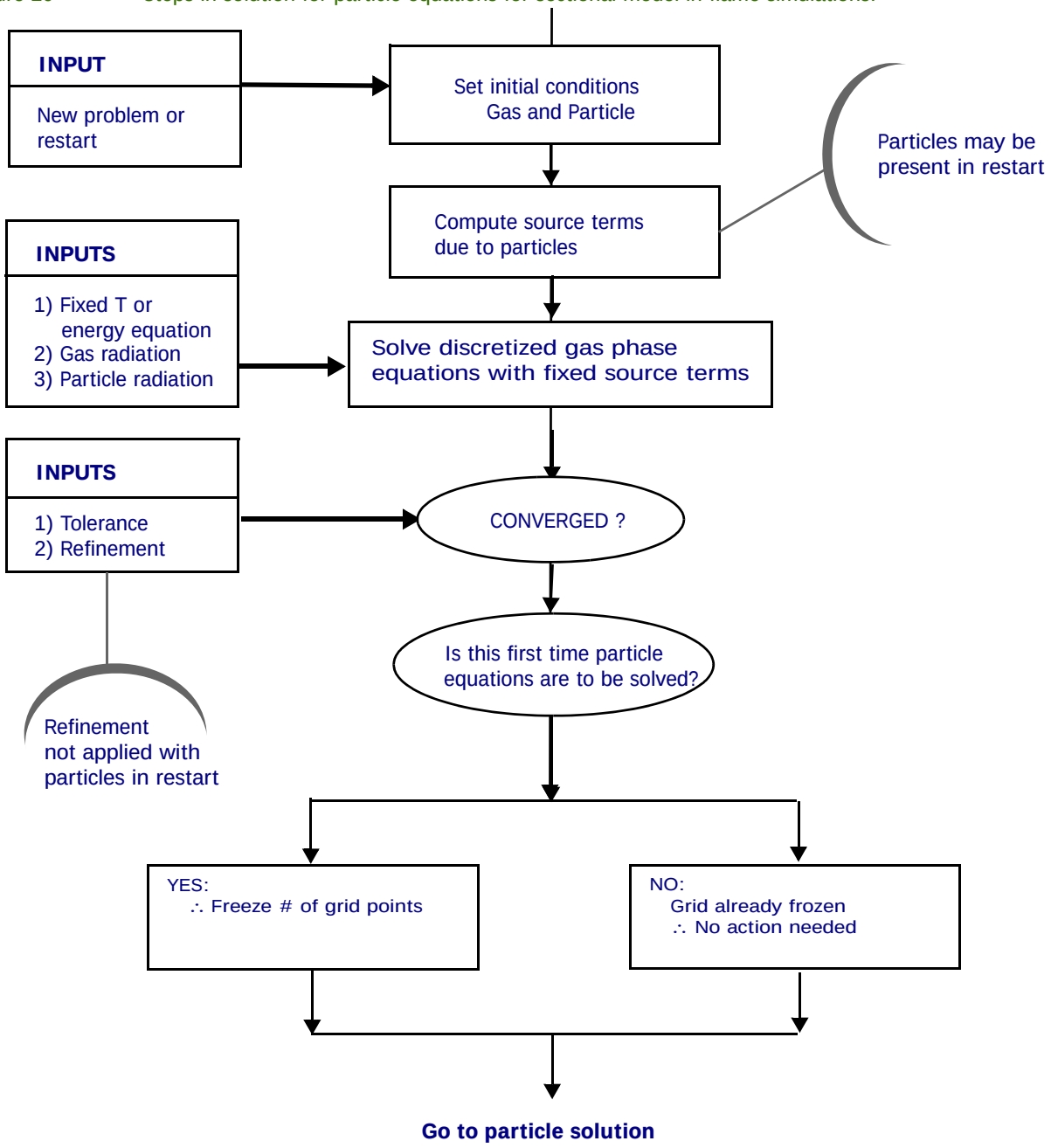

Figure 21 Expanding steps in solution for particle equations for sectional model in flame simulations.

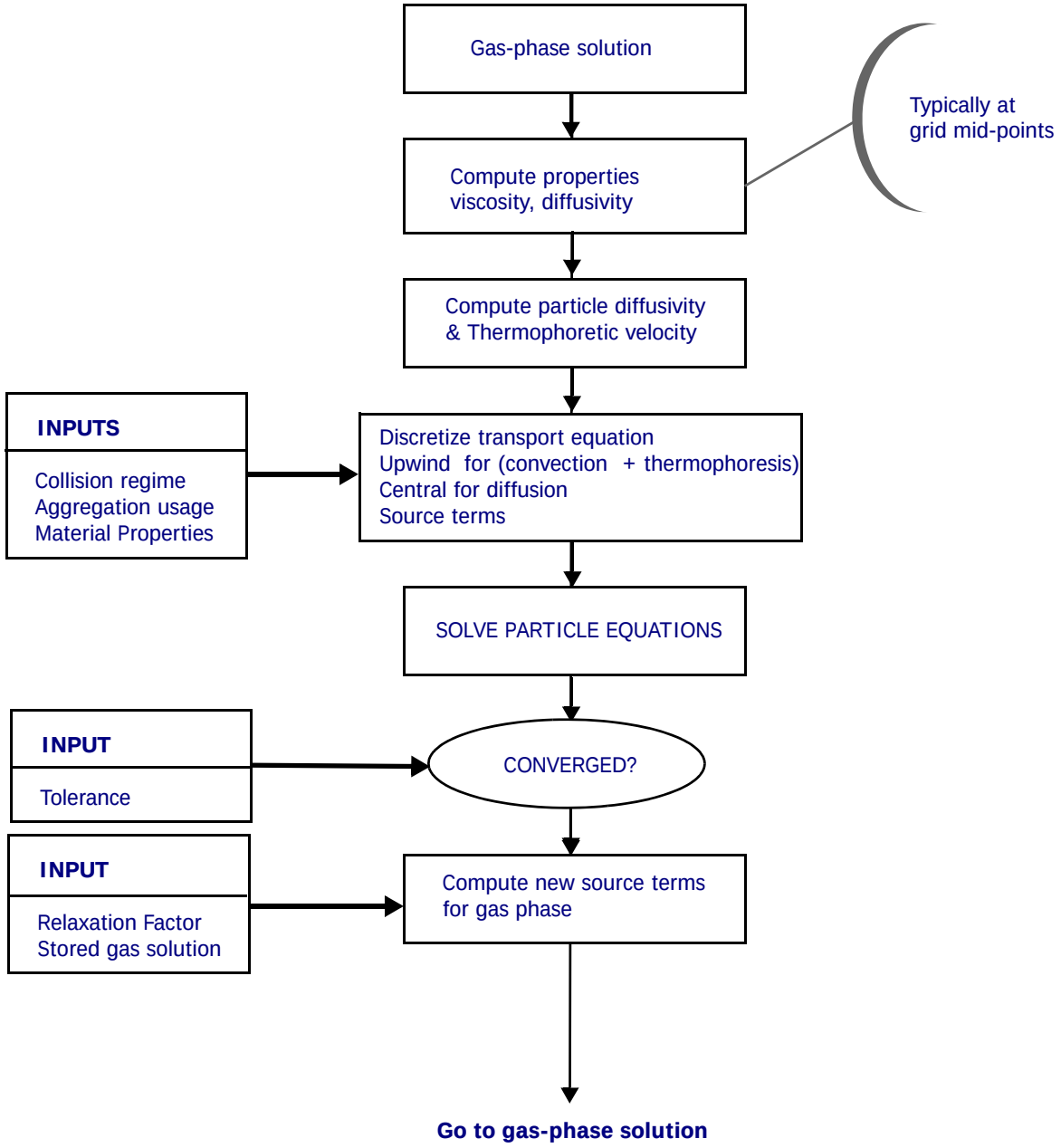

18.10 Summary of Particle Tracking Capabilities

The Particle Tracking feature provides an efficient numerical method for predicting particle formation and for tracking the evolution of particle size distributions in a reacting-flow simulation. This utility is built on proven technologies such as Chemkin's Surface Kinetics capabilities and the method of moments reported by Frenklach et al.[134,135,136] The innovation of the Particle Tracking module resides in the treatment

of particle inception, growth, and reduction processes. By expressing particle inception, growth, and reduction processes in terms of surface reactions, the user has full control over the particle growth kinetics. This implementation greatly simplifies the postulation and testing of different precursors and growth or consumption paths.

134. M. Frenklach and H. Wang, in *Soot Formation in Combustion: Mechanisms and Models*, H. Bockhorn (Ed.), Springer-Verlag, pp. 165-192 (1994).
135. J. Appel, H. Bockhorn, and M. Frenklach, *Combust. and Flame*, **121**:122-136 (2000).
136. M. Frenklach and S.J. Harris, *J. of Colloid and Interface Sci.*, **118**:252-261 (1987).

19

19 Uncertainty Analysis

Chemkin includes a generalized method for performing uncertainty analysis on reacting-flow simulations. The purpose is to determine the uncertainty of the solution as derived from the known uncertainties of one or more input parameters. In addition, the Uncertainty Analysis Facility determines the quantitative variance contribution from different inputs. This chapter provides the theoretical background for the methods used by the Uncertainty Analysis Facility.

A generic system model for chemical or materials processing can be described mathematically as:

Equation 19-1

$$\underline{y} = \underline{g}\left(\underline{y}, \underline{y}', \theta_1, \theta_2, \ldots, \theta_N\right)$$

where $\underline{y}$ is a vector of dependent variables and $\underline{g}$ is a set of differential equations that involve $\underline{y}$, the first derivative $\underline{y}'$, as well as *N* parameters θ_i. The parameters may be specified operating conditions, such as inlet temperatures or pressures, or they may be chemistry parameters such as reaction-rate coefficients. The dependent variables for this type of system would usually be chemical state variables, including pressure, temperature, species composition, and velocity components. In a deterministic approach to modeling the system, single values of the *N* parameters would be chosen, and a single result for $\underline{y}$ would be calculated. However, if θ_i is not a known constant but is better represented by a probability distribution function, $f(\theta_i)$, then the resultant $\underline{y}$ vector would also be a distribution of unknown shape and mean. Traditional methods for dealing with these stochastic problems are based on Monte-Carlo methods, where statistics on the mean and variance of $\underline{y}$ are collected based on solving $\underline{g}$ using random samplings of the distributions of θ_i values. Such methods are extremely time consuming and typically require very large numbers of model simulations (i.e., evaluations of $\underline{g}$) to produce meaningful statistics. Moreover, as the number of parameters *N* grows, the number of simulations required increases

exponentially with *N*. For such complex systems, then, the cost of Monte Carlo-based analyses is often prohibitive. In this chapter, a more computationally efficient method using polynomial chaos expansion is developed to solve the stochastic problems with large numbers of parameters.

19.1 Reducing the Dimensionality of the System through Polynomial Chaos Expansion

As mentioned above, one of the first obstacles encountered in performing uncertainty analysis on an arbitrary model is the dimensionality of the problem that arises from the number of uncertain parameters in the system. For example, we consider the evaluation of the expected value of a single model response in a multivariate system. The expected value is given as

Equation 19-2

$$E\left\{y\left(\underline{\theta}\right)\right\}=\int_{-\infty}^{\infty} y(\underline{\theta})\, f_{y(\underline{\theta})}\left(y\left(\underline{\theta}\right)\right) dy\left(\underline{\theta}\right)$$

where $\underline{\theta}=\left\{\theta_1,...,\theta_N\right\}$ is a set of uncertain parameters. Although the calculation is in the form of a one-dimensional integration, the lack of knowledge of the density function $f_{y(\underline{\theta})}\left(y\left(\underline{\theta}\right)\right)$ makes it impossible to solve. However, the one-dimensional integral can be expressed in a different form that is statistically equivalent:

Equation 19-3

$$E\left\{y\left(\underline{\theta}\right)\right\}=\int\ldots\int y(\underline{\theta})\, f_{\underline{\theta}}(\underline{\theta}) d\theta_1\ldots d\theta_N$$

where $f_{\underline{\theta}}\left(\underline{\theta}\right)$ is the joint density function of uncertain parameters $\theta=\{\theta_1\ldots\theta_N\}$. Unfortunately, the construction of the *N*-dimensional joint density function requires a prohibitively large number of samples. Furthermore, the numerical evaluation of the integral for a prescribed level of accuracy demands that the number of samples increase exponentially with the dimension *N*. To avoid this inherent dimensionality problem, we turn to principle-component techniques to reduce the dimension of the data through the implementation of polynomial chaos expansions.

Using polynomial chaos expansion, we can approximate the random parameters as summations in the form of

Equation 19-4

$$\underline{\theta}(\omega) = \sum_{j=0}^{\infty} a_j H_j[\underline{\xi}(\omega)] \cong \sum_{j=0}^{J} a_j H_j[\underline{\xi}(\omega)]$$

where $\underline{\theta}(\omega)$ denotes the distributions of $\underline{\theta}$, and $\underline{\xi}(\omega) = \{\underline{\xi}_1(\omega), \ldots, \underline{\xi}_N(\omega)\}$ is a vector of *independent* standard distributions that mimic the general behavior of $\underline{\theta}$ [137]. For example, a "standard" distribution might be a Gaussian distribution if θ_i behaves like a normal random variable. H_j is the j^{th}-derived multidimensional orthogonal polynomial functional (for example, Hermite polynomial), and a_j is the expansion coefficient to be determined by the characteristic values of the probability density function of θ_i. The transformation given in *Equation 19-4* uses a set of orthogonal polynomials to span the entire response space and allows projection of the *n*-dimensional data onto one-dimensional subspaces.

Next, before we can perform the change of variable for the integration parameter θ_i, we have to transform the multivariate probability density function $f_{\underline{\theta}}(\underline{\theta})$. A general form of orthogonal expansion for an arbitrary probability density function is given as

Equation 19-5

$$f_{\underline{\theta}}(\underline{\theta}) = p_{\underline{\theta}}(\underline{\theta}) \sum_{l=0}^{\infty} c_l L_l(\underline{\theta}) \cong p_{\underline{\theta}}(\underline{\theta}) \sum_{l=0}^{M_f} c_l L_l(\underline{\theta})$$

where $p_{\underline{\theta}}(\underline{\theta})$ is the *key probability density function*, $L_l(\bullet)$ is an orthogonal polynomial derived from $p_{\underline{\theta}}(\underline{\theta})$, and c_l are weighting coefficients. By *key probability density function,* we mean that the function should be either a "standard" probability density distribution (e.g., Gaussian) or a combination of such distribution functions, where the properties are well known and the function has a similar shape to that of the original $f_{\underline{\theta}}(\underline{\theta})$. With the projection of $\underline{\theta} = \{\theta_1, ..., \theta_N\}$ into the space of the independent random variables $\underline{\xi} = \{\underline{\xi}_1, \ldots, \underline{\xi}_N\}$ (given by *Equation 19-4*), the key probability density function can be transformed as

Equation 19-6

$$p_{\underline{\theta}}(\underline{\theta}) = p_{\underline{\xi}}(\underline{\xi}) = p(\xi_1, \ldots, \xi_N) = p_{\xi_1}(\xi_1) p_{\xi_2}(\xi_2) \cdots p_{\xi_N}(\xi_N)$$

Similarly, the derived orthogonal polynomial can be recast in terms of the independent random variables as

137. Ramkrishna, D., On Problem-specific Polynomials. Chemical Engineering Science, 1973. 28: p. 1362.

Equation 19-7

$$\sum_{l=0}^{M_f} c_l L_l(\underline{\theta}) = \sum_{l=0}^{M_f^*} u_l N_l(\underline{\xi})$$

where N_l is the transformed set of orthogonal polynomials and u_l are the new weighting coefficients. Substituting into *Equation 19-5*, the probability density function $f_{\underline{\theta}}(\underline{\theta})$ can be represented in terms of $\underline{\xi} = \{\xi_1, \ldots, \xi_N\}$ as follows

Equation 19-8

$$f_{\underline{\theta}}(\underline{\theta}) \cong \left\{\prod_{i=1}^{N} p_{\xi_i}(\xi_i)\right\}\left\{\sum_{l=0}^{M_f^*} u_l N_l(\underline{\xi})\right\}$$

Furthermore, the model response $y(\underline{\theta})$ can also be transformed into a summation of orthogonal polynomials as follows:

Equation 19-9

$$y(\underline{\theta}) = \sum_{l=0}^{\infty} b_l G_l(\xi_1(\omega),\ldots,\xi_N(\omega)) \cong \sum_{l=0}^{M_y} b_l G_l(\xi_1(\omega),\ldots,\xi_N(\omega))$$

where G_l is an algebraic function of the model-specific orthogonal polynomials $\left\{H_j^i(\underline{\xi})\right\}$, and b_l is another set of weighting coefficients.

With *Equation 19-8* and *19-9*, both the model response and its probability density function are transformed into the space of $\underline{\xi} = \{\xi_1, \ldots, \xi_N\}$. By careful selection of the type of orthogonal polynomials used in the transformations, the original integration given in *Equation 19-3* may be represented by

Equation 19-10

$$\begin{aligned} E\{y(\underline{\theta})\} = \int\cdots\int y(\underline{\theta}) f_{\underline{\theta}}(\underline{\theta}) d\theta_1 \cdots d\theta_N &\cong \prod_{k=1}^{N} \int \left\{\sum_{l=0}^{M} \alpha_l \psi_l(\xi_i)\right\} p_{\xi_i}(\xi_i) d\xi_i \\ &= \prod_{k=1}^{N} \left\{\sum_{l=0}^{M} \alpha_l \int \psi_l(\xi_i) p_{\xi_i}(\xi_i) d\xi_i\right\} \end{aligned}$$

where Ψ is an algebraic function of the model-specific orthogonal polynomials $\left\{H_j^i(\underline{\xi})\right\}$, based on G_l of *Equation 19-9* and N_l of *Equation 19-8*, and α_l are the combined weighting coefficients.

Thus, through polynomial chaos expansion techniques, we have successfully transformed the problem from one of solving the multi-dimensional integration in *Equation 19-3* to solving multiple one-dimensional integrations, which can be addressed through collocation method discussed in the next section.

For the approximations that allow us to get to *Equation 19-10* to hold, the transformation of the joint probability density function $f_{\underline{\theta}}(\underline{\theta})$, as well as the transformation of the response variable, must be based on orthogonal polynomials that are derived specifically from the probability density function of the fundamental variables $\{\xi_i\}$. The polynomial chaos expansion has the following properties:

- Any square-integrable random variable can be approximated as closely as desired by a polynomial chaos expansion
- The polynomial chaos expansion is convergent in the mean-square sense
- The set of orthogonal polynomials is unique given the probability density function
- The polynomial chaos expansion is unique in representing the random variable

For a given "standard" distribution function, there is a corresponding orthogonal expansion that meets these criteria. The correspondences between several important and common cases are given in *Table 19-1*. In general, problem-specific orthogonal polynomials can be derived by algorithms such as ORTHPOL[138, 139].

Table 19-1 Summary of General Orthogonal Expansions

Key Probability Density Function	*Polynomial for Orthogonal Expansion*	*Support Range*
Gaussian distribution	Hermite polynomials	(-∞, +∞)
Gamma distribution	Laguerre polynomials	(0, +∞)
Beta/uniform distribution	Jacobi/Legendre polynomial	Bounded, such as (0, 1)

19.2 Solving for the Coefficients of the Expansions

In this section, we describe more concretely how we determine the coefficients for the polynomial chaos expansions (PCE) described above. The expansion coefficients for the inputs are calculated using the characteristic information of the distribution of the input random variables. The coefficients for the probability density distribution of

138. Gautschi, W., Algorithm 726: ORTHPOL - A Package of Routines for Generating Orthogonal Polynomials and Gauss-type Quadrature Rules. ACS Transaction on Mathematical Software, 1994. 20(1): p. 21.
139. Szego, G., Orthogonal Polynomials. 1975, Providence, Rhode Island: American Mathematics Society.

the response surface and the error of approximation are obtained using a probabilistic collocation approach that takes advantage of the form of the polynomial chaos expansions to minimize the number of model simulations required for a given level of accuracy.

19.2.1 Polynomial Chaos Expansion for Uncertain (Variant) Input Parameters

For the probability distribution functions (PDFs) of the input data, the user will supply the characteristics of the PDF (mean, variance, lower bound, upper bound, etc.). The expansion coefficients for the inputs are calculated using the characteristic information and the standard unit distribution for the particular PDF. The number of the terms in the expansion will depend on the type of the PDFs that characterize the model inputs. For a normal distribution, for example, the expansion will be defined with two coefficients, representing the mean and the variance (standard deviation), because these values can represent the input distribution in terms of the standard normal distribution.

19.2.2 Polynomial Chaos Expansion for the Model Outputs

Once the PCEs for the model inputs are determined, the next step is to approximate the probability density distribution of the model response variable. In this case, we use the problem-specific polynomials derived from the probability density functions of the uncertain input parameters. For example, if the input parameters were characterized by normal distributions, then we use Hermite polynomials for the model output expansions, as determined by *Table 19-1*. The general form of the expansion for an output variable *y* is then

Equation 19-11

where ξ_i are the standard, independent, random variables used to describe the variant model inputs and $\{u_j\}$ are coefficients that need to be determined. In general, *Equation 19-11* will include terms corresponding to each of the input parameters plus cross-link terms for all the combinations that are relevant for the specified order of approximation. For example, a 3rd-order Hermite polynomial expansion of a model response that considers two random input parameters would have terms corresponding to those listed in *Table 19-2* below.

Table 19-2 Terms for a 3rd-Order Hermite Polynomial Expansion with Two Parameters

j	$H_j(\xi_1)$	$H_j(\xi_2)$	$H_j(\xi_1, \xi_2)$

$$y(\omega) \approx \sum_{j=1}^{J} u_j H_j(\{\xi_i(\omega)\})$$

Table 19-2 Terms for a 3rd-Order Hermite Polynomial Expansion with Two Parameters

1	ξ_1	ξ_2	
2	$\xi_1^2 - 1$	$\xi_2^2 - 1$	$\xi_1\xi_2$
3	$\xi_1^3 - 3\xi_1$	$\xi_2^3 - 3\xi_2$	$\xi_1(\xi_2^2 - 1)$, $\xi_2(\xi_1^2 - 1)$

19.2.3 Selecting the Points for Model Evaluation

To solve for this set of coefficients, we need to evaluate the model at special "points" in the ξ_i space. First, we can define the residual of the problem that we would like to minimize. For the deterministic set of model equations (i.e., the "black-box" model), the residual is given by $R\left(\underline{y},\underline{\theta}\right) = 0$, assuming fixed values for $\underline{\theta}$ and an invariant set of values for $\underline{y}$. For the stochastic problem, where $\underline{\theta}$ and $\underline{y}$ are distributions, the probabilistic residual becomes:

Equation 19-12

$$\int \ldots \int f_{\underline{\theta}}(\underline{\theta}) R\left(\underline{y}(\omega), \underline{\theta}(\omega)\right) d\theta_1 \ldots d\theta_N = 0$$

Applying PCEs, *Equation 19-12* is transformed to

Equation 19-13

$$\int_{-\infty}^{\infty} \ldots \int_{-\infty}^{\infty} f_{\underline{\xi}}\left(\underline{\xi}\right) R\left(\left\{u_j\right\}, \underline{\xi}\right) w_k\left(\underline{\xi}\right) d\xi_1 \cdots d\xi_N = 0$$

where $\{w_k(\xi)\}$ is a set of approximating functions (basis functions) that are orthogonal, such that the inner product of the residual and each member of the set of approximating functions is equal to zero[140]. The residual is now cast in terms of $\{u_j\}$, which are the set of coefficients of the polynomial chaos expansions of the $\underline{y}$ vector of outputs.

140. Tatang, M.A., Direct Incorporation of Uncertainty in Chemical and Environmental Engineering Systems. Ph.D. Thesis, 1995, Department of Chemical Engineering, Massachusetts Institute of Technology, Cambridge.

In order to solve *Equation 19-13* using an arbitrary "black-box" model, we need to find a way to perform the integration without knowing the exact form of the residual. This can be achieved using a special quadrature method, collocation, described by Tatang and Wang[140, 141], where the model is evaluated at a finite number of points. The key to this method is that it selects points corresponding to the roots of the "key" polynomials used in the response PCEs in place of the basis functions $\{w_k(\xi)\}$ in *Equation 19-13*. As a result, the residual minimization problem becomes:

Equation 19-14

$$\int_{-\infty}^{\infty} \cdots \int_{-\infty}^{\infty} f_{\underline{\xi}}(\underline{\xi}) R\left(\{u_j\}, \underline{\xi}\right) \delta\left(\underline{\xi} - \underline{\xi}^k\right) d\xi_1 \cdots d\xi_N = 0$$

where $\underline{\xi}^k$ are the collocation "points" or sets of $\underline{\xi}$ values where the model residual will be minimized. *Equation 19-14* is equivalent to:

Equation 19-15

$$R(\{u_j\}, \{\xi_i\})|_{\{\xi_i\}=\{\xi_i^j\}} = 0; \qquad k = 1, \ldots, K$$

where K is the number of collocation points required to determine the $\{u_j\}$ coefficients. In this way, the collocation method transforms the stochastic model into a deterministically equivalent model, because it solves the deterministic model at several chosen values of uncertain parameters.

The collocation method uses the roots of the key polynomial as the sampling points, because these points provide good coverage of the distribution function, capturing high-probability and transition regions. This is illustrated in *Figure 19-1*, where the location of the collocation points for a normal distribution (roots of the Hermite polynomial) are compared with the Monte Carlo approach that requires many more sampling points. The roots of Hermite polynomials are given in *Table 19-3* below. In the collocation method, we take the roots of the polynomial that represents one order higher than the one used in the PCEs of the model outputs. This choice is made to allow more of the sampling points to be high-probability points than would be possible if the roots were of the same order as the PCEs. Because of this choice, however, we have more roots than we need to define the sampling points. To select the collocation points, we start by defining an anchor point. The anchor point is the one consisting of the highest-probability root for all ξ_i values. We then fill in the remaining points by substituting the highest-probability root for the next-highest-probability root successively into each of the ξ_i values. This process is repeated until we have defined the K collocation points necessary to determine the response coefficients.

141. Wang, C., Parametric Uncertainty Analysis for Complex Engineering Systems. Ph.D. Thesis, 1999, Department of Chemical Engineering, Massachusetts Institute of Technology, Cambridge.

Figure 19-1 Comparison of collocation points for normal PDF and sampling points for Monte Carlo method

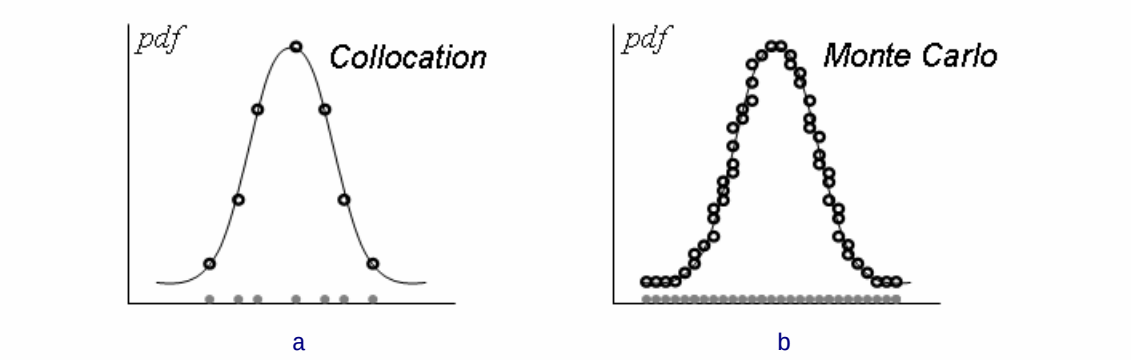

(a) Location of the collocation points that correspond to roots of the Hermite polynomial expansion for a normal probability distribution function (PDF) and (b) sampling points necessary using a Monte Carlo method to achieve the same resolution of the PDF

Table 19-3 Roots of Hermite Polynomials

j	$H_j(x)$	***Location of zeros*** *(in the order of their probability)*
1	x	0
2	$x^2 - 1$	±1
3	$x^3 - 3x$	0, ±1.7321
4	$x^4 - 6x^2 + 3$	±0.7420, ±2.3344
5	$x^5 - 10x^3 + 15x$	0, ±1.3556, ±2.8570
6	$x^6 - 15x^4 + 45x^2 - 15$	±0.6167, ±1.8892, ±3.3243
7	$x^7 - 21x^5 + 105x^3 - 105x$	0, ±1.1544, ±2.3668, ±3.7504
8	$x^8 - 28x^6 + 210x^4 - 420x^2 + 105$	±0.5391, ±1.6365, ±2.8025, ±4.1445
9	$x^9 - 36x^7 + 378x^5 - 1260x^3 + 945x$	0, ±1.0233, ±2.0768, ±3.2054, ±4.5127

19.2.4 Solving for the Expansion Coefficients for the Model Outputs

Once the collocation points have been defined, we can translate these ξ_i values into sets of model input parameters, θ_i. We then run the "black-box" model for each of these cases, and collect the resulting values for each of the uncertain output variables. With the output values, we can construct K equations for the $\{u_j\}$ coefficients. This matrix of algebraic equations can then be solved using standard linear-algebra techniques. With the coefficients determined, we now have the complete PDFs defined for all of the variant model outputs. This allows us to perform a variety of analyses including error estimation, expected value, and variance analysis, discussed further below.

19.2.5 Determining the Error of the Approximation

After obtaining the coefficients of the expansions, we need to evaluate the accuracy of the current approximation to make sure that it meets the requirements of the user. To accomplish this, a few more runs of the model are required to allow comparison of the model results with the approximation results. First we define the deviation of the expansion for one of the model output variables to be:

Equation 19-16

$$\Delta = y\left[\left\{\theta_i\left(\xi_i\right)\right\}\right] - \sum_{j=1}^{J} u_j H_j(\{\xi_i\})$$

where $y\left[\left\{\theta_i\left(\xi_i\right)\right\}\right]$ is the model evaluation for a set of ξ_i values and the right-hand summation is the polynomial approximation of y for the same ξ_i values. The error of approximation is defined as the product of the square of the deviation Δ and the joint probability density function of uncertain parameters evaluated at the collocation points.

Equation 19-17

$$\varepsilon_l = \Delta_l^2 \bullet f_{\{\xi_i\}}(r_l)$$

In order to estimate the error of approximation, we need to use collocation points that were not used previously in the solution of the problem. Here again we want points that represent high probabilities, so we need to use a polynomial of a different order than the one used in the solution of the output expansion coefficients. We choose to obtain the points for the error estimation from the key polynomial of the next higher order from the one used in the solution. The main reason for this choice is to accommodate a software system that is designed to iteratively reduce the error by extending the order of the polynomial expansions as needed. In other words, if we fail the error-test, we will need the results of running collocation points that correspond to the next order anyway. Therefore, if we are going to have to run the model, we might as well run it at points where the results can be re –used in case the error is not acceptable. To estimate the error, we use L collocation points, where L should be greater than the K collocation points used in the solution in order to adequately test the approximation over the distribution. To this end, we define L somewhat arbitrarily as equal to the number of original collocation points K plus the number of input parameters N.

To test against our error criteria we accumulate the error for each output variable over the new collocation points. Then the sum-square-root (SSR) error is calculate as the following:

Equation 19-18

$$\mathrm{SSR} = \sqrt{\frac{\sum_{l=1}^{L} \varepsilon_l}{K f_{\{\xi_i\}}(\{\xi_i^l\})}}$$

and the relative sum-square-root (RSSR) error is:

Equation 19-19

$$\mathrm{RSSR} = \frac{\mathrm{SSR}}{E\{y\}} = \frac{\mathrm{SSR}}{u_1}$$

where $E\{y\}$ is the expected value of y, which in most cases will be equal to the first coefficient of the expansion, u_1. Notice that the joint probability density function at the anchor point is used to normalize the SSR calculation. Since the SSR is usually dependent on the magnitude of the expected value, the RSSR is a more useful measure of the error. The degree of accuracy required will be specific to a problem and most likely will be specified by the user in the form of absolute and relative tolerances. Such tolerances may be different for different output variables.

19.2.6 Variance Analysis

For most applications of uncertainty analysis, it is very important to obtain not just the response surface for the outputs, but also the variance contribution from each uncertain input parameter. Such information can be used as screening criteria, as weighting factors to guide the refinement of a model, or as the basis for robust-design decisions.

From the polynomial chaos expansion of the model response variables, we have

Equation 19-20

$$y \approx \sum_j u_j H_j\left(\{\xi_i\}\right)$$

the variance contribution from the uncertain parameters can be evaluated as

Equation 19-21

$$\sigma_y = E\left\{\left(\sum_j u_j H_j\left(\{\xi_i\}\right)\right)^2\right\} - \left(E\left\{\sum_j u_j H_j\left(\{\xi_i\}\right)\right\}\right)^2$$

Since the polynomials $\left\{H_j\left(\{\xi_i\}\right)\right\}$ are all orthogonal, the expected value of cross products becomes zero. For all of the special polynomials listed in *Table 19-1*, we also have

Equation 19-22

$$E\{H_j(\{\xi_i\})\} = \int_{\{\xi_i\}} f_{\{\xi_i\}}(\{\xi_i\}) H_j(\{\xi_i\}) d\{\xi_i\} = 0 \quad for\ \forall j$$

Therefore the variance can be simplified as

Equation 19-23

$$\sigma_y = \sum_j u_j^2 E\left\{\left(H_j\left(\{\xi_i\}\right)\right)^2\right\}$$

This simple relationship between the polynomial chaos expansion coefficients and the variance contribution from all of the uncertain parameters suggests that the contribution of each input parameter can be determined from the relevant terms in the variance calculation. Then all of the terms involving only ξ_1 account for the variance contribution of the input parameter θ_1, while all of the terms involving only ξ_2 account for the variance contribution of θ_2. For the cross terms involving both ξ_1 and ξ_2, the variance contribution to the response variable is apportioned between θ_1 and θ_2, respectively.

From the variance analysis, the relative importance of uncertain input parameters can be determined simply by their contribution to the variance of the model response variable. Therefore, for large and complicated physical models, the user can readily identify the primary sources of both simulation and approximation error. This information can be used to focus resources on reducing the distribution of the output predictions by narrowing the spread of certain inputs. In addition, as we iteratively improve the error tolerances through additional model runs to extend the polynomial expansions, the variance contributions of the parameters can be used to determine which parameters need to be refined and which do not. This approach will assure the most effective use of resources in solving a particular problem.

20

20 Tear-stream Algorithm

Complex reactor networks defined in Chemkin allow for mass flow or information to flow upstream in a series of simulations. Solution of such networks requires a tear-stream algorithm. In this section, we describe the tear-stream algorithm implemented in Chemkin in some detail and the expected advantages and disadvantages of using this approach with a reactor-network simulation.

20.1 An Overview of Tearing

Tearing is a way of "breaking up" or tearing dependencies in a model formulation. It can be used in *equation based* (EO) or *sequential modeler* (SM) environments. The principle is to tear certain dependencies in the model or flowsheet and then attempt to "close" the tear using inner-outer fixed point iterations. The idea is that the inner-outer problem is easier or faster to solve than the original problem, even though several outer iterations may be required to close the tears.

20.2 Mathematical Description

In the most general case, suppose we have a set of N nonlinear equations

Equation 20-1

$$F(X) = 0$$

where X is a vector of N unknowns. When tearing is applied to *Equation 20-1* it is rewritten as:

Equation 20-2

$$g(\Theta, Y) = 0 \quad \}$$

$$G(\Theta, Y) = 0 \quad \}$$

where

g is the set of N_{torn} torn equations;
G is the set of ($N - N_{torn}$) remaining equations;
Θ is the set of N_{torn} torn variables of X;
Y the set of remaining variables in X.

The problem (*Equation 20-2*) is solved using an inner-outer iteration where in each outer iteration $g(\Theta,Y) = 0$ is solved for Θ alone and for each inner iteration, $G(\Theta,Y) = 0$ is solved for Y alone with Θ held fixed at value from the previous solution of $g(\Theta,Y) = 0$.

It is important that the choice of g, G and Θ is done using knowledge of the underlying mathematical model so that the tears make engineering sense. Otherwise the inner-outer solution to *Equation 20-2* may not converge or give a solution that is not a solution of *Equation 20-1*.

20.3 Tearing algorithm

The tearing algorithm consists of the following steps:

1. Let i=1 and assume there is an initial guess Θ_0 and Y_0 to *Equation 20-2*.
2. Solve $g(\Theta_i, Y_{i-1}) = 0$ for Θ_i (update torn variables) "outer iteration"
3. Solve $G(\Theta_i, Y_i) = 0$ for Y_i "inner iteration"
4. If $\left\|\Theta_i - \Theta_{i-1}\right\| \succ \text{Tear\_tol}$ then i=i + 1 and goto 2

Here, "Tear_tol" is the convergence error tolerance for the outer loop, typically specified by the user. In practice it is also wise to limit the number of tear iterations to some maximum value in case of non-convergence. Therefore the jump in *step 4* back to *step 2* is done provided i is less than some maximum number of tear iterations allowed.

Convergence is obtained if and only if:

Equation 20-3

$$\left|\Theta_k - \Theta_{k-1}\right| \leq \text{Tear}_{\text{Rel}} \left|\Theta_{k-1}\right| + \text{Tear}_{\text{Abs}} \quad \text{for } k=1,2,\ldots,N_{torn}$$

where $Tear_{Rel}$ and $Tear_{Abs}$ are the relative and absolute tear tolerances, respectively. In other words, we iterate until the "tear convergence ratio" is less than unity, i.e.,

Equation 20-4

$$\left|\Theta_k - \Theta_{k-1}\right| / \left(\mathrm{Tear}_{\mathrm{Rel}} \left|\Theta_{k-1}\right| + \mathrm{Tear}_{\mathrm{Abs}}\right) \le 1 \qquad \text{for all } k$$

This is both a relative and absolute convergence test. The test is absolute when Θ_k becomes close to zero and relative otherwise. It avoids using an explicit switch from a relative to absolute test when Θ_k tends towards zero.

To make the progress of the tear algorithm transparent to the user, convergence information is reported per outer iteration and includes:

1. The current iteration number "i".
2. The maximum value of $|\Theta_k - \Theta_{k\text{-}1}| \ / \ (Tear_{Rel} |\Theta_{k\text{-}1}| + Tear_{Abs})$ (the tear convergence ratio) over all k, together with the corresponding variable name corresponding to the maximum value (which is the tear stream that is showing the current largest error).
3. A diagnostic option of showing the p (default 0) largest values of the tear convergence ratios, listed in order from largest to smallest. This shows the streams that are hardest to converge (or close).

An iterative scheme based on Newton's method, is used to solve $G(\Theta_i , Y_i) = 0$ in *step 3* of the algorithm and typically this will find a solution within some prescribed non-linear equation residual or variable tolerance. Therefore the choice of values for $Tear_{Rel}$ and $Tear_{Abs}$ should take into account (and generally be larger than) the tolerances used to solve $G(\Theta_i , Y_i) = 0$.

In the formulation above, the torn equations $g(\Theta_i, Y_{i\text{-}1}) = 0$ are non-linear and also require an iterative scheme to solve for Θ_i . However in practice the torn equations are usually linear in Θ_i and therefore easy to solve and usually in one of the following forms:

1. $\Theta_i(j) = func(j)\left(Y_{i-1}\right)$ where *func* is a user-prescribed function that maps $Y_{i\text{-}1}$ to Θ_i (j), for example, a chemical properties procedural calculation;
2. $\Theta_i(j) = Y_{i-1}(j)$ — i.e., stream connectivity equations — in the case of torn recycle streams.

Nomenclature

"In the discussions and equations in this manual, "log" means $\log_{10}$, and "ln" means "natural logarithm".

21.1 Latin Equation Symbols

The table below shows the conventions used in this document for Latin equation symbols.

Latin Symbols

Symbol	*Description*	*Chapter*	*CGS Units*
a_i	Pre-exponential factor in sticking coefficient expression	*Chapter 4*	none
a_k	Activity of the *k*th bulk-phase species	*Chapter 4*, *Chapter 8*	none
a_k^o	Standard state specific Helmholtz free energy of the *k*th species	*Chapter 2*, *Chapter 4*	ergs/g
a_{nk}	Coefficients of fits to thermodynamic data	*Chapter 4*	depends on n
$\bar{a}$	Mean specific Helmholtz free energy of a mixture	*Chapter 2*	ergs/g

Latin Symbols (Continued)

Symbol	Description	Chapter	CGS Units
A	Total surface area of all materials in the reactor	Chapter 8	cm^2
	Cross-sectional area of the stream tube encompassing the flame	Chapter 12	cm^2
	Cross-sectional area available for flow downstream of the shock wave	Chapter 7	cm^2
	Surface Area	Chapter 4	cm^2
$\overline{A}$	Mean molar Helmholtz free energy of a mixture	Chapter 2	ergs/mole
A_k^o	Standard state molar Helmholtz free energy of the *k*th species	Chapter 2	ergs/mole
A_i	Pre-exponential factor in the rate constant of the *i*th reaction	Chapter 3, Chapter 4, Chapter 12, Chapter 14	depends on reaction
A_m	Surface area of the *m*th material	Chapter 8	cm^2
b_i	Temperature exponent in sticking-coefficient expression	Chapter 4	none
c_k	Concentration of the *k*th species (gas-phase or bulk-phase)	Chapter 8	$mole/cm^3$
	Concentration of the *k*th species (surface-phase)	Chapter 8	$mole/cm^2$
c_i	Activation energy in sticking-coefficient expression. By default, GAS-PHASE KINETICS and SURFACE KINETICS uses activation energies in thermal calories instead of ergs.	Chapter 4	cal/mole
c_p	Specific heat at constant pressure of gas mixture	Chapter 7, Chapter 11, Chapter 12, Chapter 14	ergs/(g K)

Latin Symbols (Continued)

Symbol	Description	Chapter	CGS Units
c_{pk}	Specific heat capacity at constant pressure of the *k*th species	Chapter 2, Chapter 4, Chapter 5, Chapter 7, Chapter 8, Chapter 11, Chapter 12, Chapter 14	ergs/(g K)
$c_{pk,\,\mathrm{int.}}$	Internal contribution to the mass specific heat of the *k*th species	Chapter 5	ergs/(g K)
$c_{pk,\,\mathrm{rot.}}$	Rotational contribution to the mass specific heat of the *k*th species	Chapter 5	ergs/(g K)
c_{vk}	Specific heat capacity at constant volume of the *k*th species	Chapter 2	ergs/(g K)
$\bar{c}_p$	Mean specific heat capacity at constant pressure	Chapter 2	ergs/(g K)
$\bar{c}_v$	Mean specific heat capacity at constant volume	Chapter 2	ergs/(g K)
C	Compression ratio for the IC HCCI engine model	Chapter 8	none
	Ratio defined by shock tube equations.	Chapter 7	none
C_{pk}	Molar heat capacity at constant pressure of the *k*th species	Chapter 2	ergs/(mole K)
C_D	Turbulent scalar-to-mechanic time scale ratio	Chapter 9	none
C_{pk}^{o}	Standard state molar heat capacity at constant pressure of the species	Chapter 2, Chapter 14	ergs/(mole K)
$C_{pk,\,\mathrm{trans.}}$	Translational contribution to the molar heat capacity of the *k*th species	Chapter 5	ergs/(mole K)
$C_{pk,\,\mathrm{vib.}}$	Vibrational contribution to the molar heat capacity of the *k*th species	Chapter 5	ergs/(mole K)

Latin Symbols (Continued)

Symbol	Description	Chapter	CGS Units
$C_{pk,\,\mathrm{rot.}}$	Rotational contribution to the molar heat capacity of the *k*th species	Chapter 5	ergs/(mole K)
C_{vk}	Molar heat capacity at constant volume of the *k*th species	Chapter 2	ergs/(mole K)
C_{ϕ}	Modeling constant for the IEM model	Chapter 9	none
$\overline{C}_p$	Mean molar heat capacity at constant pressure	Chapter 2, Chapter 9	ergs/(mole K)
$\overline{C}_v$	Mean molar heat capacity at constant volume	Chapter 2	ergs/(mole K)
$\dot{C}_k$	Chemical creation rate of the *k*th species	Chapter 3	mole/(cm^3 sec)
D	Cylinder bore diameter for the IC HCCI engine model	Chapter 8	cm
D_h	Hydraulic diameter (4 times the ratio of the cross-sectional area of the tube to the perimeter of the tube)	Chapter 7	cm
D_k^T	Thermal diffusion coefficient of the *k*th species	Chapter 4, Chapter 5, Chapter 11 Chapter 12, Chapter 13, Chapter 14	g/(cm sec)
$D_{k,\,j}$	Ordinary multicomponent diffusion coefficient of the species k in species j	Chapter 4, Chapter 5, Chapter 11, Chapter 12	cm^2/sec
D_{kj}	Binary diffusion coefficient of species k in species j	Chapter 5, Chapter 12,Chapter 14	cm^2/sec
D_{km}	Mixture-averaged diffusion coefficient of the *k*th species	Chapter 5, Chapter 11, Chapter 12, Chapter 14	cm^2/sec

Latin Symbols (Continued)

Symbol	Description	Chapter	CGS Units
$\dot{D}_k$	Chemical destruction rate of the *k*th species	*Chapter 3*	mole/(cm^3 sec)
E_i	Activation energy in the rate constant of the *i*th reaction. By default, GAS-PHASE KINETICS and SURFACE KINETICS uses activation energies in thermal calories instead of ergs.	*Chapter 3*, *Chapter 4*	[cal/mole]*
		Chapter 12, *Chapter 14*	ergs/mole
E_{ion}	Energy of a positive ionic species	*Chapter 4*	[cal/mole]*
$E_{\text{ion, 0}}$	Energy threshold in ion-energy-dependent reactions	*Chapter 4*	[cal/mole]*
$E_{\text{yield, 0}}$	Energy threshold in reaction yield expression	*Chapter 4*	[cal/mole]*
f_i	Exponential constant in ion-energy-dependent reactions	*Chapter 4*	none
F_{ki}	Forward reaction-order specified for the *k*th species in *i*th reaction	*Chapter 3*, *Chapter 4*	none
g	Acceleration of gravity	*Chapter 11*	cm/sec^2
g_i	Exponential constant in ion-energy-dependent reactions	*Chapter 4*	none
g_k^o	Standard state specific Gibb's free energy for the *k*th species	*Chapter 2*	ergs/g
$\bar{g}$	Mean specific Gibb's free energy of a mixture	*Chapter 2*	ergs/g
G	Small number (e.g. 1.E-12)	*Chapter 5*	none
G_k	Linear growth rate for the *k*th bulk species	*Chapter 4*, *Chapter 8*, *Chapter 11*, *Chapter 14*	cm/sec
G_k^o	Standard state molar Gibb's free energy for the *k*th species	*Chapter 2*, *Chapter 4*	ergs/mole

Latin Symbols (Continued)

Symbol	Description	Chapter	CGS Units
$\overline{G}$	Mean molar Gibb's free energy of a mixture	Chapter 2	ergs/mole
h_k	Specific enthalpy of the *k*th species	Chapter 2, Chapter 4, Chapter 5, Chapter 7, Chapter 8, Chapter 11, Chapter 12, Chapter 14	ergs/g
	Specific enthalpy of the *k*th species	Chapter 9	ergs/mole
h_t	Heat transfer coefficient	Chapter 8	ergs/(sec K)
$\tilde{h}_e$	Specific enthalpy of the electron upon creation of the gas-phase	Chapter 8	ergs/g
$\bar{h}$	Mean specific enthalpy of a mixture	Chapter 2, Chapter 7	ergs/g
h_{yield}	Multiplicative factor in reaction yield expression	Chapter 4	depends on reaction
H_f	Enthalpy of formation	Chapter 4	ergs/mole
H_k^o	Standard state molar enthalpy of the *k*th species	Chapter 3, Chapter 4	ergs/mole
H_k	Molar enthalpy of the *k*th species	Chapter 3, Chapter 4	ergs/mole
$\overline{H}$	Mean molar enthalpy of a mixture	Chapter 2	ergs/mole
I	Total number of reactions	Chapter 3, Chapter 4, Chapter 8, Chapter 14	none
j_k	Flux of gas-phase species k into the surface	Chapter 14	mole/(cm^2 sec)
j_k	Diffusive mass flux of the *k*th species	Chapter 5	ergs/g

Latin Symbols (Continued)

Symbol	Description	Chapter	CGS Units
J	Jacobian matrix	Chapter 12	none
	Total number of grid points	Chapter 14	none
k_B	Boltzmann Constant	Chapter 5	ergs/K
k_{fi}	Forward rate constant of the *i*th reaction	Chapter 3, Chapter 4, Chapter 12	depends on reaction
k_{ri}	Reverse rate constant of the *i*th reaction	Chapter 3, Chapter 4	depends on reaction
K	Total number of species	Chapter 3, Chapter 4, Chapter 5, Chapter 8, Chapter 12, Chapter 14	none
K_b	Total number of bulk species	Chapter 4, Chapter 11, Chapter 14	none
$K_b(m)$	Total number of bulk species on the *m*th material.	Chapter 8	none
K_b^f	Index of the first bulk-phase species in the first bulk phase	Chapter 14	none
$K_b^f(n)$	Index of the first bulk species	Chapter 11	none
	Index of the first bulk-phase species in phase n	Chapter 4	none
$K_b^f(n, m)$	Index of the first bulk-phase species in phase of the *m*th material	Chapter 8	none
K_b^l	Index of the last bulk-phase species in the last bulk phase	Chapter 14	none
$K_b^l(n)$	Index of the last bulk-phase species in phase n	Chapter 4, Chapter 11	none
$K_b^l(n,m)$	Index of the last bulk-phase species in phase of the *m*th material.	Chapter 8	none

Latin Symbols (Continued)

Symbol	Description	Chapter	CGS Units
K_{ci}	Equilibrium constant in concentration units for the *i*th reaction	Chapter 3, Chapter 4, Chapter 14	depends on reaction
K_g	Total number of gas-phase species	Chapter 4, Chapter 8, Chapter 11, Chapter 14	none
K_g^f	Index of the first gas-phase species	Chapter 4, Chapter 8, Chapter 14	none
K_g^l	Index of the last gas-phase species	Chapter 4, Chapter 8, Chapter 14	none
K_{pi}	Equilibrium constant in pressure units for the *i*th reaction	Chapter 3, Chapter 4, Chapter 14	depends on reaction
K_s	Total number of surface species	Chapter 4, Chapter 11, Chapter 14	none
$K_s(m)$	Total number of surface species on the *m*th material	Chapter 8	none
K_s^f	Index of the first surface-phase species in the first surface phase	Chapter 14	none
$K_s^f(n)$	Index of the first surface species in phase n	Chapter 4, Chapter 11	none
$K_s^f(n,m)$	Index of the first surface species in phase n of the *m*th material	Chapter 8	none
K_s^l	Index of the last surface-phase species in the last surface phase	Chapter 14	none
$K_s^l(n)$	Index of the last surface species in phase n	Chapter 4, Chapter 11	none
$K_s^l(n,m)$	Index of the last surface species in phase n of the *m*th material	Chapter 8	none

Latin Symbols (Continued)

Symbol	Description	Chapter	CGS Units
K_{phase}	Array containing the number of species in each phase	Chapter 4, Chapter 14	none
$K_{\text{phase}}(m)$	Array containing the number of species in each phase for material m	Chapter 8	none
l_m	Distance between the shock and the contact surface at infinite distance from the diaphragm	Chapter 7	cm
$L_{n,\,m}$	Film-thickness length scale	Chapter 8	cm
L_A	Crank-arm length for the IC HCCI engine model	Chapter 8	cm
L_C	Length of the connecting rod for the IC HCCI engine model	Chapter 8	cm
m_{jk}	Reduced molecular mass for the collision	Chapter 5	g
m_k	Molecular mass of the *k*th species	Chapter 4, Chapter 5	g
$\dot{m}_i$	Mass flow rate at inlet	Chapter 9	g/sec
$\dot{m}_l$	Mass loss rate at the lower boundary	Chapter 11	g/(cm$^{(1-\alpha)}$ sec)
$\dot{m}_o$	Mass flow rate at outlet	Chapter 9	g/sec
$\dot{m}_u$	Mass loss rate at the upper boundary	Chapter 11	g/(cm$^{(1-\alpha)}$ sec)
$\dot{m}_0$	Mass flux at the channel inlet	Chapter 11	g/(cm$^{(1-\alpha)}$ sec)
$\dot{m}$	Mass flux	Chapter 11	g/(cm$^{(1-\alpha)}$ sec)
	Mass flow rate	Chapter 12	g/sec
M	Number of materials in the surface reaction mechanism	Chapter 8	none
	Reactor mass	Chapter 9	g

Latin Symbols (Continued)

Symbol	Description	Chapter	CGS Units
M_k	Molecular weight of the *k*th species, replaces W_k.	Chapter 14	g/mole
$\overline{M}$	Mean molecular weight of a mixture, replace $\overline{M}$.	Chapter 14	g/mole
$[M]$	Total molar concentration of a mixture	Chapter 3	mole/cm^3
$\hat{n}$	Interior unit normal vector. Surface-normal unit vector; points from the gas into the bulk layer	Chapter 4	cm
N	Number of coefficients in polynomial fits to C_p^o/R	Chapter 2, Chapter 4, Chapter 14	none
	Total number of event (statistical) particles	Chapter 9	none
	Total number of phases	Chapter 4	none
$N(m)$	Total number of phases for the *m*th material	Chapter 8	none
N_A	Avogadro's number	Chapter 4	none
N_b	Total number of bulk phases	Chapter 4, Chapter 14	none
N_c	Number of event (statistical) particles to be effected by convection	Chapter 9	none
$N_b(m)$	Total number of bulk phases for the *m*th material	Chapter 8	none
N_b^f	Index of the first bulk phase	Chapter 4, Chapter 14	none
$N_b^f(m)$	Index of the first bulk phase for the *m*th material	Chapter 8	none
N_b^l	Index of the last bulk phase	Chapter 4, Chapter 14	none

Latin Symbols (Continued)

Symbol	Description	Chapter	CGS Units
$N_b^l(m)$	Index of the last bulk phase for the mth material	Chapter 8	none
N_g	Number of gas phases (always equal to 1)	Chapter 4, Chapter 8	none
N_m	Number of event (statistical) particles to be effected by molecular mixing	Chapter 9	none
N_s	Total number of surface site types (phases)	Chapter 4, Chapter 11, Chapter 14	none
$N_s(m)$	Total number of surface site types (phases)	Chapter 8	none
N_s^f	Index of first surface phase	Chapter 4, Chapter 14	none
$N_s^f(m)$	Index of first surface phase	Chapter 8	none
N_s^l	Index of last surface phase	Chapter 4, Chapter 14	none
$N_s^l(m)$	Index of last surface phase	Chapter 8	none
Nu_h	Nusselt number for heat transfer for the IC HCCI engine model	Chapter 8	none
o_i	Scaled circumferential velocity (W) at the inlet	Chapter 14	1/sec
P	Pressure	Chapter 3, Chapter 4, Chapter 5, Chapter 7, Chapter 8, Chapter 11, Chapter 12, Chapter 14	dynes/cm^2
P_m	Spatially-varying component of pressure in radial momentum equation.	Chapter 14	dynes/cm^2

Latin Symbols (Continued)

Symbol	Description	Chapter	CGS Units
P_{atm}	Pressure of one standard atmosphere	Chapter 3, Chapter 4, Chapter 8	dynes/cm^2
P_ϕ	Probability density function of scalar	Chapter 9	none
$\dot{P}$	Energy source term for heating of surface	Chapter 14	ergs/(cm^2 sec)
Pr	Prandtl number for the IC HCCI engine model	Chapter 8	none
$\dot{q}$	Net heat transfer from reactor to ambient	Chapter 14	ergs/sec
$\dot{q}''$	Total energy deposited into the gas from a heat source	Chapter 14	ergs/(cm^2 sec)
	Heat flux	Chapter 5	ergs/(cm^2 sec)
q_i	Rate of progress of the *i* th gas-phase reaction.	Chapter 14	mole/(cm^3 sec)
	Rate of progress of the *i* th reaction.	Chapter 3, Chapter 4	mole/(cm^2 sec)
$\dot{q}_{wall}$	Heat loss to the walls for the IC HCCI engine model	Chapter 8	ergs/sec
r	Radial coordinate	Chapter 14	cm
R	Universal gas constant	Chapter 3, Chapter 4, Chapter 5, Chapter 7, Chapter 8, Chapter 11, Chapter 12, Chapter 14	ergs/(mole K)
R_c	Universal gas constant, in units consistent with activation energy	Chapter 3, Chapter 4	[cal/(mole K)]*
R_{ki}	Reverse reaction-order specified for the *k* th species in the *i* th reaction.	Chapter 3, Chapter 4	none

Latin Symbols (Continued)

Symbol	Description	Chapter	CGS Units
R_{CA}	Ratio of L_C over L_A for the IC HCCI engine model	Chapter 8	none
Re	Reynolds number for the IC HCCI engine model	Chapter 8	none
s_k^o	Standard state specific entropy of the *k*th species	Chapter 3, Chapter 4	ergs/(g K)
$\bar{s}$	Mean specific entropy of a mixture	Chapter 2	ergs/(g K)
$\dot{s}_k$	Production rate of the *k*th species from surface reactions	Chapter 4, Chapter 8, Chapter 11, Chapter 14	mole/(cm^2 sec)
S_k^o	Standard state molar entropy of the *k*th species	Chapter 3, Chapter 4	ergs/(mole K)
S_k	Molar entropy of the *k*th species	Chapter 3	ergs/(mole K)
S_q	Spatially distributed thermal energy source	Chapter 2	ergs/(cm^3 sec)
$\bar{S}$	Mean molar entropy of a mixture	Chapter 2	ergs/(mole K)
$\bar{S}_p$	Average piston speed for the IC HCCI engine model	Chapter 8	cm/sec
t	Time	Chapter 4, Chapter 7, Chapter 8, Chapter 9, Chapter 12, Chapter 14	sec
t_l	Laboratory time	Chapter 7	sec
t_p	Gas-particle time	Chapter 7	sec

Latin Symbols (Continued)

Symbol	Description	Chapter	CGS Units
T	Temperature	Chapter 3, Chapter 4, Chapter 5, Chapter 7, Chapter 8, Chapter 9, Chapter 11, Chapter 12, Chapter 14	K
T_{ik}^{*}	Reduced temperature for the collision	Chapter 5	none
T_{k}^{*}	Reduced temperature of the kth species	Chapter 5	none
T_o	Ambient temperature	Chapter 4, Chapter 8, Chapter 14	K
T_e	Electron temperature	Chapter 4, Chapter 8	K
T_{ion}	Temperature of the ions.	Chapter 8	K
T_{surf}	Surface temperature	Chapter 8, Chapter 14	K
T_{wall}	Chamber wall temperature for the IC HCCI engine model	Chapter 8	K
	Temperature to which the surface radiates	Chapter 14	K
u	Axial velocity of fluid mixture (x direction)	Chapter 4, Chapter 8, Chapter 11, Chapter 12, Chapter 14	cm/sec
	Gas velocity in shock-fixed coordinates	Chapter 7	cm/sec
u_i	Exponential constant in reaction yield expression	Chapter 4	none
u_k	Specific internal energy of the kth species	Chapter 2, Chapter 4	ergs/g

Latin Symbols (Continued)

Symbol	Description	Chapter	CGS Units
$\bar{u}$	Mean specific internal energy of a mixture	Chapter 2	ergs/g
U	Gas velocity in laboratory-fixed coordinates	Chapter 7	cm/sec
U_k	Molar internal energy of the *k*th species	Chapter 2	ergs/mole
U_{rs}	Reflected shock velocity	Chapter 7	cm/sec
U_s	Incident shock velocity	Chapter 7	cm/sec
U_k^o	Standard state internal energy of the *k*th species	Chapter 2	ergs/mole
$\bar{U}$	Mean molar internal energy of a mixture	Chapter 2	ergs/mole
v	Fluid velocity in y direction	Chapter 11	cm/sec
$\mathbf{v}$	Gas velocity (vector)	Chapter 5, Chapter 7	cm/sec
V	Volume	Chapter 4, Chapter 8, Chapter 9, Chapter 14	cm^3
	Scaled radial velocity	Chapter 14	1/sec
V_c	Clearance volume in an engine cylinder for the engine model	Chapter 8	cm^3
	Correction velocity	Chapter 12, Chapter 14	cm/sec
V_k	Diffusion velocity of the *k*th species	Chapter 4, Chapter 5, Chapter 12, Chapter 14	cm/sec
$V_{k,y}$	Diffusion velocity of the *k*th species in the y division	Chapter 11	cm/sec
V_k	Ordinary diffusion velocity of the *k*th species	Chapter 5, Chapter 12	cm/sec

Latin Symbols (Continued)

Symbol	Description	Chapter	CGS Units
w	Ratio u_w/u_2 used shock tube equations	Chapter 7	none
	Scaled circumferential velocity	Chapter 14	1/sec
w_s	Half-width of the distribution of energy source term	Chapter 14	cm
$\overline{W}$	Mean molecular weight of a mixture	Chapter 2, Chapter 4, Chapter 5, Chapter 8, Chapter 11, Chapter 12	g/mole
W_k	Molecular weight of the *k*th species	Chapter 2, Chapter 4, Chapter 5, Chapter 7, Chapter 8, Chapter 9, Chapter 11, Chapter 12, Chapter 14	g/mole
W_k	Thermal diffusion velocity of the *k*th species	Chapter 5, Chapter 12	cm/sec
W_{ion}	Molecular weight of the positive ionic species in a Bohm-type reaction	Chapter 4	g/mole
x	Spatial coordinate along principal flow direction	Chapter 4, Chapter 11, Chapter 12, Chapter 14	cm
x_s	Position of the center of the energy source term	Chapter 14	cm
$\mathbf{X}$	Array of surface species mole fractions	Chapter 4	none

Latin Symbols (Continued)

Symbol	Description	Chapter	CGS Units
X_k	Mole fraction of the *k*th species	Chapter 3, Chapter 4, Chapter 5, Chapter 6, Chapter 7, Chapter 8, Chapter 11, Chapter 12, Chapter 14	none
$[X_k]$	Molar concentration of the *k*th species	Chapter 3, Chapter 4, Chapter 14	mole/cm^3
y	Cross-stream coordinate	Chapter 11	cm
$y_{\max}$	Maximum channel dimension	Chapter 11	cm
Y_k	Mass fraction of the *k*th species	Chapter 3, Chapter 4, Chapter 5, Chapter 7, Chapter 8, Chapter 9, Chapter 11, Chapter 12, Chapter 14	none
z	Distance	Chapter 7	cm
$\mathbf{Z}$	Array of surface species site fractions	Chapter 4	none
	Ratio $(y+1)/(y-1)$ used in Shock Reactor.	Chapter 7	none
Z_k	Site fraction of the *k*th species at a site	Chapter 14	none
$Z_k(n)$	Site fraction of the *k*th species on surface phase n	Chapter 4, Chapter 11	none
$Z_k(n,m)$	Site fraction of the *k*th species on site n of the *m*th material	Chapter 8	none

The energy CGS units that are noted by an asterisk (*****) depend upon user input at the `REACTIONS` line or in the `UNITS` auxiliary keyword for chemistry input files. The default unit is thermal calories.

21.2 Greek Equation Symbols

The table below shows the conventions used in this document for Greek equation symbols.

Greek Symbols

Symbol	Description	Chapter	CGS Units
α	Coordinate index: 0 for planar, 1 for radial coordinates	Chapter 11	none
α	Temperature ratio across the incident shock, T_2/T_1	Chapter 7	none
α'	Temperature ratio across the reflected shock, T_5/T_1	Chapter 7	none
α_i	Parameter in mechanism	Chapter 4	none
α_k	Polarizability of the *k*th species	Chapter 5	Å^3
α_k^*	Reduced polarizability of the *k*th species.	Chapter 5	none
α_{ki}	Enhanced third-body efficiency of the *k*th species in the *i*th reaction	Chapter 4	none
β	Temperature ratio across the incident shock, p_2/p_1	Chapter 7	none
β_i	Temperature exponent in the rate constant of the *i*th reaction	Chapter 3, Chapter 4, Chapter 8, Chapter 12	none
β'	Temperature ratio across the reflected shock, p_5/p_1	Chapter 7	none
Γ_n	Site density for surface phase n	Chapter 4	mole/cm^2
Γ_n^o	Initial site density for surface phase n	Chapter 4	mole/cm^2
Γ_{tot}	Site density summed over all surface phases	Chapter 4	mole/cm^2
Γ_{mix}	Characteristic time scale for the mixing process	Chapter 9	sec

Greek Symbols (Continued)

Symbol	Description	Chapter	CGS Units
Γ_{res}	Reactor residence time	Chapter 9	sec
$\dot{\Gamma}_n$	Production rate for surface phase n	Chapter 4	mole/(cm^2 sec)
γ	User-specified parameter for solution curvature resolution	Chapter 12	none
	Specified heat ratio	Chapter 7	none
γ_i	Sticking coefficient for the ith surface reaction	Chapter 4	none
Δt	Time step size for stochastic simulation	Chapter 9	sec
$\hat{\delta}$	Unit tensor	Chapter 5	none
δ^*_{jk}	Reduced dipole moment of the kth species	Chapter 5	none
δ^*_k	Effective reduced dipole moment for the collision	Chapter 5	none
ε	Small number (e.g. 1.E-12)	Chapter 5	none
	Emissivity	Chapter 4	none
$\bar{\varepsilon}$	Averaged turbulent kinetic energy dissipation rate	Chapter 9	cm^2/sec^3
ε_{jk}	Effective Lennard-Jones potential well depth for the collision	Chapter 5	ergs
ε_k	Inlet mass fraction of the kth species	Chapter 12	none
	Lennard-Jones potential well depth for the kth species	Chapter 5	ergs
ε_{ki}	Coverage parameter	Chapter 4	[cal/mole]*
η	Mixture viscosity	Chapter 5	g/(cm sec)
	Density ratio across the incident shock, ρ_2/ρ_1	Chapter 7	none

Greek Symbols (Continued)

Symbol	Description	Chapter	CGS Units
η_k	Pure species viscosity of the *k*th species	Chapter 5	g/(cm sec)
η_{ki}	Coverage parameter	Chapter 4	none
η_{air}	Viscosity of air for the IC HCCI engine model	Chapter 8	g/(cm sec)
Θ_k	Thermal diffusion ratio for mixture-averaged formula	Chapter 5, Chapter 12	none
θ	Angle between the crank arm and connecting rod for the engine model	Chapter 8	degrees
κ	Bulk coefficient of viscosity	Chapter 5	g/(cm sec)
$\tilde{\kappa}$	Averaged turbulent kinetic energy	Chapter 9	cm^2/sec^2
λ	Thermal conductivity of the gas mixture	Chapter 4, Chapter 5, Chapter 11, Chapter 12, Chapter 14	ergs/cm · sec · K
$\lambda^{(n)}$	Damping parameter for the *n*th iterate in the solution algorithm	Chapter 12	none
λ_0	Multicomponent thermal conductivity of the species	Chapter 5	ergs/cm · sec · K
λ_k	Thermal conductivity of the *k*th species	Chapter 5	ergs/cm · sec · K
λ_{air}	Thermal conductivity of air for the IC HCCI engine model	Chapter 8	ergs/cm · sec · K
μ	Mixture viscosity	Chapter 7, Chapter 11	g/(cm sec)
μ_{jk}	Effective dipole moment for the collision	Chapter 5	Debye
μ_k	Chemical potential of the *k*th species	Chapter 4	none
	Dipole moment of the *k*th species	Chapter 5	Debye
μ_k^o	Chemical potential of the *k*th species	Chapter 4	none

Greek Symbols (Continued)

Symbol	Description	Chapter	CGS Units
μ_k^*	Reduced dipole moment of the *k*th species	Chapter 5	none
μ_{ki}	Coverage parameter	Chapter 4	none
ν	Kinematic viscosity	Chapter 7	cm^2/sec
ξ	Normalized stream function	Chapter 11	none
	Density ratio, ρ_5/ρ_1	Chapter 7	none
ξ_{ij}	Relaxation collision number	Chapter 5	none
ρ	Mass density of a gas mixture	Chapter 2, Chapter 4, Chapter 5, Chapter 7, Chapter 8, Chapter 9, Chapter 11, Chapter 12, Chapter 14	g/cm^3
ρ_i	Mass density at the reactor inlet	Chapter 11	g/cm^3
ρ_k	Mass density of the *k*th bulk species	Chapter 4, Chapter 8, Chapter 11	g/cm^3
$\rho_{n,\,m}$	Site density of the *n*th bulk phase on the *m*th material.	Chapter 8	$mole/cm^2$
ρ_{air}	Mass density of air for the SI Engine Zonal Simulator model	Chapter 8	g/cm^3
σ_k	Number of sites occupied by the *k*th species.	Chapter 4	none
	Stefan-Boltzmann constant	Chapter 14	none
	Stefan-Boltzmann constant	Chapter 4, Chapter 14	$ergs/(cm^2\ sec\ K^4)$
	Lennard-Jones diameter of the *k*th species	Chapter 5	Å

Greek Symbols (Continued)

Symbol	Description	Chapter	CGS Units
σ_{jk}	Effective Lennard-Jones diameter for the collision	Chapter 5	Å
τ	Nominal residence time	Chapter 8, Chapter 14	sec
	Momentum flux	Chapter 5	g/(cm sec^2)
τ_k	Characteristic chemical destruction time of the *k*th species	Chapter 3	sec
υ_{ki}	Net stoichiometric coefficient of the *k*th species in the *i*th reaction; $\upsilon_{ki} = \upsilon'_{ki} - \upsilon''_{ki}$	Chapter 3	none
υ'_{ki}	Stoichiometric coefficient of the *k*th reactant species in the *i*th reaction	Chapter 3	none
υ''_{ki}	Stoichiometric coefficient of the *k*th product species in the *i*th reaction	Chapter 3, Chapter 4, Chapter 8, Chapter 14	none
Φ	Dependent variable vector in an application program	Chapter 4	none
χ_k	Chemical symbol of the *k*th species	Chapter 4, Chapter 8	none
ψ	Stream function	Chapter 11	g/(cm^2 sec)
Ψ	Yield enhancement factor (ion-energy-yield reaction)	Chapter 4	none

Greek Symbols (Continued)

Symbol	Description	Chapter	CGS Units
Ω	Rotation rate of the crank arm in the internal combustion engine model	Chapter 8	1/sec
	Collision integral	Chapter 5	none
$\dot{\omega}_k$	Chemical production rate of the *k*th species due to gas-phase reactions	Chapter 3, Chapter 4, Chapter 7, Chapter 8, Chapter 9, Chapter 11, Chapter 12, Chapter 14	mole/(cm^3 sec)

The energy CGS units that are noted by an asterisk (*****) depend upon user input at the `REACTIONS` line or in the `UNITS` auxiliary keyword for chemistry input files. The default unit is thermal calories.

21.3 Subscript Equation Symbols

The table below shows the conventions used in this document for subscript equation symbols.

Subscript Symbols

Symbol	Description	Chapter
0	Denotes reference condition	Chapter 7
1	Denotes condition before the incident shock	Chapter 7
2	Denotes condition immediately behind incident shock	Chapter 7
3	Denotes condition immediately behind reflected shock	Chapter 7

Subscript Symbols (Continued)

Symbol	Description	Chapter
i	Denotes reaction index, ionic species index, or inlet index.	Chapter 3, Chapter 4, Chapter 8, Chapter 14
j	Grid-point index	Chapter 12
	Reactor index in network	Chapter 8, Chapter 11, Chapter 13, Chapter 14
k	Species index	Chapter 3, Chapter 4, Chapter 5, Chapter 8, Chapter 12, Chapter 14
m	Denotes materials index m	Chapter 8
n	Phases index	Chapter 4, Chapter 8,
	Species index for a non-polar species	Chapter 5
p	Species index for a non-polar species	Chapter 5
w	Denotes condition at the wall	Chapter 7

Index

C

D

E

F

G

H

I

J

K

L

M

N

O

P

Q

R

S

T

U

V

W

X

Y

Z

